DESIGN AND MANUFACTURING OF HYBRID VERTICAL TAKEOFF AND LANDING (VTOL) UAV

A Final Year Project Report

Presented to

SCHOOL OF MECHANICAL & MANUFACTURING ENGINEERING

Department of Mechanical Engineering

NUST

ISLAMABAD, PAKISTAN

In Partial Fulfillment
of the Requirements for the Degree of
Bachelor of Mechanical Engineering

---

by

Sameer Bin Khalid

Aqib Habib

Usman Shahid

Muhammad Salman Azam

June 2022

We hereby recommend that the final year project report prepared under our supervision by:

SAMEER BIN KHALID	257215
AQIB HABIB MEMON	266993
USMAN SHAHID	255526
MUHAMMAD SALMAN AZAM	256777

Titled: "DESIGN AND MANUFACTURING OF HYBRID VERTICAL TAKEOFF AND LANDING (VTOL) UAV" be accepted in partial fulfillment of the requirements for the award of BACHELOR'S IN MECHANICAL ENGINEERING degree with grade ___

Supervisor: Dr Zaib Ali, Assistant Professor SMME (NUST)	______________________ Dated:
Committee Member: Name, Title (faculty rank) Affiliation	______________________ Dated:
Committee Member: Name, Title (faculty rank) Affiliation	______________________ Dated:

______________________ ____________

(Head of Department) (Date)

COUNTERSIGNED

Dated: ________________ ________________________

(Dean / Principal

ABSTRACT

The usage of UAVs has risen tremendously in recent years because of improved avionics and propulsion technology; nonetheless, there is a lot of demand to improve the range, endurance, speed, and ergonomics of UAVs. Neither a fixed wing nor a multi-rotor can solve all of these issues. What's required is a mix of the two configurations, which may considerably expand the usage of drones in a variety of applications. Due to the requirement for emergency operations, a novel idea is being developed in which an aircraft can fly and land vertically like a helicopter or other multi-rotor, as well as fly ahead like a fixed-wing aircraft, combining the best of both configurations.

Our Hybrid VTOL UAV can take-off and land without a runway and hover in any required area with higher endurance and range than multi-rotor. Hence due to their ideal flight requirements for reconnaissance it can be used in military, disaster management, healthcare and mapping. In this report, a concept of a UAV is developed which is fully automated and can take off and land vertically with capability of performing a range of missions from product delivery to military reconnaissance.

ACKNOWLEDGMENTS

We would like to express our deepest appreciation to all those who provided us the possibility to complete this report. A special gratitude we give to our final year project coordinator "Dr. Niaz Bahadur", whose contribution in stimulating suggestions and encouragement, helped us to coordinate our project.

Furthermore, we would also like to thank our Advisors "Dr. Zaib Ali" and "Dr. Basharat Ali Haider" who invested his full effort in guiding the team in achieving the goal. We must appreciate the guidance given by other supervisors as well as the input provided by the panel during our last project presentation, which helped us in improving and showing up for this presentation with a cogent and pragmatic approach.

ORIGINALITY REPORT

TABLE OF CONTENTS

LIST OF TABLES

LIST OF FIGURES

SYMBOLS & ABBREVIATIONS

$N_b = Number\ of\ Batteries$

$N_{sm_1} = Number\ of\ Servos\ of\ Type\ 1$

$N_{sm_2} = Number\ of\ Servos\ of\ Type\ 2$

$N_{sm_1} = Number\ of\ Motors\ of\ Type\ 1$

$N_{m_2} = Number\ of\ Motors\ of\ Type\ 2$

$W_b = Weight\ of\ Battery$

$W_{m_1} = Weight\ of\ Motor\ of\ Type\ 1$

$W_{m_2} = Weight\ of\ Motor\ of\ Type\ 2$

$W_{ESC} = Weight\ of\ Electronic\ Speed\ Controller$

$W_{p_1} = Weight\ of\ Propellers\ of\ Type\ 1$

$W_{p_2} = Weight\ of\ Propellers\ of\ Type\ 2$

$W_{FC} = Weight\ of\ Flight\ Controller$

$W_{Misc} = Weight\ of\ Miscellaneous\ Components\ (GPS\ /Accesories)$

$W_{p_1} = Weight\ of\ Propellers\ of\ Type\ 1$

$W_{sm_1} = Weight\ of\ Servos\ of\ Type\ 1$

$W_{sm_2} = Weight\ of\ Servos\ of\ Type\ 2$

$W_{LG} = Weight\ of\ Landing\ Gear$

$W_{CB} = Weight\ of\ Cables\ or\ Wires$

$W_{AF} = Weight\ of\ Airframe\ of Structure$

$W_{PL} = Weight\ of\ Payload$

$W_{MTOW} = Maximum\ Take-Off\ Weight$

$\rho_{sea} = Density\ of\ Air\ at\ Sea-Level$

$\rho_{ceiling} = Density\ of\ Air\ at\ Ceiling\ Altitude$

$\rho_{alt} = Density\ of\ Air\ at\ Cruising\ Altitude$

$CD_o = Zero-Lift\ Drag\ Coefficient$

$e = Ostawald's\ Efficiency$

$K = Drag\ due\ to\ lift\ Coefficient$

$C_D = Drag\ Polar$

$V_c = Cruise\ Speed$

$V_s = Stalling\ Speed$

$V_{max} = Maximum\ Speed$

$ROC = Rate\ of\ Climb$

$ROC_{ceiling} = Rate\ of\ Climb\ at\ Ceiling\ Altitude$

$e = Ostawald's\ Efficiency$

$Cl_{max_{w,2-D}} = Maximum\ Lift\ Coefficient\ of\ Wing\ Airfoil$

$\left(\frac{W}{S}\right)_{Stall} = Wing\ Loading\ as\ a\ function\ of\ Stall\ Speed$

$\left(\frac{W}{S}\right)_{Max} = Wing\ Loading\ as\ a\ function\ of\ Max\ Speed$

$\left(\frac{W}{S}\right)_{Take-off} = Wing\ Loading\ as\ a\ function\ of\ Take-off\ run$

$\left(\frac{W}{S}\right)_{ROC} = Wing\ Loading\ as\ a\ function\ of\ Rate\ of Climb$

$\left(\frac{W}{S}\right)_{Ceiling} = Wing\ Loading\ as\ a\ function\ of\ Rate\ of Climb$

$\left(\frac{W}{P}\right)_{Stall} = Power\ Loading\ as\ a\ function\ of\ Stall\ Speed$

$\left(\frac{W}{P}\right)_{Max} = Power\ Loading\ as\ a\ function\ of\ Max\ Speed$

$\left(\frac{W}{P}\right)_{Take-off} = Power\ Loading\ as\ a\ function\ of\ Take-off\ run$

$\left(\frac{W}{P}\right)_{ROC}$

$= Power\ Loading\ as\ a\ function\ of\ Rate\ of Climb$

$\left(\frac{W}{P}\right)_{Ceiling}$

$= Power\ Loading\ as\ a\ function\ of\ Rate\ of Climb$

$h_{Ceiling} = Absolute\ Ceiling$

$h_{alt} = Cruising\ Altitude$

$P_{alt} = Power\ at\ cruising\ altitude$

$P_{SL} = Power\ at\ sea\ level$

$K = Induced\ Drag\ Factor$

$\sigma_c = Relative\ Air\ Density\ at\ Required\ Ceiling$

$(\eta_p)_{Stall} = Efficiency\ of\ Propeller\ during\ Stall$

$(\eta_p)_{Max}$

$= Efficiency\ of\ Propeller\ during\ Maximum\ Speed$

$(\eta_p)_{Take-off} = Efficiency\ of\ Propeller\ during\ Take$

$- off$

$(\eta_p)_{ROC} = Efficiency\ of\ Propeller\ during\ Climb$

$(\eta_p)_{Ceiling} = Efficiency\ of\ Propeller\ at\ Ceiling$

$(\eta_p)_{Stall} = Efficiency\ of\ Propeller\ during\ Stall$

$\sigma_c = Relative\ Air\ Density\ at\ Ceiling$

$\sigma_{alt} = Relative\ Air\ Density\ at\ Cruising\ Altitude$

$\left(\frac{W}{P}\right)_{DP} = Power\ Loading\ Design\ Point$

$\left(\frac{W}{S}\right)_{DP} = Wing\ Loading\ Design\ Point$

$S_w = Wing\ Area$

$b_w = Wing\ Span$

$AR_w = Wing\ Aspect\ Ratio$

$C_{tip,w} = Wing\ Tip\ Chord$

$C_{root,w} = Wing\ Root\ Chord$

$P_{DP} = Power\ of\ Motor\ From\ Design\ Point$

$\left(\frac{L}{D}\right)_{w,2-D_{max}}$

$= Maximum\ Wing\ Airfoil\ Lift\ to\ Drag\ Ratio$

$\left(\frac{L}{D}\right)_{w,3-D_{max}} = Maximum\ Wing\ Lift\ to\ Drag\ Ratio$

$g = Gravitational\ Acceleration$

$\lambda_w = Taper\ Ratio\ of\ Wing$

$\alpha_{t,w} = Wing\ Twist\ Angle$

$\Gamma_w = Wing\ Dihedral\ Angle$

$\alpha_{i,w} = Wing\ Incidence\ Angle\ or\ Setting\ Angle$

$Cl_{\alpha_{w,2-D}} = Lift\ coefficient\ Slope\ of\ Wing\ Airfoil$

$Cl_{\alpha_{w,3-D}} = Lift\ coefficient\ Slope\ of\ Wing$

$\alpha_{o_{w,2-D}} = Zero\ Lift\ Angle\ of\ Attack\ of\ Airfoil$

$\overline{C_w} = Mean\ Aerodynamic\ Chord\ of\ Wing$

$\Lambda_w = Wing\ Sweep\ Angle$

$Cl_{LT_{w,3-D}}$

$= Lift\ Coefficient\ of\ Wing\ from\ Lift\ Line\ Theory$

$Cl_{c_{req,2-D}}$

$= Required\ Lift\ Coefficient\ of\ Airfoil\ at\ Crusing$

$Cl_{c_{req,3-D}}$

$= Required\ Lift\ Coefficient\ of\ Wing\ at\ Crusing$

$\overline{S_w} = Mean\ Wing\ Area$

$\left(\frac{t}{c}\right)_{max,w}$

$= Wing\ Airfoil\ Maximum\ Thickness\ to\ Chord\ Ratio$

$V_{c_{LLT}}$

$= Crusing\ Speed\ From\ Lift\ Line\ Theory\ Wing\ Lift\ Coefficient$

$P_c = Power\ Required\ in\ Cruise$

$R_{plane} = Range\ of\ Aircraft$

$t_{cruise} = Time\ of\ Total\ Cruise$

$E_{cruise} = Energy\ Consumption\ in\ Cruise$

$\left(V_{Take-off}\right)_{VTOL} = Vertical\ Take\ off\ Speed$

$\left(L_{Take-off}\right)_{VTOL} = Vertical\ Take-off\ Lift$

$P_{Take-off} = Power\ Required\ in\ Take-off$

$t_{Take-off} = Time\ of\ total\ Vertical\ Take-off$

$E_{Take-off} = Energy\ Consumption\ in\ Take-off$

$E_{Descend} = Energy\ Consumption\ in\ Descend$

$E_{Total} = Total\ Energy\ Consumption$

$\mu_{battery} = Energy\ Density\ of\ Battery$

$FOS_{Battery} = Safe\ Discharge\ of\ Battery$

$(W_b)_{req} = Required\ Weight\ of\ Battery$

$\bar{V}_H = Horizontal\ Tail\ Volume\ Coefficient$

$D_F = Diameter\ of\ Fuselage$

$K_c = Fudge\ Factor$

$(l_h)_{opt} = Optimum\ Moment-Arm\ of\ Horizontal\ Tail$

$S_h = Horizontal\ Tail\ Area$

$C_{m_{w,2-D}} = Wing\ Airfoil\ Maximum\ Pitching\ Moment$

$C_{m_{w,3-D}} = Wing\ Maximum\ Pitching\ Moment$

$h - h_o$

$= Distance\ between\ Aerodynamic\ Center\ and\ Center\ of$

$Gravity$

$(Cl_h)_{req}$

$= Required\ Lift\ Coefficient\ of\ Horizontal\ Tail$

$\Lambda_h = Horizontal\ Tail\ Sweep\ Angle$

$\Gamma_h = Dihedral\ Angle\ of\ Horizontal\ Tail$

$AR_h = Horizontal\ Tail\ Aspect\ Ratio$

$\lambda_h = Taper\ Ratio\ of\ Horizontal\ Tail$

$\left(\frac{t}{c}\right)_{max,h}$

$= Horizontal\ Tail\ Airfoil\ Maximum\ Thickness\ to$

$Chord\ Ratio$

$Cl_{\alpha_{h,2-D}}$

$= Lift\ coefficient\ Slope\ of Horizontal\ Tail\ Airfoil$

$Cl_{\alpha_{h,3-D}} = Lift\ coefficient\ Slope\ of\ Horizontal\ Tail$

$\alpha_h = Horizontal\ Tail\ Angle\ of\ Attack$

$\alpha_{i,h} = Horizontal\ Tail\ Incidence\ Angle$

$\alpha_{t,h} = Horizontal\ Tail\ Twist\ Angle$

$b_h = Horizontal\ Tail\ Span$

$C_{tip,h} = Horizontal\ Tail\ Tip\ Chord$

$C_{root,h} = Horizontal\ Tail\ Root\ Chord$

$\overline{C_h} = Mean\ Aerodynamic\ Chord\ of\ Horizontal\ Tail$

$\overline{S_h} = Mean\ Horizontal\ Tail\ Area$

$\eta_h = Horizontal\ Tail\ Efficiency$

$C_{m\alpha}$

$= Longitudinal\ Stability\ Contribution\ by\ Horizontal\ Tail$

$\bar{V}_V = Vertical\ Tail\ Volume\ Coefficient$

$(l_v)_{opt} = Optimum\ Moment-Arm\ of\ Vertical\ Tail$

$S_v = Vertical\ Tail\ Area$

$\left(\frac{t}{c}\right)_{max,V}$

$= Vertial\ Tail\ Airfoil\ Maximum\ Thickness\ to\ Chord\ Ratio$

$\lambda_v = Taper\ Ratio\ of\ Vertical\ Tail$

$AR_v = Vertical\ Tail\ Aspect\ Ratio$

$\alpha_{i,v} = Vertical\ Tail\ Incidence\ Angle$

$\alpha_{t,v} = Vertical\ Tail\ Twist\ Angle$

$\Gamma_v = Dihedral\ Angle\ of\ Vertical\ Tail$

$b_v = Vertical\ Tail\ Span$

$C_{tip,v} = Vertical\ Tail\ Tip\ Chord$

$C_{root,v} = Vertical\ Tail\ Root\ Chord$

$\overline{C_v} = Mean\ Aerodynamic\ Chord\ of\ Vertical\ Tail$

$\overline{S_v} = Mean\ Vertical\ Tail\ Area$

$FOS_p = Propulsion\ Factor\ of\ Safety$

$\eta_p = Propeller\ Efficiency$

$AR_p = Propeller\ Aspect\ Ratio$

$V_{max_{ts,p}} = Maximum\ Propeller\ Tip\ Speed$

$Cl_{p,2-D} = Propeller\ Airofil\ Lift\ Coefficient$

$D_p = Diameter\ of\ Fuselage$

$\omega_p = Propeller\ RPM$

$S_{wl} = Winglet\ Area$

$b_{wl} = Winglet\ Span$

$AR_{wl} = Winglet\ Aspect\ Ratio$

$C_{tip,wl} = Winglet\ Tip\ Chord$

$C_{root,wl} = Winglet\ Root\ Chord$

$\lambda_{wl} = Taper\ Ratio\ of\ Winglet$

$\phi_{ct} = Winglet\ Cant\ Angle$

$R_{BL} = Winglet\ Blend\ Radius$

$\rho_{mat,w} = Wing\ Material\ Density$

$K_{\rho,w} = Wing\ Density\ Factor$

$n_{max} = Max\ Load\ Factor$

$n_{ult} = Ultimate\ Load\ Factor$

$\Lambda_{QC,w} = Wing\ Quarter\ Chord\ Sweep\ Angle$

$(W_w)_{est} = Estimated\ Wing\ Weight$

$K_{\rho,h} = Horizontal\ Tail\ Density\ Factor$

$\Lambda_{QC,h} = Horizontal\ Tail\ Quarter\ Chord\ Sweep\ Angle$

$\frac{C_{tip,E}}{C_{tip,h}} = Elevator\ to\ Horizontal\ Tail\ Tip\ Chord\ Ratio$

$(W_h)_{est} = Estimated\ Horizontal\ Tail\ Weight$

$K_{\rho,v} = Vertical\ Tail\ Density\ Factor$

$\Lambda_{QC,v} = Vertical\ Tail\ Quarter\ Chord\ Sweep\ Angle$

$\frac{C_{tip,R}}{C_{tip,v}} = Rudder\ to\ Vertical\ Tail\ Tip\ Chord\ Ratio$

$(W_v)_{est} = Estimated\ Vertical\ Tail\ Weight$

$L_f = Length\ of\ Fuselage$

$K_{inlet} = Constant\ Fuselage\ Parameter$

$K_{\rho,w} = Fuselage\ Density\ Factor$

$\rho_{mat,f} = Fuselage\ Material\ Density$

$(W_f)_{est} = Estimated\ Fuselage\ \ Weight$

$(W_{LG})_{est} = Estimated\ Landing\ Gear\ \ Weight$

$(W_{total})_{est} = Estimated\ Total\ Aircraft\ Weight$

$\frac{b_{a_i}}{b} = inboard\ position\ of\ aileron\ w.r.t\ wingspan$

$\frac{b_{a_o}}{b} = outboard\ position\ of\ aileron\ w.r.t\ wingspan$

$b_A = aileron\ span$

$C_A = aileron\ chord$

$S_A = aileron\ area$

$\frac{b_A}{b} = ratio\ of\ aileron\ span\ to\ wingspan$

$\frac{C_A}{C} = ratio\ of\ aileron\ chord\ to\ wing\ chord$

$\frac{S_A}{S} = ratio\ of\ aileron\ area\ to\ wing\ area$

$\tau_a = aileron\ effectiveness$

$C_{l_{\delta A}} = rolling\ moment\ coefficient\ derivative$

$\delta_A = max\ aileron\ deflection$

$C_l = rolling\ moment\ coefficient$

$L_A = aircraft\ rolling\ moment$

$P_{SS} = steady\ state\ roll\ rate$

$\phi_l = bank\ angle\ for\ steady\ state\ roll\ rate$

$\dot{P} = aircraft\ rate\ of\ roll\ rate$

$t_2 = roll\ time$

$b_E = elevator\ span$

$C_E = elevator\ chord$

$S_E = elevator\ area$

$\frac{b_E}{b_h} = ratio\ of\ elevator\ span\ to\ horizontal\ tail\ span$

$\frac{C_E}{C_h} = ratio\ of\ elevator\ chord\ to\ horizontal\ tail\ chord$

$\frac{S_E}{S_h} = ratio\ of\ elevator\ area\ to\ horizontail\ tail\ area$

$\tau_E = elevator\ effectiveness$

$\delta_E = max\ elevator\ deflection$

$C_{m_{\delta E}} = longitudinal\ control\ power\ derivative$

$\frac{\partial C_m}{\partial \delta_E}$

$= rate\ of\ change\ of\ pitching\ moment\ coefficient\ w.r.t$

$elevator\ deflection$

$C_{L_{\delta E}} = elevator\ contribution\ to\ aircraft\ lift$

$\frac{\partial C_L}{\partial \delta_E}$

$= rate\ of\ change\ of\ lift\ coefficient\ w.r.t\ elevator\ deflection$

$C_{L_{h_{\delta E}}} = elevator\ contribution\ to\ horizontal\ tail\ lift$

$C_{L_l} = steady\ state\ lift\ coefficient\ at\ cruising\ speed$

$C_{L_o} = lift\ coefficient\ at\ zero\ angle\ of\ attack$

C_{L_o}

$= pitching\ moment\ coefficient\ at\ zero\ angle\ of\ attack$

$\overline{q} = Dynamic\ Pressure$

$\delta_R = Max\ Rudder\ deflection$

$V_{mc} = Minimum\ controllable\ speed$

$\eta_v = Vertical\ tail\ efficiency$

$\frac{b_R}{b_V} = ratio\ of\ rudder\ span\ to\ vertical\ tail\ span$

$\frac{C_R}{C_V} = ratio\ of\ rudder\ chord\ to\ vertical\ tail\ chord$

$\frac{S_R}{S_V} = ratio\ of\ rudder\ area\ to\ vertical\ tail\ area$

$\tau_R = Rudder\ angle\ of\ attack\ effectiveness$

$C_{n_{\delta R}} = directional\ control\ derivative$

$C_{L_{\alpha_V}} = vertical\ tail\ lift\ curve\ slope$

$\dot{R}_{SR} = rate\ of\ spin\ recovery$

$\alpha_{spin} = angle\ of\ attack\ during\ spin$

$N_{SR} = counteracting\ yawming\ moment$

$S_{V_e} = effective\ vertical\ tail\ area$

$\overline{V}_{V_e} = effective\ vertical\ tail\ volume\ coefficient$

$I_{xx_w} = rolling\ inertia\ in\ wind\ axis$

$I_{zz_w} = product\ inertia\ in\ wind\ axis$

$I_{xz_w} = inertia\ in\ wind\ axis$

$I_{xx_B} = rolling\ inertia\ in\ body\ axis$

$I_{zz_B} = product\ inertia\ in\ body\ axis$

$I_{xz_B} = inertia\ in\ body\ axis$

CHAPTER 1: INTRODUCTION

1.1 Background and History

The term UAV is an abbreviation for Unmanned Aerial Vehicle i.e., an aircraft that does not carry on-board crew or passengers. UAVs find extensive use in military reconnaissance, agriculture, recreational photography as well as industrial inspections. A UAV is an aircraft capable of sustained level flight, either actively controlled from a ground-based operator or managed by the device itself (provided it is an autonomous aircraft) according to a mission path specified beforehand. This definition encompasses missile systems in addition to ordinary aircraft. For the sake of simplicity, they are classified separately under weapon systems.

UAVs are commonly known as *drones* and one early example (made by the US in the early 1960s) was even called an RPV (Remotely Piloted Vehicle). The term UAS (Unmanned Aerial System) is used when one wishes to refer to the complete operational framework (i.e., the additional ground control and data-link elements) of the UAV. Although the terms "UAV" and "drone" are synonymous with each other, some people regard UAVs as having complete autonomy in operation, as opposed to drones that may or may not be autonomous.

Figure 1 Drone for Aerial Photography [1]

The development of unmanned aerial vehicles or drones as we know them today started in the 20^{th} century when new types of military missions emerged that were deemed too risky or dull for pilots. However, the earliest known unmanned aerial weapon of warfare was actually a balloon carrier (used for dropping munitions on targets) developed in the mid-nineteenth century.

As a result of over a century of development, UAVs have transformed from remotely piloted vehicles used as weapon-launching platforms to completely autonomous aircraft capable of fulfilling a multitude of mission-specific roles. Where in the past, only rotor or jet-powered drones were practicable, electric power drives many modern UAVs intended for small-scale commercial and civilian use.

UAVs have become essential assets for armed forces of almost every country in the world. Although their genesis stemmed from a military requirement, drones have quickly diversified in application over the past decade or two.

1.2 Early Days

The concept of un-crewed military aircraft was first put to the test when British engineer Geoffrey de Havilland's "Aerial Target" aircraft was launched from a pneumatically powered ramp as part of the Royal Flying Corps (RFC) Trials in Upavon on March 21, 1917. The aircraft recorded a successful powered flight using British engineer Archibald Montgomery Low's radio-control system and, in doing so, became the first known 'drone' aircraft in history.

The next major developments in UAV technology came in the form of the Kettering Bug and the Hewitt-Sperry Automatic Airplane. The former was an experiment unmanned torpedo and the latter was a flying bomb designed to carry munitions.

Figure 2 The Kettering Bug (left) and the Hewitt-Sperry Automatic Airplane (right). Both were examples of early concepts for Unmanned Aerial Vehicles [2] [3]

In 1939, Nazi Germany developed a small, unmanned remote-controlled anti-aircraft drone called the Argus as 292. A reconnaissance variant was also made for the 292.

The post-WWII period saw the emergence of the Ryan Firebee, the GAF Jindvik and the Beechcraft MQM-61 Cardinal, all three being target drones controlled remotely from ground.

The Vietnam War, especially the Gulf of Tonkin incident in 64' prompted the development of the Ryan Model 147, a jet-powered drone capable of low-altitude photography, electronic warfare, decoy, signals intelligence and surveillance amongst other mission roles. The 147 was named an RPV (Remotely Piloted Vehicle), the nomenclature of that time. The Ryan AQM-91 was also a drone of this time, but it did not see extensive production or service.

A supersonic, rocket-propelled reconnaissance drone called the Lockheed D-21 was also developed by America and it performed a couple of reconnaissance missions over Chinese territory, but ultimately did not prove sound for further development. It was only designed for a one-way trip where it would eject its camera payload before eventually self-destructing. The D-21 marked significant progress in UAV technology, as it had an Inertial Navigation System (INS) which it would use to follow a pre-programmed path, thus having a level of autonomy in operation.

Figure 3 The Lockheed D-21 supersonic UAV. [4]

During the War of Attrition and the Yom Kippur War in the Middle East, Israel used tactical UAVs from the US as reconnaissance drones and decoys against opposing forces. Their missions culminated in the development of the Tadiran Mastiff, which is regarded as the first 'modern' fixed-wing UAV as it used a data-link system to transmit high-quality video coverage of enemy territory to its operators. The aircraft had 7-hour endurance, a payload of more than 10 kg, which it could take to a distance of 30-50 km at a max speed of 185 km/h.

Figure 4 Tadiran Mastiff: Israel's first modern drone aircraft [5]

The Tadiran Mastiff also had a rival (also a compatriot), the IAI Scout with similar capabilities.

Figure 5 The IAI Scout; a UAV similar in capabilities to its compatriot: the Mastiff [6]

The General Atomics MQ-1 Predator, perhaps the UAV to have seen most extensive combat was developed in the early 1990s for the US Air Force. Primarily used for reconnaissance but also later outfitted with air-to-ground missiles, the Predator is classified as a UAS consisting of a ground control station (GCS) and a satellite link communication suite in addition to the drone itself.

Figure 6 The MQ-1 Predator; a premier example of a military drone [7]

The Predator is still in limited service and has been developed into the MQ-9 Reaper that carries several times more payload of the Predator at higher altitudes and greater speed.

1.3 Classification of UAVs

There are two main types of UAVs concerning the layout their propulsion systems and the type of flight they maintain:

1.3.1 Fixed Wing UAVs

These types of drones takeoff, cruise and land like normal airplanes do. They have wings generating lift at speed, and tail structures for stability as required. Forward thrust is attained by propellers (or in some cases, gas turbines) mounted on wings. Some drones have one central powerplant mounted on the fuselage (nose or tail), which may necessitate unconventional tail designs, like in the MQ-1 Predator and the MQ-9 Reaper.

Fixed wing UAVs are ideal when endurance and range is a priority, like in reconnaissance missions. They are fast and carry high payload. They are not very complex in design and control. Their main disadvantage is the requirement of dedicated runways to take off and land.

Another shortcoming of this platform is the inability to maintain its spatial position and 'hover' in one spot, thus precluding applications like photography and product delivery. On top of that, a fixed wing UAV requires a skilled operator for safe flight and is usually an expensive solution because of its bulky structure. Almost all military drones are of a fixed-wing type.

Figure 7 A typical fixed wing UAV, but with an unconventional "inverted-V" tail [8]

1.3.2 Multi-copter UAVs

Multi-copter or multi-rotor UAVs are the ones with propellers installed on arms arranged symmetrically around a central structure. The propellers are installed so that their thrust is directed vertically rather than horizontally.

Pitch, roll and yaw is attained by providing differential power (and thus, inducing relative velocity) between the different propellers

As the propeller thrust is always directed vertically, multi-rotor UAVs are inherently VTOL (Vertical Take Off and Landing) aircraft and thus, do not need any runways for operation. They can easily hover in one spot if required. They are very stable in the air and anyone with a basic knowledge of the controls can maneuver them with ease. These are their main advantages over the fixed-wing type UAVs. They are best suited for covering short distances at a time, as they are not good in endurance or range. They are naturally slow in forward flight and inefficient in consuming battery power. This makes them ideal for commercial applications like product delivery, photography and crop spraying etc. They cannot carry as much payload as fixed-wing UAVs, but conversely, they are lighter and smaller.

The quadcopter is the most common kind of multi-rotor seen in application all over the world. It has four propellers on the ends of four arms arranged in a ‘cross’ or ‘plus’ layout.

Figure 8 Quadcopter [1]

Here is a brief comparison of salient features of the two main UAV types:

Table 1 Fixed-wing vs. Multi-rotor

Parameter	Fixed-wing	Multi-rotor
Endurance	High	Low
Range	High	Low
Payload	High capacity	Low capacity
Cruise Speed	High	Low
Size	Large	Small
Hover	No	Yes
Takeoff & Landing	Conventional	Vertical
Stability	Difficult to achieve	Easily achieved
Maneuverability	Limited	Easy
Control Systems	Complex	Simple
Assembly	Difficult	Easy

1.4 Design Demand

Our requirement is a UAV with good endurance and cruising speed that can carry a light payload (for example, a camera) and conduct reconnaissance of an area. From the above discussion, it follows that we require a hybrid of both the fixed-wing, and the multi-copter UAV type.

1.4.1 Alternating Hybrid VTOL UAV

The alternating hybrid VTOL UAV combines the strengths of the fixed-wing and multi-rotor and aims to have none of their drawbacks. Visually, it very much approximates a fixed-wing design, but it has booms for mounting propellers like a multi-rotor UAV. Four propellers intended to produce vertical thrust are located on the booms that also carry the tail while a single, large propeller ‘pusher’ is located on one end of the fuselage.

The tail is to follow an unconventional twin-T design, thus shielding horizontal and vertical tails from the propeller wake during forward flight. The takeoff and landing regimes are responsibilities of the quad-rotor array while the singular pusher is to generate forward thrust and the wings are to provide sufficient lift for the cruise regime of flight.

The UAV has been called ‘alternating’ because in the transition stage, the motor(s) controlling all propellers will decrease the speed of vertical propellers slowly while gradually increasing the speed of the pusher propeller. It is necessary to provide a gradual transition to the aircraft as a sudden complete ‘switch’ from vertical thrust to horizontal thrust would severely destabilize it.

Figure 9 A “4+1” alternating UAV [9]

Although the design promises significant advantages over its individual inspirations, it is not without shortcomings. For one, our UAV can be costly to manufacture than both an equivalent fixed-wing and a comparable multi-rotor. It is also huge in size and requires complicated disassembly to fit in practicable packaging.

1.4.2 Advantages

- Flexible in operation: can be launched from any surface directly.
- High-endurance and long-range.
- Can carry a good amount of supplies.
- Efficient in consuming power.
- Very stable in flight.
- Can hover in one place as well as cruise forwards.

1.5 Applications of UAVs

Modern UAVs are not at all restricted to military use like their predecessor. The recent conceptualizations and advances in UAV technology have made it possible to use drones in a multitude of commercial/civilian industries and applications. Some of them include:

1.5.1 Military Reconnaissance

UAVs were basically invented for the purpose of surveillance and reporting of hostiles on the battlefield, or outside of it. It is still a major application of drones, because they are easily and swiftly deployed, and they can relay vital information in the least amount of time (i.e. when compared to aircraft and helicopters) to ground operators when needed.

1.5.2 Emergency & Disaster Management (Damage Assessment, Supply Drops etc.)

Due to being flexible in deployment and operation, UAVs can prove to be the most efficient and effective type of aircraft to use for airborne surveillance of areas affected by natural disasters or tragedies. They can even be used to ferry small amounts of vital supplies to such areas.

1.5.3 Urban Planning

With the population of Pakistan (and the whole word in general) on the rise, new towns and housing schemes are popping up regularly. Poor planning before starting construction in such areas can cause severe problems later and cause significant losses to everyone involved. The problem can be averted if drones are used to conduct extensive surveys of an area to get the best idea of how the space might be managed.

1.5.4 Product Delivery

Online marketplaces are popular these days, because they provide unparalleled convenience for people when they want to shop for something. Such companies can benefit a lot from the use of drones to deliver (some, if not all types of) products to customers. This guarantees speedy and economical deliveries.

1.5.5 Agriculture

Agriculture is the backbone of our country, and we cannot afford for it to become decrepit because of the dated practices that are still going on amongst our farmers and landowners. It is high time that jobs like crop spraying and surveying land were handed over to the drones, so that the farmers do not have to do the hard work and can focus on being more efficient elsewhere in the agricultural processes.

1.5.6 Industrial Inspections

Heavy industries such as steel mills, cement plants comprise massive machinery that requires periodic inspection for possible faults and flaws. Sometimes, these inspections carry potential hazards for human beings, whether it is due to narrow spaces, heights or chemical hazards. UAVs can offer a brilliant solution because they are not affected by any of these things, nor other hazards like them.

1.5.7 Videography & Photography

Although aerial photography is mostly done on multi-rotor UAVs, they do not make for the most efficient platforms as they consume a lot of power in for flight. Videography from the air is also done by using multi-copters. However, enthusiasts and professionals can say goodbye to the inconvenience and cost of employing multi-copters for their work, because our UAV can offer efficient forward flight for videography but can also hover in mid-air for photographic opportunities.

CHAPTER 2: LITERATURE REVIEW

2.1 Propulsion System:

The term propulsion system means the power needed for the motion of aircraft for cruising or hover. The two primary categories of propulsion systems are electric and fuel-based propulsion systems. Both can be used to operate the propellers and shroud fans. Each system has its own advantages and disadvantages all used for specified UAV applications. [10]

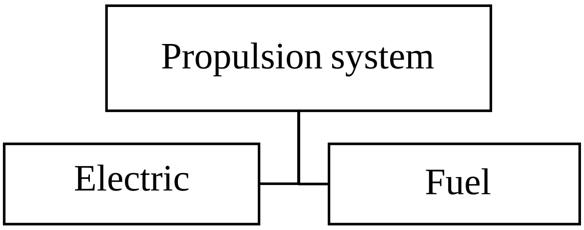

Figure 10 Types of Propulsion System [10]

2.1.1 Electric Propulsion Systems:

Electric propulsion system runs on electrical components which accumulate energy using batteries and electric motors to drive the propellers. [10]

2.1.1.1 Components:

a. Brushless Electric Motor:

Brushless motors are broadly utilized in present day UAVs. While brushed motors utilizes mechanical changes to stage the windings for engine running, brushless motors utilize Electronic Speed Controller (ESC) board for exchanging. They are better than brushed motors as they have better thrust-to-weight ratio, better efficiency, high torqueper weight and increased reliability with lower noise. They are also beneficial for effective stabilization of camera footage. [11]

b. Lithium Polymer Battery:

Lithium polymer or LiPo batteries are the most well-known kind of battery utilized in present day UAVs. They are utilized as the primary power for the drive of UAV framework and as an optional power hotspot for electronic subsystems. They have thehighest energy density among lithium-ion batteries and have the highest discharge rate [10]

which makes them the perfect candidate to be used in UAVs. Be that as it may, they can be harmed effectively or even causes fire perils if not appropriately dealt with. [12]

c. Propeller:

Propellers is utilized to create thrust in a UAV. Like a fan, propeller pivots around a fixed shaft to create a flow of air that produces thrust and the UAV pushes ahead. Thepropeller geometry is determined by its width, diameter and twist, that is the pitch of propeller. Various factors affect different parameters of the propeller, such as speed, generated thrust and mechanical efficiency. [10]

d. Electronic Speed Controller (ESC):

An electronic speed control or ESC is responsible for controlling the RPM of the electric motor. It controls speed of the motor by taking the PWM (pulse with modulation) input from the autopilot. [13]

2.1.1.2 Types of Electric Systems:

a. Single-Motor Electric Propulsion System:

The major components in a UAV electric propulsion system are batteries, brushless motors and the velocity controller. The battery is linked to the ESC, which is connectedto the motor and receiver. The receiver gets the transmission signal from the RC transmitter in the ground, and sends the signal to the speed controller, which changes the speed of the motor. Different cable gauges are used for each electric joint. Two wires, typically two thick black and red wires, make the connection from the battery to the speed controller. Three cables join the speed controller to the brushless motor. Thesecables can be linked in any order, and any two can be swapped if the motor is revolvingin the wrong direction. The speed controller connects to the receiver through a standard servo cable, which has three wires: ground, voltage and signal

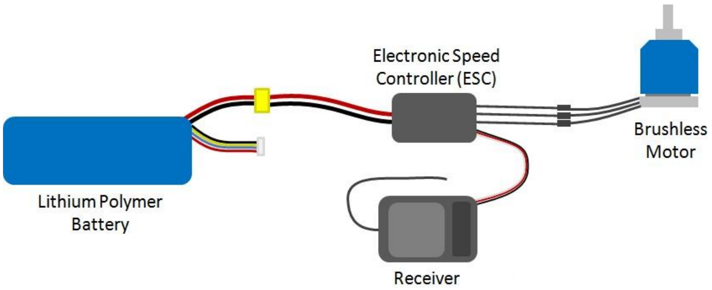

Figure 11 Single rotor Electronic propulsion system

Multi-Motor Electric Propulsion System:

Multi-motor configurations need various electric motors. The configuration is almost like the single motor system, except that a power distribution board is utilized to connectmultiple speed controllers to one battery. In multi-copter UAVs, the speed controllers are connected to a flight controller board which maintains the motor speed based on theinput from the used and stability algorithms.

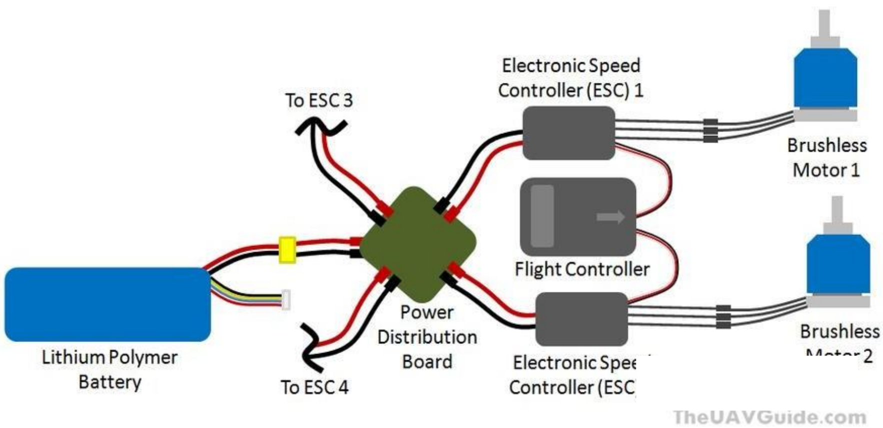

Figure 12 Multi rotor electronic propulsion system [14]

2.1.1.3 Advantages:

- Electric supported systems produce less noise than gasoline supported ones.
- The thrust in electrical systems can be precisely varied and has faster throttleresponse.
- Electric systems are more reliable due to minimum possible chances of crashdue to motor failure.
- Low serviceability, consistent performance and tough.
- Comparatively fewer heating issues and cooling requirements as IC engines.
- Great torque.
- Can be scaled.
- Lighter as compared to IC engines.
- Heat losses are minimized.
- Extremely high efficiency.
- No additional component required.
- Very simple in design and manufacturing.
- Rechargeable

2.1.1.4 Drawbacks:

The electric propulsion has significantly lower energy density per unit mass as compared to internal combustion engines, hence electric propulsion provides much less flight duration. [10]

- Fuel in the combustion engines can be added very quickly while the batteries require significantly more time to recharge.
- Electromagnetic interference can harm avionics.
- Requires high current when operated as well as low productivity due to current limits and recharge rates.

- Electric systems are vulnerable to water and other conductive fluids.
- Limited endurance.
- Heating occurs during faster charging.
- Performance can be affected from the environment

2.1.2 Fuel Propulsion System:

Gasoline propulsion have significantly higher energy density as they use fuel (such as petrol or nitro) to operate, and they use the engine power to rotate the propeller or other device. Multiple forms of engines are available such as two and four-stroke, as well as nitro or gasoline fuels. [10]

2.1.2.1 Components:

The major parts of a fuel propulsion system for a UAV are the

- Engine
- fuel storage (fuel tank)
- Throttle control linkage (throttle servo)

Multiple fuel tanks can be connected to the engine for the provision of the fuel. The throttle servo receives the signal from the radio receiver and changes the throttle valve position of the engine, a battery is required to power the receiver and to control the RPM. The servo gets the power from the receiver through the signal cable.

2.1.2.2 Working:

The power from an internal combustion engine is produced from the burning of the airfuel mixture inside the engine. The combustion which occurs inside the engine produces the desired

RPM that drives the UAV. The popular type of engines are 4-stroke & 2- stroke, while the fuel types which are used are nitro and gasoline.

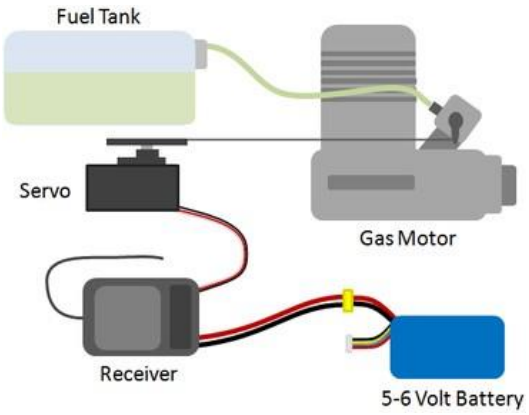

Figure 13 Fuel propulsion system [14]

2.1.2.3 Advantages:

- They provide much higher flight times.
- They can be refilled very quickly.
- Combustion engines are used in airplane UAVs that require longer flighttimes.
- Diesel engines uses low volatility heavy fuels.
- Supports fuel pumping at high altitudes. [10]

2.1.2.4 Drawbacks:

- Comparatively, fuel systems are more complex to setup, use and maintain thanelectric propulsion.
- They produce more noise, are less dependable and cannot be controlled asaccurately as electric propulsion.
- Moving parts are more.
- Need sealing and lubricants to function.
- Require cooling.
- Heat production reduces efficiency.

- Higher complexity.
- Heavier.
- Restart becomes an issue [10]

2.2 Control System:

2.2.1 Fixed Wing Movement Control

Fixed are usually controlled by the movement of their control surfaces. Control surfacesare defined as the surfaces which are moveable and are usually on the plane's tail and wings, which create a difference of air pressure to produce positive and negative lift tomaneuver the plane. The movement of the control surfaces of a plane is usually controlled by servos (for small and unmanned planes) and hydraulic/pneumatic actuators on large, commercial aircraft. [10]

The function of each control surface is as follows:

Yaw: The yaw movement is the directional change of a plane's trajectory. The yaw movement is usually controlled by the rudder.

Pitch: The pitch movement is the change in direction in the longitudinal axis. The pitch movement is usually controlled by the elevator.

Roll: The roll movement of the plane is the change in the direction in lateral axis. Theroll movement is usually controlled by ailerons.

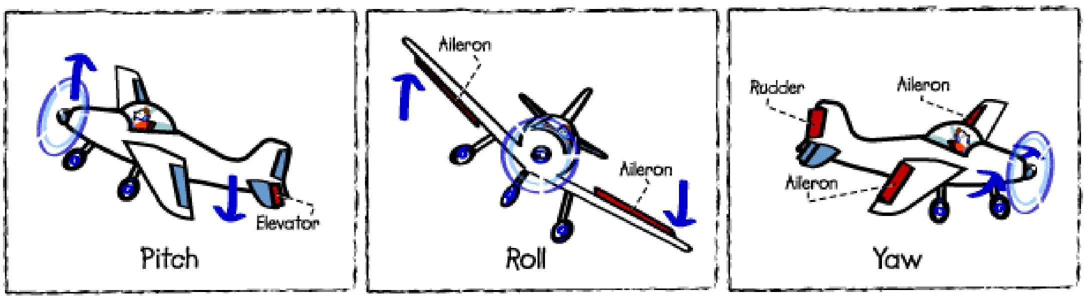

Figure 14 Control surfaces and their movements [15]

Servos will be used to actuate the control surfaces by means of a ball link and push rod.

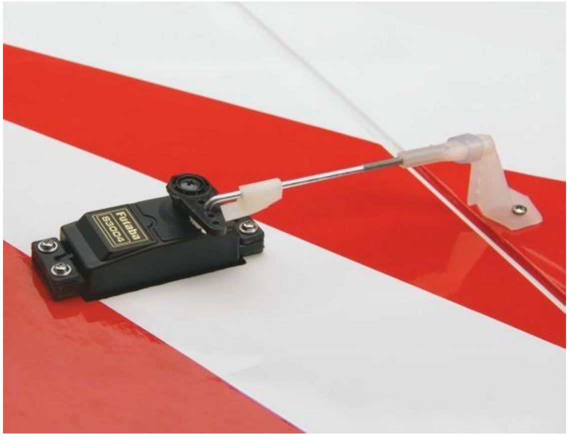

Figure 15 Servo connected to the surface through control rod [16]

2.2.2 Multi-Rotor Movement Mechanism

Multi Rotor are generally divided into two types:

- Tri-Copter
- Quadcopter

However, quad copters are used more than tri copters today, as they offer -mechanical simplicity.

2.2.2.1 Quad-Copter Movement Control:

The Quadcopter, as the name suggests, has four motors. The diagonal motors are running in the same directions will the adjacent motors are running in the opposite direction. The pitch and roll movement is actuated by varying the speed of the desiredmotors (front or back motors for pitch, left or right side motors for roll), which varies the lift generated by the propeller and the direction of the quad-copter changes.

The yaw control is achieved by augmenting the motor speed of the diagonal motors, which causes a torque inequality, hence the quad-copter yaws opposite to the directionof the uneven torque.

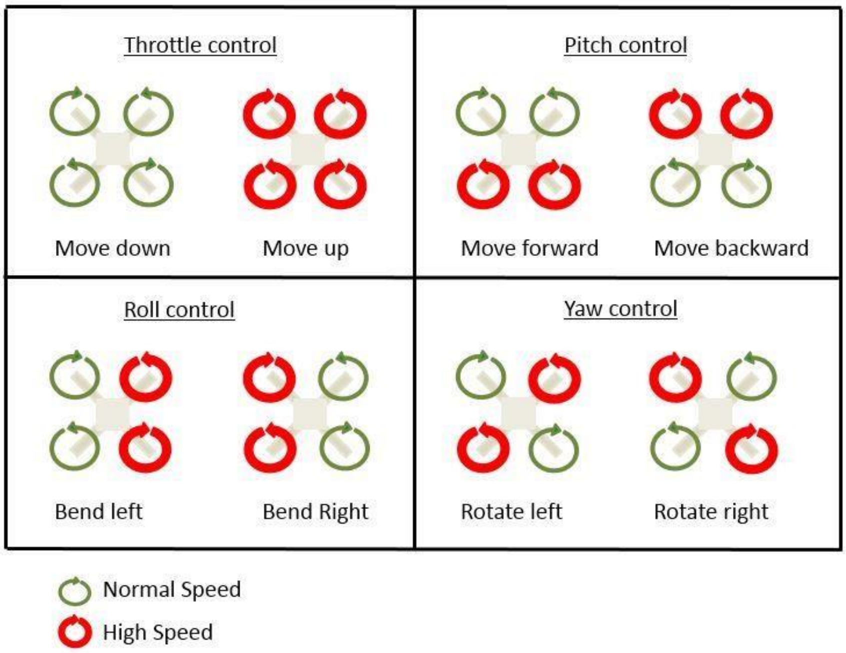

Figure 16 Quad copter movement description [17]

2.2.2.2 Tri-copter Movement Control:

Tri-Copter contains three motors, the front two motors are rotating in opposite directions, while the back motor can be run in any direction (clockwise/counterclockwise). The tri-copter is naturally unstable in the yaw direction, as in any configuration possible, the two motors will be running in the same direction, while theother motor will be running in the opposite direction, thus there will be a torque imbalance.

To counter this effect, the tail motor of the tri-copter uses thrust vectoring to control and stabilize the yaw direction by means of rotating the motor by a servo.

The pitch is controlled by augmenting the RPM of the front two motors or by increasingthe speed of the tail motor.

Roll is varied by lessening the speed of the front right or left motor, and the tail motors is thrust vectored accordingly.

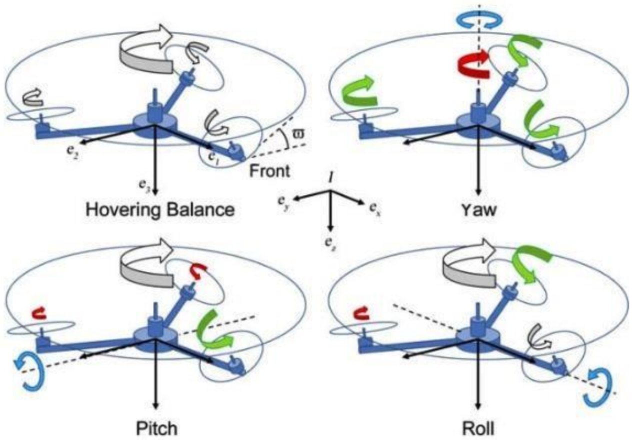

Figure 17 Tricopter movement description [18]

2.2.3 Autonomous operations

The autonomous operation of any aircraft involves input from a variety of sensors to a microcontroller, which gives output to the motor/servos to control the movement of theaircraft.

2.2.3.1 Fixed wing sensors:

The following sensors are usually required for the autonomous operations of an airplane: [19]

1. Accelerometer: measures the acceleration of the airplane, which assists the microcontroller to predict the plane's trajectory.
2. Gyroscope: senses the angular velocity/position on pitch and roll axis. Insimpler words, it tells whether the plane is level or not.
3. Compass: To tell the heading of the plane when it's in flight.
4. Barometer: senses the altitude of an airplane by sensing the difference in pressure as altitude increases/decreases.
5. Laser Altimeter: measures the distance between the plane and the ground duringthe landing approach with centimeter level accuracy, which is required as barometer data fluctuates when it's near to the ground due to turbulence.
6. GPS module: Senses the actual position of the plane by calculating latitude/longitude.

7. Airspeed Sensor: Measures the airspeed, which is a crucial component of the flight dynamics of a fixed wing.

2.2.3.2 Output:

The microcontroller after getting the input from the sensors, gives the output to the following components:

1. Electronic speed controller: it varies the speed/rpm of the motor, which increases or decreases the thrust/lift produced by the motor. By varying the RPM of the motor, airspeed, rate of climb and altitude is controlled.
2. Servos: Servos move the control surfaces of the aircraft which allows it to maneuver in different directions and stay level.

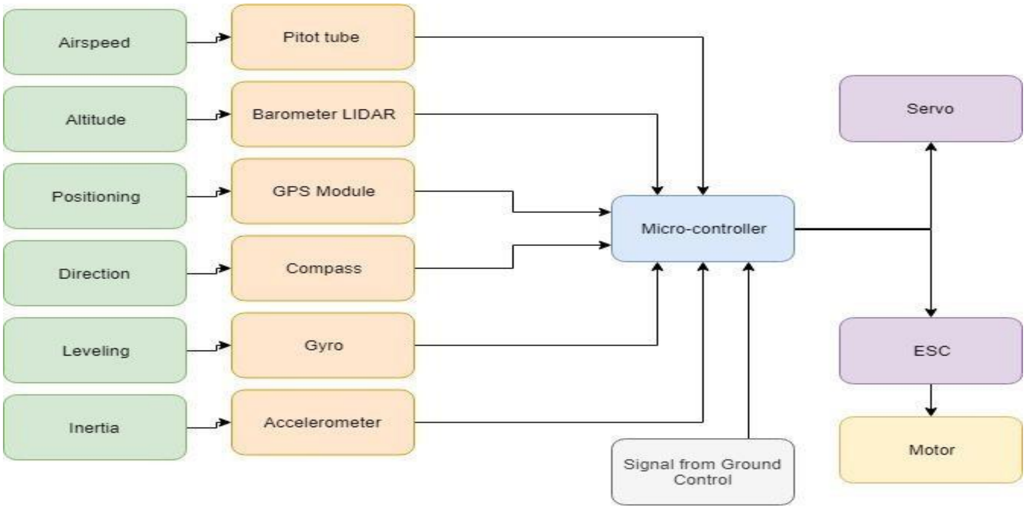

Figure 18 Sensor Feedback of fixed wing

2.2.3.3 Multi Rotor Sensors:

A Multi Rotor requires less sensor to operate as compared to the fixed wing. The following are the sensors are essential to the autonomous operations of a multi rotor: [19]

1. Accelerometer: measures the acceleration of the multi rotor, which assists the microcontroller to predict the multi rotor behavior and adjusts the motor speedaccordingly

2. Gyroscope: senses the angular velocity/position on pitch and roll axis. Insimpler words, it tells whether the multi-rotor is level or not
3. Compass: To tell the heading of the multi-rotor when it’s in flight.
4. Barometer: senses the altitude of a quadcopter by sensing the difference in pressure as altitude increases/decreases.
5. GPS module: Senses the actual position of the plane by calculating latitude/longitude, which allows the multi-rotor to stay locked in the air.

2.2.3.4 Output:

After the input, the output is given to the speed controllers (and servos for a tri- copter), which are responsible for controlling the thrust of the motors, which controlthe direction/movement around the waypoints for autonomous operations.

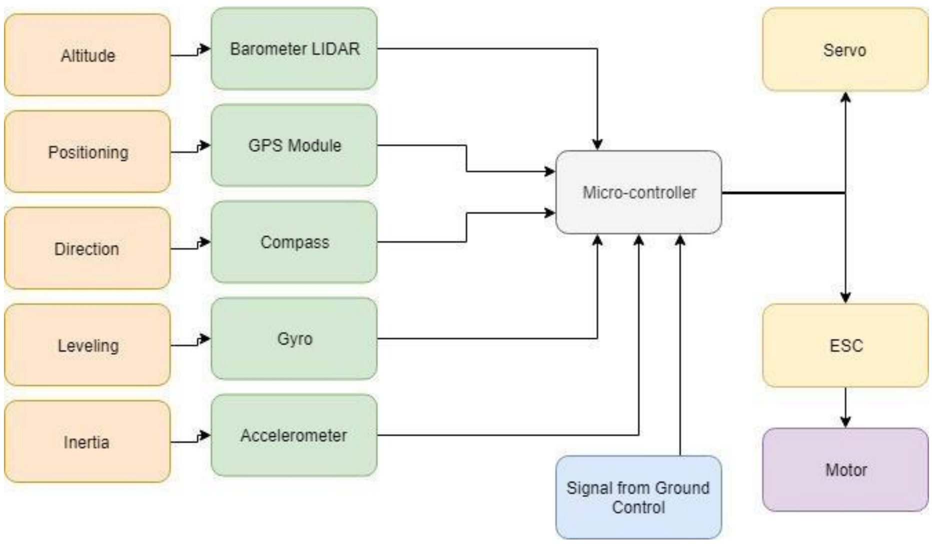

Figure 19 Sensor Feedback of multi wing

2.2.4 The VTOL Fixed Wing

Working of a VTOL Fixed aircraft is divided into the following phases:

1. First during vertical take-off the whole system works like a multi-rotor, all the movements are controlled by varying the motor speeds and the control surface are disabled. The UAV keeps ascending in multi-rotor mode until safe altitude is reached.
2. The four vertical motors are slowed down while the horizontal motor is run with increased thrustto induce forward motion. As the UAV gains airspeed, the wings start producing lift.
3. When airspeed data shows that sufficient airspeed has been reached, such that the UAV does not drop its altitude, the control surface are used for maneuvering and the vertical motors are completely turned off. The UAV will behave like a fixed wing.

2.2.4.1 Flight Controller:

The initially selected flight controller for a fully autonomous guided flight is a 32bit ARM based Pixhawk 2 Cube. Featuring dedicated chips for failsafe ops, it gets 14PWMouts (8 with manual failsafe & override feature) for servos, 6 auxiliaries, and abundantconnectivity options for peripherals like GPS, Pitot tubes, rangefinders, alert alarms (LEDs or Buzzers) on 5 UART serial ports. Further internal sensors include 2 compasses, a barometer, and a gyroscope that provide us with essential navigational parameters for autonomous flight. Allows receiver interfacing on SBUS mode and hasa dedicated SD card slot for inflight data-logging of system for flight analysis. It utilizespower from 3 separate units so a triple redundancy in system in case of power shutdownautopilot never fails, and all outputs are over-current protected.

2.3 Lift Line Theorem:

A use mathematical model to determine the lift of an airfoil over a 3-dimensional geometry of the wing. The theorem applies numerical methods over the sections of wing along its span to check the coefficient of lift at each interval. In this model, the vortex loses strength along the entire wingspan since it is shed as a vortex-sheet from the trailing edge, as opposed to exactly at the wingtips. [20]

The lift line equation is solved at each interval

$$\mu(\alpha_o - \alpha) = \sum_{n=1}^{N} A_n \sin(n\theta)(1 + \mu\frac{n}{\sin(\theta)})$$

The equation initially developed by Prandtl. In this equation, N symbolizes number of segments; α segment's angle of attack; α_o segment's zero-lift angle of attack; and coefficients are the intermediary unknowns. The parameter μ is given as follows:

$$\mu = \frac{(\bar{C_i} * C_{l_\alpha})}{4b}$$

Where μ represents the segments' mean geometric chord, $Cl\alpha$ denotes segment's lift curve slope in 1/rad; and "b" is the wingspan. If the wing has a twist (αt), the twist angle should be applied to all segments linearly. Thus, the angle of attack for each segment is reduced by reducing the corresponding twist angle from wing setting angle.If the theory is applied to a wing in a take-off operation, at flap deflection location, theinboard sections have greater zero-lift angle of attack (αo) than outboard sections. Liftcoefficient is calculated by:

$$C_{L_i} = \frac{4b}{\overline{C_l}} \sum \mathrm{A_n} \sin(n\theta)$$

2.4 Important Terminologies:

Before we proceed to the discussion of UAV's design aspect, following terminologiesare important to be known for better understanding of working and designing of UAVs:

2.4.1 Lift

An aerodynamic force exerted by the fluid on a mechanical body opposite to the direction of gravity when it passes over it. [21]

2.4.2 Drag

It is the aerodynamic resistive force acts opposite to the direction of motion on a mechanical body when it passes through a fluid. [21]

2.4.2.1 Types of Drag

2.4.2.1.1 Induced drag

It is the lift dependent drag which is proportional to the amount of lift generated by the aircraft.

2.4.2.1.2 Parasitic Drag

The drag due to the motion of a mechanical object through a fluid, proportional to the relative speed between object and fluid. It is composing of three subtypes:

A. **Form drag:** It depends upon the shape of the object. Higher the frontal surfacearea greater would be the drag.
B. **Interference drag:** It is due to the mixing of two different streamline flows in between the body.
C. **Friction drag:** It generates due to the contact between the moving fluid and the body. Higher the fluid viscosity greater would be a drag. [21]

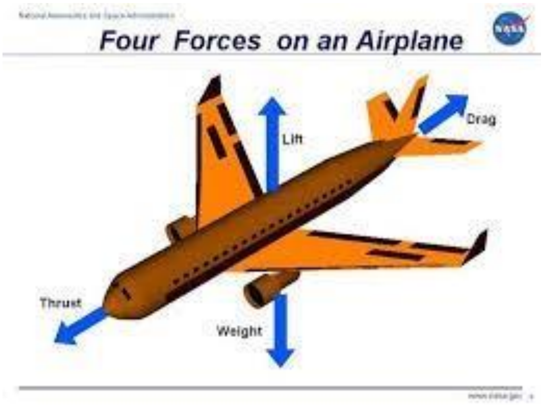

Figure 20 Principle of Aerodynamics [22]

2.4.3 Angle of attack (AOA)

Angle formed between mean line of the mechanical body and relative air flow. [20]

2.4.4 Coefficient of lift (C_L)

A dimensionless constant that relates the lift of the body. It is dependent on the shape,AOA and flow conditions of fluid. [20]

2.4.5 Coefficient of drag (C_d)

A dimensionless constant that relates the drag of the body. It is dependent on the shape,AOA and flow conditions of fluid. [20]

2.4.6 Coefficient of moment (C_m)

A moment generated due to the lift force on an aircraft also known as pitching moment.This moment is depending on the angle of attack of an airfoil. [20]

2.4.7 Center of Pressure

A point on an aircraft where net pressure field act on a body also known as a neutralpoint where lift acts. [20]

2.4.8 Aerodynamic Center

A hypothetical reference point on a wing where pitching moment acting on a wingdoesn't vary with the variation in angle of attack and coefficient of lift. [20]

2.4.9 Lift to drag ratio

It is the ratio of lift generated to the drag produced, used to determine the efficiency ofan aircraft. Can be determine by taking the ratio of C_L and C_d. [20]

2.4.10 Reynolds Number (Re)

A Quantity used to measure the pattern of fluid in nature, it is dimensionless quantitywhich is the ratio of inertial and viscous element of forces. [20]

2.4.11 Mach Number

It is a dimensionless quantity which is used for the comparison of fluid flow velocitythrough the body to the speed of sound in air. [20]

2.4.12 Stall

It is an aerodynamic phenomenon where lift starts to decrease when the angle of attackupsurges beyond a certain point. [20]

2.4.13 Stall speed

The lowest speed aircraft should have to create desire amount of lift for maintainingflight level. [20]

2.4.14 Thrust

Force induced in aircraft to move it through air. [20]

2.4.15 Thrust to weight ratio

It is a dimensionless ratio of thrust and weight of an aircraft which is used to measurethe performance of aircraft versus its engine power. [20]

2.4.16 Pitch

It is the change in direction of aircraft around lateral axis cause the nose up or downward motion [20]

2.4.17 Roll

It is the change in direction of aircraft around longitudinal axis cause the nose to rotateor wings to bank. [20]

2.4.18 Yaw

It is the change in direction of aircraft around vertical axis let the nose left or rightmotion. [20]

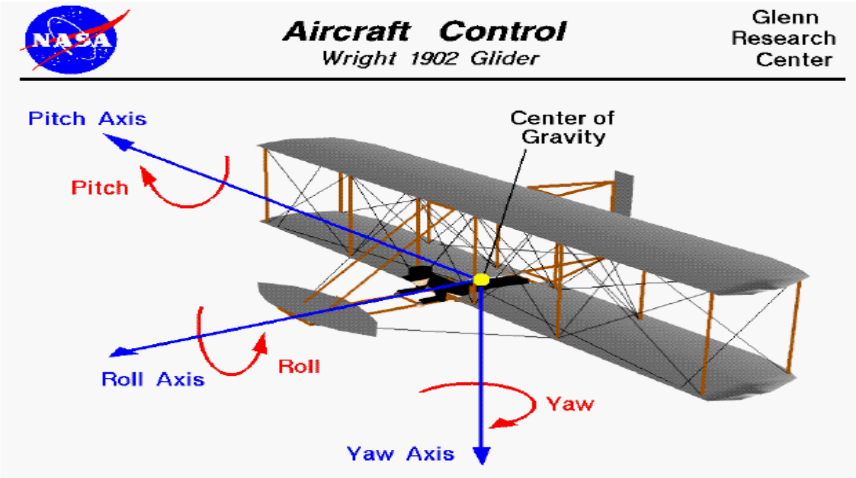

Figure 21. Aircraft control

2.4.19 Wingspan

Straight distance from left wing tip to the right-wing tip of an aircraft. [20]

2.4.20 Wing Chord

A line parallel to wing cross section center from leading to the trailing edge. [20]

2.4.21 Wing Incidence Angle

The wing incidence angle is the angle existing between the center line of fuselage and the wind chord line at its root as shown in the figure below. It is also known as wing setting angle. [10]

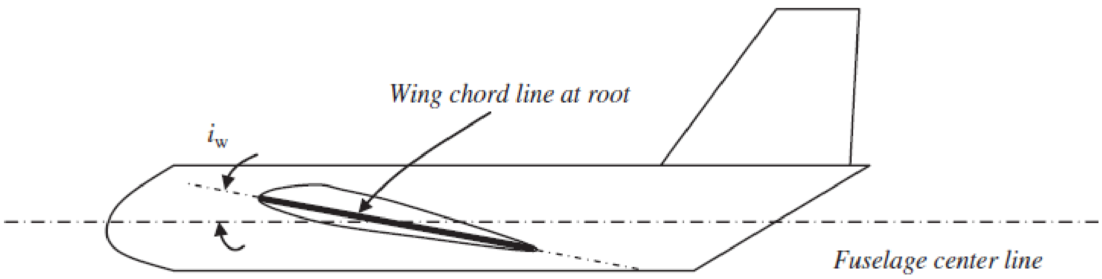

Figure 22 Wing Incidence Angle [10]

2.4.22 Wing Sweep Angle

The angle between the wing leading edge and the y-axis of the aircraft is called the leading-edge sweep. [20]

2.4.23 Aspect Ratio

The ratio between wingspan to the mean chord line. It can also be found out by thesquaring the wingspan and dividing by its area. [20]

2.4.24 Taper ratio

A dimensionless quantity measure by the ratio of root and tip chord for a half wing. [20]

2.4.25 Dihedral

It is the upward inclination of a wing from parallel mounting plane. [20]

2.4.26 Anhedral

It is the downward inclination of a wing from parallel mounting plane. [20]

2.4.27 Airfoil

An airfoil is the cross-sectional shape of the wing which when passes through the fluidproduces aerodynamic forces utilized for lift or drag. [20]

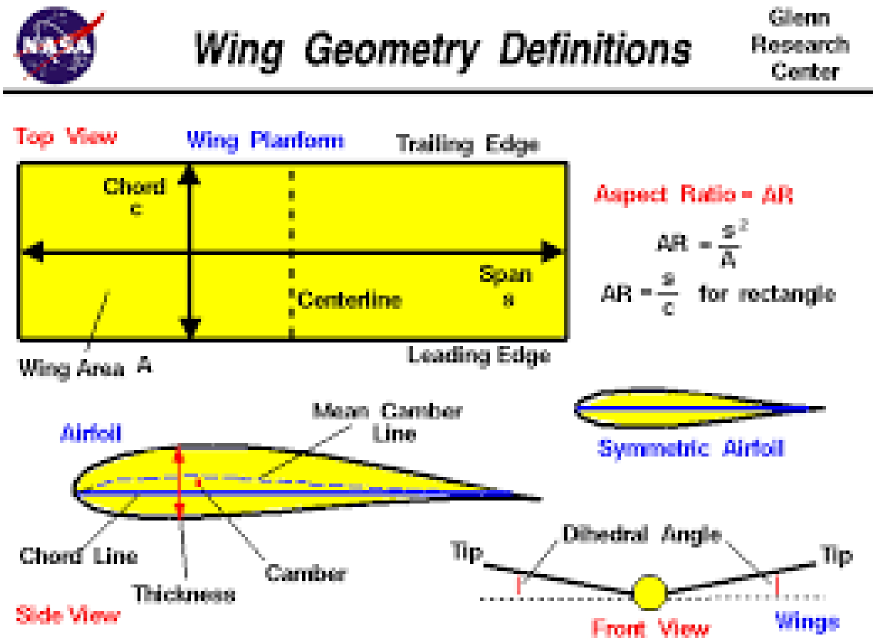

Figure 23 Wing geometry [23]

2.4.28 Mean Camber Line

Mean chamber line is a curve obtained by cutting upper and lower surfaces between thehalfway of an airfoil from its leading to trailing edge. [20]

2.4.29 Bank Angle

Angle to which wing rolls with respect to its angle of attack. [20]

2.4.30 Turn load factor

A dimensionless quantity used to determine the force exerted on the aircraft duringbanking, measure in gravitational acceleration. [20]

2.4.31 Wing loading

The ratio of the total aircraft weight to its wing area is wing loading. [10]

2.4.32 Power loading

It is the measuring performance parameter for an aircraft which is the ratio of totalweight of the aircraft to the power generated by its engine. [10]

2.4.33 Static stability

On a disturbance, the capability of an aircraft to come back to its original position isstatic stability. There are three types of static stability:

- **Positive:** On a disturbance, the aircraft tends to regain its original position.
- **Neutral:** On a disturbance, the aircraft remains in its newly obtained position.
- **Negative:** On a disturbance, the aircraft continues to go surge from its original position. [24]

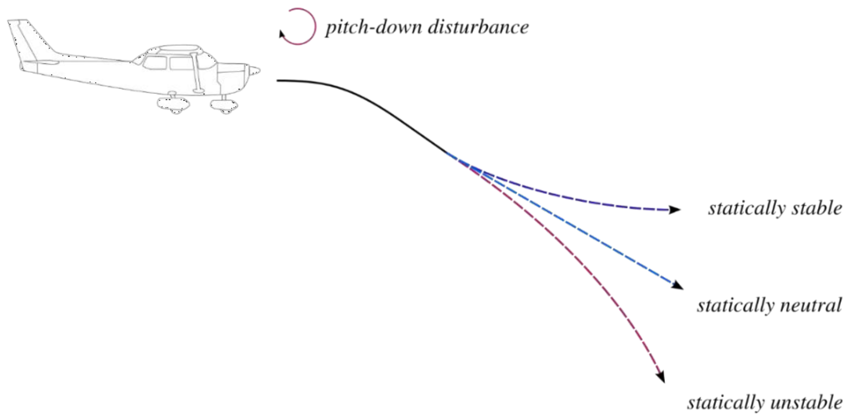

Figure 24 Static Stability [24]

2.4.34 Dynamic Stability

Dynamic stability takes place when, on a disturbance, the response of the aircraftinduces with respect to some time. There are three kinds of dynamic stability.

- **Positive:** In it, oscillation generated due to disturbance gets damped out withtime.
- **Neutral:** Oscillation generated due to disturbance never dampens out.
- **Negative:** Oscillation generated due to a disturbance increases with time. [24]

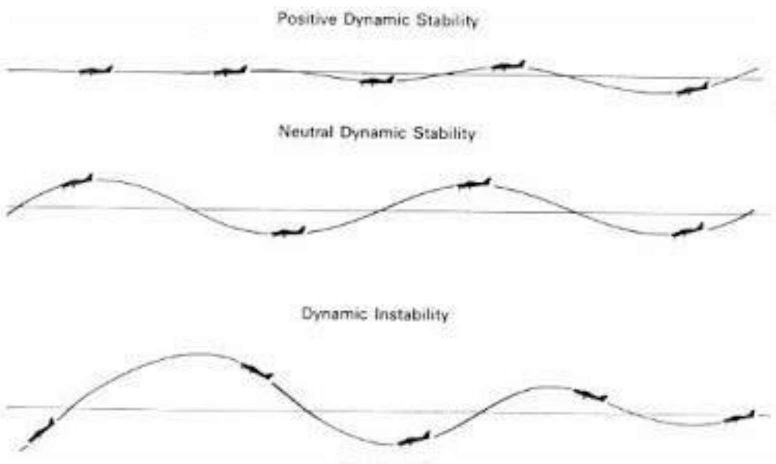

Figure 25 Dynamic Stability [24]

2.4.35 Gyroscope

A device used for stability and to maintain navigation system reference direction. [19]

2.4.36 Accelerometer

A device used to measure the acceleration in instantaneous rest frame of a body. [19]

2.4.37 Barometric altimeter

A device for measuring air pressure which is calibrated as per atmospheric condition used to measure the altitude of an aircraft. [19]

2.4.38 Remote Sensing

A phenomenon of accusation of data regarding particular thing without any direct contact with the object. Usually adopt by aircraft and high-tech satellites. [19]

2.4.39 LIDAR

LIDAR stands for Light detection and ranging, which is a remote sensing sensor used to measure the distance by using pulse laser and its reflection. [19]

2.4.40 PID Loop

Proportional–integral–derivative controller uses all three operations together to give a controlled mechanism of loop feedback. A system which required continuous monitoring and controlled use PID for its purpose. [19]

2.4.41 Pitot Tube

It is a fluid dynamic sensor which is used for measuring the velocity of fluid flow by measuring static and dynamic pressure of the fluid passing over it. [19]

2.4.42 Global Positioning System (GPS)

Global positioning system, a satellite navigation system, which uses radio signal to determine the position and velocity of an object anytime and anywhere in the world. [19]

2.4.43 Inertia Measurement Unit

An inertial measurement unit (IMU) is an electronic device. This device determines and reports a body's specific force, angular rate, and sometimes the magnetic field surrounding the body. This is done by using a combination of accelerometers and gyroscopes, sometimes also magnetometers. [19]

2.4.44 Attitude and Heading Reference System (AHRS)

An Attitude and Heading Reference System (AHRS) is an inertial sensor installation. This device provides critical attitude reference along with the heading referenceinformation of the aircraft. [19]

2.4.45 Flight Controller

A microcontroller built to control flight using integrated sensors. It receives commandsand controls the different systems. [19]

2.4.46 Tele Command

A phenomenon of controlling and operating things from far location. Usually, internet is being used to communicate. [19]

2.4.47 Telemetry

A communication process in which data and measurements collected in the remote area is transfer automatically to the monitoring system. [19]

2.4.48 Ground Control Station

A control center from where unmanned aerial vehicles are monitored and controlled. [19]

2.4.49 Radio Frequency

A range of frequency suitable for telecommunication. Usually in the range of 10^4 to 10^{12} Hz. [19]

CHAPTER 3: CONCEPTUAL DESIGN

This design phase is closely related to the design requirements and concepts itself than calculations and derivations. Firstly, the requirements of the drone are identified and then based on these requirements, the configuration of different aircraft systems is selected such as wing, tail, and engine etc. A very detailed design flowchart is show in **Figure 26.**

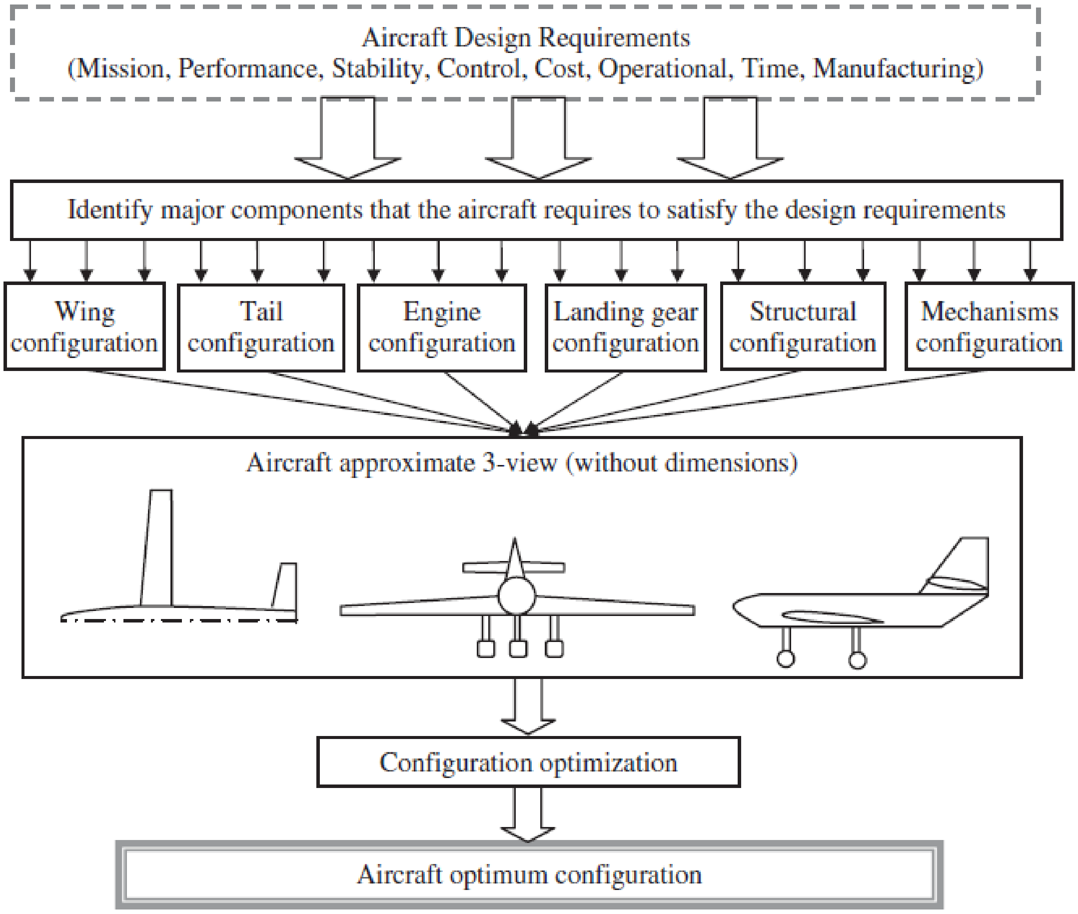

Figure 26 Aircraft Conceptual Design [10]

3.1 UAV Configuration

The review of literature leads us to the comparison of different types of Drones/UAVs which gives us below mentioned table:

Table 2 Comparison of UAV Configurations

Type	Pros	Cons
Fixed Wing	• greater endurance • greater speed • higher stability	• requires runway • more expensive • low maneuverability
Multi-copter	• good maneuverability • less expensive • compact	• less payload • lower endurance • prone to cross winds
Hybrid VTOL	• greater endurance • greater speed • higher stability • No runway required	• Expensive technology • Complex

After reviewing the feasibility and advantages of each type, Hybrid VTOL configuration was eventually decided for the design of the UAV, as it combined the benefits of both Fixed Wings and Multi-copters and gave the optimum desired results for our application.

3.2 Propulsion System Configuration

The review of literature leads us to the comparison of different types of propulsion systems which gives us below mentioned table:

Table 3 Comparison of UAV Propulsion Systems

Criteria	**Weightage**	**Electric Propulsion**		**Engine Propulsion**	
		Rating	Weighted Rating	Rating	Weighted Rating
Cost	10	5	0.5	4	0.4
Availability	20	3	0.6	4	0.8
Ease of Operation	20	4	0.8	3	0.6
Light Weight	20	5	1	3	0.6
Reliability	20	4	0.8	3	0.6
Operational Cost	10	4	0.4	2	0.2
Total	**100**		**4.1**		**3.2**

After reviewing the feasibility and advantages of the system, and after putting all the values through a weighted rated matrix, electric propulsion system was eventually decided for the design of the UAV, as it gave the optimum desired results and was found to be more efficient than the engine propulsion.

3.3 Hybrid VTOL Drone Configuration

After selecting Hybrid Vertical Take Off and Landing. Literature was reviewed to study various configurations of VTOL Drones. Some notable configurations are compared in table below:

Table 4 Comparison of major Hybrid VTOL UAV types [25], [26], [27]

		Tilt Rotor		Tilt Wing		Dual System		Tail Sitter	
Criteria	**Weightage**	**Rating**	**W. Rating**	**Rating**	**W. Rating**	**Rating**	**W. Rating**	**Rating**	**W. Rating**
Flight Efficiency	10%	3	0.3	3	0.3	3	0.3	3.5	0.35
Ease of Manufacturing	5%	3.5	0.18	2	0.1	3	0.15	4	0.2
Complexity of the design	25%	2.5	0.63	3	0.75	5	1.25	1	0.25
Cost	20%	3.5	0.7	2	0.4	4	0.8	2	0.4
Aerodynamics	5%	3.75	0.19	3.6	0.18	3	0.15	3	0.15
Stability/Controllability	15%	4.25	0.64	3.5	0.53	3.75	0.56	3	0.45
Vertical Flight Performance	10%	5	0.5	4	0.4	3	0.3	1	0.1
Horizontal Flight Performance	10%	4	0.4	3	0.3	2	0.2	4.5	0.45
TOTAL	**100%**		**3.53**		**2.96**		**3.71**		**2.35**

After reviewing the feasibility and advantages of all systems, and after putting all the values through a weighted rated matrix, Tilt Rotor and Dual System configurations were eventually shortlisted for the design of the UAV.

After shortlisting Tilt Rotor and Dual System configurations. Literature was reviewed to study various sub-configurations of these systems. Some notable configurations are compared in table below:

Table 5 Comparison of sub-configurations of VTOL UAVs [25], [26], [27], [28]

	Bi-rotor	**Tri-rotor (front 2 tilting & rear tilt for yaw)**	**Quad-rotor (front two motors tilting)**	**Quad-Rotor w/ Pusher/Puller**
Requirements Criteria / Constraint	**Rating**	**Rating**	**Rating**	**Rating**
Flight Performance Efficiency	3.5	3.5	3.35	2.75
Ease of Manufacturing	3	3.25	3.25	3.25
Complexity of the design	3	2.5	3.5	4.5
Cost	4	3.75	3	2.5
Aerodynamics	4	3.6	3	3
Stability/Controllability	2	3	3.75	4
Vertical Flight Performance	2	3	3.5	3.5
Horizontal Flight Performance	4	3	3.5	3
TOTAL	**25.5**	**25.6**	**26.85**	**26.5**

After reviewing the feasibility and advantages of all systems, and after putting all the values through a weighted rated matrix, Quad Rotor with Pusher configuration was eventually shortlisted for the design of the UAV.

CHAPTER 4: PRELIMINARY DESIGN

During the preliminary design phase, we estimate some of the most important parameters required for a VTOL drone and particularly for when it is in cruise. After completing this stage of design phase, we will be able to successfully estimate maximum take-off weight (MTOW), wing area and motor thrust required.

4.1 Estimation of MTOW

MTOW is estimated by considering the weight of five major components of the drone which includes weight of payload, avionics and electronics, battery, miscellaneous components and airframe. Weight of some components are calculated by defining the performance parameters of the drone such as cruising speed and target flight time. Defining these two will help us in calculation of the weight of the battery. Similarly, as we fix more parameters for the drone as per requirement, we will be able to estimate the weight and dimensions of more components in the aircraft.

4.2 Weight Estimation of Payload:

The weight of the payload can be determined by specifying the type of mission the drone will carry out. Since we are using our drone for purposes such as agriculture, rescue and reconnaissance, the payload will be limited to the usage of surveillance camera, small package of 1-1.5 kg and designated volume of pesticide. For reference, typical payloads are shown in **Table 6.**

Table 6 Typical Payloads for a UAV [29]

S.No	Payload Type	Type/Brand	Weight
1	Optical Camera	TL300MN FPV	15g
2	Optical Camera	DJI Zenmuse X5	530g
3	Video Camera	CC-IXHRM	0.29 kg
4	Radar	Garmin GSX 70	4.31 kg
5	Radar	Lincoln Lab	175 lb
6	Decoy	ALE-50	4.5 kg
7	ECM system	IDECM	73.4 kg
8	Radar warning receiver	AN/ALR-67	45 kg
9	Laser Range Finder	XP SSXP	2.5 kg
10	Laser Range Finder	BOD 63M-LA01-S115	0.26 kg

4.2.1 Weight Estimation of Avionics and Electronics

For successfully working of a drone, range of electronics are used onboard. Their weight can be estimated by defining some requirements and from the data sheet of that specific component. A detailed break-down of the quantity and their weights are given in **Table 7.**

Table 7 Weight of the Electronics

S No.	Part Name	Manufacturer or Company	Quantity	Weight per Part
1	BLDC Motor	T- Motor AM Series	4	300-350g
2	Electronic Speed Controller	Hornet 80A ESC	4	40-50g
3	Flight Controller	Pixhawk 4	1	35-40g
4	GPS	Pixhawk	1	350-400g
5	Servos for Control Surface	SG-90 Servo Motor	5	10-15g
7	Wires	-	-	5% of MTOW

4.2.2 Weight Estimation of Airframe

At the preliminary design phase, the design of airframe is usually not available so we can take approximate the weight of airframe by taking it be 40% of MTOW [30] as the weight of our airframe. To be on the safe side, we have taken a **factory of safety of 1.5** and the real estimated airframe weight fraction had been taken to be **60%.** This approximation will be replaced by more accurate value in later iterations when a CAD model is developed from the first iteration of the design.

4.2.3 Weight Estimation of Battery

The weight of the battery is calculated by defining the required flight time and performance of the drone. By using the parameters calculated during parametric analysis, the weight of the battery can be calculated by the overall energy consumption in different flight modes such as cruising, vertical take-off, loiter and descend. Knowing the speeds, range, time needed for each maneuver, we can calculate the total energy required for the drone and with the knowledge of battery density, the weight of the battery can be calculated. A MATLAB script had been created for the calculation of the battery weight and is listed in **APPENDIX I: Power Required and Battery Weight Calculation**. From the final calculations, the battery weight comes out to be **824g .**

4.2.4 Final Estimate of MTOW

Once we have an approximate value of the different components of the aircraft, we can easily calculate the MTOW of the aircraft. Some of the components, that were suitable for our requirements, were weighed physically on a weight balance. Finally, the overall weight of each component is shown in **Table 8**.

Table 8 Estimation of MTOW

Part Name	Manufacturer	Quantity	Weight Per Part	Total Weight
5000mAh LIPO Battery	Turnigy	1	824g	824g
BLDC Motor	Chinese	4	300g	1200g
80A ESC	Hornet	4	50g	200g
12x4 in Propellers	-	4	20g	80g
Flight Controller	Pixhawk	1	38g	38g
GPS and Miscellaneous	Pixhawk	1	350g	350g
SG-90 Servo Motors	SG	5	10g	50g
JR Servo DSB425	JR	2	60g	120g
Landing Gear	-	1	300g	300g
Wires/Cables	-	-	5% of MTOW	-
Airframe	-	1	60% of MTOW	-
Total				**11.892 kg**

4.3 Matching Plot and Estimation of W/S and P/S

Once maximum take-off weight had been defined, the next step was to calculate the required wing loading (W/S) and power loading (W/P) of the drone. This was achieved by specifying the capabilities of our aircraft such as stall speed, maximum speed, rate of climb, maximum ceiling, and absolute ceiling etc. Based on these parameters, a dimensionless graph of power loading vs wing loading is plotted to determine the design and operating point of the drone [10]. This is accomplished by expressing the mentioned parameters in terms of power and wing loading. A MATLAB user interface and program was constructed for easer revision of design parameters, design point and matching plot. The script is listed in **APPENDIX I: Matching Plot**

4.3.1 Wing Loading as a Function of Stall Speed

Stall speed is the minimum speed required by a fixed-wing airplane to be airborne. Stall speed is an important parameter and is different for different types of missions. According to mission requirements, the stall speed can change drastically but it is also dependent on the size of the aircraft [10].

According to the lift equation during cruise,

$$L = W = \frac{1}{2}\rho_{alt}\, V_s^2 S_w Cl_{max_{w,2-D}}$$

This equation provides us with the first graph for the estimation of W/S and W/P.

$$\left(\frac{W}{S_w}\right)_{Stall} = \frac{1}{2}\rho_{alt} V_s^2 Cl_{max_{w,2-D}}$$

If we rearrange **Equation** Error! Reference source not found.**,** we see that the wing loading is i ndependent of power loading, and hence it will be a straight vertical line in our matching plot.

Initially, the stall speed had been taken as **10.5 m/s** from the comparison and statistics of similar drones [10]. $Cl_{max_{w,2-D}}$ is a quantity that dependent on the geometry of the airfoil. A value of **1.8** had been taken for $Cl_{max_{w,2-D}}$ from the selection of the airfoil of the wing which can be seen in **Section 5.1.3 Airfoil Selection** and density of air had been taken as **1.15 kg/m^3** which is nearly the same as the value of sea level i.e 1.225 kg/m^3 because the cruising height of our drone is very low and hence its effect is not as significant.

The contribution of stall speed in the matching plot is shown in **Figure 27**.

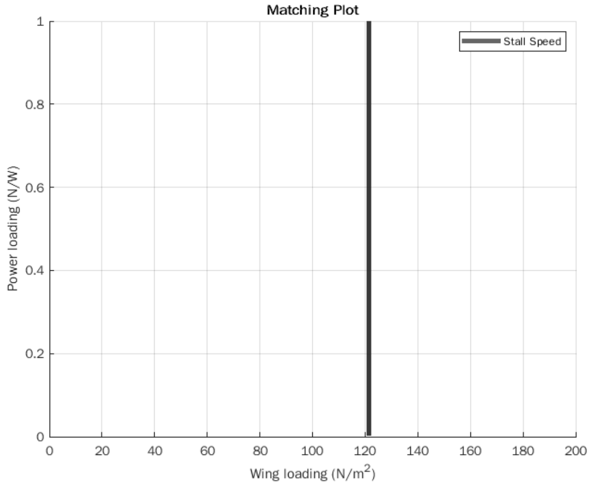

Figure 27 Contribution of Stall Speed in Matching Plot

4.3.2 Power Loading as a Function of Stall Speed

Another important parameter for the drone is its maximum speed which is usually approximated to be 1.3 times of the cruise speed [10]. From the comparison of the drones, the cruising speed of most drones lie in the range of 17-20 m/s [10] and hence we have taken our cruising speed to be **17 m/s.**

Considering our aircraft to be flying with maximum constant speed and at the cruising altitude, we can relate the maximum motor power to be equal to required power which is thrust times velocity.

$$P_{req} = TV_{Max}$$

There is also difference between the requirement of engine power at sea level and at some altitude because of the differences in the density of the air and so we can relate these two powers by relative density as

$$P_{alt} = P_{SL}\sigma_c$$

By manipulating lift equation and equation of drag polar [10], the final expression for the power loading as a function of maximum is:

$$\left(\frac{W}{P}\right)_{Max} = \frac{\sigma_c(\eta_p)_{Max}}{\frac{1}{2}\rho_{alt}V_{max}^3 C_{D_o}\frac{1}{\left(\frac{W}{S}\right)_{Max}} + \frac{2K}{\rho_{alt}\sigma_c V_{max}}\left(\frac{W}{S}\right)_{Max}}$$

The contribution of Maximum speed in the matching plot has been shown in **Figure 28**.

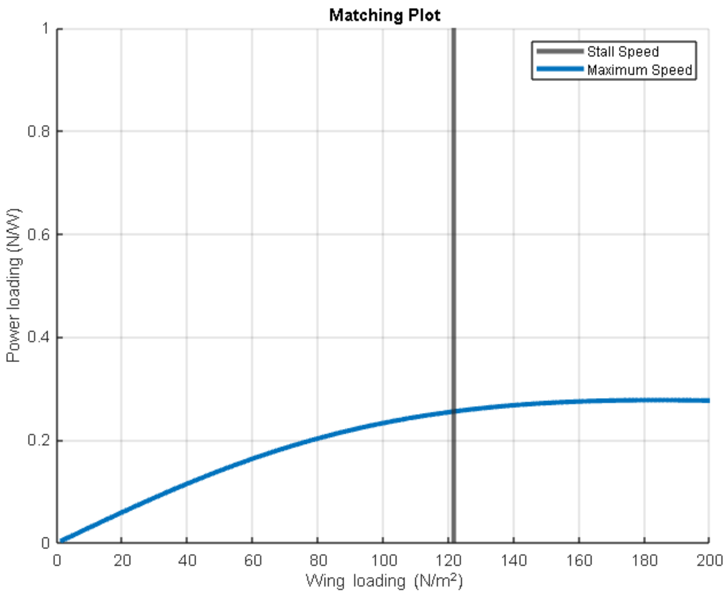

Figure 28 Contribution of Maximum Speed in the Matching Plot

4.3.3 Power Loading as a Function of Rate of Climb

A drone must have sufficient climbing speed in order to avoid obstacles in its path by climbing at relatively high speed. A general estimation of maximum ROC has been used from statistics and a value of **3 m/s** has been chosen [10].

For a prop driven aircraft, manipulating the power and drag equations [10], the final expression of our function is:

$$\left(\frac{W}{P}\right)_{ROC} = \frac{1}{\frac{ROC}{\eta_p} + \sqrt{\frac{2}{\rho\sqrt{\frac{3C_{D_o}}{K}}}\left(\frac{W}{S}\right)}\left(\frac{1.155}{\left(\frac{L}{D}\right)_{max}\eta_p}\right)}$$

The contribution of Rate of Climb in the matching plot has been shown in **Figure 29**.

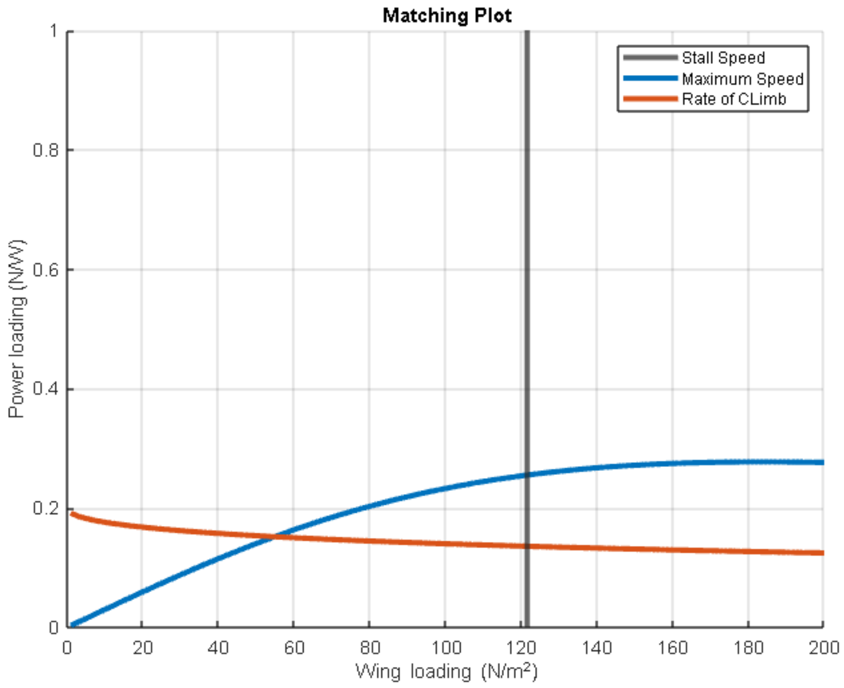

Figure 29 Contribution of Rate of Climb in the Matching Plot

4.3.4 Power Loading as a function of Absolute Ceiling

Finally, the last parameter that is to be decided during the design of the drone is the absolute ceiling. Absolute ceiling is the maximum altitude the drone will reach during its flight. According to airspace regulations of different countries [31], the maximum ceiling of the drones is 400 feet.

For a prop driven aircraft, manipulating the expression of rate of climb and power [10], the final equation of absolute ceiling is:

$$\left(\frac{W}{P}\right)_{Ceiling} = \frac{\sigma_{AC}}{\sqrt{\frac{2}{\rho\sqrt{\frac{3C_{D_o}}{K}}}\left(\frac{W}{S}\right)}\left(\frac{1.155}{\left(\frac{L}{D}\right)_{max}\eta_p}\right)}$$

4.3.5 Final Matching Plot

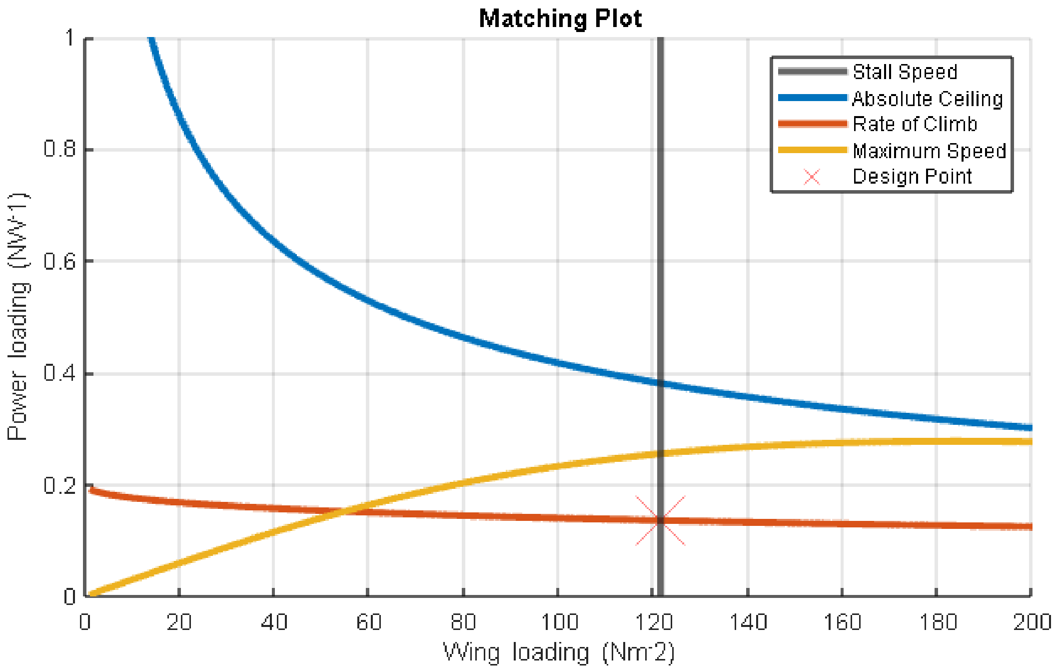

Figure 30 Complete Matching Plot

After plotting the contribution of each function in the matching plot, we choose the design point which has maximum power requirements and maximum wing loading. The design point in the matching plot is shown by a cross red marker in **Figure 30.**

Usually, take-off run is also incorporated in the matching plot but since we are designing a VTOL drone, it doesn't require a runway and so its contribution in the graph would be meaningless and confusing.

From the identified design point, we calculate the following important parameters for our drone, and they are summarized in **Table 9.**

Table 9 Resulting Parameters from the Matching Plot

Parameter	**Value**
$\left(\frac{W}{P}\right)_{DP}$	121.551 N/W
$\left(\frac{W}{S}\right)_{DP}$	0.1359 N/m^2
P_{DP}	858.23 W
S_w	0.9598 m^2
b_w	1.9594 m
$C_{tip,w}$	0.48984 m

CHAPTER 5: DETAILED DESIGN

5.1 Wing Design

5.1.1 Introduction

After completion of preliminary design phase, three parameters were derived from extensive calculations i.e., W_{MTOW} , P_{DP} and S_w . These parameters will be further used in the design of wing. In this section, a detailed design of wing will take place and the geometry, and the airfoil of the wing will be decided and calculated according to the requirements.

There are many parameters in the proper functioning of the wing but 17 of them are the most important and considered during the design of the wing.

Before starting our design, we must specify a step-by-step design process that would help us to follow a chronological order during the design and will help us later in the optimization process. Such a design flowchart has been shown in **Figure 31.**

It is to be noted that every design process is iterative and hence it is imperative that we construct our MATLAB scripts or any design programs to accommodate easy changes later in the design process.

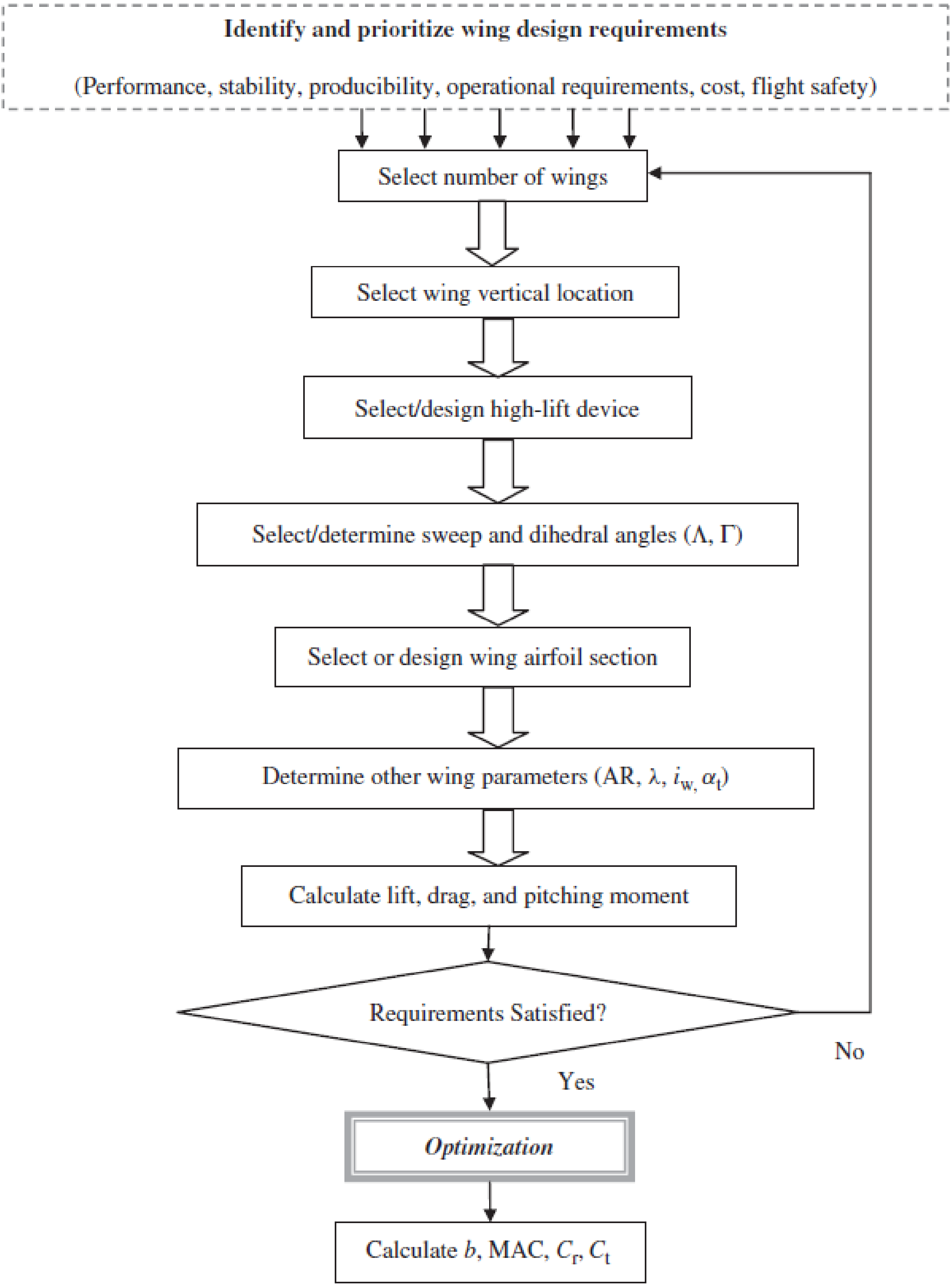

Figure 31. Design flowchart of the Wing [10]

5.1.2 Wing Vertical Location

The first decision in the design of a wing, is its vertical location relative to the plane. There are three very popular configurations of a wing and there are:

1. High-Wing
2. Mid-Wing
3. Low-Wing

Each of them has their pros and cons and so to decide which of them are better suited for the drone we must identify some of the parameters that are affected by the decision of selecting a particular configuration. A very effective method that is used for the weighing the different options is to use a design decision matrix. Such a decision matrix has been made and shown in **Table 10.**

In this matrix, firstly the design objectives are specified and then according to the requirements, a weightage is assigned to each design parameter. Based on the reviewed literature [10], requirements are scored by the team members and then the option with the highest is chosen as the optimal solution for the requirement.

Mid-wing had been scored highest in our decision matrix and hence we chose this configuration of wing for our drone. A mid-wing is a conventional balanced wing which are parameters in the range of between the low and high wing. It is very suitable for a drone as it doesn't require struts for support as a high-wing does and it doesn't have any effect on lift as a low-wing does [10]

Table 10 Wing Vertical Location Matrix

Design objectives	**Weightage (%)**	**High wing**	**Low wing**	**Mid-wing**	**SCORES OUT OF 5**		
					High	Low	Mid
Lateral Stability	10	4	1	3	0.4	0.1	0.3
Longitudinal Stability	10	3	4	3	0.3	0.4	0.3
Lateral Control	7.5	1	3	5	0.075	0.225	0.375
Longitudinal Control	7.5	5	1	4	0.375	0.075	0.3
Cost	15	4	5	4	0.6	0.75	0.6
Producibility	20	5	4	4	1	0.8	0.8
Stall Speed	10	5	1	3	0.5	0.1	0.3
Drag	10	1	3	5	0.1	0.3	0.5
Weight	10	4	5	4	0.4	0.5	0.4
Summation	100	32	27	26	3.75	3.25	**3.875**

5.1.3 Airfoil Selection

Selection of airfoil is a very important decision in the design of a wing which will have effect on the design of the tail and aerodynamics is also affected by the airfoil of the wing. Having said, there are countless types of airfoils available and each one of them have unique geometry and unique properties. Since we are only selecting an airfoil and not designing one, again the decision matrix can be used once we have identified our ideal requirements of the drone. There are various parameters that are associated and important during the selection of an airfoil, but a compromise but be maintained as no airfoil can give us all the best results at a single time.

From all the available parameters, 7 of them have been identified to be the most important for our drone and further weighing them into a decision matrix will effectively allow us to choose our airfoil for the wing.

Some descriptions of these parameters are given below:

1. **C_{dmin}** : A parameter that directly affects the battery and power requirements of the drone and hence minimizing the minimum drag coefficient will give us more endurance. [10]
2. **C_{mo}**: Coefficient of moment is important and considered during the design of tail. That is, greater the coefficient of moment, the greater the tail size would be required and will result in a bulky drone. [10]
3. **α_s**: The stall angle is the maximum angle that at which the plane will stall. The value should be optimum so that during climbing, the drone should not stall. [10]
4. **Cl_{max}**: A very important parameter that directly affects the lifting capability of the drone. A greater maximum lift coefficient will allow us to generate enough lift with a small wing and hence a small wing will have lower drag. [10]
5. **$(Cl/Cd)_{max}$**: A ratio of the two parameters that also complements both the MTOW and endurance requirements of the mission of the drone but it is not necessary that the drag is minimized if the MTOW is maximized and will require some compromise in between. [10]
6. **Cl_{α}**: It is the lifting-curve slope of an airfoil that indicates the rate of change of lift coefficient with respect to angle of attack of the wing. Greater slope allows us to generate more lift at lower angle of attacks. [10]
7. **Stall quality**: A stall quality indicates the type of stalling behavior when it has reached the stall angle. A gentle stalling behavior is always preferred over the rest of them but this

parameter is not that important because the operating range of a drone is usually not in the range of stalling. [10]

Based on the selected parameters, a decision matrix as seen in **Table 11** have been constructed. Different airfoils have been weighed in the matrix depending on their values of the parameters. According to the weightage, **MH-114** was the most optimal choice for the design as it provides lesser drag and good lifting capabilities.

Table 11 Airfoil Selection Matrix

Design Objectives	**Weightage (%)**	**MH-113 14.62%**	**MH-114 13.02%**	**EPPLER-396 (e396-il)**	**GOE-446 (goe446-il)**
Cd_{min}	25	0.00906	0.00827	0.00834	0.00834
C_{mo}	15	-0.1937	-0.1944	-0.1704	-0.1584
α_s	15	16.25	15	14.75	9.75
Cl_{max}	10	1.8356	1.8034	1.5626	1.5827
$(Cl/Cd)_{max}$	20	124.3 @ 3.75	131.2 @ 3.5	135.1 @ 5.5	122 @ 4
Cl_{α}	10	6.314	4.092	4.24	5.263
Stall quality	5	gentle	gentle	gentle	moderate
Summation	100				

5.1.4 Wing Incidence Angle

At cruising speeds, usually there is an optimum value of angle of attack for which the Cl/Cd ratio is maximum and consumes the minimum power. There are two ways to achieve this angle, that is either we can tilt the whole fuselage to an angle or, we can mount the wing at an angle which is known its wing incidence angle.

There is a range of angle of attack where the lift coefficient varies linearly and that is usually ± 8 degrees. Moreover, drag also varies linearly with the angle and so we chose an incidence angle that fulfilled our lift requirements and kept drag at minimum.

The ideal incidence angle is derived from the graph of lift coefficient vs angle of attack, which also gives us the information of maximum Cl/Cd ratio, and hence we choose the angle where Cl/Cd is maximized. In our case, an incidence angle of **3.5°** suffices our operational lift coefficient requirements and these are depicted in **Figure 32** and **Figure 33** which are derived from XFLR5.

5.1.5 Aspect Ratio of the Wing

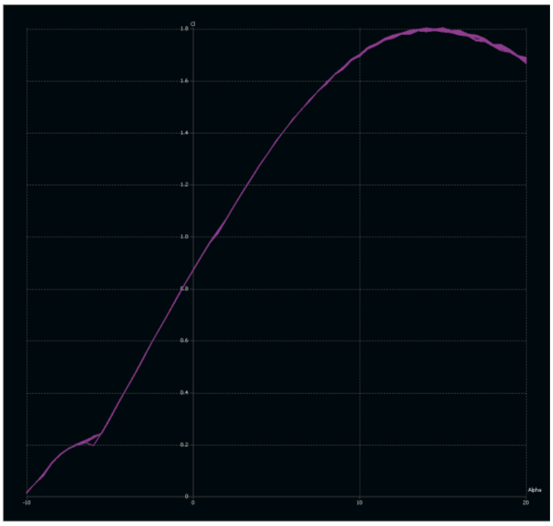

Figure 32 Variation of Lift-Coefficient with Angle of Attack

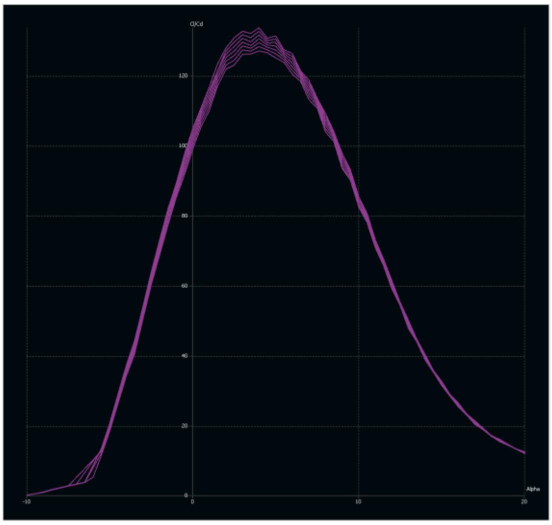

Figure 33 Variation of Cl/Cd with Angle of Attack

Aspect ratio directly influence the induced drag and weight of the airframe and hence it is really important that an optimum value of the aspect ratio is to be chosen for good performance.

Wings with higher aspect ratios have longer spans and thin chords and vice versa. Induced drag is inversely proportional to aspect ratio [4] and hence a high value of aspect ratio will allow us to have reduced drag but in a drone such a high value of aspect ratio is usually not incorporated so keeping in mind the manufacturability and structural constraints, the aspect ratio of our UAV was taken to be **4** [2]. This aspect ratio is on the lower end and hence there will be significant wing-tip vortices, but these will cater later by adding a winglet to the wing.

5.1.6 Taper Ratio

The choice of taper ratio is basically dependent on the lift distribution on the wing. Different values of taper ratio provide different shapes of lift distribution but the ideal shape in an ellipse [10] . To achieve an elliptical lift distribution, a value of **0.95** for taper ratio had been chosen. The choice of taper ratio was iteratively calculated from the lift line theory.

5.1.7 Lift Line Theorem's Mathematical Model & Lift Distribution

A mathematical model of lift line theory was modeled in MATLAB which can be found in **APPENDIX I: Lift Line Theory Wing**. There are basically two main outputs from this MATLAB script. The first one is the lift distribution curve and as seen from **Figure 34** different parameters have been optimized to achieve an elliptical distribution. Secondly, we achieve the overall lift coefficient of the wing which is less than the ideal infinite wing [10].

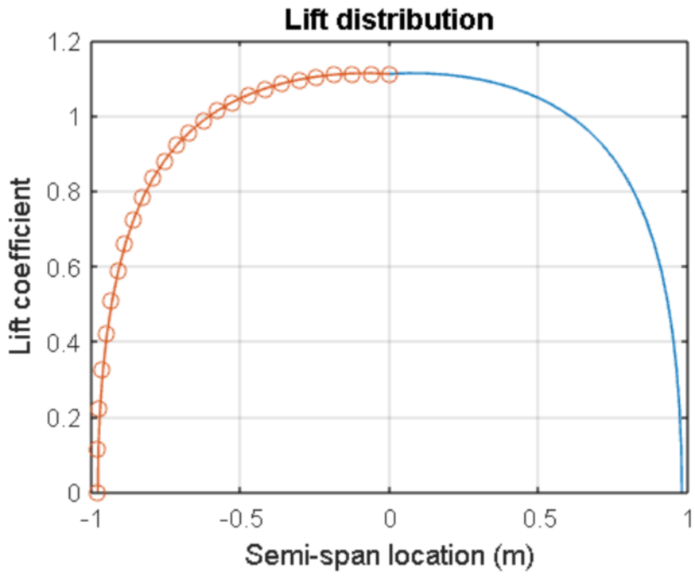

Figure 34 Lift Distribution Curve

An elliptical distribution enhances the flight safety during stall as the wing root has lower lift than that of the tip and hence gives enough time to the system for spin recovery. It also provides us with a lower bending moment and leads to a lighter but stronger wing structure as load distribution is the function of lift.

5.1.8 Sweep Angle

At speeds lower than Mach 0.3, the overall disadvantages introduced because of sweep outweigh the improvements. For example, if we apply 5 degrees of sweep angle to our wing, the overall drag will decrease by 2% but the manufacturing cost will increase by 15%. Finally, we also must keep in mind the manufacturing complexity by adding a sweep angle and for our purposes, the sweep angle was kept **zero**. [2]

5.1.9 Twist Angle

Twist angle is also a parameter that changes the shape of lift distribution and changing this angle also reduces the overall lift of the wing and furthermore, it is also difficult to manufacture a twisted wing and hence **no twist** had been used in our design. [2]

5.1.10 Dihedral Angle

The main goal of including a dihedral angle in a wing is to improve the lateral stability of the aircraft. When the dihedral angle is included in the wing, the effective planform area is reduced leading to a reduction in lift which is unfavorable in our case and hence **no dihedral** is included. [2]

5.1.11 Design & Use of Winglets

Because a low aspect ratio was used in the design of the wing, it was mandatory to include winglets so that induced drag can be reduced.

After we designed our wing, we noticed that even though we achieved our required lift but the difference between the theoretical requirements and parametric results were not up to the mark. The introduction of winglets decreased our drag coefficient by 10% and increased the lift of our wing by 7%.

For the design of winglets, an iterative approach had been taken in which different winglet parameters were varied and its effect on lift coefficient and drag were taken into notice and this was accomplished by using XFLR5. Firstly, cant angle was varied followed by taper ratio and span of the winglet. We chose PSU 94-097 the winglet airfoil due to its proven performance in many experiments and research [6]. After applying winglets, the comparison between a wing without a winglet and with a winglet has been shown in **Figure 35, Figure 36, and Figure 37.**

Keeping in view our requirements and constructional constraints we finalized our winglet design having the following parameters:

Table 12 Final Winglet Parameters

Parameter	**Value**
$\gamma_{winglet}$	0.4
$\alpha_{cant,winglet}$	90º
$b_{winglet}$	0.173 m
$C_{root,winglet}$	0.465 m
$C_{tip,winglet}$	0.186 m

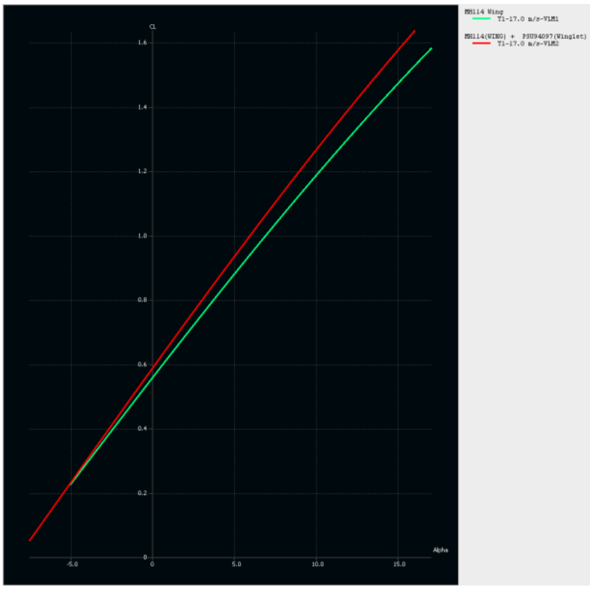

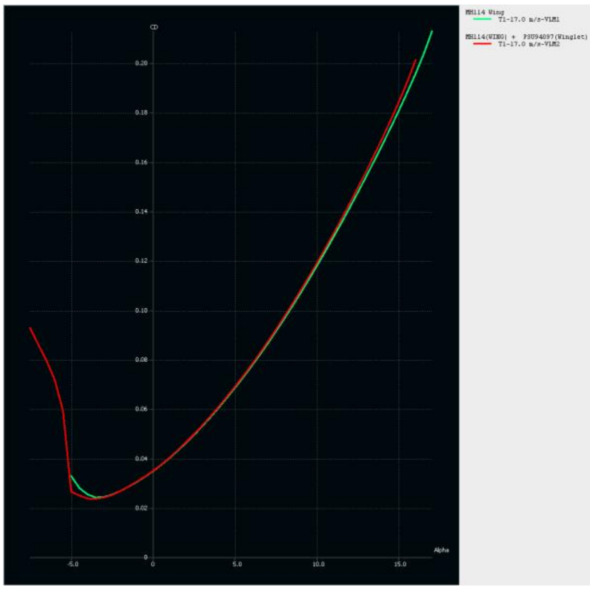

Figure 35 Comparison of Lift

Figure 36 Comparison of Drag

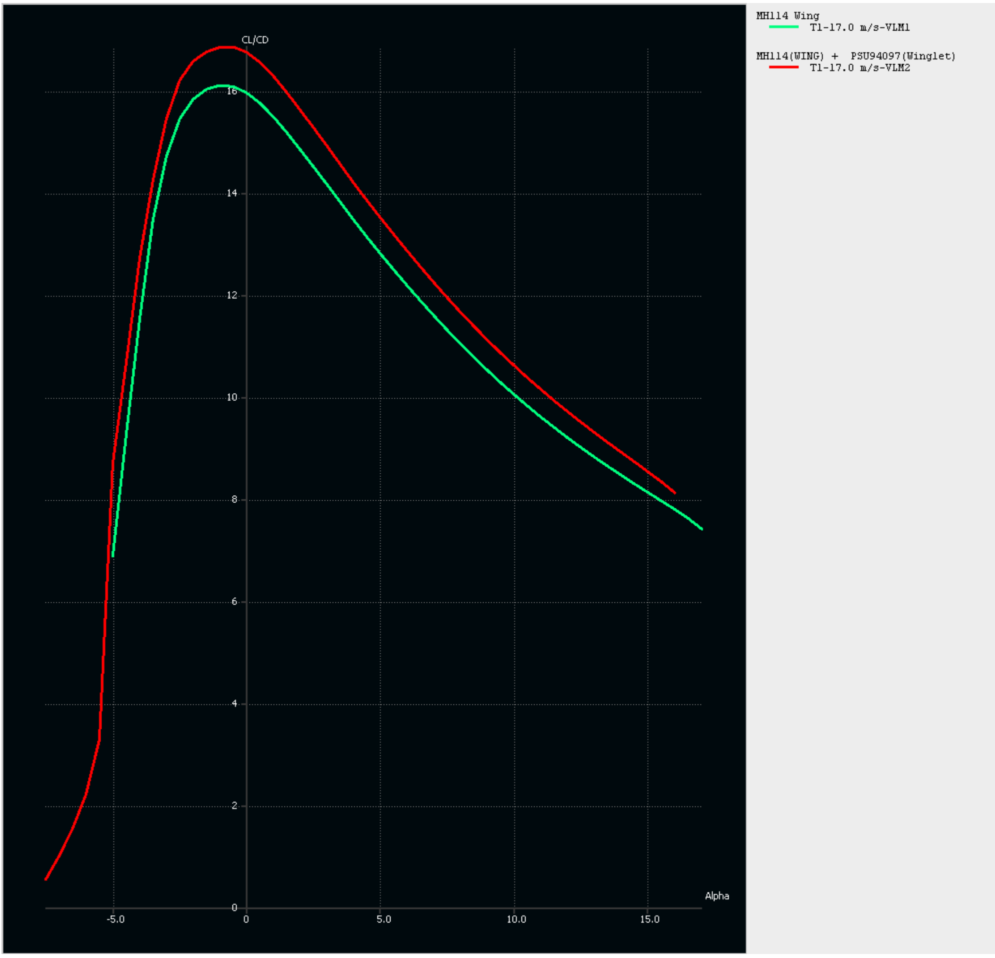

Figure 37 Comparison of Cl/Cd

5.1.12 Summary of Wing Parameters

After going through all the design steps, the parameters that were calculated or derived are listed in

Table 13**.**

Table 13 Final Wing Parameters

Parameter	**Value**
S_w	0.9598 m^2
AR_w	4
Λ_w	0
$\alpha_{t,w}$	0
$\alpha_{i,w}$	3.5°
$Cl_{\alpha_{w,2-D}}$	6.247
b_w	1.9594 m
$\overline{C_w}$	0.463 m
$C_{root,w}$	0.454 m
$C_{tip,w}$	0.4653 m

5.2 Tail Design

Tail Design has some steps components in common with wing design, but there is an important distinction between the two. The wing is responsible for generating lift while the tail primarily provides trim and stability, and secondarily the control. The tail also generates lift, but only a fraction of the amount managed by the wing. The design must be so that the tail does not ever approach its max angle of attack during any mission. It can prove catastrophic for the aircraft.

Most of our UAV's flight time is to spend in cruise, and we require it to have good endurance. Furthermore, the rotor handling the cruise regime is mounted directly on the fuselage centerline. The tail has, thus, been designed for reducing drag and wake as much as possible.

Figure 38 describes the complete tail design process:

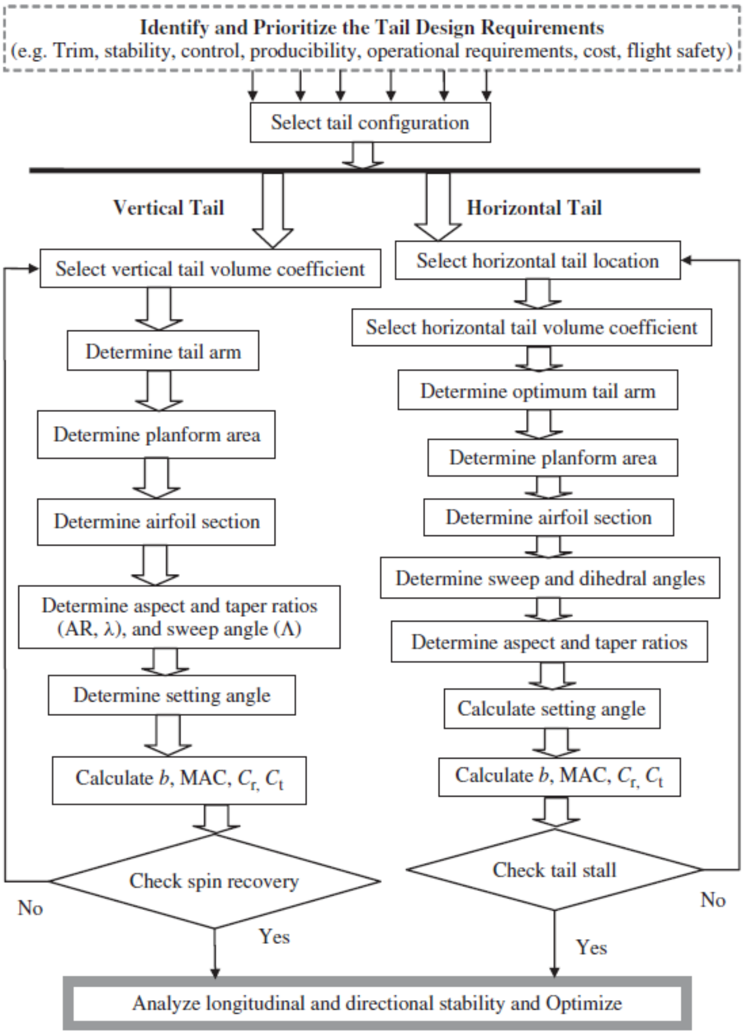

Figure 38. Tail Design Flow Chart [10]

5.2.1 Tail Configuration

The review of literature leads us to the comparison of different types of Tail Configurations which gives us below mentioned table:

Table 14. Tail Design Matrix [32], [10]

		Rating out of 5			
Design Parameters	Weightage (%)	Conventional Tail	V-Tail	Twin-boom Inverted-V	Boom-mounted Twin-T
Stability	17.5	4	2	3	4
Control	17.5	4	3	3.5	5
Drag	10	4	5	4	3
Weight	15	4	5	3	2
Manufacturability	10	4.5	4	3	2
Relevance	20	1	1	5	5
Cost	10	5	4	3.5	3
Summation	100	3.55	3.125	3.6375	3.675

The tail will be mounted conventionally i.e., aft of the fuselage, but its configuration will be unconventional. Based on the parameters most important to us, the inverted Twin-T tail is an ideal choice. It features booms for the tail structure, which can be extended forwards from the wings so that separate booms are not needed for the lifting propellers.

The tail itself provides an empty space for the cruise propeller's wake, so that none of it can impact horizontal or vertical tails.

A good example of an aircraft with the boom-mounted twin-T tail is the de Havilland DH-110 "Sea Vixen" (pictured below), a British carrier-based fighter.

Figure 39. de Havilland DH-110 [33]

As this tail configuration includes two separate (but identical) vertical tails, it is important to note that the dimensional parameters of the tail like volume coefficient and planform area will be calculated for one tail only, and then factored in twice as required in subsequent calculations.

5.2.2 Horizontal Tail Design

5.2.2.1 Configuration Selection

Three configurations of tail were available fixed, adjustable & all-moving tail. A **fixed horizontal tail** is selected because it much lighter, cheaper, and structurally easier to design. The longitudinal maneuverability requirement will be achieved using control surface i.e., Elevator hence a moving tail is not required.

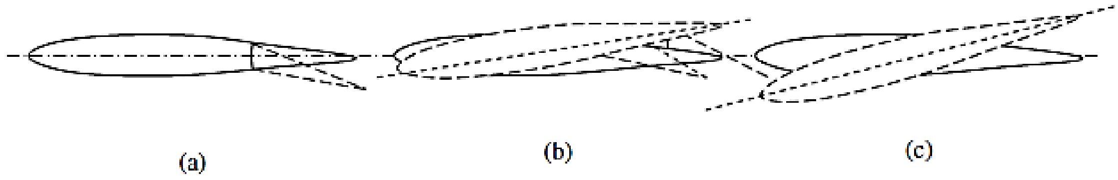

Figure 40. Three horizontal tail setting configurations. (a) Fixed; (b) Adjustable; (c) All moving [10]

5.2.2.2 Horizontal Tail Volume Coefficient

The horizontal tail volume coefficient, $\boldsymbol{\overline{V}_H}$ is determined primarily based on the longitudinal stability requirements. A higher value for $\boldsymbol{\overline{V}_H}$ results in a longer fuselage, and/or a smaller wing, and/or a larger horizontal tail. [10]

As the value of $\boldsymbol{\overline{V}_H}$ is increased, the aircraft becomes longitudinally more stable and less controllable. Hence, a lower value for $\boldsymbol{\overline{V}_H}$ causes the aircraft to become longitudinally more controllable and less stable. [10]

The value is selected from the data of previously made UAV closely resembles with our controls and stability requirement.

$$\bar{V}_H = 0.45$$

5.2.2.3 Horizontal Tail Moment Arm & Planform Area

Optimum tail moment arm determines the distance between the center of gravity of plane and the tail aerodynamic center. Both tail arm and platform area are interrelated to one another if tail arm increases platform area decreases and vice versa. [10]

Optimum tail arm is the most efficient length at which there will be minimum tail friction drag at a reasonable addition to the weight of the UAV.

$$(l_h)_{opt} = \sqrt{\frac{4\bar{C} S_w \bar{V}_H}{\pi\, D_f}}$$

From the MATLAB script **Horizontal and Vertical Tail Design** after inserting values we get,

$$(l_h)_{opt} = \ 1.3440\ m$$

Using the optimum tail moment arm we calculate horizontal tail planform area,

$$S_h = \frac{\bar{V}CS}{l}$$

Again, from the MATLAB script **Horizontal and Vertical Tail Design** we get

$$S_h = 0.1547\ m^2$$

5.2.2.4 Wing/fuselage Aerodynamic Pitching Moment Coefficient

Longitudinal trim is calculated for the cruising flight condition, trim in the other phases of flight is made by the help of control surfaces. Two major moments that are acting on a UAV along the y-axis are wing pitching moment and lift with respect to aircraft center of gravity, in order to balance it out tail moment is needed so that it will remain in equilibrium. [10]

Total moment equation is applied at center of gravity along x axis and coefficient of moment for tail is calculated at equilibrium in longitudinal direction then the most suitable airfoil is chosen from the air foil data base which matches.

$$C_{m_{w,2-D}} = -0.1948$$

Wing fuselage aerodynamic pitching moment ($C_{m_{o_{wf}}}$) is given by,

$$C_{m_{w,3-D}} = C_{m_{w,2-D}} \frac{AR_w\ \cos^2 \Lambda_w}{AR_w + 2\cos \Lambda_w} + 0.01\alpha_t$$

From the MATLAB script **Horizontal and Vertical Tail Design** after inserting values we get,

$$C_{m_{w,3-D}} = -0.1299$$

5.2.2.5 Desired Lift Coefficient at Cruise

The Required Lift Coefficient of Wing at Cruising speed is,

$$Cl_{c_{req,3-D}} = 0.7315$$

Desired Lift Coefficient at Cruise is given by,

$$(Cl_h)_{req} = \frac{C_{m_{w,3-D}} + Cl_{c_{req,3-D}}(h - h_o)}{\bar{V}_H}$$

From the MATLAB script **Horizontal and Vertical Tail Design** after inserting values we get,

$$(Cl_h)_{req} = -0.3699$$

5.2.2.6 Airfoil Section

A negative lift is required by the horizontal stabilizer for longitudinal trim, two symmetrical airfoils NACA 0012 and NACA 0009 are shortlisted of which **NACA 009** is selected having

$$Cl_{h,2-D} = -0.4292$$

at an angle of attack α = -3 degree. It has docile stall characteristics and low gradient. Moreover, it was verified that the tail does not stall before the wing.

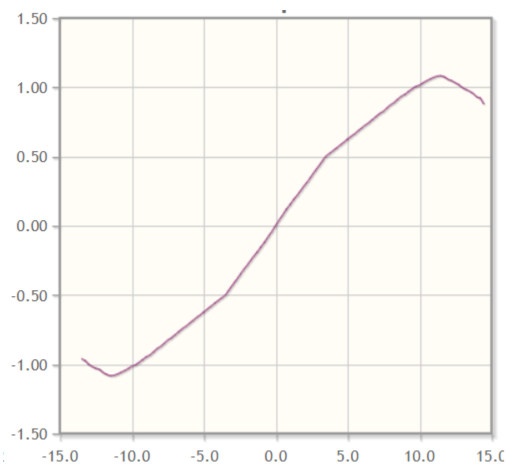

Figure 41. $\boldsymbol{Cl\ vs\ \alpha}$ for NACA 0009 [34]

5.2.2.7 Sweep angle

Horizontal Tail Sweep Angle Λ_h is defined as the angle between the tail leading edge and the y-axis in the x-y plane.

The horizontal tail sweep angle has influences on the aircraft longitudinal and lateral stability and control, aircraft performance, tail aerodynamic efficiency, and aircraft center of gravity. Most of the tail sweep angle effects are very similar to those of the wing effects, but on a smaller scale. [10]

Sweep is introduced to improve the aerodynamic features at transonic, supersonic, and hypersonic speeds by delaying the compressibility effects. However, we do not have any such requirement since the drone will be flying in subsonic regime. Therefore, horizontal tail sweep angle is kept **zero**.

$$\Lambda_h = 0$$

5.2.2.8 Dihedral Angle

The primary reason for applying a wing dihedral is to improve the lateral stability of the aircraft. The lateral stability is mainly the tendency of an aircraft to return to its original trim level-wing flight condition if disturbed by a gust and rolls around the x-axis. [10]

The dihedral angle is initially assumed the same as wing i.e., **zero**. The final value for the tail dihedral angle will be determined based on the aircraft stability and control, and performance analysis evaluations after the other aircraft components have been designed.

$$\Gamma_{\mathrm{h}} = 0°$$

5.2.2.9 Aspect Ratio

The tail aspect ratio is defined as the ratio between the tail span and the tail MAC. The tail aspect ratio has influences on the aircraft lateral stability and control, aircraft performance, tail aerodynamic efficiency, and aircraft center of gravity. The tail aspect ratio $\boldsymbol{AR_h}$ tends to have a direct effect on the tail lift curve slope. As the tail aspect ratio is increased, the tail lift curve slope is increased. [10]

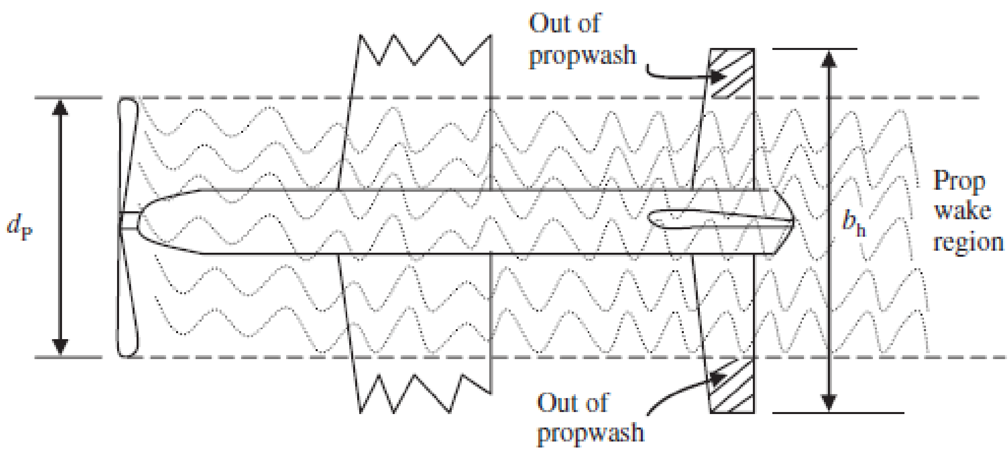

Figure 42. Tail span and prop wash [10]

Practically speaking, a lower aspect ratio is desirable for the tail, compared with that of the wing. The reason is that the deflection of the elevator creates a large bending moment at the tail root. Hence, a lower aspect ratio results in a smaller bending moment. Secondly in a single-engine prop-driven aircraft, it is recommended to have an aspect ratio such that the tail span ($\boldsymbol{b_h}$) is longer than the propeller diameter $\boldsymbol{D_p}$. This provision ensures that the tail flow field is fresh and clean of wake and out of the propellor wash area. [10]

Based on the above reasoning, an initial value for the tail aspect ratio is determined as follows:

$$AR_h = \frac{2}{3} AR_w$$

$$AR_h = 2.6667$$

5.2.2.10 Taper Ratio

The tail taper ratio λ_h is defined as the ratio between the tail tip chord and the tail root chord.

The major difference from the wing taper ratio is that the elliptical lift distribution is not a requirement for the tail. Thus, the main motivation behind the value for the tail taper ratio is to lower the tail weight. [10]

The final value for the tail taper ratio is determined to be **one** based design requirements and manufacturing constraints.

$$\lambda_h = 1$$

5.2.2.11 Lift Curve Slope

The Airfoil Maximum Thickness to Chord Ratio for NACA 0009 is as follows:

$$\left(\frac{t}{c}\right)_{max,h} = 0.09$$

In order to determine this parameter, we not only need to consider all the tail parameters, but also the wing downwash. At the beginning, the tail angle of attack is determined based on the tail lift curve slope. In the next step, the lifting line theory is used to calculate the tail generated lift coefficient. If the tail generated lift coefficient is not equal to the tail required lift coefficient, the tail incidence will be adjusted until these two are equal. In the last, downwash is applied to determine the tail incidence. The tail lift curve slope is:

$$Cl_{\alpha_{h,2-D}} = 1.8\pi\left(1 + 0.8\left(\frac{t}{c}\right)_{max,h}\right)$$

$$Cl_{\alpha_{h,3-D}} = \frac{Cl_{\alpha_{h,2-D}}}{1 + \frac{Cl_{\alpha_{h,2-D}}}{\pi AR_h}}$$

5.2.2.12 Angle of Attack at Cruise

The tail angle of attack in cruise is:

$$\alpha_{i,h} = \frac{Cl_h}{Cl_{\alpha_{h,3-D}}}$$

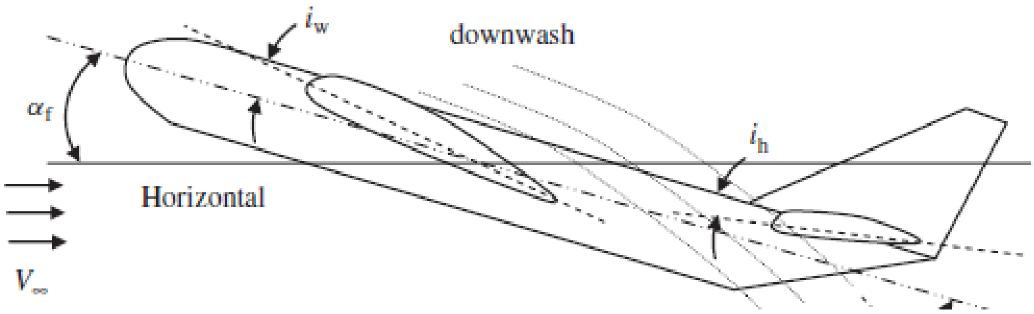

Figure 43. Horizontal tail effective angle of attack [10]

From the MATLAB script **Horizontal and Vertical Tail Design,** we get the value

$$\alpha_{i,h} = -0.1052°$$

However, the fuselage angle of attack is:

$$\alpha_f = -2°$$

Therefore, the horizontal tail incidence angle will be:

$$i_h = \alpha_f - \alpha_{i,h}$$

$$i_h = -1.8948°$$

5.2.2.13 Tail Span, Root Chord, Tip Chord, MAC

The other horizontal tail parameters are determined by solving the following four equations simultaneously.

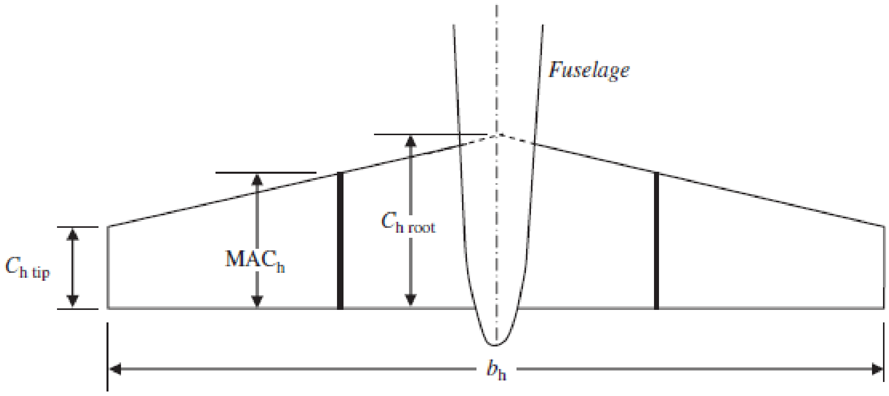

Figure 44. Horizontal tail geometry [10]

Horizontal Tail Span is given by

$$b_h = \sqrt{AR_h \times S_h}$$

$$b_h = 0.6479\ m$$

Horizontal Tail Tip Chord will be

$$C_{tip,h} = \frac{b_h}{AR_h}$$

$$C_{tip,h} = 0.2430\ m$$

Horizontal Tail Root Chord can be determined using

$$C_{root,h} = \lambda_h \times C_{tip,h}$$

$$C_{root,h} = 0.2430\ m$$

The Mean Aerodynamic Chord of Horizontal Tail is given by

$$\overline{C_h} = \frac{2}{3} C_{root,h} \frac{1 + {\lambda_h}^2 + \lambda_h}{1 + \lambda_h}$$

$$\overline{C_h} = 0.2430\ m$$

Finally Mean Horizontal Tail Area will be calculated using

$$\overline{S_h} = b_h \overline{C_h}$$

$$\overline{S_h} = 0.1574\ m^2$$

5.2.2.14 Lifting Line Theory

In the next step, the lifting line theory is used to calculate the tail generated lift coefficient. If the tail generated lift coefficient is not equal to the tail required lift coefficient, the tail incidence will be adjusted until these two are equal. In the last, downwash is applied to determine the tail incidence. To calculate the tail created lift coefficient, the lifting line theory is employed in **APPENDIX I: Lift Line Theory Horizontal Tail**. The output of the m-file is:

$$Cl_h = -0.3846$$

The tail is expected to generate a $(Cl_h)_{req}$ of -0.3699 and it generates a Cl_h of -0.3846 which is greater than requirement. Hence the designed tail is sufficient to fulfill our requirement.

5.2.2.15 Longitudinal Stability Check

The Horizontal Tail Efficiency is assumed based on actual data of other commercial aircraft with similar configurations.

$$\eta_h = 0.9$$

The last step is to examine the aircraft static longitudinal stability. The aircraft has a fixed tail, so the aircraft static longitudinal stability derivative is determined as follows:

$$C_{m\alpha} = Cl_{\alpha_{w,3-D}}(h - h_o) - Cl_{\alpha_{h,3-D}}\ \eta_h \frac{S_h}{S}\left(\frac{l}{\overline{\overline{C_w}}} - h\right)\left(1 - \frac{d\varepsilon}{d\alpha}\right)$$

$$C_{m\alpha} = -3.0243$$

where we assume that the wing/fuselage lift curve slope is equal to the wing lift curve slope.

Since the derivative $C_{m\alpha}$ is negative, the aircraft is statically longitudinally stable

5.2.2.16 Summary of Horizontal Tail Parameters:

The parameters of horizontal tail have been summarized below:

Table 15 Horizontal Tail Parameters

Parameter	**Value**
$\bar{V}_H$	0.45
$(l_h)_{opt}$	1.3440 m
S_h	0.1547 m^2
Λ_h	0
Γ_h	0°
AR_h	2.6667
λ_h	1
i_h	$-1.8948°$
b_h	0.6479 m
$C_{tip,h}$	0.2430 m
$C_{root,h}$	0.2430 m
$\overline{C_h}$	0.2430 m
Cl_h	-0.3846

5.2.3 Vertical Tail Design

5.2.3.1 Vertical Tail Volume Coefficient

The Vertical Tail Volume Coefficient used in the first iteration is assumed to be the same as that of a Cessna 177. This basis of assumption stems from the fact that the Cessna is a small, low-speed, high-wing aircraft powered by a single propeller, much like our UAV.

$$\bar{V}_v = 0.14$$

This volume coefficient is representative of the aircraft directional stability, as it relates the vertical tail area and tail arm (i.e., its moment arm) to the wing area and span. The greater the value of volume coefficient, the more directionally stabilizing the vertical tail becomes. [10]

5.2.3.2 Vertical Tail Arm

The horizontal tail is mounted on two vertical tails, so the tail arm will be the same for either tail. Thus, the optimum vertical tail moment arm is:

$$(l_v)_{opt} = 1.4259\ m$$

5.2.3.3 Vertical Tail Planform Area

The vertical tail planform area is the complete area including the fixed section and the movable section (i.e., the control surface). It was calculated from the volume coefficient as follows:

$$\bar{V}_v = \frac{(l_v)_{opt} S_v}{b S_w}$$

$$S_v = \frac{\bar{V}_v b S_w}{(l_v)_{opt}} = 0.1847\ m^2$$

5.2.3.4 Vertical Tail Airfoil Section

We shall use a symmetric airfoil for both vertical tails because they are not required to generate lift (which is a sideways force in this case). The NACA 0010 is one such airfoil. It has low-drag characteristics and a desirable lift curve slope.

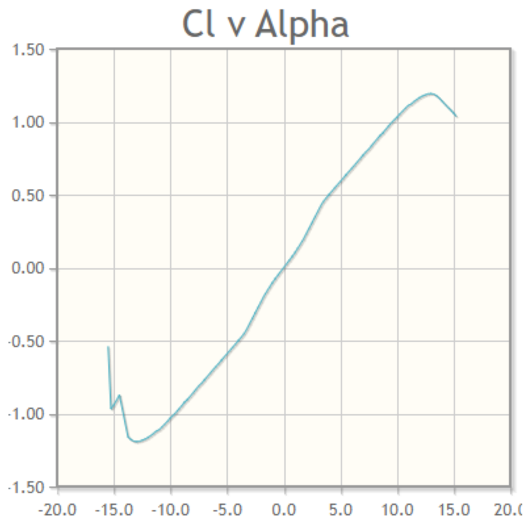

Figure 45. Cl vs Alpha [10]

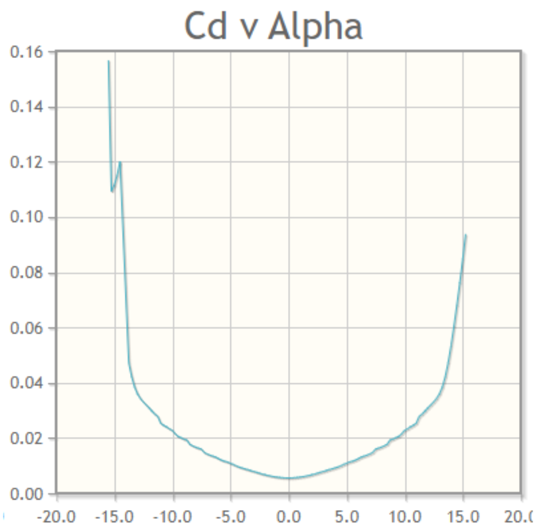

Figure 46. Cd vs Alpha [10]

The airfoil has a $(t/C)_{max}$ of 0.1/0.3 i.e., a 10% max thickness at 30% chord. This value is suitably lower compared to that of the wings to be viable for the vertical tails.

The 2D lift curve slope, according to the lift-line theory, of each vertical tail is found by:

$$C_{L_{\alpha\_v_{2-D}}} = 1.8\pi\left(1 + 0.8\left(\frac{t}{c}\right)_{max,v}\right) = 7.1628$$

Likewise, the 3D lift curve slope is:

$$C_{L_{\alpha\_v_{3-D}}} = \frac{C_{L_{\alpha\_v_{2-D}}}}{1 + \frac{C_{L_{\alpha\_v_{2-D}}}}{\pi AR_v}} = 2.7370$$

5.2.3.5 Aspect Ratio (AR_v) and Taper Ratio (λ_v)

A high aspect ratio generally improves directional stability and control along with aerodynamic efficiency but weakens lateral control and makes the tail structure heavier. Since our tail has a twin-T configuration, higher AR for the vertical tails will make horizontal tail more prone to wing wake during deep stall. [10]

The Aspect Ratio for vertical tails on most aircraft is between 1 and 2. [10] We have assumed the same value for AR as that of the Cessna 177 i.e.

$$AR_v = 1.41$$

Higher taper ratios result in reduced directional control and lateral stability, aside from increased complexity and empennage weight. Taper is generally applied for decreasing bending stresses on vertical tail roots, and to allow for vertical tail sweep. [10] The former is not enough to offset the disadvantages, and the latter is not required, in our case. Hence, the ratio for our vertical tails is:

$$\lambda_v = 1$$

5.2.3.6 Incidence Angle ($\alpha_{i,v}$)

The vertical tail on most conventional aircraft is not given any incidence. It is, however, an important consideration for designing of single-prop aircraft such as our UAV. This is because the single propeller induces a rotational reaction in the fuselage or aircraft body, thus disturbing lateral trim. [10]

To counteract this effect, most such aircraft are given 1-2 degrees of vertical tail incidence after experimental testing. In giving incidence to the vertical tail, we encounter another complication: setting two vertical tails on our aircraft in the configuration of choice will be tricky.

Considering these points, we have decided against giving the vertical tails an incidence angle, for the time being at least. Therefore,

$$\boldsymbol{\alpha_{i,v}} = 0^{\circ}$$

5.2.3.7 Sweep Angle (Λ_v)

Vertical tail sweep has affects directional and longitudinal (indirectly) stability and control. A high sweep angle increases directional control but decreases stability. In case of a T-tail, this sweep may also make the aircraft more stable and controllable in the longitudinal direction. [10]

However, such effects are significant at high speeds, which we do not plan to reach. For this reason, and to keep it simple, our design does not have sweep in the vertical tails. Therefore:

$$\Lambda_v = 0^{\circ}$$

5.2.3.8 Dihedral Angle (Γ_v)

Dihedral angle is usually applied in aircraft with two vertical tails, but only after other parameters have been specified and evaluated for efficacy in stabilizing the aircraft laterally and directionally. [10] Until then, the dihedral angle for our UAV's vertical tails is:

$$\Gamma_v = 0^\circ$$

5.2.3.9 Tip Chord ($C_{tip,v}$), Root Chord ($C_{root,v}$) & Mean Aerodynamic Chord ($\overline{C_v}$)

Our tail structure design mandates that the vertical tail tip chords be equal to the horizontal tail tip chords. Therefore,

$$C_{tip,v} = C_{tip,h} = 0.2409\ m$$

Since the taper ratio is 1 (meaning that there is no taper), the chord remains the same throughout the span of each vertical tail, and:

$$C_{root,v} = C_{tip,V} = 0.2409\ m$$

MAC for our vertical tail is given by this relation:

$$\overline{C_v} = \frac{2}{3} C_{root,v} \left(\frac{1 + {\lambda_v}^2 + \lambda_v}{1 + \lambda_v} \right)$$

Because $\lambda_v = 1$, we have:

$$\overline{C_v} = C_{root,v} = 0.2409\ m$$

5.2.3.10 Span (b_v)

The span of vertical tail is ascertained as follows:

$$b_v = \sqrt{AR_v * S_v} = 0.51\ m$$

5.2.3.11 Directional Trim & Stability

The vertical tail in a spinnable aircraft is to contribute significantly to the static directional stability derivative $C_{n_{\beta\_v}}$. The more positive the value of this derivative, the more directionally stable an aircraft is. [10] It is a function of fuselage contribution parameter K_{fl}, the vertical tail lift curve slope $C_{L_{\alpha\_v}}$, the sidewash gradient $\frac{d\sigma}{d\beta}$, the dynamic pressure ratio at vertical tail η_v as well as the tail arm, tail area, and wingspan and area.

$$C_{n_{B\_v}} = K_{\text{fl}} C_{L_{\alpha\_v}} \left(1 - \frac{d\sigma}{d\beta}\right) \eta_v \frac{(l_v)_{opt} S_v}{b S_w}$$

The value of K_{fl} is assumed to be 0.77, right in the middle of the prescribed values of 0.65 and 0.85. The dynamic pressure ratio η_v (that dictates efficiency) is taken to be 1 because the vertical tails will be under no wake from the propeller during level flight. The sidewash gradient has also been taken as zero, for the sake of simplicity.

Therefore, the directional stability derivative is:

$$C_{n_{B\_v}} = 0.2936$$

The derivative has a positive value, indicating that our vertical tail design does give directional stability to the aircraft.

Another phenomenon to consider while designing the tail is spin. Spin is a dangerous and potentially catastrophic flight condition in which the aircraft stalls, and then goes into a deep spiral like motion. Therefore, a spinnable aircraft must be able to recover from the spin in time.

The tail arm should be such that it keeps the vertical tail out of the wake of the horizontal tail during a deep stall. Experimentally, a recoverable spin is possible when at least half of the vertical tail planform area is out of the wake region of the horizontal tail. [10]

However, this stipulation applies to more conventional aircraft whereas our design has the horizontal tail itself hoisted by two vertical tails, thus precluding any situation where the vertical tail and rudder’s ability to stabilize a spinning UAV is impacted significantly.

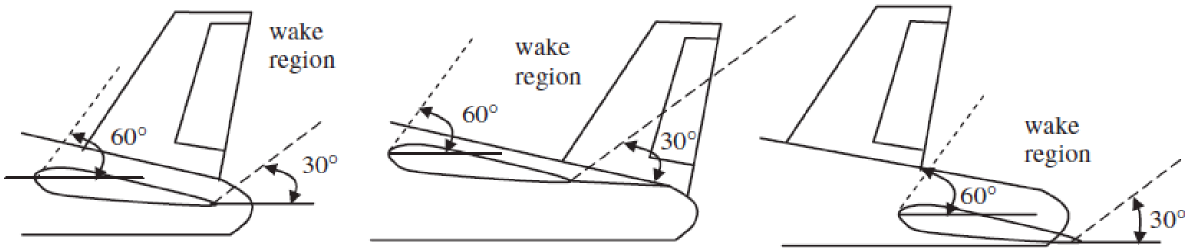

Figure 47. Vertical Tail Effectiveness [10]

5.3 Fuselage Design

In the design of fuselage, we must consider three things. Firstly, it should have plenty of space to accommodate all the electronics and battery of the drone. Secondly, it should be streamlined so it should produce minimum drag as possible during cruising. Finally, it should provide structural integrity and assembly of different components of the drone such as wings, tail, and payload.

A mixed of parametric and practical approach has been used to design and optimize the fuselage. In the beginning, a CAD model of the fuselage was developed in SolidWorks to serve as a foundation for optimization. The first iteration can be seen in **Figure 48**.

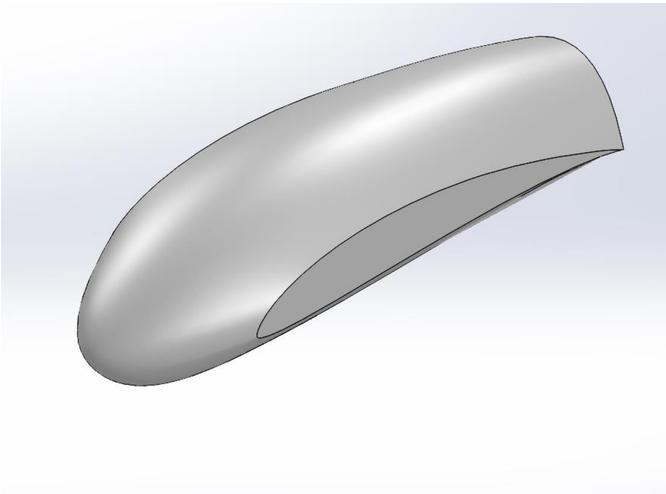

Figure 48 First iteration of Fuselage

The first design was further optimized by changing the splines connecting the different curves and it was made sure that complete blending should occur. The design obtained after another iteration is shown in **Figure 49.** Three airfoil shape have been utilized for the final design and these are MH-112, MH-113, MH-114. The thickness of the each of these airfoils decreases as the number increases and hence a blending profile is achieved at the end. The airfoil at both ends have been chosen as the same as the wing airfoil so that wing can be easily attached to the fuselage.

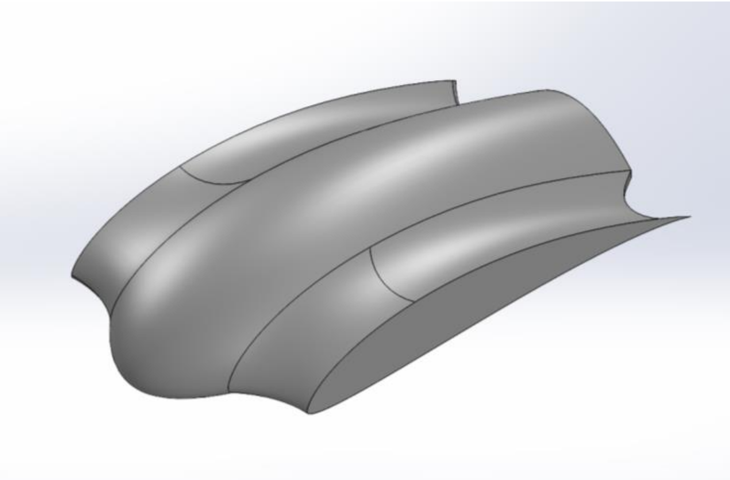

Figure 49 Revised Design of Fuselage

CFD was also performed on the fuselage to have an understanding of the lift and drag coefficients produced and based on these there were further optimized. The results have been summarized in **Table 16** and **Table 17.**

Table 16 Results from the First design of Fuselage

Goal Name	Unit	Value	Averaged Value	Minimum Value	Maximum Value
Lift Force	[N]	1.380	1.382	1.374	1.403
Drag Force	[N]	0.667	0.675	0.680	0.667

Table 17 Results from the Revised Fuselage Design

Goal Name	Unit	Value	Averaged Value	Minimum Value	Maximum Value
Lift Force	[N]	0.854	0.870	0.845	0.904
Drag Force	[N]	-0.468	0.461	0.470	0.453

A comparison of pressure distribution can also been seen from **Figure 50** and **Figure 51**

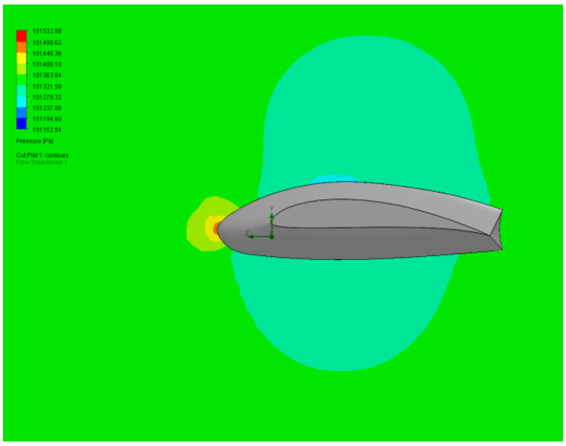

Figure 50 Pressure Distribution of First Design

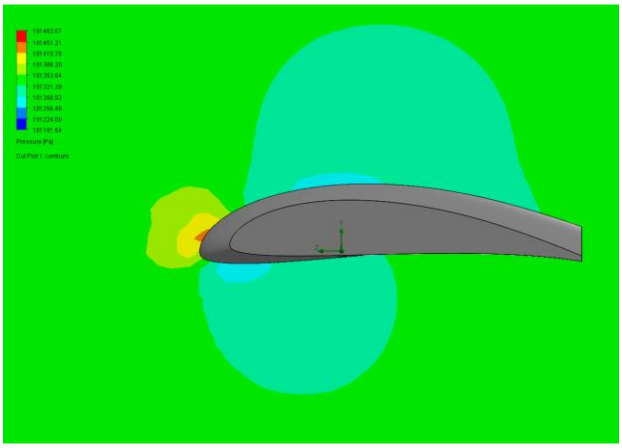

Figure 51 Pressure Distribution of Final Design

Comparing the both results, drag has reduced by 29.84% and lift is also decreased by 38.2% which is a compromise that must be made due to change in the shape of the fuselage.

5.4 Propulsion System:

An aircraft engine produces thrust based on Newton's third law. An aircraft engine usually generates a backward force to displace (accelerate) the air flow, thus the aircraft, in reaction, is pushed forward. The magnitude of engine thrust needed to fulfill a desired aircraft performance is calculated by the technique of matching plots. We will now finalize aspects of the propulsion system such as propulsion type selection, number of & locations of propellors.

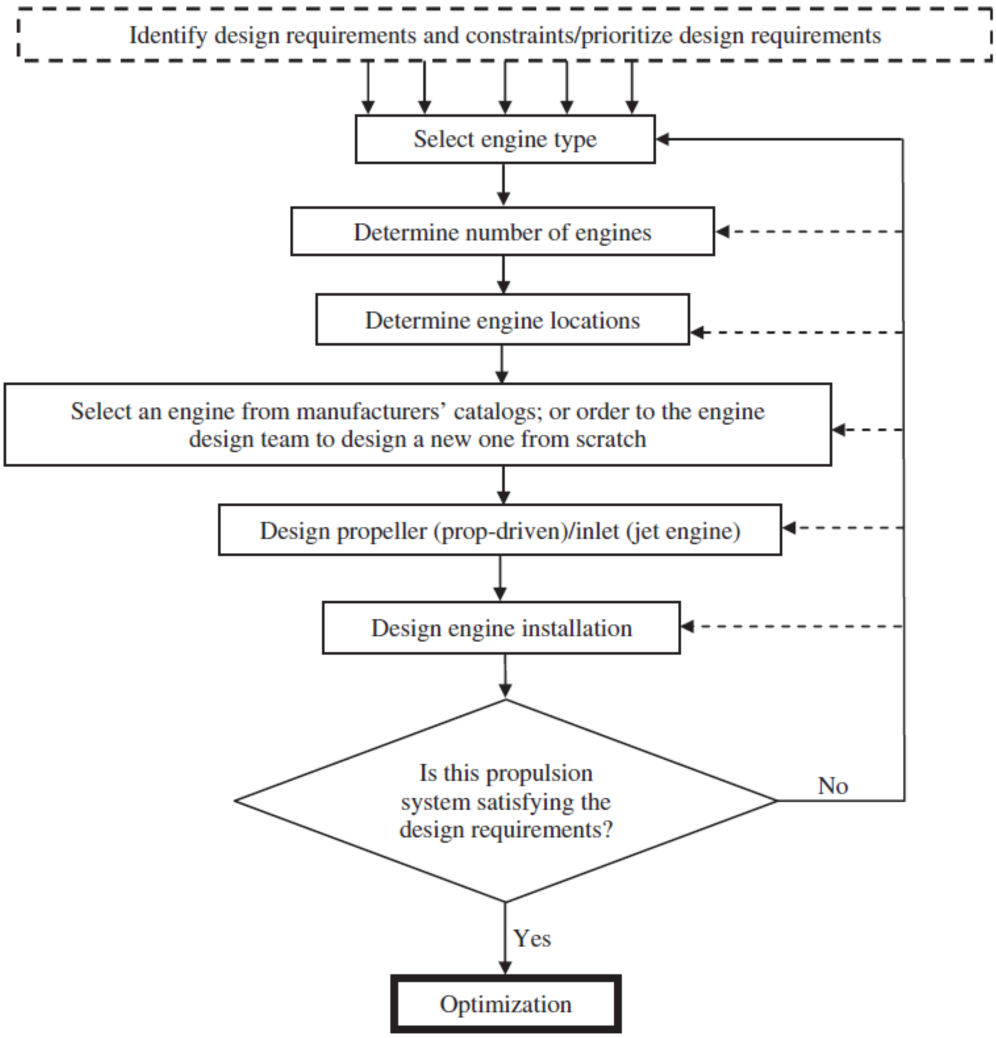

Figure 52 Propulsion system design flowchart

5.4.1 Design Requirements

The following design requirements are identified and listed in order of importance: Cost, Availability, Ease of Operation, Light Weight, Reliability, Operational Cost.

5.4.2 Engine Type

Generally speaking, the electric engine is the most maintainable engine, while the turbojet engine is the least maintainable engine. An electric engine requires less space than a piston-prop engine, even when the battery is added. The cheapest type of engine is the electric engine, after which is the solar-powered engine. Based on the all, a Prop-driven Electric Propulsion System was selected.

5.4.3 Number of Engines

There are a number of reasons to recommend a single-engine propulsion system. The negative side of a multi-engine configuration includes factors such as a heavier engine weight, larger engine size, and more direct operating cost. As the number of employed engines increases, the aircraft propulsion system tends to become heavier.

Moreover, as the number of employed engines is increased, the aircraft propulsion system tends to get larger in size. If this leads to a larger frontal area the aircraft drag is increased too, which in turn degrades the aircraft performance.

As the number of employed engines increases, the direct operating cost is increased too. Two prop-driven engines with x hp of power each will cost slightly more for a flight operation than one prop-driven engine with 2x hp.

Therefore, a **single prop-driven electric propulsion system** is selected.

5.4.4 Engine Location

The engine must be in a place resulting in the least negative aerodynamic interference with the wing and tails and the most favorable aerodynamic interferences. This guideline is applied for both buried and podded configurations. In contrast, an engine ahead of the horizontal tail will decrease the downwash behind the wing, so the longitudinal trim and stability will be influenced.

When the engine location, particularly in the case of a single-engine configuration, is compared with respect to the aircraft center of gravity, two categories of propulsion systems are identified: (i) pusher, where the engine is located behind the aircraft center of gravity and (ii) tractor, where the engine is located ahead of the aircraft center of gravity.

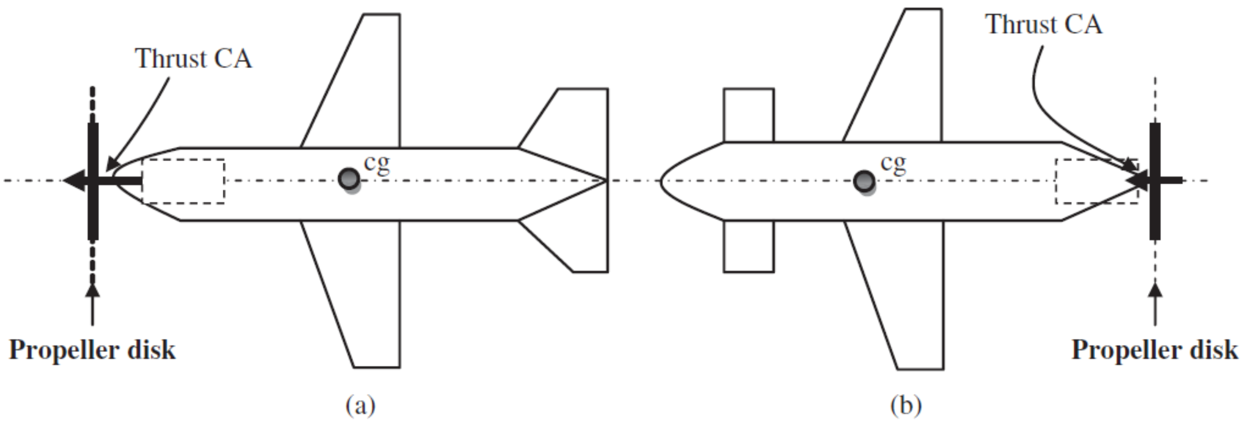

Figure 53 Pusher and tractor configurations: (a) Tractor; and (b) Pusher

A pusher aircraft has a better longitudinal controllability. Therefore, the motor is buried inside **rear fuselage nose** with a **pusher configuration** is selected.

5.4.5 Engine Selection

Based on the power requirement, T-Motor AM 480 KV 650 is selected. It has a maximum power of 1150 W which is greater than our requirement. We intentionally selected a more powerful motor for future design precautions and considerations. Specifications can be seen in Figure 54.

Test Item	KV650	Weight (Incl. Cable)	145g
Motor Dimensions	Φ49*70mm	Internal Resistance	32mΩ
Lead	Enameled Wire 90mm	Configuration	24N28P
Shaft Diameter	IN : 6mm OUT : 6mm	Rated Voltage(Lipo)	5-6S
Idle Current(10V)	1.55A	Peak Current(180s)	55A
Max. Power(180s)	1150W		

Figure 54 Specification Sheet for AM 480 KV 650 [35]

5.4.6 Propellor Design

The engine power required is:

$$P = 858.2303\, W$$

We can obtain the prop diameter using the following formula:

$$D_p = K_{np}\sqrt{\frac{2P\eta_p AR_p}{\rho\left(0.7V_{tip_{cruise}}\right)^2 C_{L_p} V_c}}$$

In a cruising flight and with the optimum angle of twist (the best propeller pitch), the propeller efficiency (η_p) may be around 75–85%. Hence, an **efficiency** of **75%** is assumed.

The propeller cruise tip speed limit is chosen based on material. For Composite material the Tip speed limit ($V_{tip_{cruise}}$) is **250 m/s**.

The typical value for the propeller aspect ratio is between 7 and 15; and a typical propeller lift coefficient is between 0.2 and 0.4. Hence, **aspect ratio** is chosen as **12** and the **propeller lift coefficient** is **0.2.**

The prop diameter is calculated to be:

$$D_p = 0.3719\, m = \ 14.64\, in$$

Propeller rotational speed is calculated using the following:

$$V_{tip_{static}} = \sqrt{\left(V_{tip_{cruise}}\right)^2 - (V_c)^2}$$

$$V_{tip_{static}} = 249.5618 \frac{m}{s}$$

$$\omega = \frac{2V_{tip_{static}}}{D_p}$$

$$\omega = 12814\, rpm$$

Therefore, a propellor of approximately 15 in is required which will rotate at approximately 13000 rpm.

5.5 Design of Control Surfaces

5.5.1 Aileron Design

The primary function of an aileron is the lateral (i.e., roll) control of an aircraft; however, it also affects the directional control. Lateral control is governed primarily through a roll rate (P). The generated rolling moment is a function of aileron size, aileron deflection, and distance from the aircraft fuselage center line. Any change in the aileron geometry or deflection will change the roll rate, which subsequently varies constantly the roll angle. [10]

5.5.1.1 Design Requirements

5.5.1.2 Roll Surface Configuration

Due to the aircraft configuration, simplicity of design, and desire for low cost, a conventional roll control surface configuration (i.e., aileron) is selected.

5.5.1.3 Maneuverability and Roll Control Requirements

Hence, table [10] will be the reference for the aileron design, which expresses the requirement as the time to achieve a specified bank angle change. We have to select aircraft class and check the Maneuverability and Roll Control Requirements from table.

5.5.1.4 Aircraft Class & Critical Flight Phase

Our UAV falls in the category of Small, light aircraft (maximum take-off mass less than 6000 kg) and with low maneuverability. So, **Class I** selected. [10]

Based on examples of flight operations [10], **Flight Phase Category B** was selected. This is because our flight operations would include Climb (CL), cruise (CR), loiter (LO), descent (D); deceleration (DE).

To leave no uncertainty in safe flight, **Level of Acceptability 1** was selected. Flying qualities will be clearly adequate for the mission flight phase.

Table 18 Aircraft Class & Flight Phase

Class	Flight phase	Level of acceptability
I	B	1

5.5.1.5 Handling Quality Design Requirements

The roll control handling qualities design requirement is identified from [10], which states that the aircraft in Class I, flight phase B, for a level of acceptability of 1, is required to be able to achieve a bank angle of 45◦ in 1.7 seconds. [10]

5.5.1.6 Aileron Position

The inboard and outboard positions of the aileron as a function of wing span (i.e., bai/b and bao/b) are tentatively selected to be at 70% and 95% of the wing span respectively.

$$\frac{b_{a_i}}{b} = 0.7$$

$$\frac{b_{a_i}}{b} = 0.95$$

5.5.1.7 Aileron Chord to Wing Chord Ratio

Given the ratio between aileron chord and wing chord, the aileron effectiveness parameter is obtained using a graph [10]. Aileron chord to wing chord ratio is 0.2.

5.5.1.8 Aileron Effectiveness Parameter

Aileron effectiveness is a measure of how effective the aileron deflection is in producing the desired rolling moment. Aileron effectiveness is a function of its size and its distance from the aircraft center of gravity. [10]

Given the ratio between aileron chord and wing chord, the aileron effectiveness parameter is obtained using a graph. Using aileron chord to wing chord ratio of 0.2, we find the effectiveness parameter for Aileron.

$$\tau_a = 0.4$$

5.5.1.9 Aileron Rolling Moment Coefficient Derivative

The aileron rolling moment coefficient derivative is calculated employing the following equation:

$$C_{l_{\delta A}} = \frac{2C_{l_{\alpha w}}\tau\, C_r}{Sb}\left[\frac{y^2}{2} + \frac{2}{3}\left(\frac{\lambda - 1}{b}\right)y^3\right]_{y_i}^{y_o}$$

$$C_{l_{\delta A}} = 0.0305$$

5.5.1.10 Maximum Aileron Deflection

A maximum aileron deflection of ±20 deg is selected.

5.5.1.11 Aircraft Rolling Moment Coefficient

Aircraft Rolling Moment Coefficient is a function of aircraft configuration, sideslip angle, rudder deflection, and aileron deflection. [10] In a symmetric aircraft with no sideslip and no rudder deflection, this coefficient is linearly modeled as:

$$C_l = C_{l_{\delta A}}\delta_A$$

The parameter $C_{l_{\delta A}}$ is referred to as the aircraft rolling moment coefficient due to aileron deflection derivative and is also called the aileron roll control power.

The aircraft rolling moment coefficient when the aileron is deflected with the maximum deflection is calculated from MATLAB Script **Aileron Design**:

$$C_l = 0.0106$$

5.5.1.12 Aircraft Rolling Moment

The aircraft rolling moment (LA) when the aileron is deflected with the maximum deflection is calculated. The typical approach velocity is 1.1–1.3 times the stall speed, thus the aircraft is considered to approach with a speed of 1.3 Vs. In addition, the sea-level altitude is considered for the approach flight operation. Using MATLAB Script **Aileron Design**, we have:

$$L_a = \frac{1}{2}\rho V_{app}^2 S C_l b$$

$$L_a = 2.1545$$

5.5.1.13 Steady-State Roll Rate

The aircraft rate of roll rate response to the aileron deflection has two distinct states a transient state and a steady state. The integral limit for the roll rate (P) is from an initial trim point of no roll rate to a steady-state value of roll rate. Since the aileron is featured as a rate control, the deflection of the aileron will eventually result in a steady-state roll rate

The steady-state roll rate is determined using MATLAB Script **Aileron Design**:

$$P_{ss} = 7.4066$$

5.5.1.14 Bank Angle

Calculating the bank angle at which the aircraft achieves the steady-state roll rate using **Aileron Design**:

$$\Phi_1 = 46.9068 \text{ rad}$$

5.5.1.15 Aircraft Rate of Roll-rate

Calculate the aircraft rate of roll rate that is produced by the aileron rolling moment until the aircraft reaches the steady-state roll rate using **Aileron Design**.

$$\dot{P} = 0.5848 \frac{rad}{s^2}$$

5.5.1.16 Roll Time

$$\mathrm{t}_2 = 1.3431 \, s$$

The roll time obtained is compared with the required roll time (t req) expressed in step 5. The roll time obtained in step to achieve the bank angle of 45 deg (i.e., 1.3431 seconds) is shorter than the roll time expressed in step 5 (i.e., 1.7 seconds). Hence the current aileron satisfies the requirements.

5.5.1.17 Aileron Geometry

The span will be:

$$b_A = y_o - y_i$$

$$b_A = 0.1922\,m$$

The chord will be:

$$C_A = 0.2C_w$$

$$C_A = 0.0890\,m$$

The aileron planform area will be:

$$S_A = b_A C_A$$

$$S_A = 0.0342$$

5.5.1.18 Summary of Aileron Parameters:

The MATLAB code used to calculate these parameters is provided in **Aileron Design**. After going through all the design steps, the parameters that were calculated or derived are listed in **Table** 19**.**

Table 19 Final Aileron Parameters

Parameter	**Value**
S_A	0.0290 m^2
b_A	0.5183 m
C_A	0.0559 m
δ_{Amax}	±20°

5.5.2 Elevator Design

The primary function of an elevator is to provide longitudinal control which is achieved by providing an incremental lift force on the horizontal tail. Since the horizontal tail is located at some distance from the aircraft's center of gravity, this lift force creates a pitching moment about the plane's center of gravity thus the elevator is also considered as a pitch control device. In conventional symmetric aircrafts, the longitudinal control is not coupled with lateral and directional controls so the design of the elevator is independent of the design of aileron and rudder. While designing the elevator, four main parameters need to be determined being the elevator planform area, elevator chord, elevator span and the maximum elevator deflection. [10] The elevator design flowchart is shown in **Figure 55**.

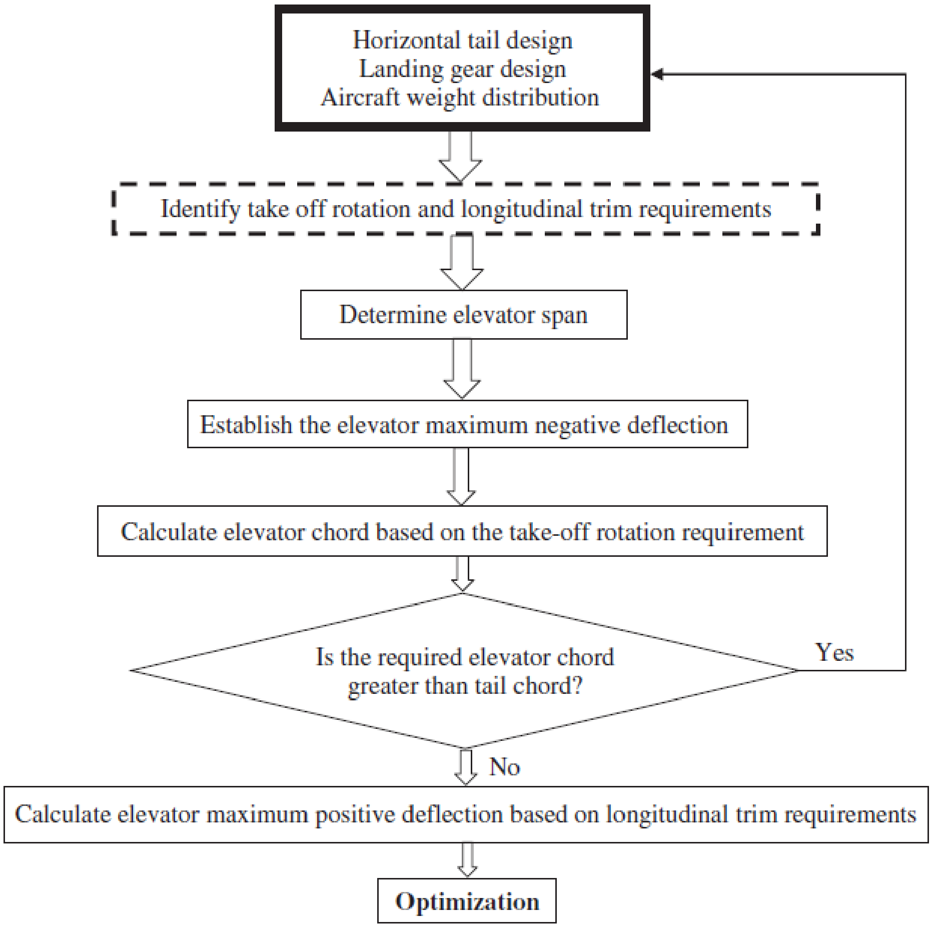

Figure 55. Elevator Design Flowchart [10]

5.5.2.1 Elevator requirements:

As step one, we need to enlist our requirements for our elevator. The elevator should be easily manufacturable and have a low cost while fulfilling our longitudinal control requirements. Our aircraft is a vertical takeoff and landing vehicle so we do not consider elevator requirements at runway during takeoff and only deal with longitudinal control during cruise.

5.5.2.2 Elevator span:

The first parameter we choose is the elevator span ratio based on intuition from typical values used in aircrafts flying today. The span ratio chosen for our elevator is 0.8. [10]

$$\frac{b_E}{b_h} = 0.8$$

5.5.2.3 Maximum elevator deflection:

The maximum elevator deflection is chosen on the basis of two things. The elevator needs to fulfill our required pitch control magnitude and rate while keeping the tail from stall. The maximum elevator deflection set in our case is ±15 degrees. [10]

5.5.2.4 Desired tail lift coefficient:

The desired tail lift coefficient needs to be defined on the basis of which we verify our elevator design. This is usually the same lift coefficient as that of horizontal tail.

5.5.2.5 Elevator angle of attack effectiveness:

The parameter τ_e is the angle of attack effectiveness of the elevator, which is primarily a function of elevator to tail chord ratio. The angle of attack effectiveness of our elevator is calculated is using the equation below.

$$\tau_E = \frac{\frac{C_{L_h}}{cl_{\alpha_{h,3-D}}} - \alpha_h}{\delta_E}$$

5.5.2.6 Elevator chord ratio:

The effectiveness of our elevator calculated in step 6 is used to find the elevator chord ratio from **Figure 56**.

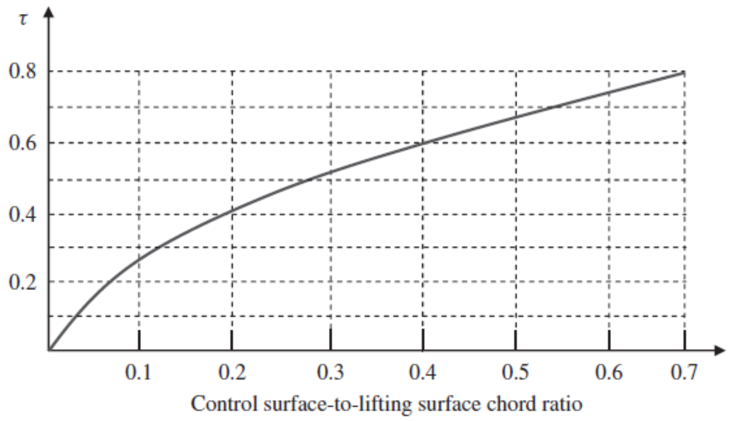

Figure 56. Elevator effectiveness to elevator chord ratio graph [10]

5.5.2.7 Elevator planform area:

The elevator planform area is the product of elevator span and chord. After finding the planform area we can draw the top view of the elevator.

$$S_E = b_E * C_E$$

5.5.2.8 Verification of Elevator parameters:

Using CFD techniques at maximum negative elevator deflection, the tail lift coefficient is calculated and compared with the required tail lift coefficient. If equal, the design of elevator is verified. Furthermore, the horizontal tail stall is also checked in this step.

5.5.2.9 Longitudinal control power derivative:

The non-dimensional derivative which represents the longitudinal control power derivative is the rate of change of aircraft pitching moment coefficient with respect to elevator deflection [10]. This is determined by:

$$C_{m_{\delta E}} = \frac{\partial C_m}{\partial \delta_E} = -cl_{\alpha_{h,3-D}} * \eta_h * \bar{V}_H * \frac{b_E}{b_h} * \tau_e$$

5.5.2.10 Contribution of elevator to aircraft lift derivative:

This non-dimensional derivative is the rate of change of aircraft lift coefficient with respect to elevator deflection [10] and is defined as follows:

$$C_{L_{\delta E}} = \frac{\partial C_L}{\partial \delta_E} = cl_{\alpha_{h,3-D}} * \eta_h * \frac{S_h}{S} * \frac{b_E}{b_h} * \tau_e$$

5.5.2.11 Contribution of elevator to tail lift coefficient derivative:

This derivative is the rate of change of tail lift coefficient with respect to elevator deflection [10] and is defined as follows:

$$C_{L_{h\delta E}} = \frac{\partial C_{L_h}}{\partial \delta_E} = cl_{\alpha_{h,3-D}} * \tau_e$$

5.5.2.12 Calculate elevator deflection for required longitudinal trim:

When all longitudinal moments and forces are in equilibrium, it is said that the aircraft is in longitudinal trim [10].We calculate the required elevator deflection by first calculating the angle of attack at which maximum deflection is required and then using that angle to calculate the deflection.

$$\alpha = \frac{\left(C_{L_1} - C_{L_o}\right)C_{m_{\delta E}} + \left(C_{m_o}\right)C_{L_{\delta E}}}{C_{L_\alpha}C_{m_{\delta E}} - C_{m_\alpha}C_{L_{\delta E}}}$$

$$\delta_E = -\frac{\left(C_{L_1} - C_{L_o}\right)C_{m_\alpha} + \left(C_{m_o}\right)C_{L_\alpha}}{C_{L_\alpha}C_{m_{\delta E}} - C_{m_\alpha}C_{L_{\delta E}}}$$

5.5.2.13 Summary of Elevator Parameters:

The MATLAB code used to calculate these parameters is provided in **APPENDIX I: Elevator Design**. After going through all the design steps, the parameters that were calculated or derived are listed in

Table 13.

Table 1 Final Elevator Parameters

Parameter	**Value**
S_E	0.0290 m^2
b_E	0.5183 m
C_E	0.0559 m
δ_{Emax}	±15°

5.5.3 Rudder Design

The rudder is the main control surface responsible for the directional control of an aircraft. When it is deflected on either side, a side force acts on it and produces a yawing moment about the aircraft cg. This yaw is accompanied by a small rolling moment, because most rudders are placed above the cg of the aircraft. [10]

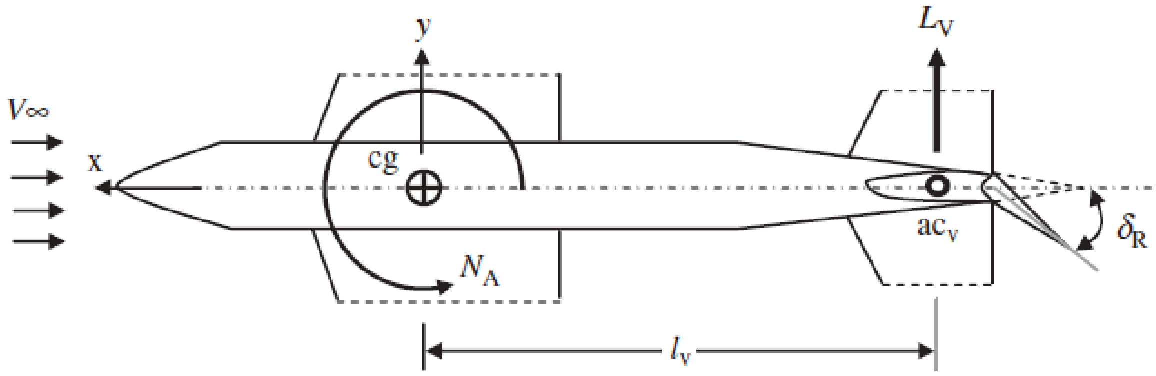

Figure 57. Directional control via rudder deflection [10]

Along with directional control, directional trim makes up the fundamnetal roles of the rudder in an aircraft. By convention, rudder deflection to the left is taken as positive, and any deflection will produce a yawing moment about the cg in the completely opposite direction. [10]

Designing the rudder involves determining its area, span, chord and maximum deflection on either side. The process is based on engineering selection, and goes like this:

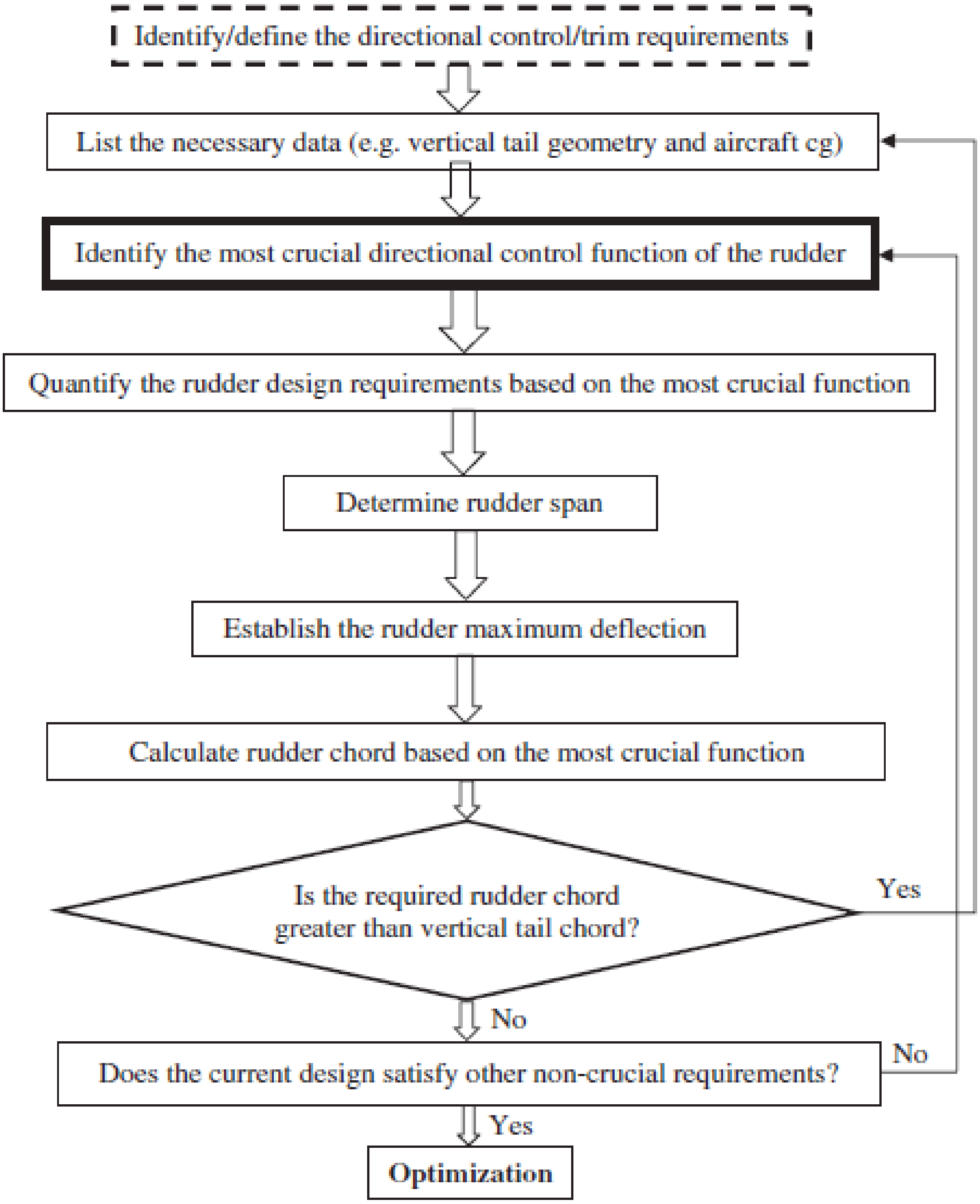

Figure 58. Rudder Design Flow Chart [10]

5.5.3.1 Vertical Tail Geometry

Before we determine the dimensional and performance-related parameters for the rudder, it is important to reiterate relevant parameters of the vertical tail:

Table 20 Vertical Tail Parameters

Parameter	**Value**
Lift Curve Slope $C_{L_{\alpha\_v_{3-D}}}$	2.7370
Planform Area S_v	$0.1847\ m^2$
Span b_v	$0.51\ m$
Chord $\overline{C_v}$	$0.2409\ m$
Aspect Ratio AR_v	1.41

5.5.3.2 Spin Recovery (Governing Design Consideration)

Initially, our most design consideration for the rudder has been spin recovery, which requires our UAV to be fast enough in coming out of a spin once it has entered it. The rudder is the most important control surface in the event of a spin maneuver. A powerful rudder can easily overcome the spinning motion of the aircraft with an adequate amount of yaw. [10]

Spin is a situation high angle of attack and low airspeed, which is usually close to the stall speed of the aircraft. An aircraft enters spin once it stalls and particularly when the inboard wing stalls first, prompting a spiral motion downward around the yaw and pitch axes. [10]

Aside from the rudder, the aircraft mass moments of inertia in different axes as well as the fuselage geometry also play an important role in spin recovery characteristics. [10]

5.5.3.3 Angle of Attack during Spin

The angle of attack during a spinning motion is measured experimentally and usually lies between 30 and 60 degrees, depending upon the type of aircraft. [10] Since we did not have access to extensive experimental facilities, the assumption is that the angle of attack during spin will be:

$$\alpha_{spin} = 40^{\circ}$$

This assumption is based on data from a comparable aircraft.

5.5.3.4 Mass Moments of Inertia

Three mass moments of inertia i.e. rolling inertia (I_{xx}), yawing intertia (I_{zz}) and the product of inertia (I_{xz}) are important to determine for a spin-recovery rudder. These moments of inertia will be determined in the body-axis coordinate system using CFD, and then in the wind-axis coordinate system using a transformation matrix related to the spin angle of attack:

$$\begin{bmatrix} I_{xx_w} \\ I_{zz_w} \\ I_{xz_w} \end{bmatrix} = \begin{bmatrix} \cos^2 \alpha_{spin} & \sin^2 \alpha_{spin} & -\sin 2\alpha_{spin} \\ \sin^2 \alpha_{spin} & \cos^2 \alpha_{spin} & \sin 2\alpha_{spin} \\ \frac{1}{2}\sin 2\alpha_{spin} & -\frac{1}{2}\sin 2\alpha_{spin} & \cos 2\alpha_{spin} \end{bmatrix} \begin{bmatrix} I_{xx_B} \\ I_{zz_B} \\ I_{xz_B} \end{bmatrix}$$

Subscripts "B" and "w" denote the moments of inertia about body-axes and wind-axes respectively. This transformation is necessary because, during a spin, the aircraft is no longer rotating around its own axes, but it is being rotated by the wind. [10] Now, our CFD yielded these values:

$$\begin{bmatrix} I_{xx_B} \\ I_{zz_B} \\ I_{xz_B} \end{bmatrix} = \begin{bmatrix} 1.23 \\ 2.00 \\ 0.02 \end{bmatrix}$$

Consequently,

$$\begin{bmatrix} I_{xx_w} \\ I_{zz_w} \\ I_{xz_w} \end{bmatrix} = \begin{bmatrix} 1.5284 \\ 1.7016 \\ -0.3757 \end{bmatrix}$$

5.5.3.5 Desirable Rate of Spin Recovery ($\dot{\boldsymbol{R}}_{\mathbf{SR}}$)

Most general aviation aircraft are designed to be able to recover from a one-turn spin in no more than 3 seconds, which mandates a rate of spin recovery as follows:

$$\dot{R}_{\mathrm{SR}} = 1.4 \frac{rad}{s^2} = 80 \frac{deg}{s^2}$$

This value is standard throughout the world of commercial aviation. It is determined from the observed rate of spin for different aircraft, which lies in the 20-40 rpm or 120-240 deg/s range. [10]

5.5.3.6 Desired Counteracting Yawing Moment ($\boldsymbol{N}_{\mathbf{SR}}$)

The counteracting moment of yaw is produced by the rudder deflection, and necessary to stop the spinning maneuver in time. Its value for our UAV came out to be:

$$\boldsymbol{N}_{\mathrm{SR}} = \dot{R}_{\mathrm{SR}} \left(\frac{I_{xx_w} I_{zz_w} - I^2{}_{xz_w}}{I_{xx_w}} \right) = 2.2529\ Nm$$

5.5.3.7 Effective Vertical Tail Area & Volume Ratio

During a spin maneuver, an aircraft with a conventional aft tail will experience wake from the horizontal tail influencing the performance of the vertical tail and the rudder. Thus, the effective vertical tail area (and subsequently the volume coefficient) will be less than the actual value.

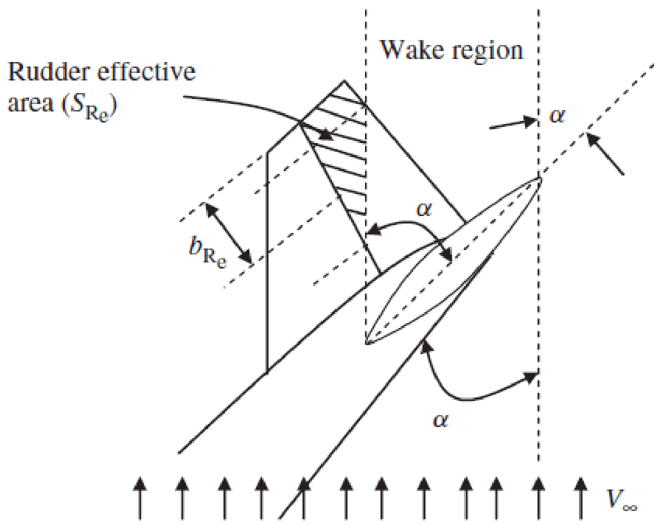

Figure 59. Rudder Effectiveness under Wake [10]

However, as our design comprises a horizontal tail that sits on top of the vertical tails, the effective vertical tail area and volume coefficient for our UAV will be the same as actual ones. Therefore,

$$S_{v_e} = S_v$$

$$\bar{V}_{v_e} = \frac{(l_v)_{opt} S_{v_e}}{b S_w} = \frac{(l_v)_{opt} S_v}{b S_w} = \bar{V}_v$$

5.5.3.8 Rudder – Vertical Tail Span Ratio (b_R/b_v)

This ratio is another important parameter to be determined as part of the process. The convention is to select a rudder to vertical tail span ratio of between 0.7 and 1. We have selected it as:

$$\frac{b_R}{b_v} = 0.8$$

5.5.3.9 Effective Rudder Span (b_{R_e})

The rudder will not be under any wake effects from the horizontal tail during spin. Therefore,

$$b_{R_e} = b_R$$

5.5.3.10 Max Rudder Deflection (δ_R)

The maximum deflection a rudder is allowed to have must be limited to avoid flow separation and its negative effects. The typical limits of deflection for rudders are 30 degrees on either side. So,

$$\delta_R = \pm 30°$$

It is the convention to take rudder deflection to the left (of the pilot) as positive and negative if it is towards their right. This value is used as a benchmark for optimizing our rudder design. If the calculated max deflection exceeds this value, the rudder needs to be redesigned.

5.5.3.11 Rudder – Vertical Tail Chord Ratio (C_R/C_v)

As with the span ratio, the chord ratio between the rudder and the vertical tail has a typical range of values (between 0.15 and 0.4) out of which, we have selected this for our rudder:

$$\frac{C_R}{C_v} = 0.3$$

This ratio will also be used for validation of our rudder design. If the calculated value exceeds 0.5 (meaning that the rudder covers more than half of the chord of the tail), then it is better to use a fully rotating vertical tail i.e. the rudder and the tail will be the same. [10]

5.5.3.12 Rudder Angle of Attack Effectiveness (τ_R)

This parameter is a function of the rudder – tail chord ratio and it measures the contribution of rudder size towards the effectiveness of rudder control. It is ascertained from a graph of observed values between itself and the chord ratio.

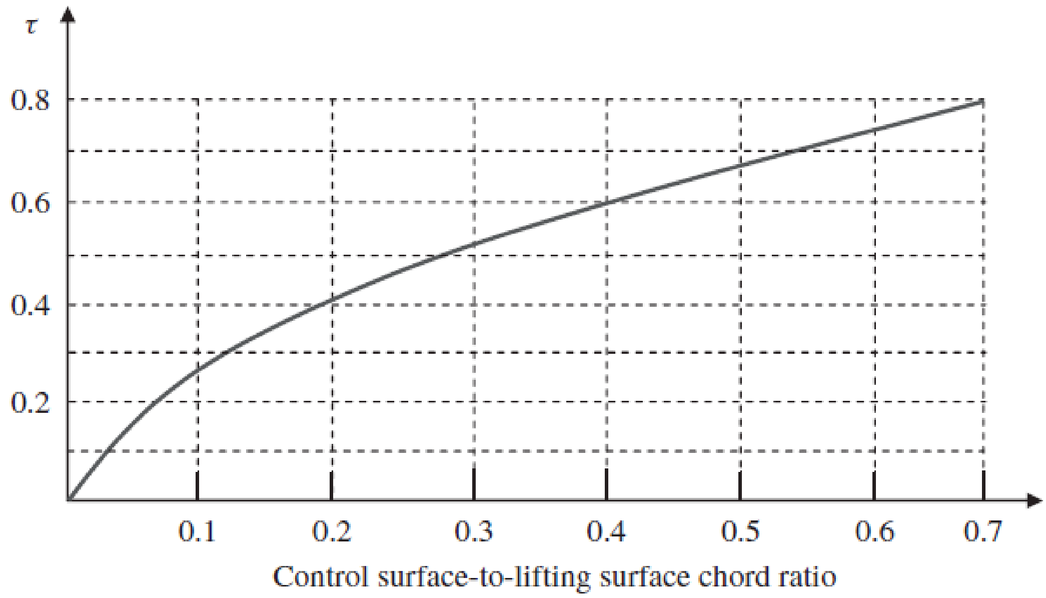

Figure 60. Elevator effectiveness to elevator chord ratio graph [10]

Our rudder has the following effectiveness:

$$\tau_R = 0.525$$

5.5.3.13 Rudder Control Derivative ($C_{n\delta R}$)

It is the directional control derivate, or the yawing moment coefficient due to rudder deflection derivative. It is also called the rudder yaw control power. Basically, this derivative tells us how fast or slow the yawing rate will become in response to increasing or decreasing the rudder deflection. It is expressed as follows: [10]

$$C_{n\delta R} = -C_{L_{\alpha_{v_{3-D}}}} \bar{V}_v \eta_v \tau_R \frac{b_R}{b_v} = -0.1609356 \frac{1}{rad}$$

5.5.3.14 Optimization

Now, we shall calculate the max rudder deflection from other relations to verify that our design is correct. The desired counteracting yawing moment (previously found) is also given by:

$$N_{\mathrm{SR}} = \frac{1}{2} \rho V_s{}^2 S_w b_w C_{n\delta R} \delta_R$$

Therefore,

$$\delta_R = \frac{2N_{\mathrm{SR}}}{\rho {V_s}^2 S_w b_w C_{n\delta R}} = -0.1167875\,rad = -6.69°$$

Considering that this above value is well within the maximum deflection specified earlier, rudder design is acceptable for spin recovery and there is no need for optimization.

5.5.3.15 Summary of Parameters

Table 21. Rudder parameters

Rudder Parameter	Value
b_R	$0.408\,m$
C_R	$0.07\,m$
S_R	$0.02856\,m^2$
$\delta_{R_{max}}$	$\pm 30°$
Required δ_R	$\pm 6.69°$

5.6 Vertical Take-Off and Landing

Thus far in detailed design, we have concerned ourselves with the cruise regime of the flight, in which the UAV functions like an ordinary fixed-wing aircraft. It is now time to go over the details of the takeoff and landing stages of flight, which will be carried out by the UAV working like a quad-rotor drone.

Required thrust must be greater than the takeoff weight, otherwise the UAV will simply not lift itself off the ground. The question of how much greater is answered by observing trends of comparable UAVs. The MTOW of our UAV had already been calculated in section **4.2.4: Final Estimate of MTOW** which is:

$$W_{MTOW} = 11.892\ kg$$

For general applications, quad-rotor drones should have a thrust-to-weight ratio of 1.5 - 1.9 [36]. We have selected a thrust-to-weight ratio of 1.5. This is to allow the motor(s) carry the UAV to a sufficient altitude.

Therefore,

$$Thrust\ Required = 1.5 \times Weight$$

If one motor is to be used for each propeller, each motor must be able to produce:

$$Thrust\ Required\ per\ motor = \frac{Thrust\ Required}{4}$$

$$Thrust\ Required\ per\ motor = 4.4595\ kg$$

Based on the power requirement, Gartt ML 5210 340 KV is selected. It has a maximum thrust of 4.620 kg which is greater than our requirement [37]. We intentionally selected a slightly more powerful motor for future design precautions and considerations.

5.7 CG Balancing (Theoretical)

Once all the avionics were finalized in the design, we created a very detailed CAD model of the aircraft in Solidworks including the geometry and weight of each individual avionics component to establish the resulting position of the CG for the whole assembly. The target with this step was to conform to the location of CG as prescribed by the static margin calculation (See **Section 6.5.1 Aerodynamic Stability Analyses**). The next step was to align the VTOL motors in such a way that the lines joining them in a cross would intersect precisely at the CG.

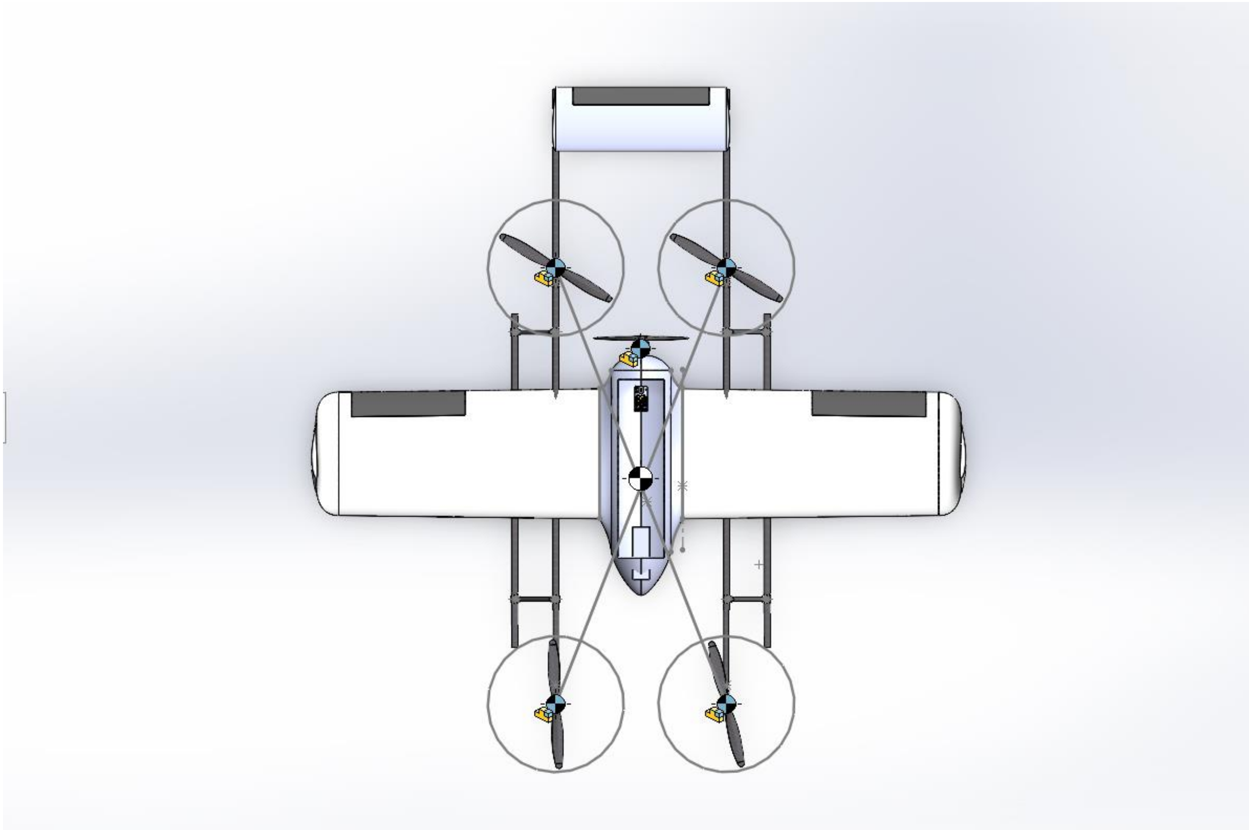

Figure 61. CG Balancing with motors

Thus, the complete assembly became balanced when in a neutral position on the ground (disarmed or ready to takeoff).

5.8 Final Iteration Parameters

In the very first iteration, we were facing a major problem with the MH-114 airfoil. The issue was that the coefficient of pitching moment was unacceptable. Because of this, the design dimensions of the tailplane were increased, which itself increased the optimum tail arm. Thus, CG balancing was becoming a problem because of the weight distribution leaning towards the back.

Another problem was our assumption regarding the weight of the airframe. We considered it as being 60% of the MTOW which turned out to be unrealistic, since we observed a 4kg difference in the parametric analysis and markedly different dimensions of structural components as compared to the preliminary design.

We resolved the issue in two ways:

- We created a CAD model in Solidworks and evaluated it with the relevant materials to obtain a reference weight of the airframe. Using this weight, we reached the final set of parameters through several iterations.
- Using the dimensions from iteration 1, we estimated the weight of the airframe for multiple other iterations by parametric analysis in MATLAB. (See **Section 12.7 Airframe Weight Calculation**)

5.8.1 Wing Design

Table 22 Final Iteration Wing Parameters

Parameter	**Value**
Airfoil	MH-116
S	0.7674 m^2
AR	4
λ	0.95
Λ	0
Γ	0
$\alpha_{t,w}$	0
$\alpha_{i,w}$	4.5
$Cl_{\alpha_{w,2-D}}$	6.0620
$Cl_{\alpha_{w,3-D}}$	4.0893
$Cl_{c_{req,2-D}}$	0.5265
$Cl_{c_{req,3-D}}$	0.5542
Cl_i	0.6158
b_w	1.752 m
$\overline{C_w}$	0.4271 m
$C_{root,w}$	0. 4380 m

$C_{tip,w}$	0.4161 m

Table 23 Final Iteration Winglet Parameters

Parameter	**Value**
$\gamma_{winglet}$	0.4
$\alpha_{cant,winglet}$	90º
$b_{winglet}$	0.137 m
$C_{root,winglet}$	0. 4161 m
$C_{tip,winglet}$	0.1664 m

5.8.2 Tail Design

The final parameters regarding the tails were under a lot of influence from the change in MTOW of the aircraft and, subsequently, the change in parameters of the wing. Therefore, they are slightly different from those obtained in the earlier stages of design.

Table 24 Horizontal Tail Parameters

Parameter	**Value**
$\bar{V}_H$	0.45
$(l_h)_{opt}$	1.2936 m
S_h	0.1404 m^2
Airfoil	NACA 0009
Λ_h	0°
Γ_h	0°
AR_h	2.6667
λ_h	1
i_h	$-1.9307°$
b_h	0.5734 m
$C_{tip,h}$	0.2150 m
$C_{root,h}$	0.2150 m
$\overline{C_h}$	0.2150m
Cl_h	-0.2662

Table 25 Vertical Tail Parameters

Parameter	**Value**
$\bar{V}_v$	0.14
$(l_v)_{opt}$	1.2936 m
S_v	0.1574 m^2
Airfoil	NACA 0010
Λ_v	0°
Γ_v	0°
AR_v	1.5
λ_v	1
i_v	0°
b_v	0.4858 m
$C_{tip,v}$	0.2150 m
$C_{root,v}$	0.2150 m
$\overline{C_v}$	0.2150 m

5.8.3 Propulsion Design

Because of the significant change in the weight of the drone in final iterations, the Power Loading was also decreased significantly, and it was also necessary to change the choice of the cruise motor according to the new power loading requirements. Of course, we have added factor of safety for safe maneuverers in adverse flight conditions.

Parameter	**Value**
P_{dp}	500.2896 W
D_p	0.2741 m = 10.79 in
${V_{tip}}_{static}$	249.4951 m/s
ω	17383 rad/s
Motor Selection	T Motor AT4125 KV 540

5.8.4 Fuselage Design

As a result of iterative changes in the wing design, we optimized the fuselage design to use three airfoils MH-114, MH-115 and MH-116 instead of MH-112, MH-113 and MH-114 as stated for the first iteration. The final design of the fuselage we also iterated aerodynamically using CFD analysis to perform better aerodynamically. The final design has less drag than its first iteration counterpart.

The final rendition of the fuselage is illustrated in **Figure 62**.

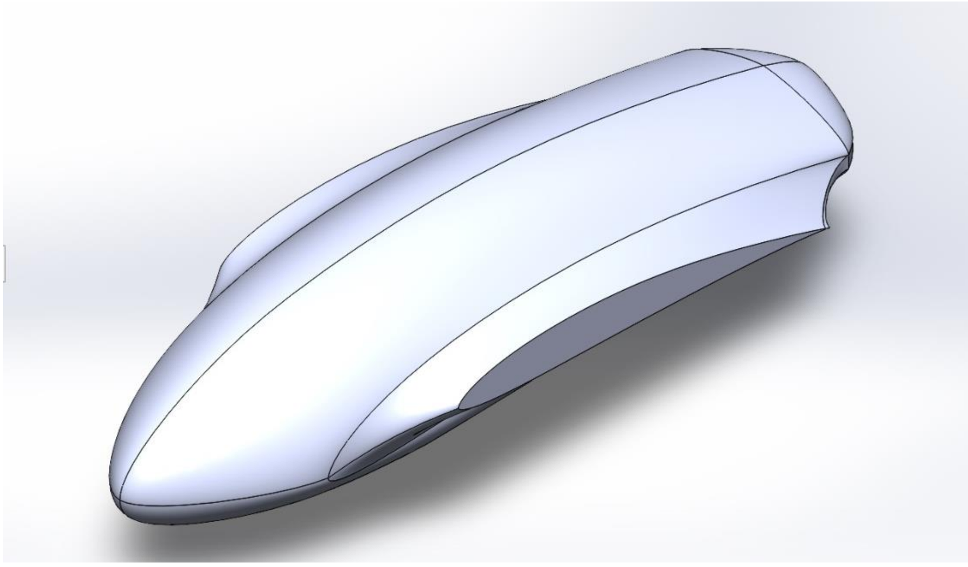

Figure 62. Finalized Fuselage Design

5.8.5 Design of Control Surfaces

The control surfaces also underwent dimension changes throughout the multiple iterations of wing and fuselage design. The MATLAB codes used to obtain these final control surface parameters can be found in sections **12.8**, **12.9** and **12.10** respectively, under **APPENDIX I: MATLAB CODES**.

Table 26 Final Aileron Parameters

Parameter	**Value**
S_A	0.0325 m^2
b_A	0.382 m
C_A	0.085 m
$\delta_{A_{max}}$	±20°

Table 27 Final Elevator Parameters

Parameter	**Value**
S_E	0.0275 m^2
b_E	0.458 m
C_E	0.06 m
δ_{Emax}	±15°

Table 28 Final Rudder Parameters

Rudder Parameter	**Value**
S_R	0.0126 m^2
b_R	0.1943 m
C_R	0.0647 m
δ_{Rmax}	$\pm 30°$
δ_R	$\pm 5.6339°$

5.8.6 Final Estimate of MTOW:

Table 29 Final MTOW Calculation

Part Name	Qty.	Weight	Total Weight
TATTU 6S 22.2V 10000 mAh Li-Po Battery	1	1352g	1352g
T-Motor AT4125 (540 KV) Long Shaft BLDC (Cruise Motor)	1	355g	355g
Gartt ML5210 (340 KV) 4.6 kg Thrust BLDC Motor (VTOL Motor)	4	230g	920g
Hobbywing Skywalker 80A ESC (Cruise)	1	82g	82g
Hobbywing X-Rotor 40A ESC (VTOL)	4	26g	104g
Gemfan 15x8 Nylon Propeller (Cruise)	1	47g	47g
18x5.5 Carbon Fiber Propeller (VTOL)	4	44g	176g
Flight Controller Kit: Holybro Pixhawk 5X + Baseboard + Power Module + M8N GPS + Power Distribution Board (PDB) + Cables	1	120g	120g
Radio Receiver: FlySky FS-iA10B Receiver	1	20g	20g
Servo: Tower Pro SG-90	5	9g	9g
Telemetry: Holybro SiK Telemetry Radio V3	1	15g	15g
UBEC	1	11g	11g
Misc.	-	150g	150g
Payload	1	1500g	1500g

Airframe (Theoretical)	1	2050g	2050g
Airframe (Experimental)		2960g	2960g
Total (Theoretical)		6911g	6911g
Total (Experimental)		7821g	7821g

5.8.7 Endurance

Because the first iteration gave an incorrect value of empty weight of aircraft, we installed a 5000 mAh battery in the UAV. However, later stages of design reduced the MTOW to such an extent that we felt comfortable installing a larger capacity battery so that we could increase the maximum flight time of the aircraft. Therefore, the final MTOW includes a 10000 mAh battery, more than double the capacity of the previous one.

CHAPTER 6: ANALYSES

The preliminary and detailed stages of design produced dimensional constraints and parameters around which we have designed the UAV. Also taken into consideration were the materials and manufacturing processes available locally. This chapter is concerned with the Finite Element & CFD Analyses of major components in the aircraft's structure.

6.1 Fuselage

The fuselage is an empty composite shell made of 1 mm thick composite fabric. It is a two-part component with both parts seamlessly blending from the top and bottom of the wing. It is to carry avionics and electronics components such as the battery, airspeed sensor, GPS module, radio receiver, flight controller etc. The battery fits snugly at the front of the fuselage in a dedicated slot. The positioning of the battery is influenced by the necessity to keep the CG as close to the front as possible in order to counterbalance the moment(s) generated by the tail.

6.1.1 CFD Analysis

The fuselage was designed from the beginning to contribute somewhat to the total lift generated by the UAV. Its profile is borne of multiple airfoils, with the ones at the ends being the same as that of the wing. Several iterations were required to reach a point where the fuselage was producing a sufficiently low amount of drag. The analysis was performed in Solidworks and the UAV was simulated in an airstream of 17 m/s, which is its maximum attainable velocity in stable forward flight.

Table 30 Results of Fuselage CFD Analysis

Goal Name	Unit	Value	Averaged Value	Min Value	Max Value
Lift	N	1.069	1.059	1.015	1.085
Drag	N	-0.634	-0.638	-0.642	-0.633

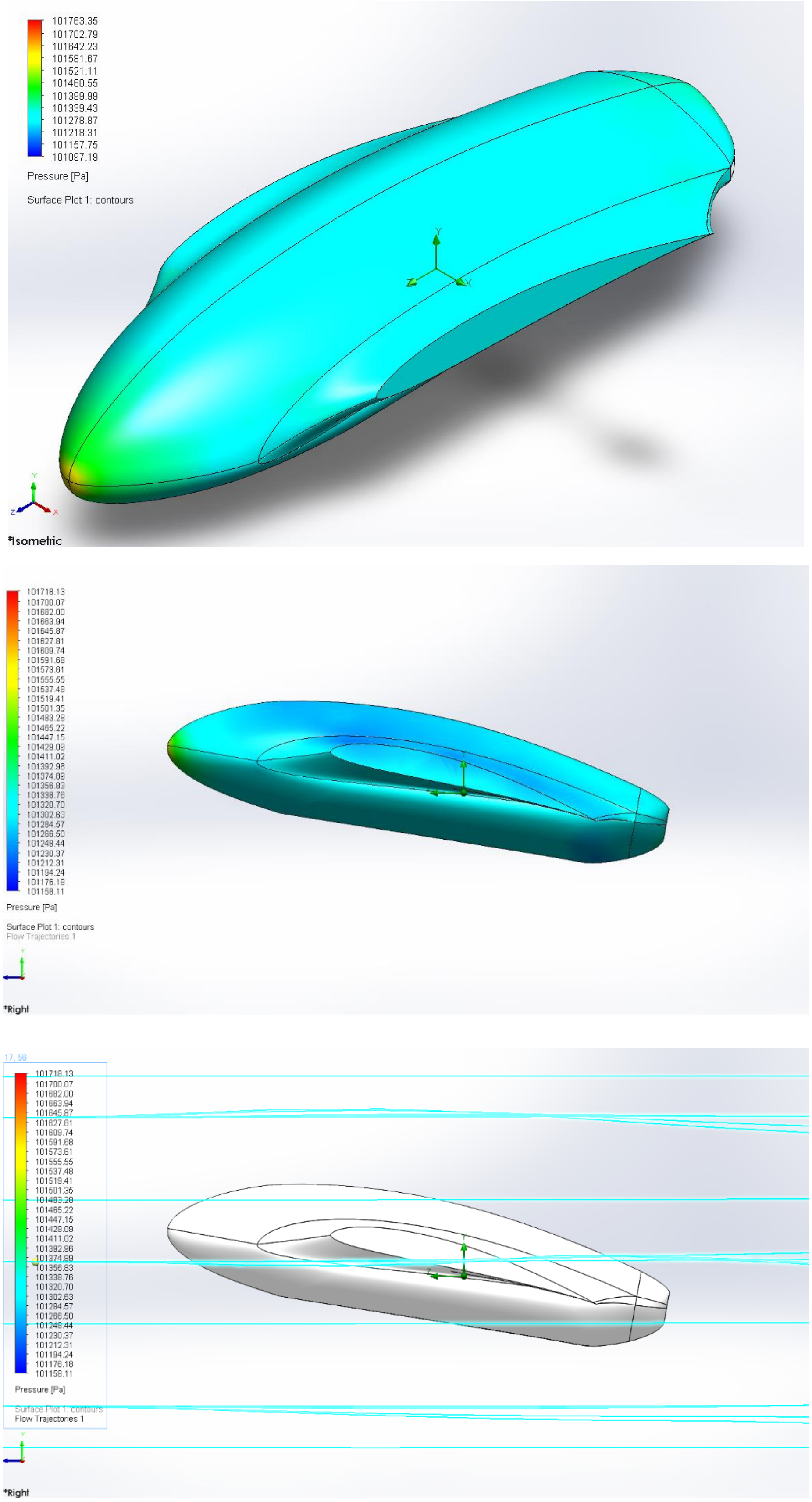

Figure 63. CFD of Fuselage

6.2 Wing & Winglets

The wing is made of a composite skin wrapped around high-density styrene foam cut in the shape of the MH-116 airfoil. There are no ribs or spars used for the basis of the wing. The winglets use different airfoil at the outer ends and the wing airfoil at the ends which are affixed on both sides of the wing. They are also made of foam wedges enclosed in tight composite fiber skin. The airfoil used for each winglet is PSU 94-097.

6.2.1 Finite Element Analysis

For the FEA, we have chosen Carbon Fiber as the material and simulated the left half of the wing under a distributed load of 180 N. Span-wise aerodynamic loads have been neglected for the sake of simplicity in the analysis. It should be stressed that the FEA is for the wing only and does not include the winglets, again for simplicity. The FOS is 2 according to the given load but overall FOS is much higher, and the mesh quality used was extremely fine.

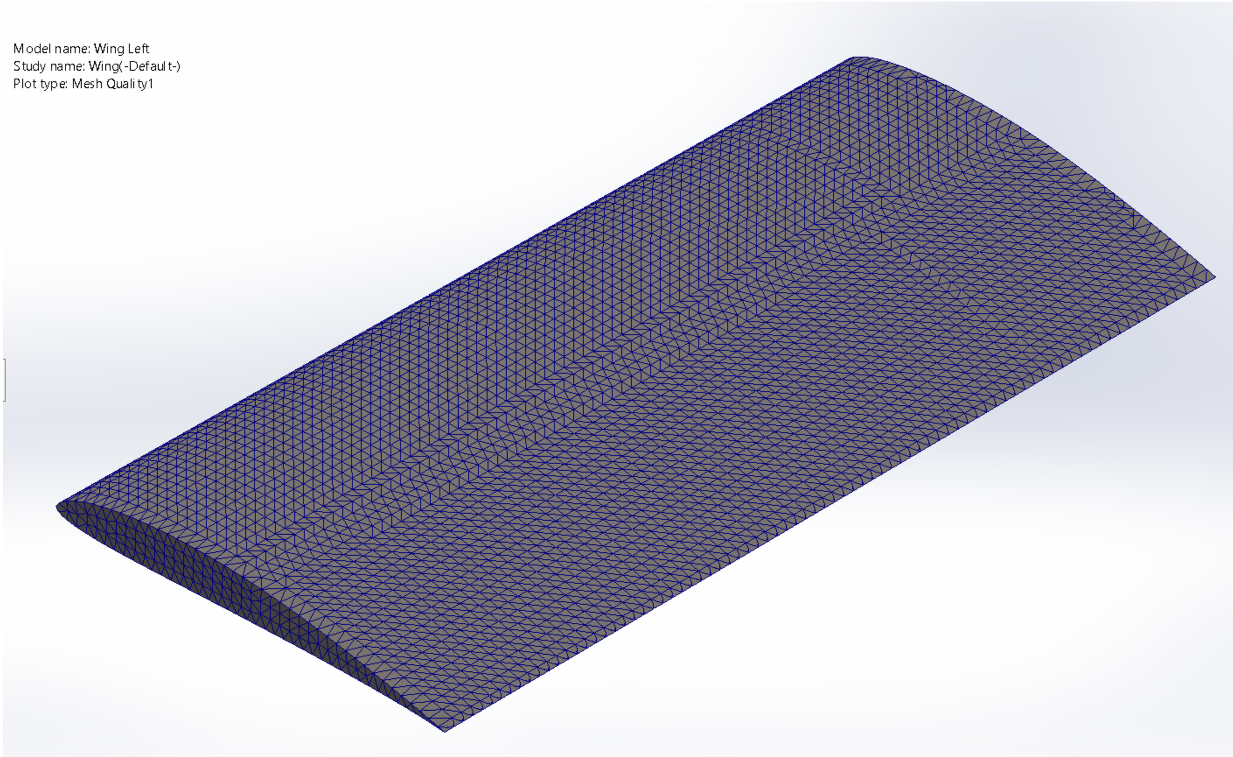

Figure 64 Wing Structured Mesh

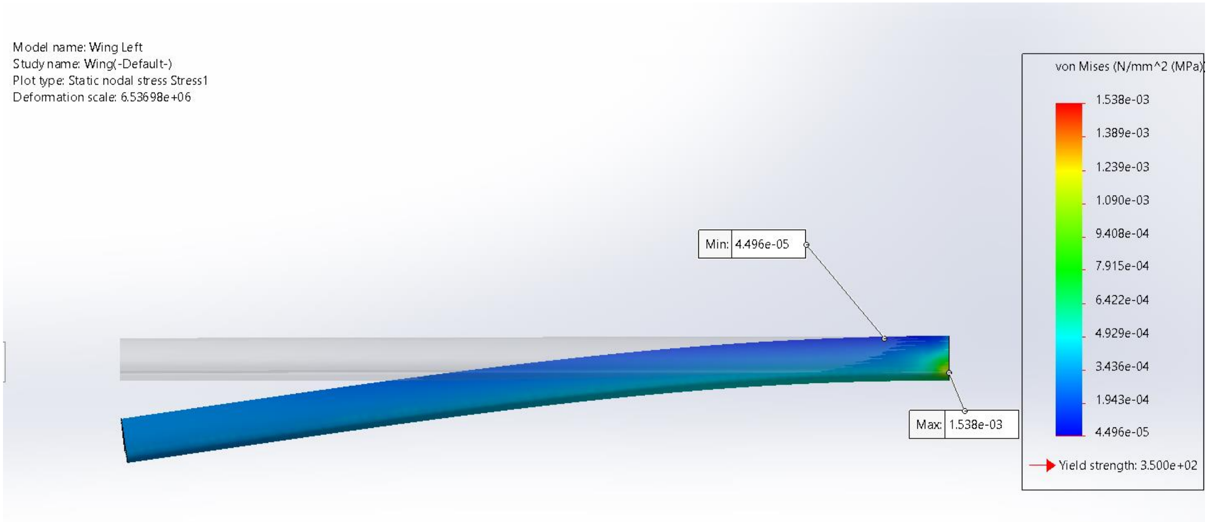

Figure 65. FEA of wing (from aft)

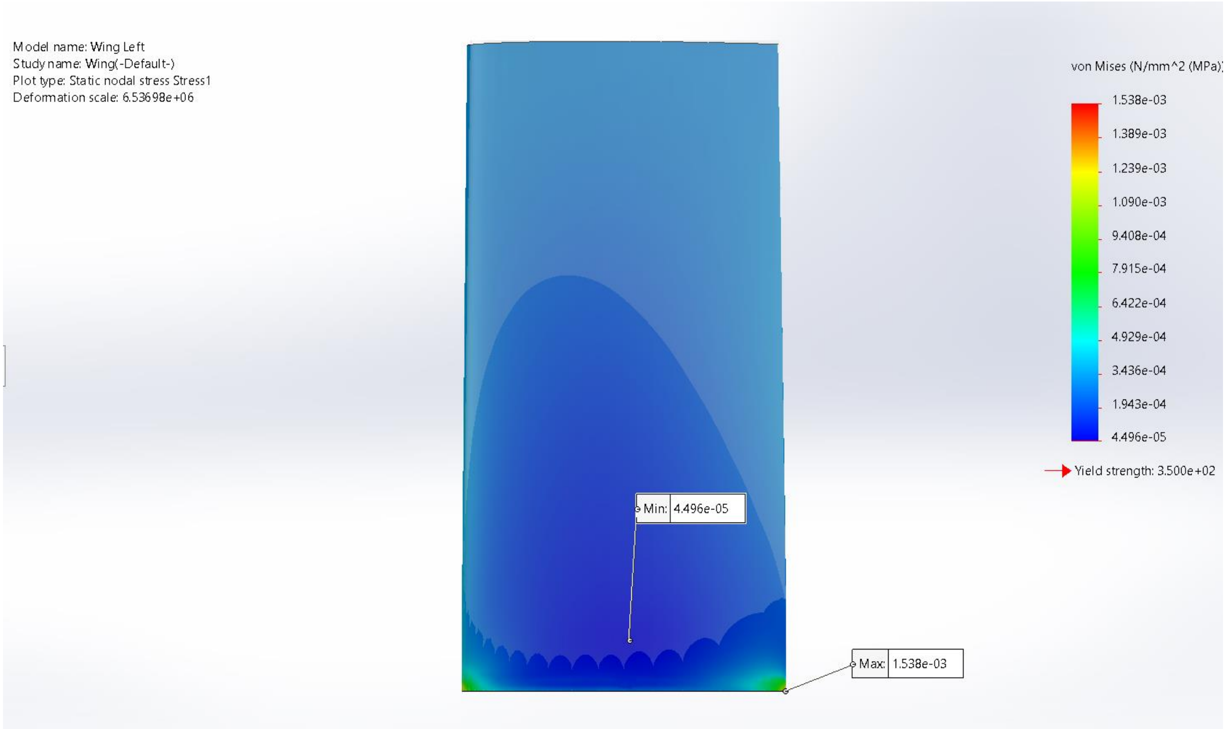

Figure 66. FEA of wing (from top)

6.3 Booms

There are two booms that run under the wing and extend to its front while providing the support for the complete tailplane. The booms are hollow and made of Carbon Fiber. They are attached under the wing and the vertical tails via adhesion with super glue and Carbon dust. The booms also carry the mounts for the 'vertical' 4 motors and 4 propellers. Thus, they undergo bending stresses in the aircraft.

6.3.1 Finite Element Analysis

Finite Element Analysis of booms was carried out in SolidWorks and was based on the tail load and the motor/propeller loads only. The results are visible in **Figure 67** and **Figure 68**.

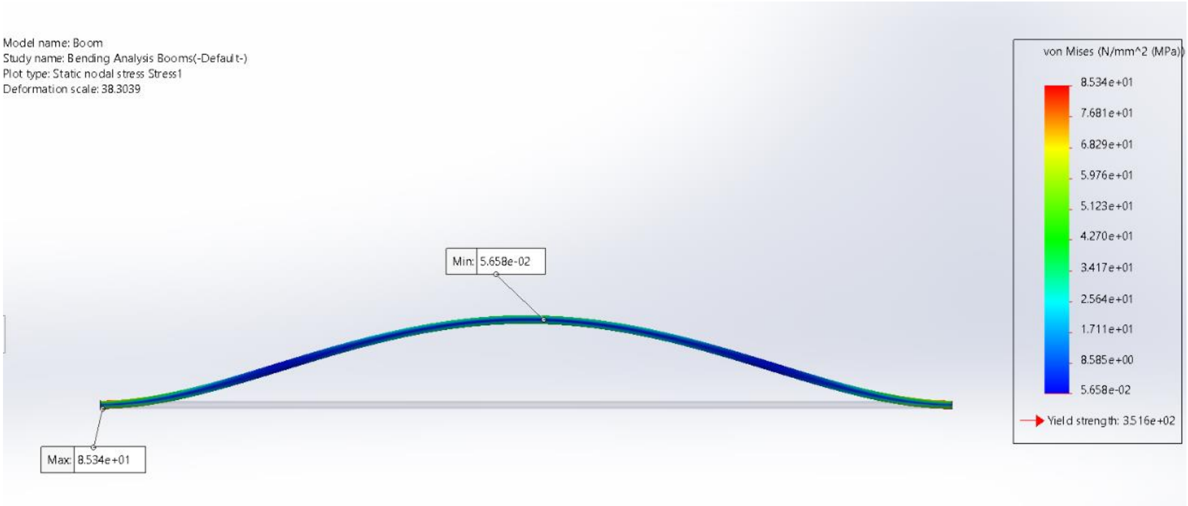

Figure 67. FEA of boom (side view)

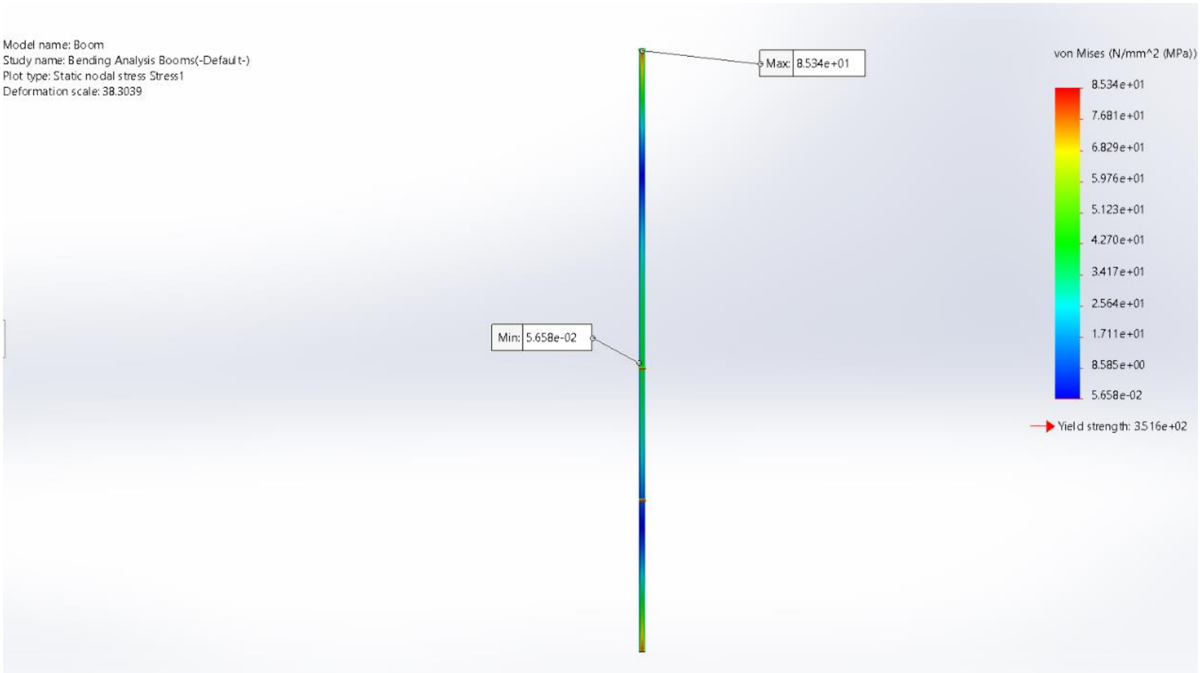

Figure 68. FEA of boom (top view)

6.4 VTOL Motor Mounts

Since it would not be possible to fit the VTOL motors directly to the booms, we designed special mounts for them and had the mounts 3d printed. The material of choice was PLA (Poly Lactic Acid), owing to its ease of use, greater availability, and lower cost. The mounts have been designed to press fit onto the composite booms.

The maximum von Mises stress occurring in the mount is a little more than 7 MPa which is comfortably within the strength of the material i.e., PLA. The conclusion, therefore, is that these motor mounts are fit to bear the loads applied to them.

6.4.1 Finite Element Analysis

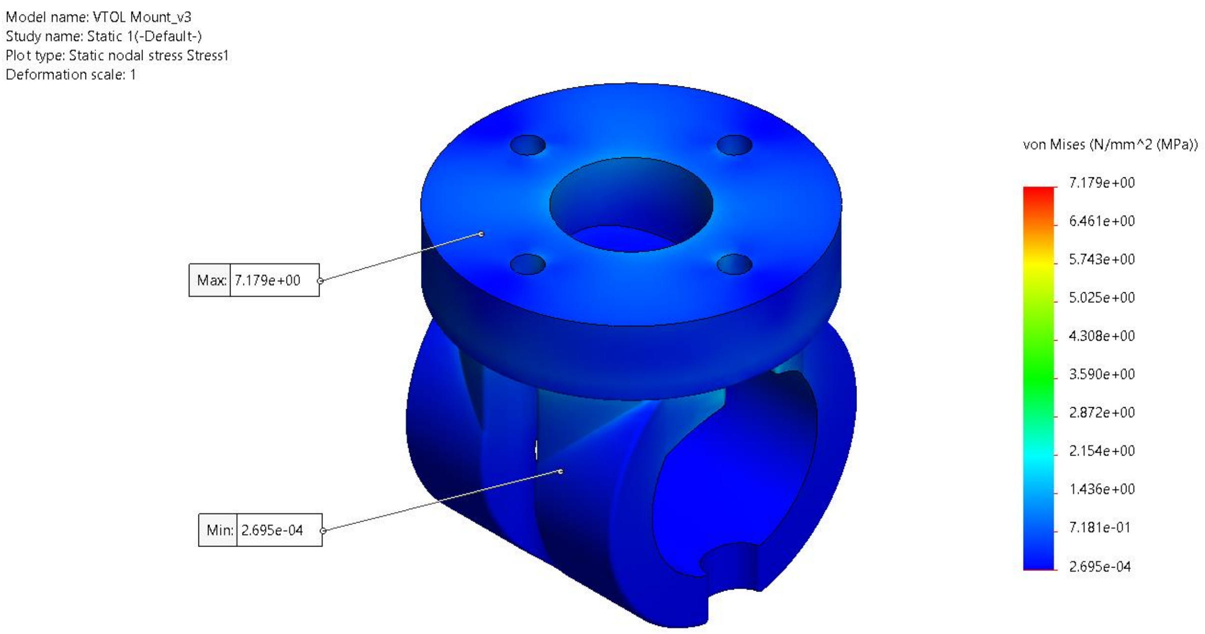

Figure 69. FEA of motor mount (isometric view)

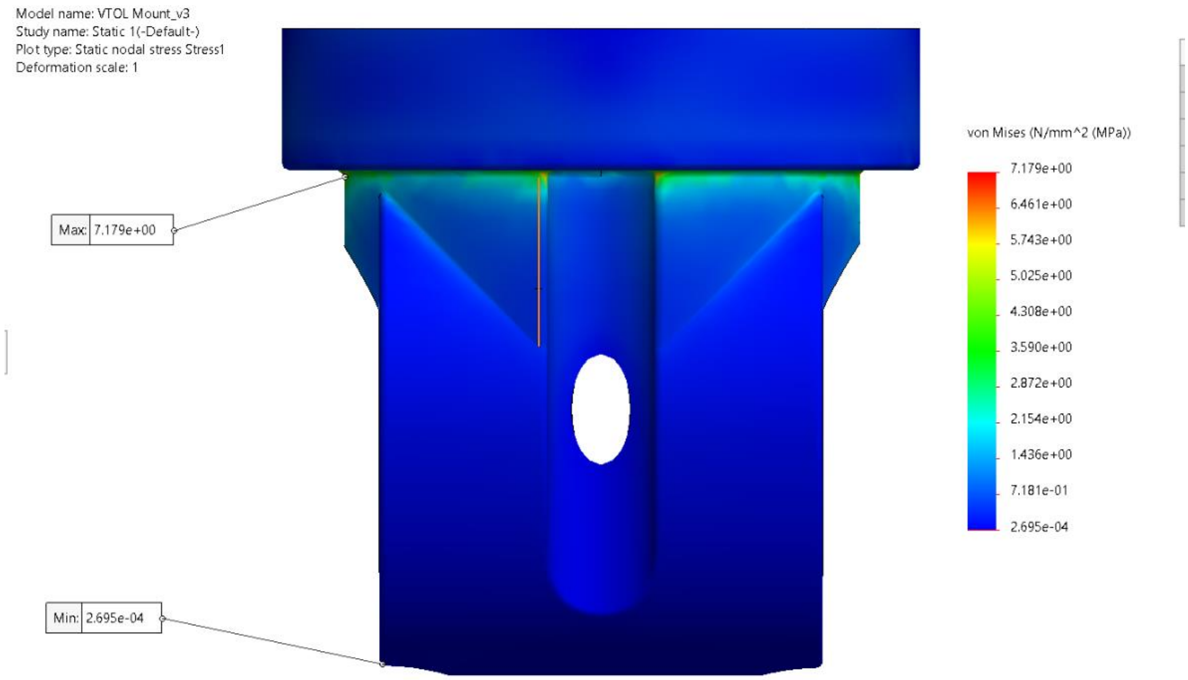

Figure 70. FEA of motor mount (front view)

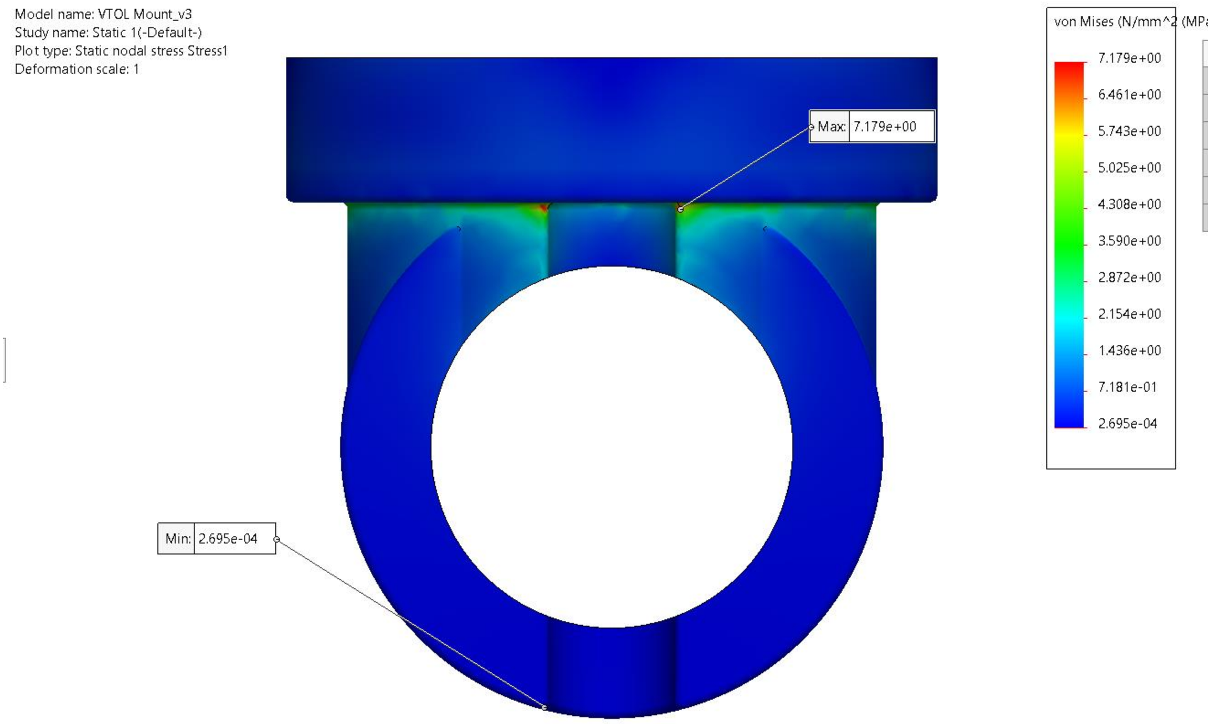

Figure 71. FEA of motor mount (side view)

6.5 Wing + Tail

Aside from the structural and/or fluid analyses of major load-carrying and lift-generating components, it is also crucial to validate the stability of the aircraft in its primary axes of freedom. The UAV must have sufficient lateral and longitudinal stability to sustain level flight in cruise mode.

6.5.1 Aerodynamic Stability Analyses

From the final assembly in Solidworks, we calculated the location of the point mass of each avionics component with respect to the leading edge of the wing. The locations were imported as x, y and z points in XFLR5 as shown in **Figure 72** and **Table 31**. By adding these points masses, the software determines the CG location and the stability of the drone.

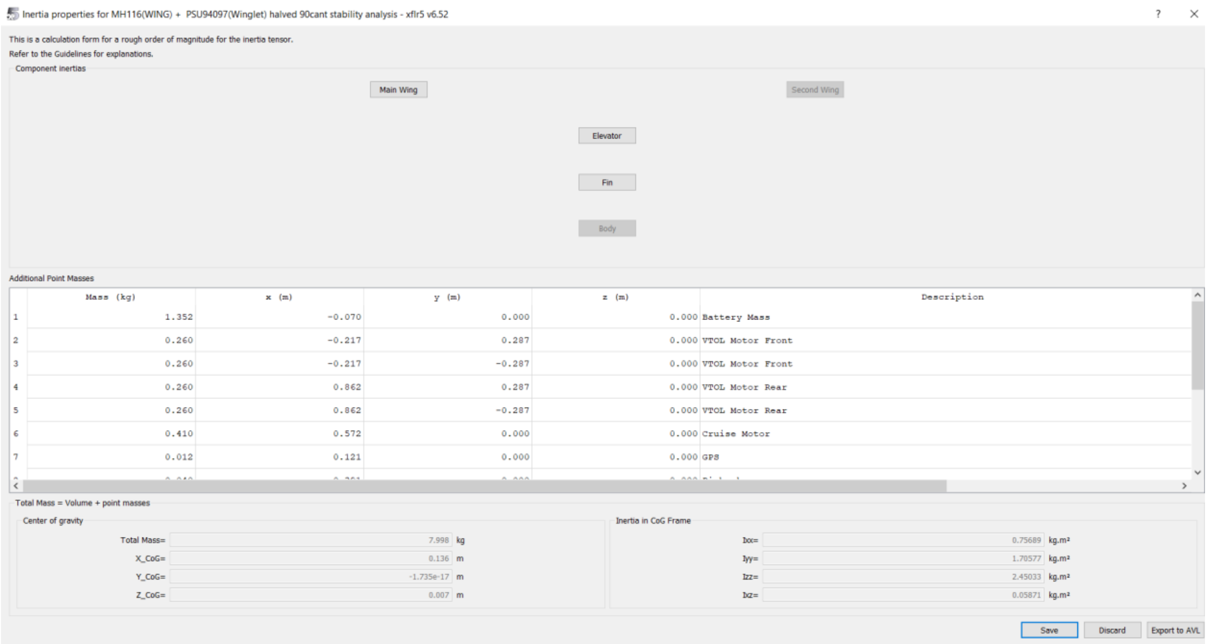

Figure 72. Component locations in XFLR5

Table 31 Component locations in XFLR5

Mass (kg)	x (m)	y (m)	z (m)	Description
1.352	-0.070	0.000	0.000	Battery Mass
0.260	-0.217	0.287	0.000	VTOL Motor Front
0.260	-0.217	-0.287	0.000	VTOL Motor Front
0.260	0.862	0.287	0.000	VTOL Motor Rear
0.260	0.862	-0.287	0.000	VTOL Motor Rear
0.410	0.572	0.000	0.000	Cruise Motor
0.012	0.121	0.000	0.000	GPS
0.040	0.391	0.000	0.000	Pixhawk
0.4	0.255	0.000	0.000	Fuselage
0.297	0.217	0.287	0.000	Boom Left
0.297	0.217	-0.287	0.000	Boom Right
1.6	-0.432	0.000	0.000	Payload

The first thing to check is the static margin of the plane which indicates how stable is the plane in cruise. Static Margin is calculated by:

$$SM = \frac{X_{NP} - X_{CG}}{MAC_W}$$

X_{NP} refers to the location of the neutral point on which the aerodynamic pitching moment is independent of the angle of attack. As indicated by **Figure 73,** $X_{NP} = 0.179m$, MAC_W =0.427m and finally $X_{CG} = 0.136m$ from **Figure 72.**

The static margin, then, is $SM = \frac{0.179-0.136}{0.427}\ x\ 100 = 10.07\%$; a good value [38] but it will increase to 12% by shifting the VTOL motors slightly forwards during assembly of the drone.

The next stage is to investigate the pitching moment of the drone at zero angle of attack and the phugoid modes besides longitudinal and lateral behavior of the plane.

The horizontal tail was given no static incidence because it was calculated to -1 degree which can be easily balanced by using elevator deflection. As seen from **Figure 74,** a -1-degree rudder deflection produces zero pitching moment at most of the angle of attacks, but this value will be calibrated experimentally using mission planner and initial flight tests.

Finally, the longitudinal and lateral stability was checked in XFLR5 by analyzing the stability derivatives and phugoid responses as shown in **Figure 75** and by **Table 32.**

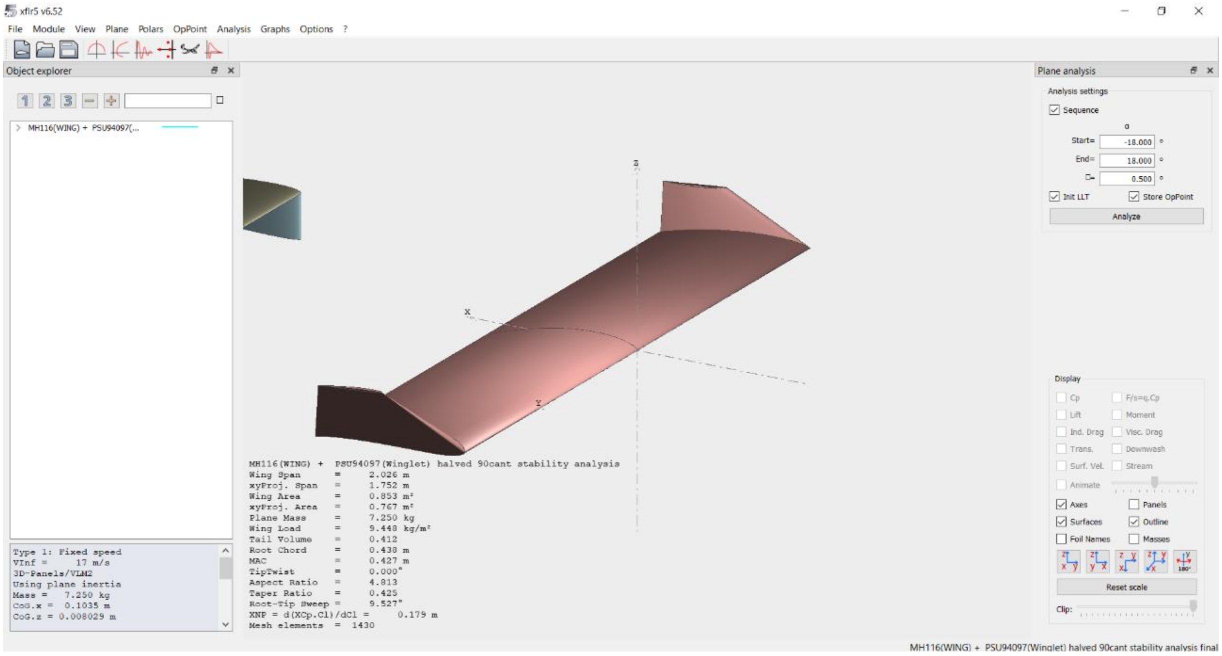

Figure 73. Location of neutral point

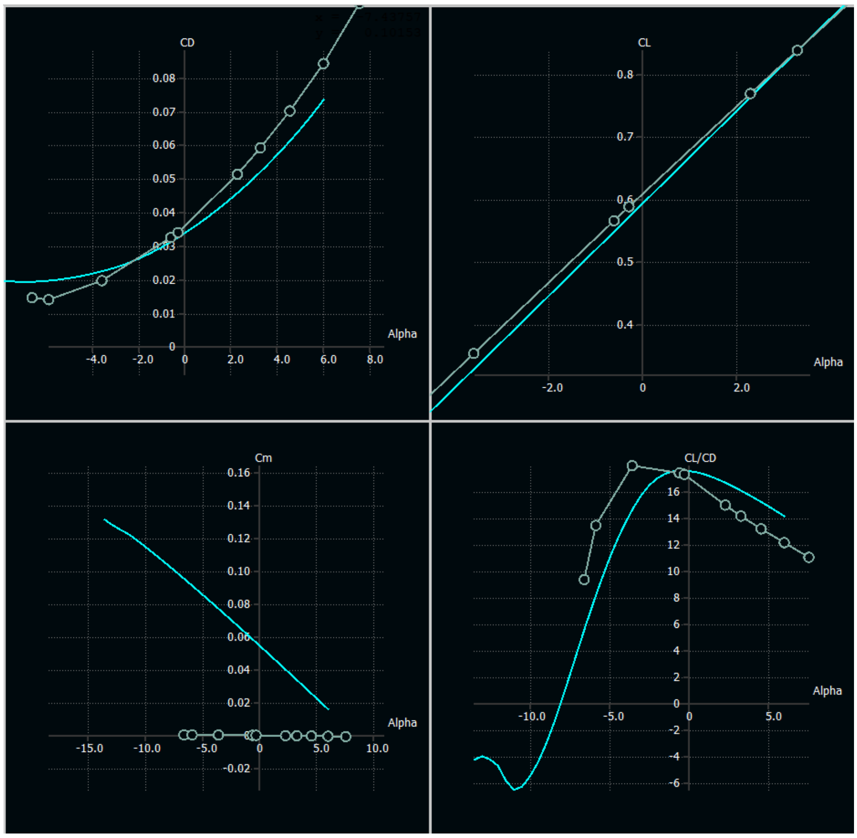

Figure 74. Stability Analysis with Elevator deflection

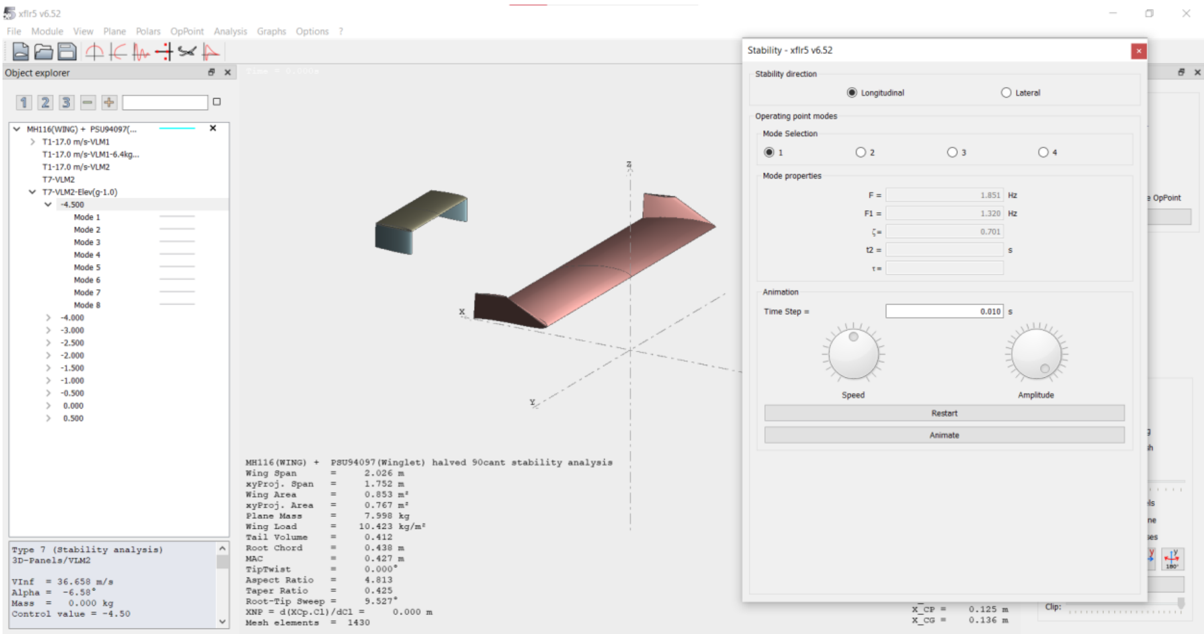

Figure 75. Longitudinal and Lateral stability in XFLR5

Table 32 Stability Derivatives

AOA	Cma	Cla	Cnb	Cyb	Clb	Cnb/Cyb (Directional)	Cma/Cla (Longitudnal)
0.5	-0.3829	4.05489	0.01914	-0.20941	-0.09711	9.139964663	9.442919537
0	-0.40507	4.15621	0.0242	-0.21466	-0.08976	11.27364204	9.74613891
-0.5	-0.40507	4.15621	0.0242	-0.21466	-0.08976	11.27364204	9.74613891
-1	-0.42866	4.19899	0.02807	-0.21953	-0.08629	12.78640732	10.20864541
-1.5	-0.49905	4.34536	0.05727	-0.24643	-0.07097	23.23986528	11.4846641
-2	-0.49905	4.34536	0.05727	-0.24643	-0.07097	23.23986528	11.4846641
-2.5	-0.49905	4.34536	0.05727	-0.24643	-0.07097	23.23986528	11.4846641
-3	-0.49905	4.34536	0.05727	-0.24643	-0.07097	23.23986528	11.4846641
-4	-0.49905	4.34536	0.05727	-0.24643	-0.07097	23.23986528	11.4846641
-4.5	-0.49905	4.34536	0.05727	-0.24643	-0.07097	23.23986528	11.4846641

Clb is zero for all values of angle of attack. This is very ideal because it indicates that the aircraft is likely to be very stable in forward flight.

CHAPTER 7: MANUFACTURING & ASSEMBLY

Initially, we did research on the materials typically used in UAV manufacturing, their characteristics, the availability of those materials and the associated processes locally. It was decided that a composite material would be used to form the surface of the wings, tails as well as the fuselage. For the internal structure of the wing (and tails), a typical setup of spars and ribs was proposed. However, this was ultimately dropped in favor of using foam as the basis because it is lightweight and easier in construction.

With regards to the composite material, Carbon Fiber was chosen instead of Glass Fiber, because it would decrease the weight of the airframe a little bit and improve performance. The cost increase was not an issue because the total was still within our allocated budget.

7.1 Principal Materials

7.1.1 Carbon Fiber

Used in:

- Wing skin
- Winglets' skins
- Fuselage shell
- Tails' skins
- Booms

The Carbon Fiber cloth we used in our UAV was of a 3k plain weave – 200 gsm specification. A plain weave CF cloth offers high fabric stability and is easier to work. It is ideal for applications where geometries are not too complex, such as in our drone. 200 gsm refers to the density of the fabric, which is moderately high considering the value.

The fabric was imported from Taiwan and is branded as TAIRYFIL TC-33 PAN-based Carbon Fiber. Physical properties are tabulated below:

Table 33. Carbon Fiber properties [39]

Property	**Value**
Number of Filaments	3000
Filament Diameter	7 µm
Yield TEX	200 g/1000m
Tensile Strength	500 Ksi
	3450 MPa
Young's Modulus	33 Msi
	230 GPa
Elongation	1.5 %
Density	1.8 g/cm^3

Since the booms are tubular structures, they were made from multiple layers of the same composite yarn by roll wrapped prepregs.

7.1.2 Styrene Foam

Used in:

- Wing body
- Winglet body
- Tails' bodies

The type of foam featured in our drone's construction is a closed-cell, high-density foam made of Styrene. It has been chosen for its high durability and less permeability, therefore allowing the internal structure of the UAV to be sufficiently rigid, simple, and lightweight. Important properties have been displayed below:

Table 34. Styrene Foam properties

Parameter	Unit	Value
Color	---	Pink
Cell structure	---	Closed, very fine
Density	kg/m^3	32-35
Compressive Strength	kPa	250-350
Thermal Conductivity @ 25 mm thickness	BTU in/ft^2 hr °F	0.1789
	W/mK	0.0258
Coefficient of Linear Thermal Expansion	mm/mK	0.07
Temperature Limits	°C	-50 to +75

7.2 Principal Processes

7.2.1 CNC Routing

Used for:

- Fuselage molds (Lasani Boards)

CNC Routing involves the same kinds of processes as milling, but at higher speeds and quick, intermittent cutting action. CNC Routers use rotational speed to make cuts and are usually able to work in three axes. They are also different in the respect that mills are used for tougher materials (metals, for example) while routers cut softer materials efficiently and precisely. [40] They are especially ideal for use with all kinds of wood.

Figure 76. A typical CNC Routing Machine [41]

7.2.2 High Intensity Laser Cutting

Used for cutting of guiding plates in the shape of airfoil(s).

Figure 77. Laser Cutting of mild steel sheet

A laser cutting machine stimulates a lasing material by electrical discharges or inside lamps which is then reflected in an internal mirror until it gains sufficient energy to form a coherent monochromatic beam of light. Additional mirrors or fiber optics focus this extremely powerful laser onto the desired work area. In addition to its high intensity, a laser beam is also very small in diameter at its narrowest point. [42] This gives very precise, high-quality cuts in the workpiece.

7.2.3 Hot Wire Cutting

Used for:

- Cutting foam for wing, tail and winglets

A hot write foam cutter has table and an arm structure that holds a wire in tension. When electricity is run through the wire, it is heated up to such an extent that it will easily cut through and sculpt pieces of foam as desired. [43] Apart from manual hot wire cutters, there are also CNC Foam Cutting machines for applications that require very accurate cutting of foam.

Figure 78. Hot Wire Foam Cutter [44]

7.2.4 Wet Layup

Used for:

- Carbon Fiber skin

Wet layup is a process in which layers of Carbon Fiber cloth are added to a mold one by one. Before that, each layer is wetted with epoxy by hand using a brush or roller (and removing excess epoxy with a scraper). Once each layer has been wetted and arranged in the mold, it is left to cure at room temperature for some time. [45] The CF cloth we have used in our UAV requires 1.5-2 hours in summer months to fully cure at room temperature.

Figure 79. Epoxy being applied to composite cloth [46]

7.3 Wings

7.3.1 Structural Description

The wing body is made of dense foam whereas the skin is Carbon Fiber. The wing has been manufactured as a single part for greater resistance to bending loads and to reduce the number of adhesive joints. There is a 95% taper on the wing. The use of foam has eliminated the need for balsa ribs and spars to form the basis of the wing. Small slots and holes are provided in the wing's skin and body for the wiring and electronics coming from the fuselage.

Running under both sides of the wing (and bonded to it via adhesion) are Carbon Fiber booms that serve as supports for the complete tail structure as well as the quadrotor "VTOL" array. Initially, these booms were supposed to penetrate the leading edge of the wing and exit out the trailing edge, but this approach was abandoned after advice from reputable vendors.

Ailerons have been cut and hinged on the trailing edge. They are controlled by rods connected to servos mounted inside the wing body.

Figure 80. Right aileron (deflected)

7.3.2 Major Components

The following are the principal components involved with or related to the wing:

- Foam (styrene) body
- Carbon Fiber skin
- Carbon Fiber booms

- Winglets
- Ailerons
- Hinges
- Control rods
- Servos

7.3.3 Fabrication

To form the basis of the wing, the foam had to be cut very precisely in the shape of the MH-116 airfoil. This was accomplished by using a hot wire cutter guided by a ‘rib’ of 1.5 mm thickness. We used a high intensity laser cutting machine on a mild steel plate to obtain the rib.

Figure 81. Cutting of airfoil-shaped plates

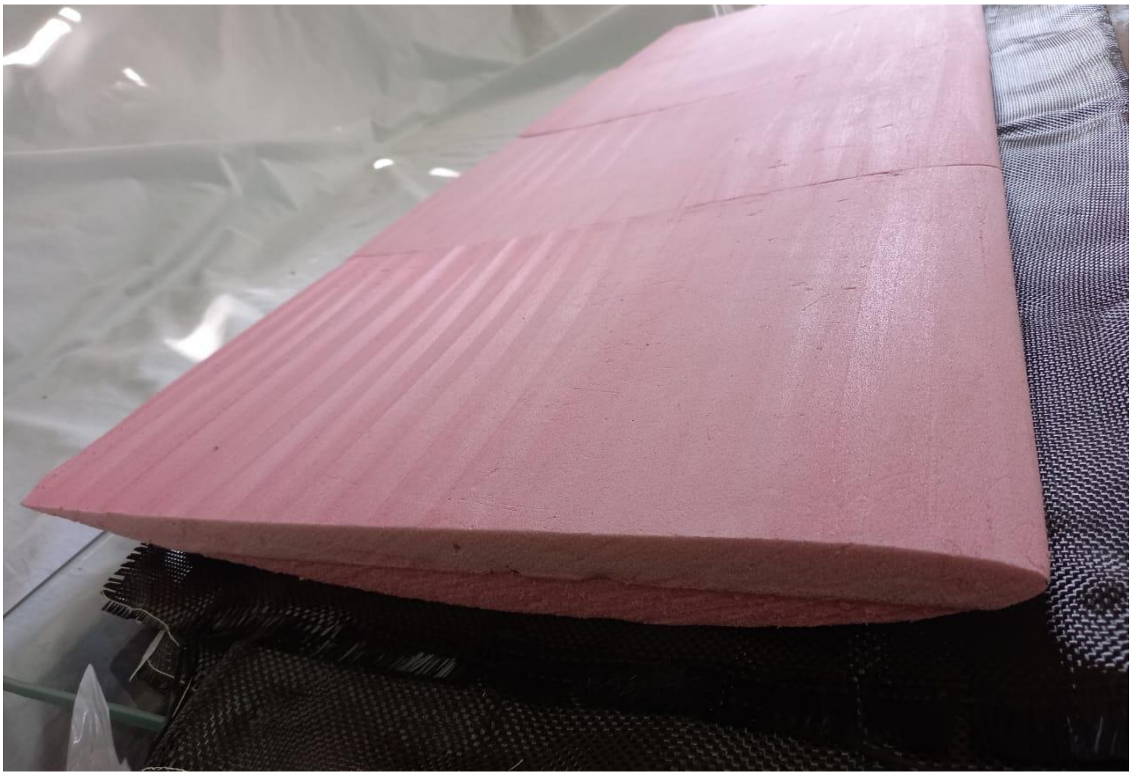

Figure 82. Side view of the foam wing (hot wire cut)

Figure 83. Measurement of wing chord

Figure 84. Measurement of wingspan

Once the foam base was ready, we applied prepregs of Carbon fabric to it and removed excess epoxy resin. The finalized wing and winglets are illustrated below:

Figure 85. Wing and winglets blended with fuselage

7.4 Winglets

7.4.1 Structural Description

The winglets follow the same structural scheme as the wings and are affixed to them via adhesion. The end of each winglet is angled at 90° to the wing surface and is itself airfoil shaped. The winglet structure features a well-defined curve for good aerodynamic performance.

Figure 86. Right winglet (front view)

7.4.2 Major Components

- Foam (styrene) body
- Carbon Fiber skin

7.4.3 Fabrication

As stated before, there is a definite curvature in the composition of the winglets. This manifested itself as a complex problem during manufacturing. The solution we devised was to divide the foam into small wedges (with decreasing lengths as per the profile) and arrange them so as to allow a neat curve of composite skin to form afterwards.

Figure 87. Right winglet before manufacturing

Figure 88. Both winglets before manufacturing Fuselage

7.4.4 Structural Description

The structural concept of our fuselage is that of an empty shell made of two parts bonding perfectly with each other from the top and bottom of the wing to create a smooth blended surface between itself and the wing.

The fuselage skin is made from the same Carbon Fiber skin as the wings. It is 1 mm thick. There are slots on front and back of the fuselage to allow for easy access to the avionics and payload inside. The avionics components have safety guards to prevent their movement during flight. Special mounts were installed for heavier components such as the battery and cruise motor.

Since Carbon Fiber is not Radio Frequency transparent, a special slot was made so that the antenna could be outside the body.

7.4.5 Major Components

- Carbon Fiber Shell
- Avionics

7.4.6 Fabrication

For a hollow Carbon Fiber shell, the fuselage mold had to be a wooden structure. We used high-quality Lasani boards and made the mold by CNC routing in multiple steps, which were necessitated by of the complexity of the shape and the nominal thickness of the wood. Molds for both parts of the fuselage can be seen in **Figure 89** and **Figure 90**

Figure 89 Lower side of Lasani mold for Lower part of Fuselage

Figure 90 Inside of Lasani board for Upper part of Fuselage

When the wooden molds were ready, we covered them with layers of prepreg of the same Carbon Fiber fabric as the wing. Final step in fuselage fabrication was to create slots and holes for the wiring and avionics etc.

7.5 Tailplane

7.5.1 Structural Description

The tail structure is much the same in construction to the wing. Horizontal tail and Vertical tails have foam bodies wrapped in Carbon Fiber. There is one elevator and two rudders, all actuated by control rods and servos. The horizontal tail sits inside and atop the two vertical ones, which are supported by the same boom structure that runs under the wing.

Figure 91 Tail structure (front view with servo slots showing on the insides)

Figure 92 Tail structure from the rear (control surfaces deflected)

7.5.2 Major Components

- Foam (styrene) bodies
- Carbon Fiber skins
- Carbon Fiber booms
- Elevator
- Rudders
- Control rods
- Hinges
- Servos
- Booms

7.5.3 Fabrication

All three tail pieces were obtained in a similar fashion to the wing: by hot wire cutting of foam with help of an airfoil-shaped mild steel plate cut from the laser machine and then laying up CF cloth over them. The control surfaces were then cut, and wiring was laid down along with the servos being set up.

7.6 Landing Skids

7.6.1 Structural Description

The landing skids are each a network of three of the same Carbon Fiber booms that support the tail structure and the VTOL motors. They are mounted at an angle to increase the ground area between them and provide more stability while on the ground.

Figure 93 A single skid with epoxy on joints left to dry

7.6.2 Major Components

- Carbon Fiber booms

7.6.3 Fabrication

For fabricating the network of landing skids, we notched Carbon Fiber tubes on a milling machine as shown in **Figure 94**, and then proceeded to make adhesive joints with super glue and Carbon dust. Afterwards, we glazed the still forming joints with epoxy for reinforcement.

When both skids were affixed to the main booms on the UAV, the joints were found to be lacking in rigidity and strength. Therefore, we decided to cover all the landing skid joints with Carbon Fiber cloth (after wet layup) as a tape and made the cloth smooth by sanding after it had hardened properly.

Figure 94 Notching of Booms on a Milling machine

Figure 95 Close-up of CF cloth tape on a boom

Figure 96 CF tape adjacent to a 'T' joint in the boom

Figure 97 Taping up the T-joints

Figure 98 Using scraper to wind the tape tightly

Figure 99 Taping up the T-joints

7.7 Assembly

The assembled airframe is visible in. The front top hatch is affixed in its slot with duct tape for easy removal and access to internal components, primarily the battery. It was not put on the UAV here because calibrations were still under way. The wiring is to be secured along the length of the booms and under the wing, also with duct tape.

CHAPTER 8: AVIONICS AND SOFTWARE

In this section, we will discuss the electronics/avionics components present in our UAV and the computer programs that complement those components for the proper working of the UAV.

8.1 Flight Controller and Autopilot: Pixhawk 5X and PX4

Figure 100 Pixhawk 5X with M8N GPS, Power Distribution Board and other accessories [47]

Pixhawk 5X by Holybro comes with the latest PX4 Autopilot pre-installed, triple redundancy, temperature-controlled, isolated sensor domain, delivering incredible performance and reliability. Pixhawk 5X is a high-performance module that is ideal for use by academic as well as commercial autonomous vehicles. Some of the features in device are:

- Modular flight controller with a separated IMU, FMU, and Base system connected via 100-pin and 50-pin bus connector for flexibility and high degree of customization.
- High redundancy (3 IMU and 2 Barometer sensors on separate buses, allowing parallel and uninterrupted operation even in the event of failure of a sensor).
- Temperature-controlled IMUs
- Vibration isolation system for reducing noise and ensuring highly accurate results.
- Ethernet interface for high-speed mission computer integration.
- Automated sensor calibration eliminating varying signals and temperature

- Two smart batteries monitoring on SMBus
- Additional GPIO line and 5V for the external NFC reader
- Secure element for secure authentication of the drone (SE050)
- 16- PWM servo outputs
- R/C input for Spektrum / DSM
- Dedicated R/C input for PPM and S.Bus input
- Dedicated analog / PWM RSSI input and S.Bus output
- 4 general purpose serial ports (3 with full flow control, 1 with separate 1.5A current limit, 1 with I2C and additional GPIO line for external NFC reader)
- 2 GPS ports (1 full GPS & Safety Switch Port and 1 basic GPS port)
- 1 I2C port
- 1 Ethernet port
- 100Mbps
- 1 SPI bus
- 2 CAN Buses for CAN peripheral (CAN Bus has individual silent controls or ESC RX-MUX control).
- 2 Power input ports with SMBus
- 1 AD & IO port (2 additional analog input, 1 PWM/Capture input, 2 dedicated debug and GPIO lines).
- Multicolor LED visual indicators

8.2 Radio: FlySky FS-i6X Transmitter and FS-iA10B Receiver

Figure 101 The FS-i6X Transmitter [48]

The FS-i6X is a 10-channel transmitter designed to work best with small fixed-wing, glider and helicopter models. It has proprietary AFHDS (Automatic Frequency Hopping Digital System) technology that allows for reliable communication with the receiver while consuming lower power and being less vulnerable to interference. The RF (Radio Frequency) range in which the i6X works is 2.408-2.475 GHz and it is capable of two-way data exchange with an array of sensors and servos. The transmitter has a high-quality display and comes with a very powerful firmware so that it can be used fully and easily with a vast majority of aircraft types.

The main motivation to use this transmitter in our UAV was its available number of channels i.e. 10 which is exactly how much we need to fly our aircraft in a controlled manner.

For superior security, all transmitters and receivers come with unique IDs. Once they are paired with each other, a particular transmitter or receiver will only work with that receiver or transmitter.

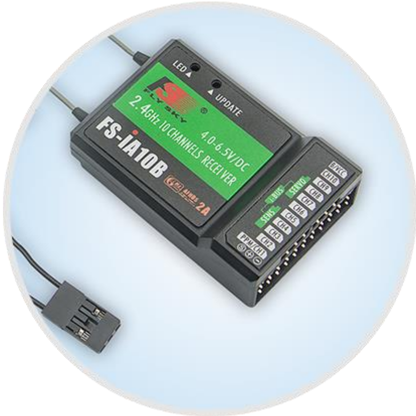

Figure 102 The FS-iA10B receiver [49]

The FS-iA10B receiver is extremely sensitive, up to -105 dBm. It has an i-BUS interface as well as one for data acquisition.

8.3 Telemetry: Holybro SiK Telemetry Radio V3

Figure 103 SiK Telemetry Radio [50]

For seamless integration with Mission Planner, it is necessary to have a telemetry radio in the UAV. Since our flight controller is from Holybro, we decided to acquire the telemetry radio from the same manufacturer. The SiK V3 has a max output power of 100 mW and a -117 dBm receive sensitivity. The air and ground radios are interchangeable, and the antennas can rotate for easy installation, thus making it ideal for our application.

8.4 Battery: TATTU 6S 22.2V 10000 mAh 25C Li-Po

Figure 104 TATTU 10000 mAh Li-Po Battery [51]

In order to meet the constraints laid out by our design, the battery had to compact and of high capacity. Furthermore, it also had to be of high-quality and durability to increase the UAVs life and retain performance over time. Taking into account all these requirements, we acquired the TATTU 6s 22.2V battery. It offers 10000 mAh of peak charge and a high discharge rate of 25C in a hard casing that measures 165*64*59 mm and weighs around 1.35 kg.

8.5 Cruise Motor: T-MOTOR AT4125 KV540 Long Shaft BLDC Motor

Figure 105 T-MOTOR 540 KV BLDC Motor [52]

Mounted at the back of the fuselage is the motor responsible for rotating the pusher propeller. For easier installation with the fuselage, a long shaft motor was desired. The AT4125 540KV brushless DC motor by T-MOTOR was ideal for the application since it provides adequate RPM to the propeller for sustained forward flight and is very reliable.

8.6 Cruise ESC: Hobbywing Skywalker 80A ESC

Figure 106 The Skywalker 80A ESC [53]

Electronic Speed Controllers are needed for better management of motor RPMs, something that is very important in UAV applications. The Hobbywing Skywalker 80A ESC is a high-quality product designed to work with continuous loads of up to 80 amps and bursts of 100 amps for up to 10 seconds. It is fully capable with a 6s Li-Po battery and programmable via different methods according to the user's needs. The ESC is good for speeds reaching 35000 RPM in case of a 12-pole BLDC motor. It has safe arming feature, overheat protection, throttle signal loss protection as well as low-voltage cutoff protection.

8.7 Cruise Propeller: Gemfan 15x8 Nylon Propeller

Figure 107 15x8 Nylon Propeller [54]

The cruise propeller has a diameter of 15 inches and a pitch of 8 inches. It was meant to be a Carbon Fiber propeller from the design stage which could not be found. Instead, we acquired a Nylon propeller which does the job equally well.

8.8 VTOL Motors: GarttML 5210 340KV

Figure 108 Gartt 340KV BLDC motor [55]

Each of the four motors used to rotate the ‘vertical’ propellers is a 340KV BLDC motor. It is compatible with a 6s Li-Po battery. The maximum continuous current for the motor is 40 amps. Each motor will be screwed to a specially designed 3d printed mount. The design has been made to reduce temperature during operation and keep performance at a maximum.

8.9 VTOL ESCs: Hobbywing X-Rotor 2-6S Li-Po 40A ESC

Figure 109 The X-Rotor 40A ESC [56]

Since each of the VTOL motors is less powerful than the one for cruise, we did not need ESCs of 80A for them. Thus, each VTOL motor gets Hobbywing’s X-Rotor Li-Po 40A ESC. It can bear a current of 60A for up to 10 seconds on top of the continuous 40A load. The ESC is programmable, has a high refresh rate, MOSFET for its integrated circuits and other useful features as well.

8.10 VTOL Propellers: 18x5.5 Carbon Fiber Propellers

Figure 110 18x5.5 CF Propellers [57]

Each propeller responsible for vertical flight is made of Carbon Fiber and has a diameter of 18 inches. Its pitch is 5.5 inches.

8.11 Connectors

We used XT 90 (90A rated) connectors for the battery and XT 60 (60A rated) connectors for the individual motors. The signal wires used JST-XH connectors, ranging from 3-pin to 8-pin types.

Figure 111 XT90 connector (male and female) [58]

Figure 112 XT60 connector (male and female) [59]

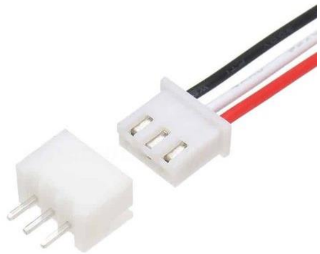

Figure 113 3-pin JST-XH connector (male and female) [60]

8.12 Servos: Tower Pro SG90 9G Mini Servo

Figure 114 SG90 Mini Servo [61]

Servos were necessary to give movement to control surfaces i.e., rudders, elevator and ailerons during flight. The Tower Pro SG90 servo is a small, 9-gram motor that is ideal for application in model UAVs and other small aircraft. It works from -30 to +60°C so temperature is not an issue for us. Its operating voltage is 3-7.2V and operating speed is 0.12 sec/60° under no load.

8.13 Wiring Diagram

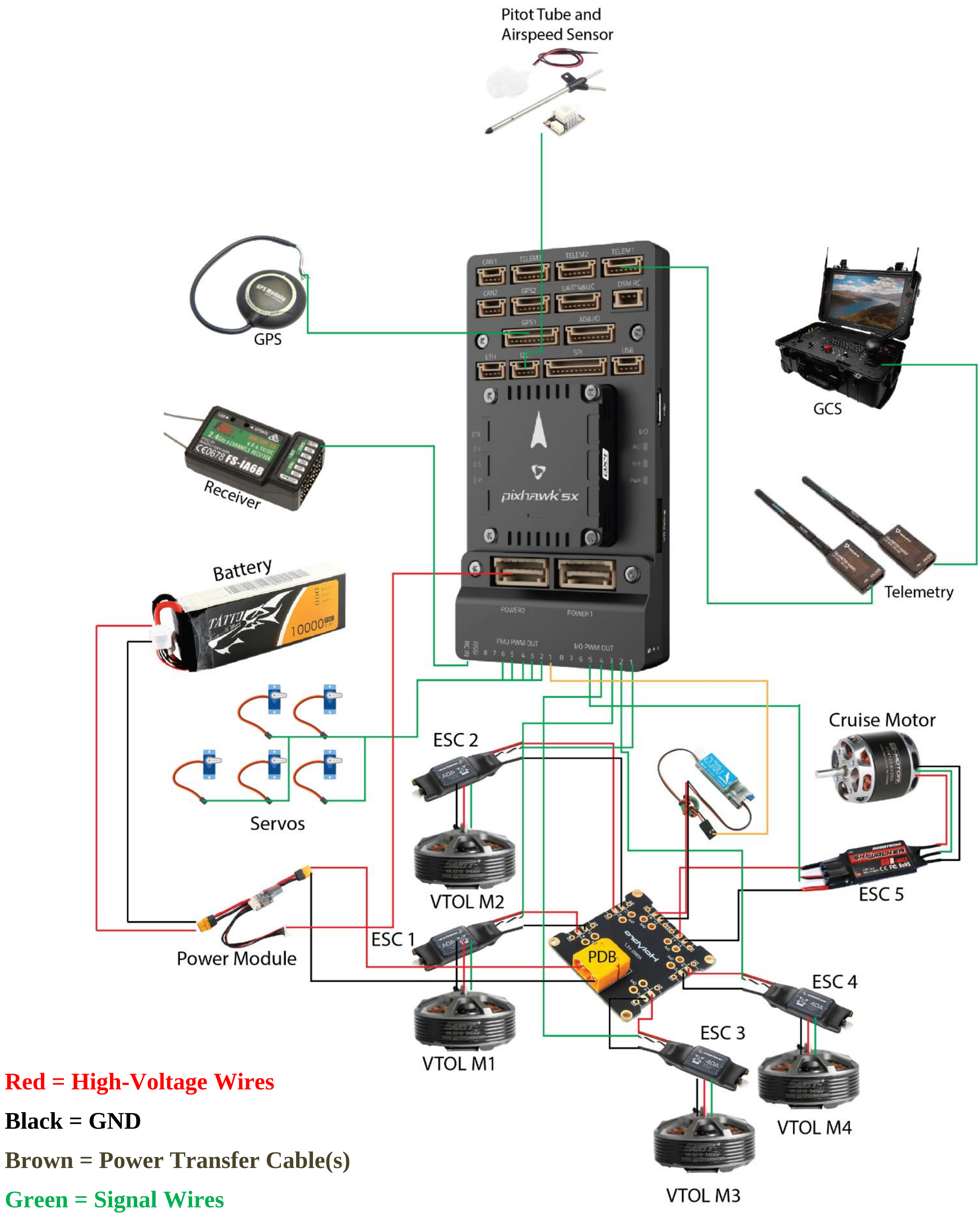

Figure 115 Wiring Diagram

8.14 ArduPilot Mission Planner

We used the Mission Planner ground control software from ArduPilot for calibrations of sensors and flight testing of our UAV. It is a powerful software in popular use for RC aircraft and UAVs.

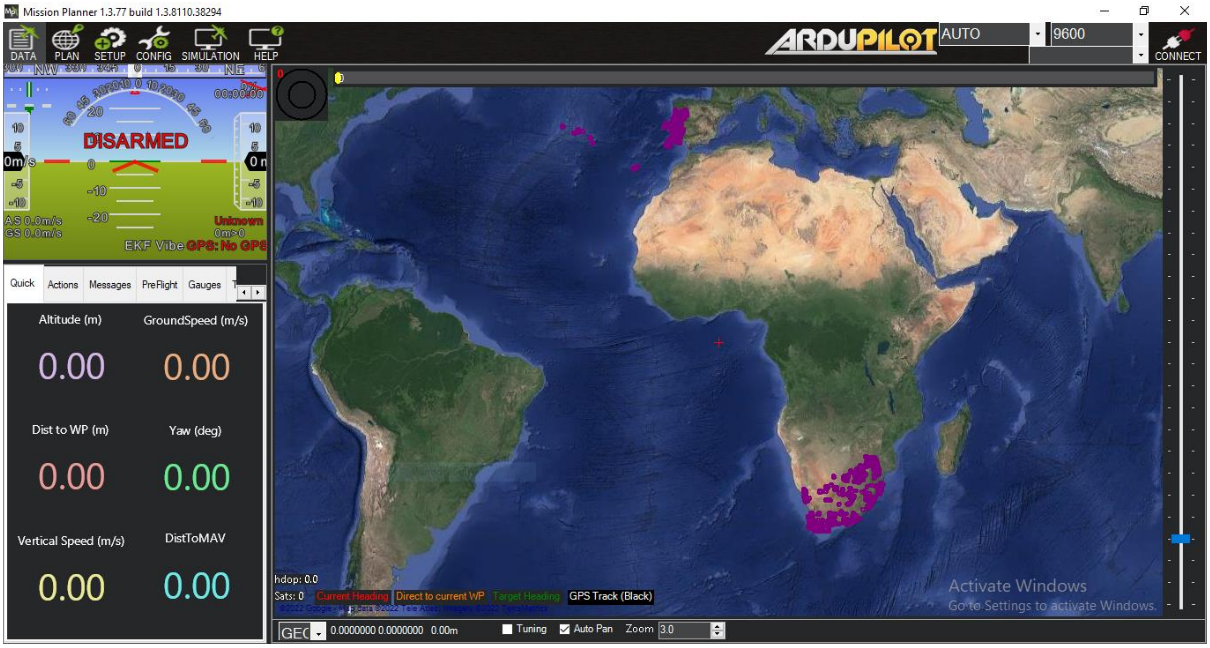

Figure 116 Mission Planner home screen

8.15 Sensor Calibration

To calibrate different sensors, the flight controller module is connected (Pixhawk 5X) on the Mission Planner screen and then Setup is opened. There, from the left pane, we select Mandatory Hardware. Different sensors were calibrated in this order:

8.15.1 Accelerometer

The accelerometer is zeroed in three axes by placing and holding the vehicle on all its six sides (level, left, right, nose-down, nose-up and back) as prompted on the Mission Planner one by one after clicking the Calibrate Accel button. These modes can be seen illustrated for a quadcopter in **Figure 117**.

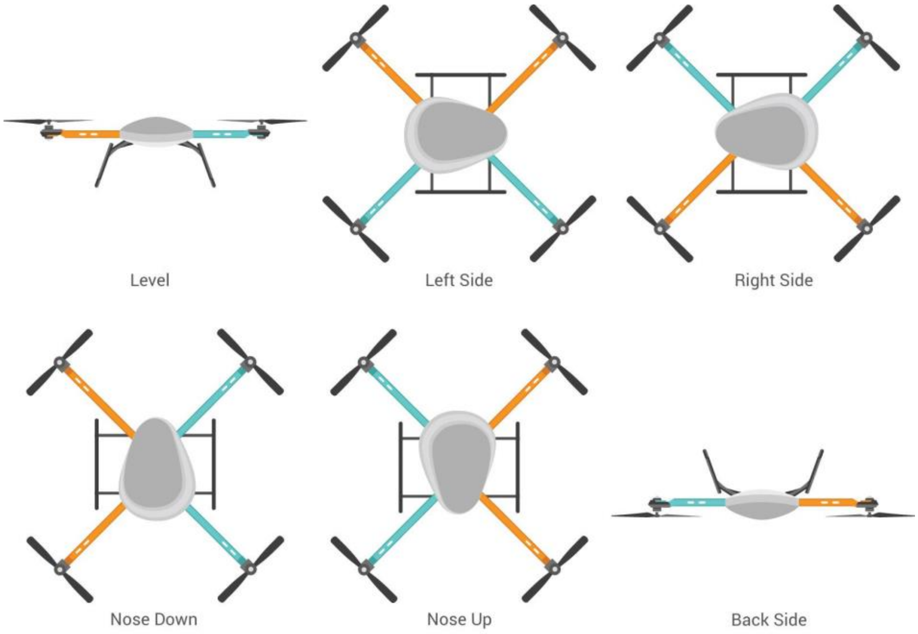

Figure 117 Accelerometer Calibration modes for Quadrotors [62]

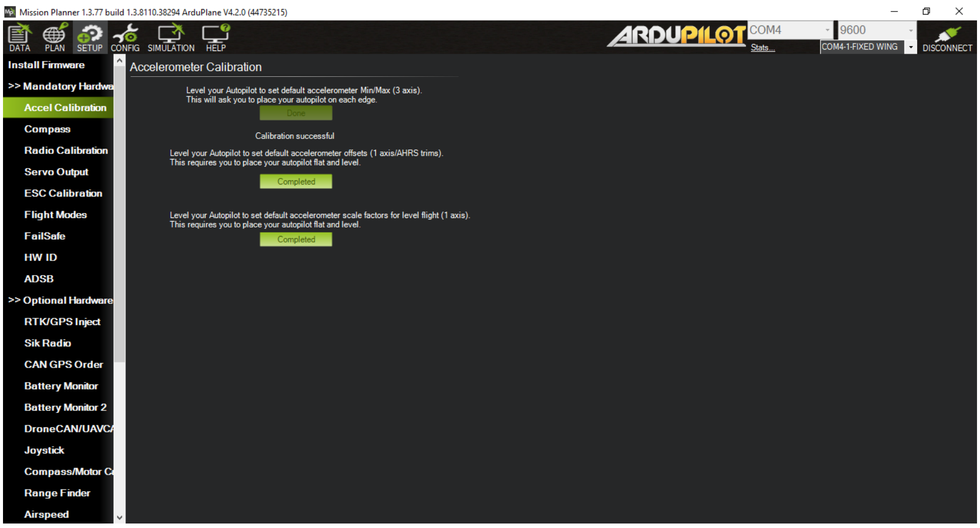

Figure 118 Accelerometer calibration screen

Secondly, we calibrate the level by placing the autopilot on a level surface and then clicking the button for level calibration. There is also a third option for setting default scale factors that is done in the same way as the level calibration.

8.15.2 Compass

Compass calibration requires rotating the autopilot module about all 3 axes and also in between after pressing Start in the mag calibration tab. Once complete, the user is required to reboot and then reconnect the autopilot.

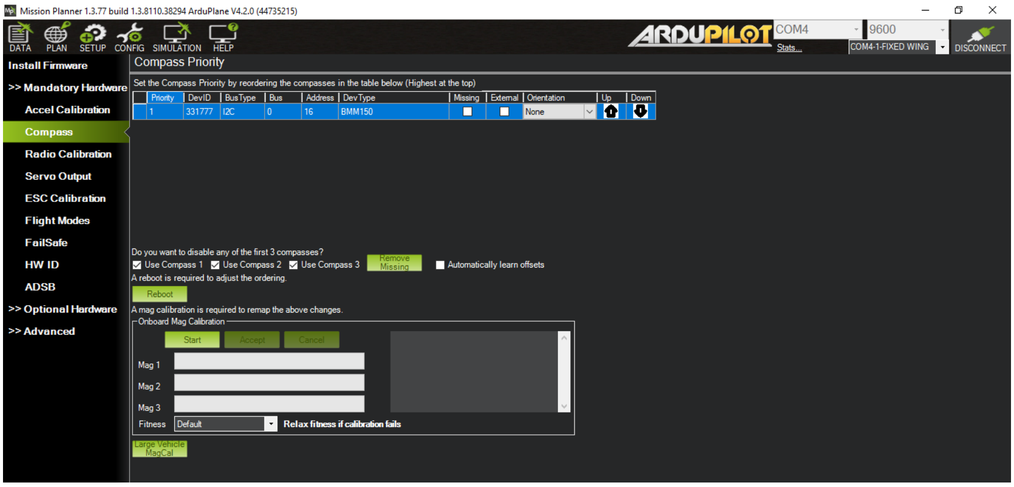

Figure 119 Compass calibration screen

8.15.3 Radio

For Radio calibration, we connect the transmitter device and then press Calibrate Radio before moving all the knobs and switches on the transmitter between their minimum and maximum positions to establish their limiting values for the Mission Planner.

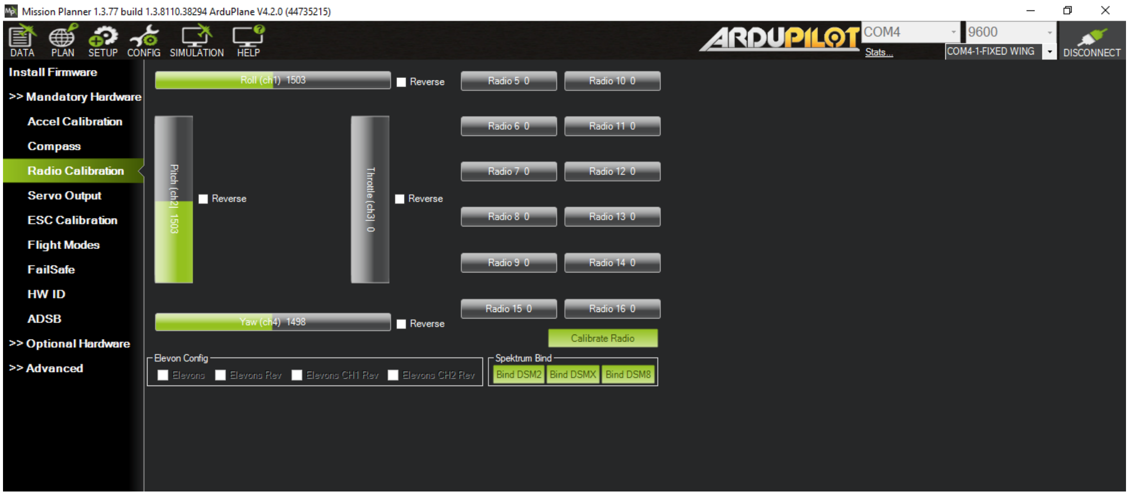

Figure 120 Radio calibration screen

8.15.4 Servo Output

By connecting all the servos to the autopilot module, we can configure the component that each servo is responsible for, and then set the minimum, maximum and trimming deflections for it.

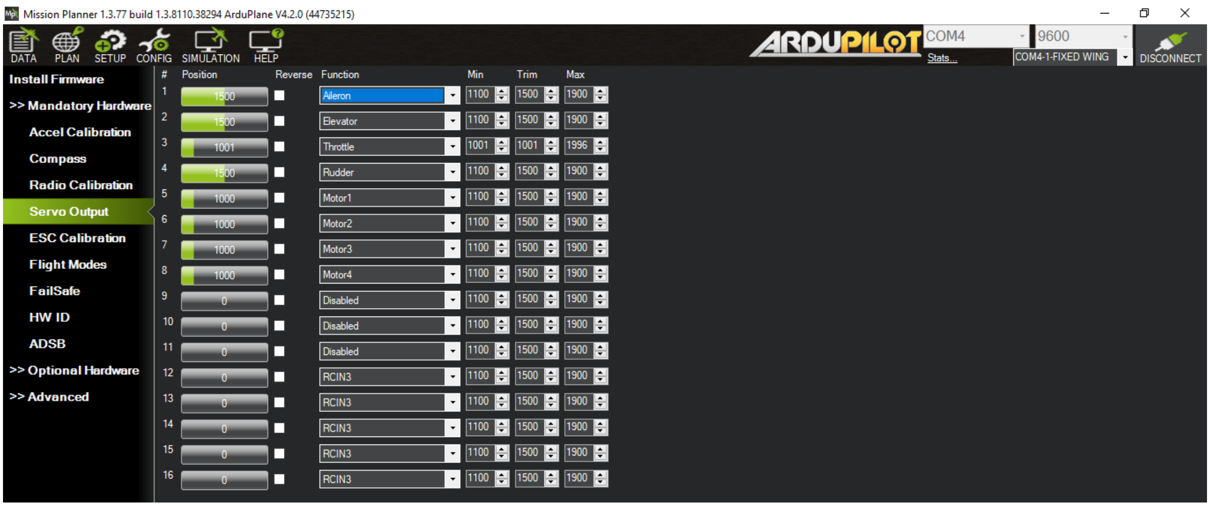

Figure 121 Servo output calibration

8.15.5 ESC

Follow the on-screen instructions beside the Calibrate ESCs button and then connect the transmitter. Increase power to each motor one by one, hold each at full speed for 2 seconds before decreasing speed to 0. The Mission Planner will automatically decide how quickly each ESC should throttle its motor.

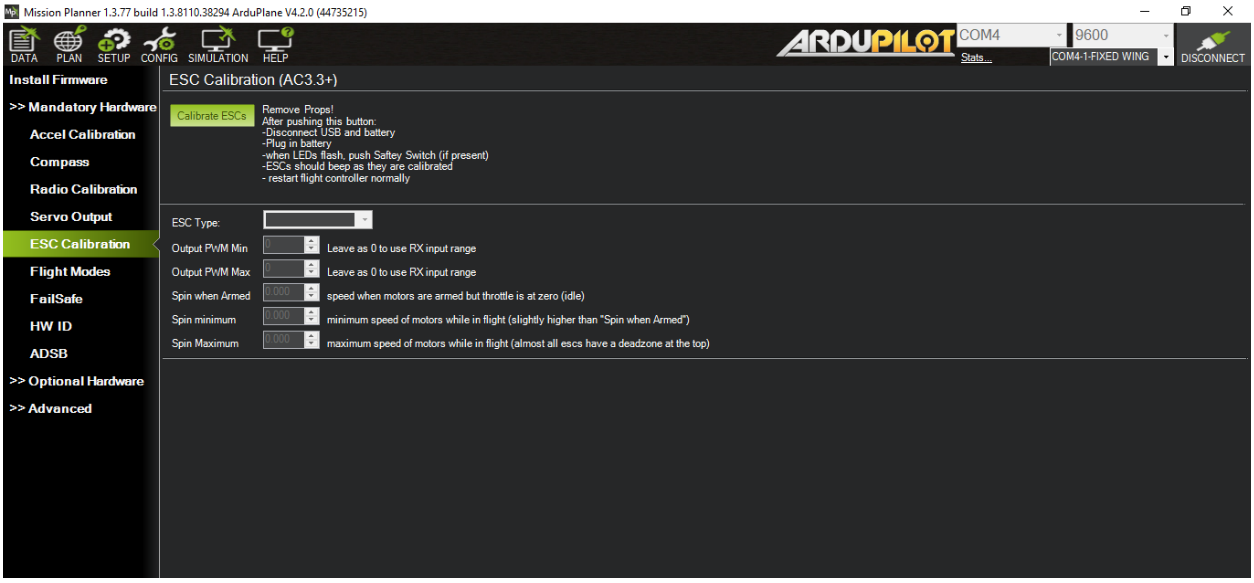

Figure 122 ESC calibration screen

8.15.6 Airspeed

The airspeed sensor setup is not present in Mandatory Hardware. Rather, it is categorized under Optional Hardware. Once the window is opened, we enable airspeed, select the pin on the autopilot in which the airspeed sensor is plugged. Then we select its type. The rest of the calibration needs to be carried out in the Full Parameter List under the Config section of Mission Planner. Here, we change the value of “ARSPD_AUTOCAL” to 1, cover the opening of the sensor, let it read the value, then change to 1 again and blow air into the opening for it to take a second value.

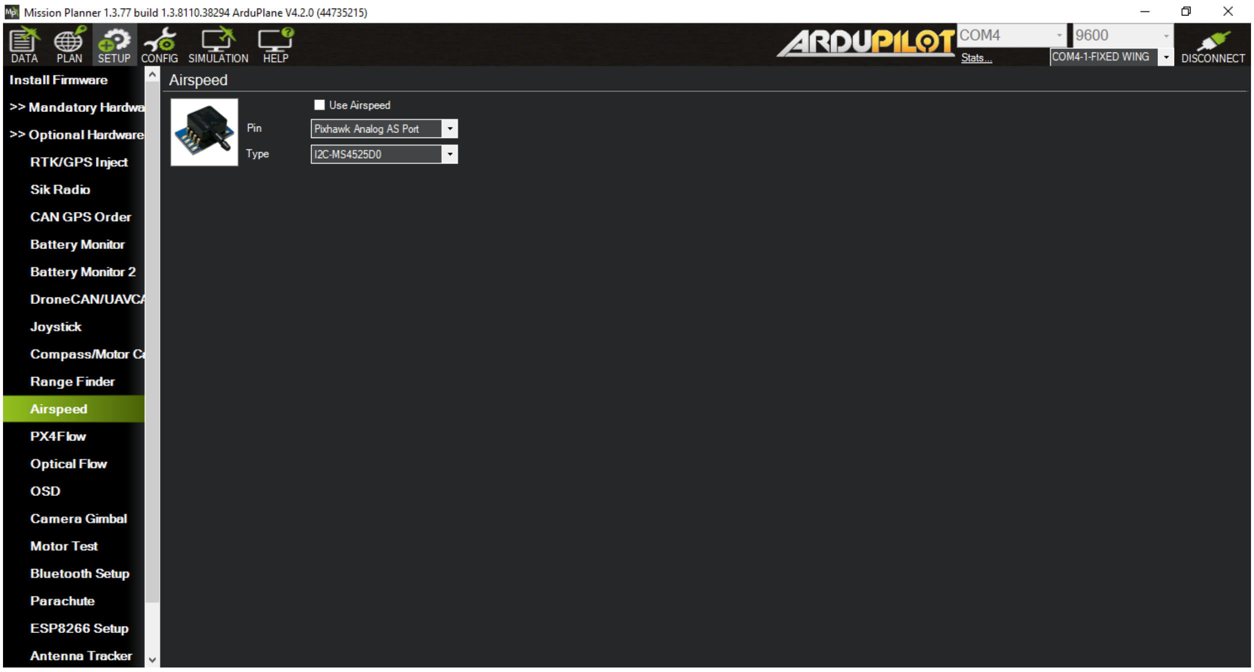

Figure 123 Airspeed sensor configuration

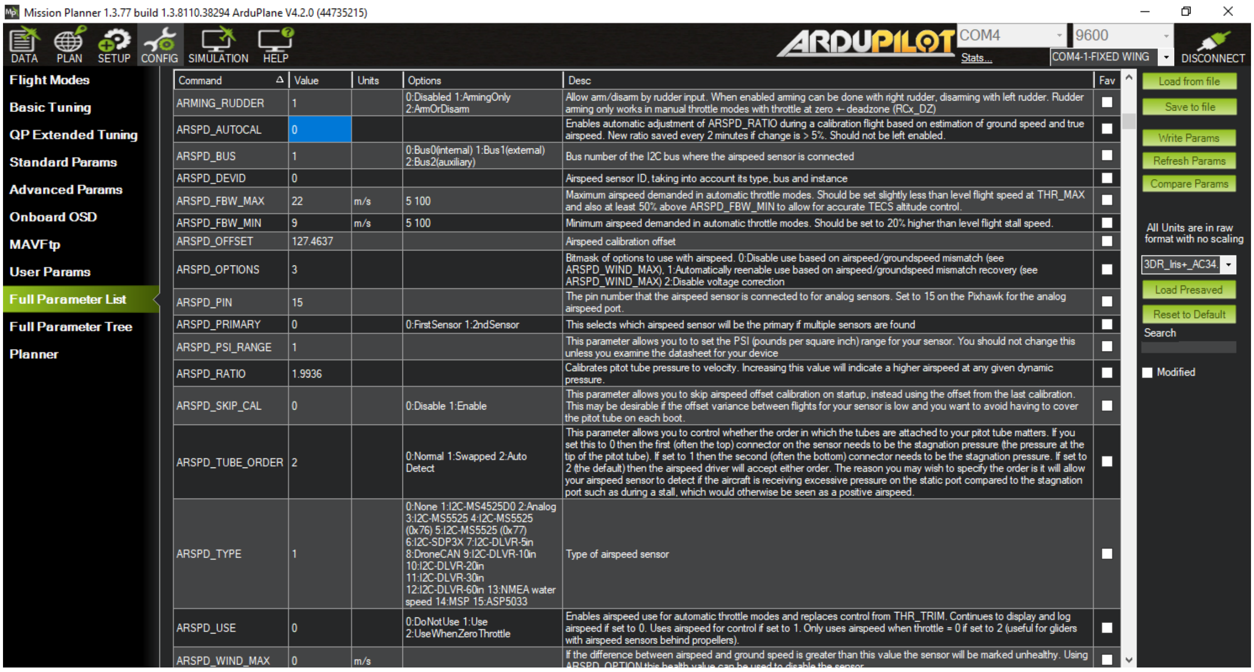

Figure 124 Airspeed sensor calibration

8.16 Flight Modes

There are several flight modes available for configuration in Mission Planner. The most important ones for us to configure are shown in the **Figure 125**.

Figure 125 Flight modes configuration

8.16.1 Manual

This is the simplest flight mode in which we will have full control of the UAV from takeoff to landing. Only the arming of the UAV will have to be done in Mission Planner.

8.16.2 Auto

This flight mode is for fully autonomous flight in which a program will be made in Mission Planner containing all the coordinates of the waypoints that the UAV must follow on a path planned by us. To start the flight, we will simply load and run the program we saved earlier. The drone takes off itself, makes a transition from hover to cruise, completes the trip, makes a transition back to hover and lands vertically itself, disarming at the end automatically.

8.16.3 QSTABILIZE

This mode allows the user to fly the quad plane by themselves but continually resets the aircraft's roll and pitch behavior after every input, thus preventing any conditions of unstable flight that can be triggered by abnormal rolling or pitching maneuvers. [63]

8.16.4 QLOITER

As the name suggests, the QLOITER mode maintains the aircraft's current location, heading and altitude when the control sticks are released. Before releasing the sticks, one may continue to fly the drone manually by giving inputs on the remote transmitter. As soon as it is set free from manual input, the UAV will self-level and slow down to a stop in the air. [64]

8.16.5 QHOVER

In this mode, the user is in control of the roll, pitch and yaw of the aircraft. However, any changes in altitude as a result of any of the above inputs will be compensated for and the quad plane will attempt to maintain a consistent altitude throughout. [65]

8.16.6 QRTL

The QRTL (Return to Land) mode, when activated mid-flight, guides to UAV back to its home position from where it took off in a controlled manner. Depending upon the subsequent mode setting, QRTL will either make the UAV simply circle around the home location as a fixed wing, fly as a VTOL aircraft to the home position and land, or fly as a fixed-wing and make a transition to VTOL before landing when close to the home location. [66]

8.16.7 QLAND

When the QLAND mode is activated, the UAV will descend and attempt to land right below its position in the air. [67]

8.16.8 FBWA Mode (FLY BY WIRE_A)

This mode is mostly used by inexperienced flyers and is the most popular mode. In this mode, roll and pitch are controlled and hold by the sticks. In FBWA mode, throttle is manually controlled and is limited by **THR_MIN** and **THR_MAX.** Control surfaces can be manually controlled or set to automatic depending on the settings.

CHAPTER 9: TESTING

9.1 Static Wing Loading Test

Static wing loading tests involve placing distributed loads on the wing while the UAV is stationary on the ground to approximate the expected elliptical load distribution in flight. A 45N load of sandbags was applied on one half of the wing, which it sustained successfully.

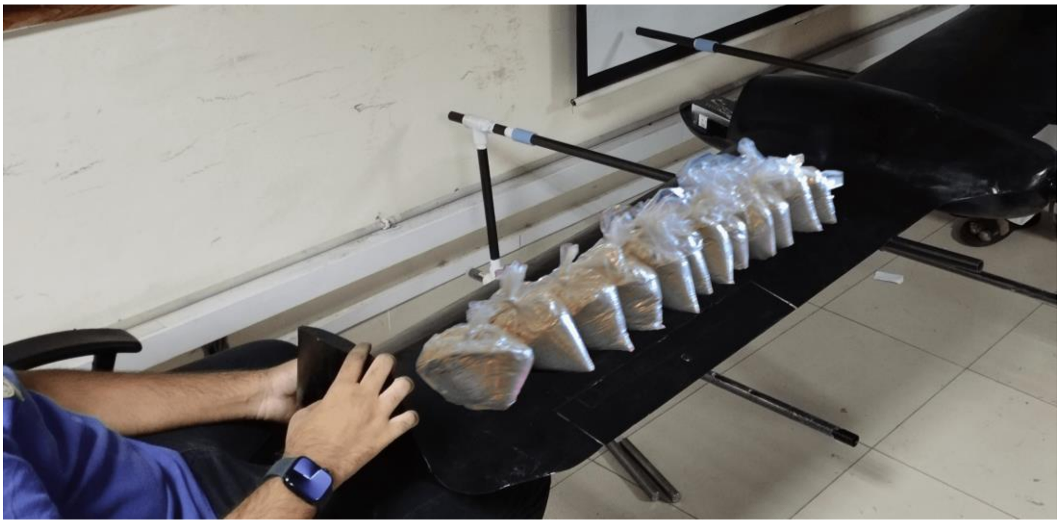

Figure 126 Static Wing Loading Test

9.2 VTOL Tuning

Flight testing of the UAV was done in a staggered manner. Initially, it was only commanded to the vertical takeoff, hover, and vertical landing maneuvers. This itself comprised several steps in Mission Planner:

9.2.1 Battery and Expo Settings

The thrust curve of VTOL motors must be as linear as feasible for steady takeoff and flight, i.e. the thrust delivered by a motor had to be in direct proportion to the thrust expected from it by Mission Planner.

The first part of this step involves tuning the battery properly. To help the voltage range of battery cope with the voltage sag, we set the following parameters:

- **Q_M_BAT_IDX**: 0
- **Q_M_BAT_VOLT_MAX**: 25.2V
- **Q_M_BAT_VOLT_MIN**: 19.8V

The adjustment to the thrust expo parameter, namely **Q_M_THST_EXPO** was done by extracting a value from the following graph according to the propeller size:

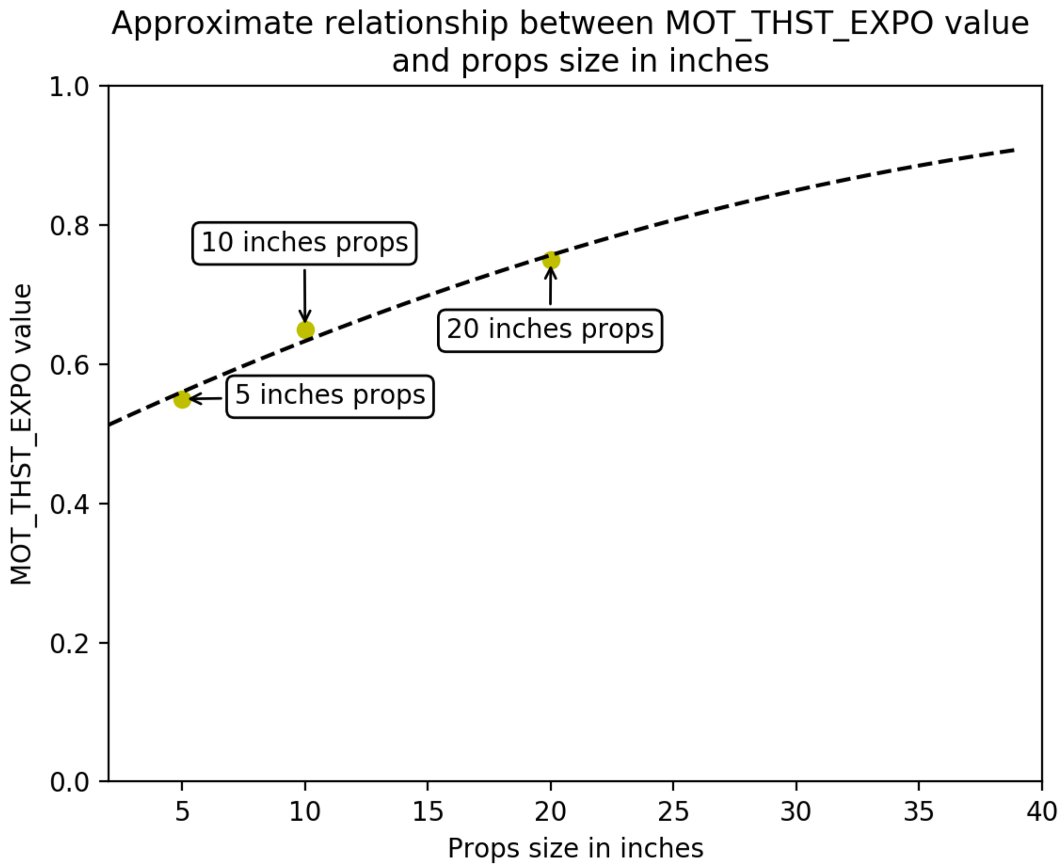

Figure 127 Prop Size vs. MOT_THST_EXPO value [68]

Q_M_THST_EXPO: 0.73

9.2.2 Motors Setup

The PWM output range transmitted to the ESCs is defined by the motor settings. It was critical to keep the range of throttle values employed in flight within the propulsion system's linear range.

For standard PWM-based ESCs, **Q_M_PWM_MIN** is tuned until it is approximately 20 seconds below the minimum value that causes the motors to just start spinning.

Q_M_PWM_MIN: 1000

- Afterwards, we adjust **Q_M_PWM_MAX** upto the value where the ESCs stop producing more thrust. This should be done with the propellers removed.

  Q_M_PWM_MAX: 2000

The first two parameters from the ones given below are used to select a linear sub-range of outputs for the motors:

- **Q_M_SPIN_MAX**: 0.95.
- **Q_M_SPIN_MIN** was determined from the motor test feature.
- **Q_M_SPIN_ARM** was also determined from the motor test feature.
- **Q_M_THST_HOVER**: 0.45

9.2.3 PID Controller Initial Setup

PID control parameters are a critical part of the tuning process. They are meant to yield the correct approximate range of acceleration and filter settings for the PID controller. They were set to be as follows:

- **INS_ACCEL_FILTER**: 12
- **INS_GYRO_FILTER**: 21
- **Q_A_ACCEL_P_MAX**: 58000
- **Q_A_ACCEL_R_MAX**: 58000
- **Q_A_ACCEL_Y_MAX**: 18700
- **Q_A_RAT_YAW_P**: 2.078
- **Q_A_RAT_PIT_FLTD**: 10.5

- **Q_A_RAT_PIT_FLTT**: 10.5
- **Q_A_RAT_RLL_FLTD**: 10.5
- **Q_A_RAT_RLL_FLTT**: 10.5
- **Q_A_RAT_YAW_FLTE**: 2
- **Q_A_RAT_YAW_FLTT**: 10.5

If prop size does not match with the values stated above, the relevant parameters can be found in the following graphs:

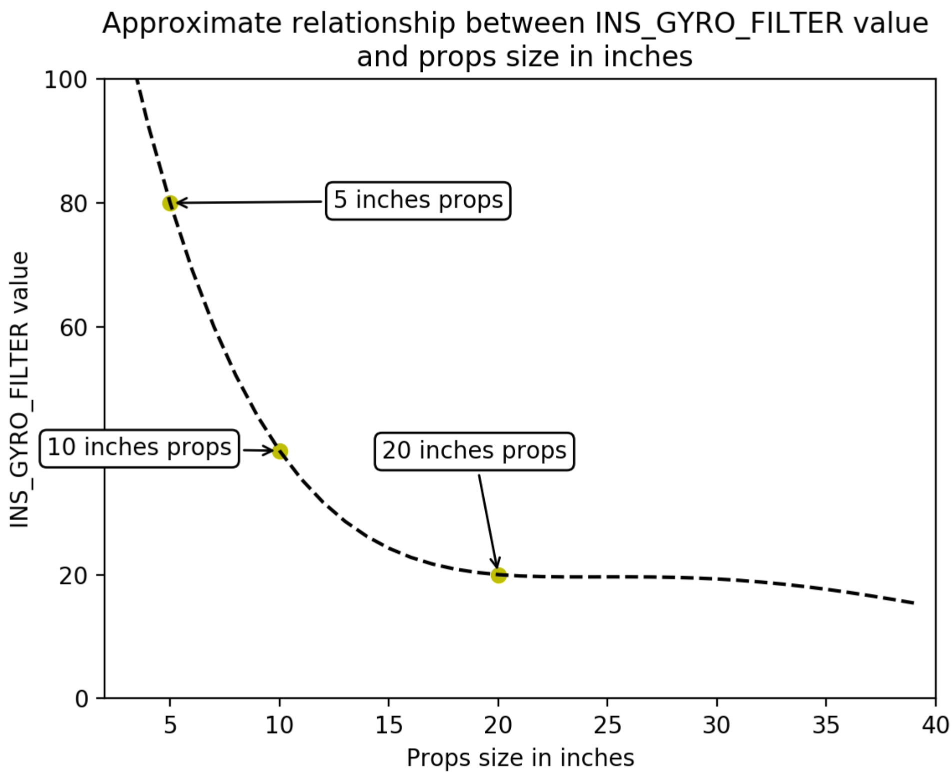

Figure 128 Prop Size vs. INS_GYRO_FILTER [68]

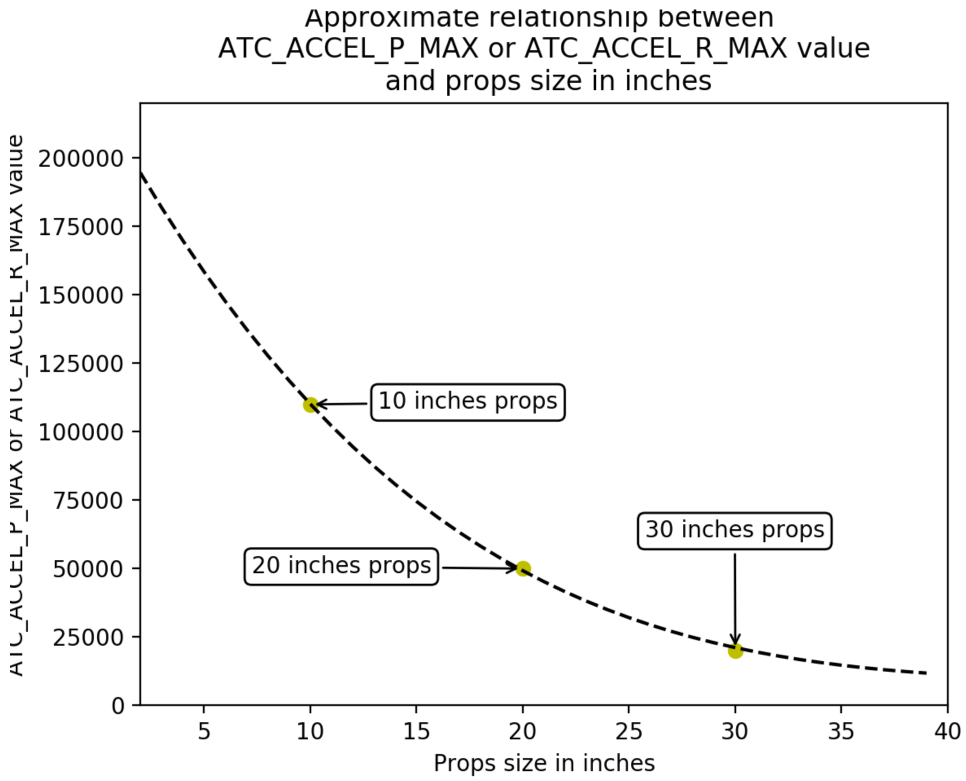

Figure 129 Prop Size vs. ATC_ACCEL_P_MAX or ATC_ACCEL_R_MAX [68]

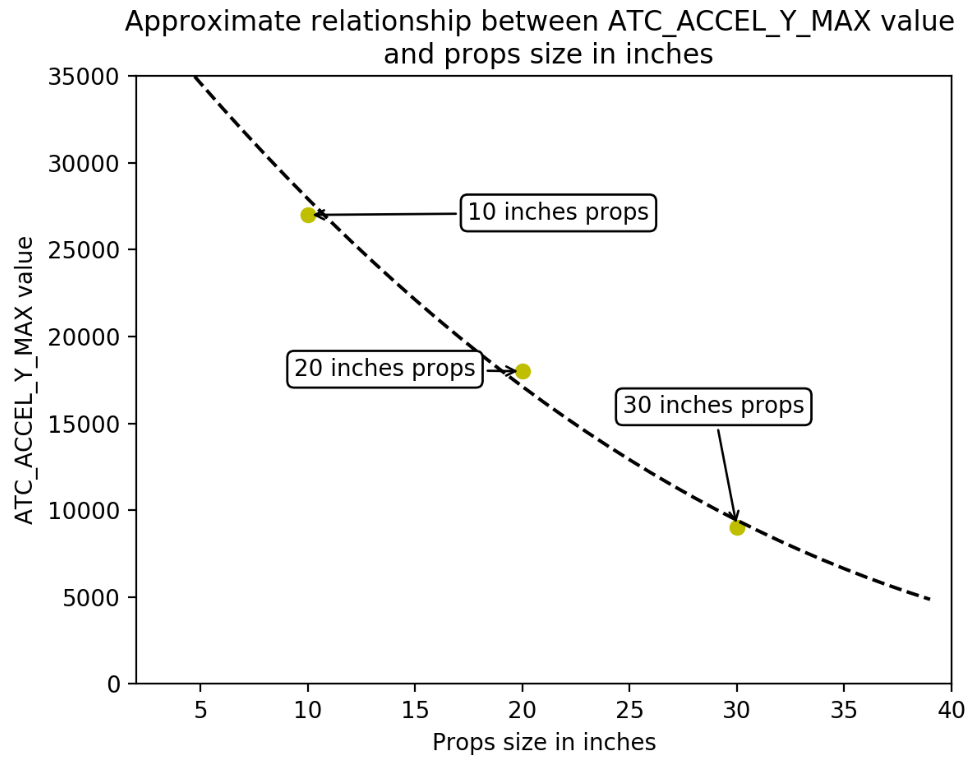

Figure 130 Prop Size vs. ATC_ACCEL_Y_MAX [68]

9.2.4 Pilot Preparation for First Flight

The first takeoff of a VTOL UAV is the most dangerous part of the aircraft's life. This is where the aircraft could be very unstable causing a sudden increase in power when then results in the aircraft jumping into the air, or it may be so poorly tuned that one has insufficient control over the aircraft once it is airborne.

There are several steps the operator can take for safety of aircraft and human life before flight. For example, we took the following precautions:

- Performed a motor number and orientation check. Confirmed that the correct frame type was selected in Mission Planner. Ensured that:
    - **Q_M_SPIN_ARM** is set high enough to spin the motors cleanly.
    - **Q_M_SPIN_MIN** is set high enough to spin the motors with minimal thrust.
- Every flight after a significant tuning change was done in the QSTABILIZE mode. This meant that the vibrations were kept in check, and we had more command over the UAV's movement than we would in complete manual mode.
- We avoided using QHOVER mode for takeoff until we had tested the altitude controller during flight by switching to QHOVER from QSTABILIZE.
- Set **Q_A_THR_MIX_MAN** to 0.1 and **Q_M_THST_HOVER** to 0.25 or below the expected hover throttle.
- Calibrated the radio correctly.
- Configured the ARM/DISARM switch properly and tested it.
- Performed tuning flights in low-wind conditions and normal weather/temperature i.e. no rain and at 15-25°C.

9.2.5 First Tuning Flight

As discussed before, the first flight is a crucial time for the UAV. Therefore, before we proceeded with the takeoff, we made sure of the following things:

- All spectators were standing at a safe distance (at least 20m away in every direction).
- The aircraft was in QSTABILIZE mode.
- The aircraft was armed.
- It was then immediately disarmed to verify that the disarm option was working properly.
- The UAV was armed again.
- The throttle was increased slowly to observe any oscillation or wobble in the airframe due to the long landing gear.
- The throttle was increased further till the aircraft took off from the ground.
- The UAV was immediately landed and the parameters were tuned again so that it the range of thrust that could be demanded from the motors was ideal.
- We armed the aircraft again and initiated the takeoff.
- We let it hover at 2-3m of altitude and applied small degree inputs to roll and pitch controls to see any oscillations.
- The UAV was then landed.

9.2.6 Initial Aircraft Tune

In order to free the aircraft of any disturbing oscillations on takeoff and the initial part of the flight, we needed to achieve a stable tune and perform further tests. We followed these steps:

- The aircraft was armed in QSTABILIZE
- The throttle was increased slowly until the aircraft left the ground

- Following parameters were reduced by 50% until oscillations stopped.
  - **Q_A_RAT_PIT_P**
  - **Q_A_RAT_PIT_I**
  - **Q_A_RAT_PIT_D**
  - **Q_A_RAT_RLL_P**
  - **Q_A_RAT_RLL_I**
  - **Q_A_RAT_RLL_D**

We repeated this type of tuning until we could not see any more vibrations in the UAV during the takeoff and hover phase.

9.2.7 Test QHOVER

This procedure was for verifying our altitude controller and to ensure the stability of the UAV. It comprised these steps:

- Checked that **Q_M_HOVER_LEARN** is set to 2. This will allow the controller to learn by itself the correct hover value when flying.
- Take off in QSTABILIZE and increase altitude to 5m. Switch to QHOVER and be ready to switch back to QSTABILIZE. If the aircraft is hovering at a very low hover throttle value, there may be a fast oscillation in the motors. Ensure the aircraft has spent at least 30 seconds in hover to let the hover throttle parameter converge to the correct value. Land and disarm the aircraft.
- Set these parameters on ground and preferably disarm:
  - **Q_P_ACCZ_I** to 2 x **Q_M_THST_HOVER**
  - **Q_P_ACCZ_P** to **Q_M_THST_HOVER**
- If the quadplane in QHOVER starts to move up and down, the vertical position and velocity controllers (**Q_P_POSZ_P** and **Q_P_VELZ_P**) need to be reduced by 50%.

9.2.8 Yaw Bias

The amount of thrust being used to maintain yaw was checked by looking RATE YOut value in the hover logs. The value for the QHOVER flight test was 0.02. The value was less than 0.1 so there was no problem with yaw symmetry. Moreover, we have an H frame compared to X frame which works best to cater such issues.

9.2.9 Notch Filtering

After eliminating the vibrations in QHOVER through tuning, the next was to implement a notch filter to reduce noise to the VTOL PID controllers.

The plane was set to hover for 2 minutes with **INS_LOG_BAT_MASK** set to 1 and during this time no pilot input was given. This enables the FFT logging system which is used for the correct setup of the filter.

During the setup of notch, any cause of vibration is investigated especially by the motors. By doing this we will be able to reduce noise and come to know of any resonances.

A dynamic notch filter is used for our purposes. A dynamic harmonic notch filter can be linked to the motor rotational frequency for multicopter motors and provides notches at the primary frequency and its harmonics.

There are different modes of the dynamic notch filter but for our purposes we have used the default mode 1.

INS_HNTCH_MODE = 1: It is a throttle position-based filter where the frequency variation is determined from the logs, and it is also used to track the noise frequency.

9.2.10 Setting up Notch-Filter

First you must select the mechanism used for controlling the harmonic notch frequency which we have used to be Mode 1. Flight log is also required for the tuning of notch filter. We have also set **INS_HNTCH_REF** and **INS_HNTCH_HMNCS** to 1 which means no scaling and three harmonics for notches

A baseline is first established to identify the noise at hover throttle level to configure the throttle-based filter. We need to use batch sampler of mission planner for this purpose.

To enable the batch sampler, **INS_LOG_BAT_MASK** was set to 1, **LOG_BITMASK** and **INS_LOG_BAT_OPT** was set to 0

9.2.11 Determination of Notch Frequencies

Firstly, a hover flight of 30 seconds was done in altitude hold and after that the log was downloaded from the mission planner. As seen from the graph **Figure 131** the significant peak in the noise corresponding to the rotational frequency is identified.

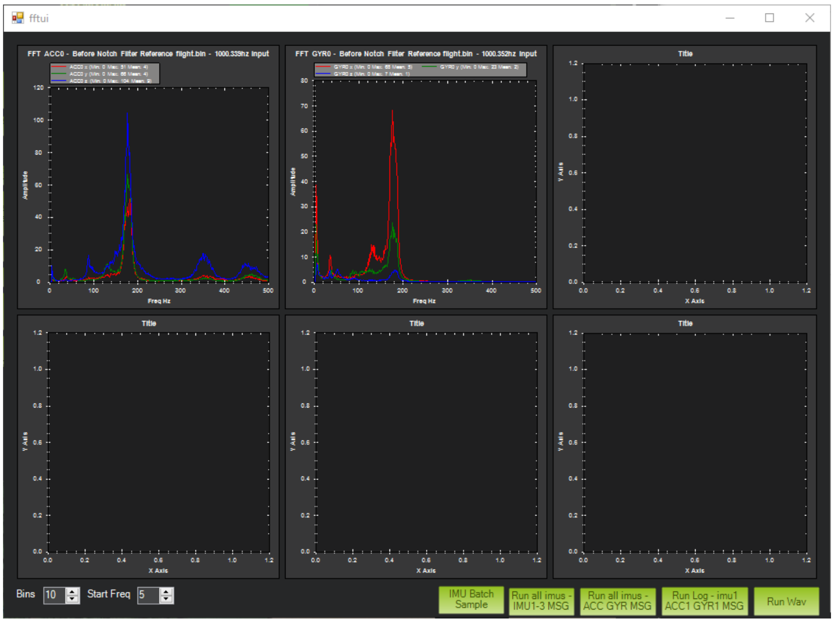

Figure 131 Noise Graph

Throttle value was also graphed, and average hover throttle value was determined. This will give us hover motor frequency and thrust value of the hover. Based on the results, **INS_HNTCH_REF** was set to reference hover thrust and **INS_HNTCH_FREQ** to the hover thrust frequency. This completes the tuning of the dynamic throttle-based notch filter

9.2.12 Manual tuning of Roll and Pitch

A solid manual tune cuts down on the time it takes for a QAUTOTUNE, which is important considering the short VTOL hover times of many quadplanes.

In low wind, with a decent sky view and good GPS lock, we hovered the aircraft in QSTABILIZE or QHOVER modes. To try to generate oscillation, the rate gains were varied as detailed below, with slight "twitches" on the sticks after each adjustment.

The parameters we adjusted were as follows:

Q_A_RAT_RLL_D

Q_A_RAT_RLL_P and Q_A_RAT_RLL_I

Q_A_RAT_PIT_D

Q_A_RAT_PIT_P and Q_A_RAT_PIT_I

We started with the roll parameters, then moved onto the pitch.

- Increased the D term in steps of 50% until oscillation was observed
- Reduced the D term in steps of 10% until the oscillation disappeared
- Reduced the D term by a further 25%
- Increased the P term in steps of 50% until oscillation was observed
- Reduced the P term in steps of 10% until the oscillation disappeared
- Reduced the P term by a further 25%

A good manual tune reduces the amount of time a QAUTOTUNE will take so we thoroughly tuned these parameters.

9.2.13 Evaluation of aircraft tune

We accessed the aircraft's tune to determine whether the previous stages resulted in a tune suitable for a transition flight or QAUTOTUNE.

1. QHOVER mode was used for taking off.
2. Small roll and pitch inputs were given. Approximately 5-degree inputs were given and stick was released to center for pitch, left, right, roll forward back, and finally all four diagonal points.
3. Gradually inputs were increased until the stick was fully deflected.

The aircraft did not overshoot or wobble following the stick input which was a sign of tuning being successful.

The parameter Q A RATE FF ENAB was set to 0 to test the stabilization loops independent of the input shaping.

1. QHOVER mode was used for taking off.
2. Roll or pitch input were given.
3. The stick was released and overshoot was observed as the aircraft leveled itself.
4. The stick deflection was gradually increased to 100%.

The overshoot of UAV was very small which meant that tuning was fine. Q_A_RATE_FF_ENAB was set back to 1.

9.2.14 QAUTOTUNE

This mode automatically improves and fine tunes the parameters without having to manually adjust PIDs. We performed takeoff using QHOVER mode. Then we switched to QAUTOTUNE mode and the process automatically started. It took approximately 5 minutes to tune about each of the axis.

A stable hover flight indicated that the tuning process was complete. We safely landed the UAV and then adjusted rest of the parameters.

QAUTOTUNE will attempt to tune each axis as tight as the aircraft can tolerate. In some aircraft this can be unnecessarily responsive. A guide for most aircraft:

Q_A_ANG_PIT_P was reduced by 8

Q_A_ANG_RLL_P was reduced by 8

Q_A_ANG_YAW_P was reduced by 8

Q_A_RAT_YAW_P was reduced by 0.6

Q_A_RAT_YAW_I : Value was 0.06

9.2.15 Conclusion

The final values of all parameters tuned are attached as **APPENDIX II: AUTOPILOT TUNING PARAMETERS**

9.3 Final Flight Test

For the final test, firstly the pre-flight checks are done which are explained in **Chapter 10.1: Pre-flight Measures.** The RC controller has been configured in such a way that the through the channel switch we can change the flight modes of the plane. During take-off, QHOVER mode is selected. After the cruising altitude has reached (**Figure 135**), the next flight mode to FBWA (Fly-by-Wire A). In this mode, the cruise motor starts and when stall speed is reached, the VTOL motors slow down proportionally. When the VTOL motors stop completely the transition is complete (**Figure 136**). Similarly, once it travels some horizontal distance in cruise, we then switch back to QHOVER mode for its transition from cruise to VTOL and finally, the mode is switched to QLAND for its successfully landing.

Figure 132 UAV in Neutral Position

Figure 133 UAV Pre-Flight Checks

Figure 134 UAV in VTOL Mode 5 m

Figure 135 UAV in VTOL Mode 10 m

Figure 136 UAV Transition to Cruise at 60m

Figure 137 From FBWA To QHOVER and To QLAND

CHAPTER 10: OPERATING PROCEDURES

This chapter describes how to handle the aircraft during different stages of flight. The process comprises precautionary measures before flying, in-flight maneuvering and supervision and post-flight diagnostics/maintenance.

10.1 Pre-flight Measures

- The landing skids and the booms are inspected for rigid connection with the wings.
- The top hatch at the front of fuselage is opened, and battery is installed before being secured into place.
- Connections are established between electronics/avionics.
- Payload, if any, is also loaded inside the fuselage.
- Other lighter avionics components are secured in their places.
- Both top and bottom hatches are secured into place with duct tape.
- The aircraft's CG is checked.
- The FlySky radio transmitter is switched on and initialized.
- Autonomous flight (if desired) is configured in Mission Planner.
- Motor Test is carried out to check if all motors are working.
- Response of control surfaces to stick inputs on Radio Transmitter is checked.
- Arm and disarm using Radio is checked.
- UAV is finally armed and ready for flight.

10.2 In-flight Operation

- The UAV can be operated in assisted mode using the Radio Controller or in completely autonomous mode using telemetry and pre-planned mission.
- In autonomous operation, UAV takes off vertically when the program is run via Mission Planner for planned flight. In case of manual flight, the VTOL propeller speeds are increased from radio transmitter for takeoff in QLOITER or QHOVER Mode.
- Upon reaching a certain preplanned altitude, the aircraft turns the cruise motor ON and switches to FBWA mode.
- It then makes a transition from hover mode to cruise mode completely after a certain airspeed is attained.
- The UAV completes its route through several waypoints as prescribed in the mission plan in forward flight.
- Having crossed the final waypoint, the UAV makes a second transition from cruise back to hover and lands vertically.

10.3 Post-flight Measures

- Fuselage top hatch is opened, and battery is disconnected.
- Battery level is checked, and it is put on charging as required.
- Pitot tube (airspeed sensor) opening is cleaned and covered.
- UAV is inspected for any visible damage.

CHAPTER 11: CONCLUSION

In this chapter, we shall present the experimental results for the UAV and see how well they conform to the expected/theoretical results. Furthermore, we have discussed the performance of our aircraft relative to similar contemporary and existing designs. Finally, there are recommendations for future endeavors in relation to the design and manufacture of the UAV.

11.1 Theoretical vs. Actual Performance

Table XX shows the comparison of results with regards to several important parameters:

Table 35 Design vs. Experimental performance of UAV

Parameters	Theoretical	Actual
MTOW	7.25 kg	8.1 kg
Stall Speed	10.5 m/sec	11 m/s
Cruise Speed	17 m/sec	20m/s
Max Speed	23 m/s	28 m/s
Rate of Climb	3 m/s	4 m/s
Endurance	50 minutes	33 minutes

11.2 Comparable Designs

There are several VTOL UAVs available in both national and international markets that employ 5 propellers in a "4+1" configuration. However, almost all of them, save for one or two, use a tilting mechanism for transition between the two major modes of flight i.e., hover and cruise. For a suitable comparison, we shall focus on two examples of electric-powered "4+1" UAVs of dimensions, construction, MTOW or speed not too dissimilar from our solution.

11.2.1 Mugin 2 V2930ES VTOL UAV

Figure 138 Mugin 2 V2930ES (airframe only) [69]

The V2930ES is a UAV fabricated from composite material and made by Mugin, a reputable Chinese manufacturer of drones. It is very much like our own UAV in that it uses 5 propellers to conduct hybrid flight. During transition, the UAV simply 'alternates' between which rotor(s) are providing the thrust, and no tilting mechanism is employed as such.

The wingspan is 2.93 m and the MTOW is 25 kg with a max payload of 3 kg. The aircraft can stay airborne for up to 90 minutes. It is not restricted to any one application. Rather, it is sold as a general-purpose UAV. The tail configuration is of particular importance, as it is very similar to what we have used in our design. The one difference is that our UAV does not incorporate a dihedral angle in the vertical tails for easier assembly/manufacturing.

11.2.2 Foxtech BABY SHARK 260 VTOL

Figure 139 Foxtech BABY SHARK 260 [70]

Foxtech is a Singapore-based company that manufactures drone systems for commercial use. Their BABY SHARK 260 VTOL is a UAV designed for inspection, survey and mapping according to the product website. Featured in the drone are four fixed propellers that help it move vertically, and one that propels it during forward flight.

The BABY SHARK boasts a wingspan of 2.5 m and an endurance of up to 2.5 hours. With a lightweight composite airframe, the drone can carry 2.1 kg of max payload in an MTOW of 13 kg. The tail is almost an inverted-V tail but with a narrow horizontal portion provided as well.

11.2.3 Comparison with Buraq VTOL UAV

Table 36 Comparison with other UAVs [69] [71]

Parameters	**Buraq Hybrid VTOL UAV**	**Mugin 2 V2930ES VTOL UAV**	**Foxtech BABY SHARK 260 VTOL**
Max Payload	1.5 kg	3 kg	2.1 kg
MTOW	8.1 kg	25 kg	13 kg
Endurance	33 minutes	Up to 90 min	Up to 150 min
Stall speed	11 m/s	13 m/s	16 m/s
Cruise speed	20 m/s	24.44 m/s	21.5 m/s
Max speed	28 m/s	33.33 m/s	30.55 m/s
Cost (exclusive of shipping)	Rs. 500,000/-	Rs. 1,481,000/-	Rs. 1,520,000/-
Landing Cost	Rs. 500,000/-	Rs. 3,000,000/-	Rs. 3,050,000/-

In comparison with contemporary products, our UAV lacks in endurance, max speed and max altitude. However, it is not so far short of the others in relative terms, especially if one considers their total costs. This is the main area where the Buraq outclasses its intended rivals. Since its production was indigenous, it incurred far lower costs than the others, even though it has Carbon Fiber construction, and the others mostly make use of Glass Fiber. This means that it is stronger and more lightweight (when considering empty weight of the airframe) while being less expensive.

The tail design of all three UAVs is based around minimizing the effects of the pusher propeller's wake on the tail surfaces. However, the extent to which they accomplish this is slightly different from each other. Our UAV has a very simplistic H-Tail which has no dihedral in the vertical parts to make the manufacturing aspect easier aside from keeping the tails are as far out of the propeller's wake as possible. The Mugin VTOL features a small dihedral but still follows the configuration of the H-Tail. The Foxtech VTOL, however, has a horizontal tail that is very narrow, and the vertical tails are angled so that they almost form an inverted-V tail configuration.

11.3 Future Recommendations

Thus far, the project is fulfilling nearly all of its design requirements. Due to the time constraint, a lot of areas of improvement have been left in the UAV. For one, the processes used for manufacturing and especially finishing the Carbon Fiber parts were not the best that could have been. We wish to use vacuum bagging for the wing, tail and fuselage profiles in the future.

From the design stage, the wing was meant to be manufactured in two parts and those two parts would be blended to either side of the fuselage. However, in the manufacturing phase, it was discovered that manufacturing the complete wing as a single piece was easier and more suitable when the wing body is made of foam rather than ribs and spars. It also makes for a stronger structure when the fuselage is of two-part construction and must blend with the wing. The downside was that most of the space inside the fuselage was occupied by the wing, although enough space was left for all our avionics plus some for payload.

With regards to the above problem, we intend to redesign the fuselage and increase its volume without producing any wake on the pusher propeller as well as the tailplane.

Another step we can take is to produce a version of the UAV that is made of Glass Fiber instead of Carbon Fiber. This will involve some redesigning to account for the increased weight but will diversify our product in terms of cost while retaining good performance.

Last but not least, tailoring different versions of the UAV to different applications will be an important milestone in the future of our drone program. The model currently made is a general-purpose aircraft used to showcase the chief characteristics of the “4+1”, “H-Tail” and ‘alternating’ thrust concepts and does not feature components specific to any of its intended applications. We aim to change that in the near future by increasing the range of product types available.

As a demonstrator UAV, we believe that the Buraq VTOL UAV is a good representative of hybrid VTOL drones and can be influential in bringing about their popularity in the Pakistani commercial and industrial space, and, to a limited extent, the defense sector as well.

With Buraq, we will revolutionize Hybrid VTOL UAVs forever!

APPENDICES

APPENDIX I: MATLAB CODES

12.1 Matching Plot

Variables and Initializations

```
prompt={'Number of Batteries:','No of Servos of Type 1:','No of Servos of Type 2:','No of Motors of Type 1:','No of Motors of Type 2:','Payload Mass:','Battery Mass:','Motor Mass of type 1:','Motor Mass of type 2:','ESC Mass of Type 1:','ESC Mass of Type 2:','Propeller Mass of Type 1:','Propeller Mass of Type 2:','Flight Controller Mass:','Mass of GPS:','Mass of Servo of Type 1:','Mass of Servo of Type 2:','Mass of Landing Gear:','Weight Fraction of Wires:','Weight Fraction of Airframe:','Aspect Ratio of the Wing:','Zero Lift Drag Coefficient','Ostawalds Efficiency','Maximum Lift Coefficient'};

dim=[1 60];

title_prompt='Enter the Parameters: ';

default_Values={'1','5','0','4','1','1.5','0.885','0.255','0.145','0.109','0.109','0.0279','0.0265','0.0158','0.068','0.055','0.0601','0.250','0.05','2.0477','4','0.036','0.9344','1.3729'}; %% Oswald Efficiency came out to be around 0.93 for AR 4 Wing with Elliptical Distribution. (https://wingsofaero.in/calculator/oswald-efficiency-factor-for-straight-wing/)

Inputs=inputdlg(prompt,title_prompt,dim,default_Values);

%All Weights are in kgs

N_b= str2double(Inputs(1)); %No of batteries

N_s_1= str2double(Inputs(2)); %no of servos of type 1

N_s_2= str2double(Inputs(3)); %no of servos of type 2

N_m_1=str2double(Inputs(4)); %No of Motors of type 1

N_m_2=str2double(Inputs(5)); %No of Motors of type 2

W_PL=str2double(Inputs(6)); %payload weight
```

From Specsheet of Tattu 25C 22.2V 6S 10000mAh Lipo

```
W_b=N_b*str2double(Inputs(7)); %battery weight
```

From Specsheet of Gartt ML5210 (340 KV) 4.6 kg Thrust

```
W_m_1= N_m_1*str2double(Inputs(8));  %motor weight of type 1

W_m_2= N_m_2*str2double(Inputs(9));  %motor weight of type 2
```

From Spechsheet of Hobbywing Skywalker 80A ESC Hobbywing Skywalker 40A ESC

```
W_ESC_1= N_m_1*str2double(Inputs(10)); %ESC Weight of type 1

W_ESC_2= N_m_2*str2double(Inputs(11)); %ESC Weight of type 2
```

From Specsheet of Gemfan 15x8 Nylon Propeller and 18x5.5 Carbon Fiber Propeller

```
W_p_1= N_m_1*str2double(Inputs(12)); %Propellers Weight of type 1
W_p_2= N_m_2*str2double(Inputs(13)); %Propellers Weight of type 2
```

From Specsheet of Pixhawk 5x Holybro

```
W_FC=str2double(Inputs(14)); %Flight Controller weight
```

Weight of Pixhawk 5x Holybro M8-N GPS

```
W_Misc= str2double(Inputs(15)); %Accessories Weight or Miscellaneous Weight
```

Weight of SG-90 Servo Motor

```
W_SM_1= N_s_1*str2double(Inputs(16)); %Servo Motors for Control Surfaces weight
```

Weight of JR Servo DS8425 (Not Included Because No Tilt Rotor)

```
W_SM_2= N_s_2*str2double(Inputs(17)); %Servo Motors for Tilt Mechanism
```

General Estimation From Internet (Real Estimation From Solidworks)

```
W_LG= str2double(Inputs(18)); %Landing Gear Weight
```

Weight of Wires/Cables (Estimation from Research Paper)

```
W_CB=str2double(Inputs(19));
```

Weight of the Airframe (Calculated from Scripts and Solidworks)

```
W_AF=str2double(Inputs(20)); % Estimate from Weight.mlx
W_MTOW_NAF=W_PL+W_b+W_m_1+W_m_2+W_ESC_1+W_ESC_2+W_p_1+W_p_2+W_FC+W_Misc+W_SM_1
+W_SM_2+W_LG+W_AF; %Maximum Takeoff Weight without airframe
W_MTOW=(W_MTOW_NAF)/(1-W_CB);
```

Wing Reference Area and Required Thrust

```
rho_sea= 1.225; %Density at Sea Level in kg/m^3
rho_ceiling= 1.15 ;%Density at Maximum Height in kg/m^3
sigma_ceiling= rho_ceiling/rho_sea; %ratio of desnity of working altitude to
sea level
Cdo=str2double(Inputs(22)); %zero_lift_drag_coefficient
AR_w=str2double(Inputs(21)); %Wing Aspect Ratio
Ostawald_Efficiency= str2double(Inputs(23));
K=1/(pi()*AR_w*Ostawald_Efficiency); %drag_due_to_lift_coefficient
eta_p_stall= 0.85;
Vc=17.5; %Cruise Speed (Estimation from Book and Statistics)
Vs=10.5; %Stall Speed (Estimated from Statistics and Book)
```

Wing Loading as a Function of Stall Speed

```
Power_Loadng_Stall_Speed=1:0.5:200;
Wing_Loading_Stall_Speed=0.5*rho_sea*Vs.^2*Cl_max_w_2d;
```

Estimation of Maximum Speed

```
V_max=1.3*Vc; % 30% greater than cruise speed Vmax = 1.2VC to 1.3VC (4.58)

Wing_Loading_Vmax=1:0.5:200;

Power_Loading_Vmax=(sigma_ceiling*eta_p_stall)./((0.5*rho_sea.*V_max.^3*Cdo.*(
Wing_Loading_Vmax).^-
1)+(2*K.*Wing_Loading_Vmax)./(rho_sea*sigma_ceiling.*V_max));
```

Aircraft Zero Lift Drag Coefficient Estimation

```
% Average of 0.4 (Sadraey Book)
```

Estimation of Rate of Climb:

```
Wing_Loading_Rate_Of_Climb=1:0.5:200;

eta_climb=0.6; %Prop Efficiency for CLimb (Estimation from Book)

ROC= 3; %Rate of Climb (Hardcore Estimation)

Lift_to_Drag_Ratio= 11; % (Estimated from Tabl 4.11)

c_ROC=(ROC/eta_climb);

d_ROC=sqrt((2.*Wing_Loading_Rate_Of_Climb)/(rho_sea*sqrt(3*Cdo/K)))*(1.155/(Li
ft_to_Drag_Ratio*eta_climb));

Power_Loading_Rate_Of_Climb=(1./(c_ROC+d_ROC));
```

Absolute Ceiling Estimation

```
h_alt=400; %Altitude in Feet

sigma_relative_density=(1-6.873*10^-6*h_alt)^4.26;

Wing_Loading_Absolute_Ceiling=1:0.5:200;

ROC_Ceiling=0.1;

e_ceiling=(ROC_Ceiling/eta_climb);

f_ceiling=sqrt((2.*Wing_Loading_Rate_Of_Climb)/(rho_ceiling*sqrt(3*Cdo/K)))*(1
.155/(Lift_to_Drag_Ratio*eta_climb));

Power_Loading_Absolute_Ceiling=sigma_relative_density./(e_ceiling+f_ceiling);

figure('Position',[0 0 1920 1080])

hold on

xline(Wing_Loading_Stall_Speed,'linewidth',3);

S_w=(W_MTOW*g)/Wing_Loading_Stall_Speed;

index=round(Wing_Loading_Stall_Speed/0.5);

Power_Loading_DP=Power_Loading_Rate_Of_Climb(index);

P_DP=(W_MTOW*g)/Power_Loading_DP;

b_w=sqrt(AR_w*S_w);

C_tip_w=b_w/AR_w;
```

Plots and Results

```
plot(Wing_Loading_Absolute_Ceiling,Power_Loading_Absolute_Ceiling,Wing_Loading
_Rate_Of_Climb,Power_Loading_Rate_Of_Climb,Wing_Loading_Vmax,Power_Loading_Vma
x,'linewidth',3)

grid on

axis([0,200,0,1])

set(gca,'YTick',0:0.20:1)

title('Matching Plot')

xlabel('Wing loading (Nm^-2)')

ylabel('Power loading (NW^-1)')

disp("The Maximum Take Off Weight is: " +W_MTOW+ " kg")

disp("The Power Required is: " + P_DP + " Watt")

disp("The Wing Area Required is: " + S_w +" m^2")

disp("The Wing Span is: " +b_w+" m" )

disp("The Wing Chord is:"+C_tip_w+" m")

plot(Wing_Loading_Stall_Speed,Power_Loading_DP,"Marker","x","MarkerSize",30,"M
arkerEdgeColor",'red','Color',[1 1 1])

legend('Stall Speed','Absolute Ceiling','Rate of Climb','Maximum
Speed','Design Point')

set(gca, 'visible', 'on')

hold off
```

12.2 Lift Line Theory Wing

```
N = 9; % (number of segments - 1)
S_w;
AR_w % Aspect ratio
lambda_w = 0.95; % Taper ratio
alpha_twist = 0.000000000000000001; % Twist angle (deg)
i_w = 4.5; % wing setting angle (deg)
tbyc_max_w=0.0984;
CL_alpha_w_2d = 1.8*pi*(1+0.8*tbyc_max_w); % lift curve slope 2-D
CL_alpha_w_3d=CL_alpha_w_2d/(1+CL_alpha_w_2d/(pi*AR_w));lift curve slope 3-D
CL_alpha_w_3d=CL_alpha_w_2d/(1+CL_alpha_w_2d/(pi*AR_w)); %lift curve slope 3-D
alpha_0 = -4.75; % zero-lift angle of attack (deg)
b_w; % wing span (m)
MAC = S_w/b_w; % Mean Aerodynamic Chord (m)
Croot = (1.5*(1+lambda_w)*MAC)/(1+lambda_w+lambda_w^2); % root chord (m)
theta = pi/(2*N):pi/(2*N):pi/2;
alpha = (i_w+alpha_twist):-alpha_twist/(N-1):i_w;
% segment's angle of attack
z = (b_w/2)*cos(theta);
c = Croot * (1 - (1-lambda_w)*cos(theta)); % Mean Aerodynamics
%Chord at each segment (m)
mu = c * CL_alpha_w_2d / (4 * b_w);
LHS = mu.*(alpha-alpha_0)/57.3; % Left Hand Side
% Solving N equations to find coefficients A(i):
for i=1:N
for j=1:N
B(i,j) = sin((2*j-1) * theta(i)) * (1 + (mu(i) * (2*j-1)) /sin(theta(i)));
end
end
A=B\transpose(LHS);
for i = 1:N
sum1(i) = 0;
sum2(i) = 0;
for j = 1 : N
sum1(i) = sum1(i) + (2*j-1) * A(j)*sin((2*j-1)*theta(i));
sum2(i) = sum2(i) + A(j)*sin((2*j-1)*theta(i));
```

```
end
end
CL = 4*b_w*sum2 ./ c;
CL1=[0 CL(1) CL(2) CL(3) CL(4) CL(5) CL(6) CL(7) CL(8) CL(9)];
y_s=[b_w/2 z(1) z(2) z(3) z(4) z(5) z(6) z(7) z(8) z(9)];
plot(y_s,CL1,'-o')
grid
title('Lift distribution')
xlabel('Semi-span location (m)')
ylabel ('Lift coefficient')
CL_w_3d = pi * AR_w * A(1)
```

CL from Operational Requirements:

Section's Ideal Lift Coefficient:

```
Cl_c_req_2d=(W_MTOW*g)/(0.5*rho_ceiling*Vc^2*S_w)
Cl_c_req_3d=Cl_c_req_2d/0.95
Cl_i=Cl_c_req_3d/0.9
```

Section's Maximum Lift Coefficient:

```
CL_max=(2*W_MTOW*g)/(rho_sea*Vs^2*S_w)
CL_max_w=CL_max/0.95
CL_max_gross=CL_max_w/0.9
```

Wing_Parameters Final:

```
C_root_w
C_tip_w=C_root_w*lambda_w
MAC_w=(2/3)*C_root_w*((1+lambda_w+lambda_w^2)/(1+lambda_w))
Mean_Wing_Area=b_w*MAC_w
```

12.3 Power Required and Battery Weight Calculation

```
V_c_LLT=sqrt((2*Wing_Loading_Stall_Speed)/(rho_ceiling*CL_w_3d))

Coefficient from Lift Line Theory

CD=Cdo+K*CL_w_3d^2;

P_C=sqrt((2*(W_MTOW*g)^3*CD^2)/(rho_ceiling*S_w*CL_w_3d^3)) % Power Required
for Cruise

R_plane=50*1000 % Range of Plane in meters

t_cruise=(R_plane/V_c_LLT)/3600 % Time of cruising in Hours

E_cruise=(t_cruise*P_C) % Energy for cruising in Wh

V_take_off=5 % Vertical take-off velocity in m/s

L_take_off=(W_MTOW*g)+0.5*rho_sea*V_take_off^2*S_w*Cdo % Lift required for
vertical take-off in newtons

P_take_off=L_take_off*V_take_off % Power Required for Vertical Take-off in W
h_alt=100 % Cruising Altitude in m

t_take_off= (h_alt/V_take_off)/3600 % Time required for take-off in hours

E_take_off=t_take_off*P_take_off % Power Required for take-off in Wh

E_descend=E_take_off; % Both assumed to be same

E_total=E_take_off+E_cruise+E_descend % Total Energy Required

mu_battery=200; % Battery density in Wh/kg

FOS_battery=0.85; % Percentage of safe discharge for battery

W_b_req=E_total/(mu_battery*FOS_battery) % Battery weight in kg
```

12.4 Horizontal and Vertical Tail Design

Horizontal Tail Design

Step 1+2: Configuration Selection

H-Tail

Step 3: Horizontal Tail Volume Coefficient

```
V_h = 0.45; %0.45 from Table 6.2 (Sadraey Book)
```

Step 4: Horizontal Tail Moment Arm

```
D_F = 0.2; % assumption from CAD model area known
% As a general rule, for a single-seat single-engine prop-driven GA aircraft, the factor Kc is assumed to be 1.1
Kc = 1.25; % Fudge Factor
l_h_opt = Kc*sqrt((4*MAC_w*Mean_Wing_Area*V_h)/(pi*D_F))
```

Step 5: Horizontal tail Planform Area

```
S_h = (V_h*MAC_w*S_w)/l_h_opt
```

Step 6: Wing/Fuselage Aerodynamic Pitching Moment Coefficient

```
Cm_w_2d = -0.1230 % Maximum Airfoil Pitching Moment MH-116 -0.1230(Airfoil Tools)
sweep_angle_w = 0;
alpha_w_t = 0;
Cm_w_3d = Cm_w_2d*((AR_w*(cos(sweep_angle_w)^2))/(AR_w+(2*cos(sweep_angle_w)))) + 0.01*alpha_w_t
```

Step 7: Cruise Lift Coefficient

```
Cl_c_req_3d % From Lift Line Theory of Wing
```

Step 8: Horizontal tail desired lift coefficient at cruise

```
h = 0.2; % From SolidWorks
ho = 0.25; % From SolidWorks
Cl_h_req = (Cm_w_3d + (Cl_c_req_3d*(h-ho)))/V_h % Required Tail Lift Coefficient
```

Step 9: Horizontal Tail Airfoil Selection

NACA 0009

- Optimum -ve Cl at -3 degree
- Does not stall before wing.
- Need to check actual tail and wing

Step 10: Horizontal Sweep & Dihedral Angle

```
sweep_angle_h = 0
dihedral_angle_h = 0
```

Step 11: Horizontal Tail Aspect Ratio & Taper Ratio

```
AR_h = (2/3)*AR_w
Lambda_h = 1
```

Step 12: Horizontal Tail Lift Curve Slope

```
tbyc_max_h=0.09 %NACA 0009
CL_alpha_h_2d=1.8*pi*(1+0.8*tbyc_max_h);
CL_alpha_h_3d=CL_alpha_h_2d/(1+CL_alpha_h_2d/(pi*AR_h));
```

Step 13: Horizontal Tail Angle of Attack at Cruise

```
alpha_h_i = Cl_h_req/CL_alpha_h_3d % Required tail incidence angle
alpha_f= -2 %Fuselage angle of attack
i_h = alpha_f - alpha_h_i % Effective tail incidence angle
```

Step 14: Horizontal Tail Span, Root Chord, Tip Chord, MAC

```
b_h = sqrt(AR_h * S_h)
C_root_h = b_h/AR_h
C_tip_h = Lambda_h*C_root_h
MAC_h=2/3*C_tip_h*((1+Lambda_h^2+Lambda_h)/(1+Lambda_h))
Mean_Tail_Area=b_h*MAC_h
```

Step 15: Horizontal Tail Lifting Line Theory

```
run("Lift_Line_Theory_Tail.mlx") %Should be greater than achieved in step 8
```

Step 16: Checking for Tail Stall

```
%Will be checked in XFLR5
```

Step 17: Final Check for Longitudinal Stability Check

```
eta_h=0.9; %Efficienciy of horizontal tails
C_m_alpha=CL_alpha_w_3d*(h-ho)-
CL_alpha_h_3d*eta_h*(Mean_Tail_Area/Mean_Wing_Area)*(l_h_opt/C_root_h-h) %If
negative than tail is stable , (Lognitudinal_Stability)
```

Vertical Tail Design

Step 1: Configuration Selection

H-Tail

Step 2: Vertical tail volume coefficient

```
V_v = 0.14; %From Table 6.6 of Sadraey (Cessna 177)
```

Step 3: Vertical Tail Moment Arm

```
l_v_opt = l_h_opt;
```

Step 4: Vertical tail Planform Area

```
S_v = (b_w*S_w*V_v)/l_v_opt
```

Step 5: Vertical Tail Airfoil Section

NACA 0010

Reason: less drag + symmetric + lift curve slope

```
tbyc_max_v=0.1 %For NACA 0010 Airfoil
```

Step 6: Vertical tail Aspect Ratio

```
AR_v = 1.5 % Initial assumption from Table 6.6 of Sadraey Book
CL_alpha_v_2d=1.8*pi*(1+0.8*tbyc_max_v)
CL_alpha_v_3d=CL_alpha_v_2d/(1+CL_alpha_v_2d/(pi*AR_h))
```

Step 7: Vertical Tail Taper Ratio

```
Lambda_v = 1
```

Step 8: Vertical Tail Incidence Angle

```
i_v = 0
```

Step 9: Vertical Tail Sweep Angle

```
Alpha_Sweep_v= 0
```

Step 10: Vertical Tail Dihedral Angle

```
dihedral_v = 0
```

Step 11: Vertical Tail Span, Root Chord, Tip Chord, MAC

```
b_Vtail=sqrt(S_v*AR_v)
C_tip_v = C_root_h
C_root_v = Lambda_v*C_tip_v
MAC_v = (2/3)*C_root_v*((1+Lambda_v+(Lambda_v^2))/(1+Lambda_v))
Mean_S_v=b_Vtail*MAC_v
save("Tail_Design.mat")
```

12.5 Lift Line Theory Horizontal Tail

```
N = 9; % (number of segments-1)
S_h; %Tail Area
AR_h; %Aspect Ratio
Lambda_h; % Taper ratio
alpha_twist = 0.00001; % Twist angle (deg)
a_h = -4.5; % tail angle of attack (deg)
tbyc_max_w=0.09;
CL_alpha_w_2d = 1.8*pi*(1+0.8*tbyc_max_w); % lift curve slope 2-D
CL_alpha_w_3d=CL_alpha_w_2d/(1+CL_alpha_w_2d/(pi*AR_w));lift curve slope 3-D
CL_alpha_w_3d=CL_alpha_w_2d/(1+CL_alpha_w_2d/(pi*AR_w)); %lift curve slope 3-D
alpha_0 = 0.000001; % zero-lift angle of attack (deg)
b_h; % tail span
MAC = S_h/b_h; % Mean Aerodynamic Chord
Croot = (1.5*(1+Lambda_h)*MAC)/(1+Lambda_h+Lambda_h^2); % root chord
theta = pi/(2*N):pi/(2*N):pi/2;
alpha=a_h+alpha_twist:-alpha_twist/(N-1):a_h;
% segment’s angle of attack
z = (b_h/2)*cos(theta);
c = Croot * (1 - (1-Lambda_h)*cos(theta)); % Mean
%Aerodynamics chord at each segment
mu = c * CL_alpha_w_2d / (4 * b_h);
LHS = mu .* (alpha-alpha_0)/57.3; % Left Hand Side
% Solving N equations to find coefficients A(i):
for i=1:N
for j=1:N
B(i,j)=sin((2*j-1) * theta(i)) * (1+(mu(i) *(2*j-1))/sin(theta(i)));
end
end
A=B\transpose(LHS);
for i = 1:N
sum1(i) = 0;
sum2(i) = 0;
for j = 1 : N
sum1(i) = sum1(i) + (2*j-1) * A(j)*sin((2*j-1)*theta(i));
sum2(i) = sum2(i) + A(j)*sin((2*j-1)*theta(i));
```

```
end
end
CL_tail = pi * AR_h * A(1)
```

12.6 Sizing of Motor and Propeller (Cruise Mode)

Diameter of Propeller:

```
FOS_p=1.2; %factor of safety for propulsion power
K_np = 1; %Propeller Efficiency
eta_p= 0.75; %Propeller Efficiency
AR_p= 7; %Propeller Aspect Ratio
V_max_ts=250;   % m/s (Maximum Propeller Motor Tip Speed Table Sadraey)
Cl_p_2d=0.2; %Propeller Lift Coefficient
D_p=K_np*sqrt((2*P_DP*AR_p*FOS_p)/((rho_ceiling*(0.7*V_max_ts)^2)*Cl_p_2d*V_c_LLT)) % Diameter of propeller in meters
```

RPM of Propeller:

```
V_ts=sqrt(V_max_ts^2-V_c_LLT^2)_% Maximum Tip Speed
omega_p=vpa((2*V_ts)/D_p*(60/(2*pi)),5) % RPM of Motor
```

12.7 Airframe Weight Calculation

Wing weight:

```
tbyC_max_w = 0.13;
rho_mat = 160; % Material Density taken for Balsa Wood from Table 10.6 Sadraey
K_rho_w = 0.001; % Wing Density factor taken for RC from 10.8 Sadraey
n_max = 1.5; % Max load factor taken for RC from 10.9 Sadraey
n_ult = 1.5*n_max; % Ultimate load factor
sweep_qc_w = sweep_angle_h; % Quarter-chord sweep angle in rad.
W_w=S_w*MAC_w*tbyC_max_w*rho_mat*K_rho_w*(((AR_w*n_ult)/(cos(sweep_qc_w)))^0.6)*(lambda_w^0.04)*g
```

Horizontal Tail Weight:

```
K_rho_h = 0.0175; % Horizontal Tail Density factor for RC taken from 10.10. Sadarey
sweep_qc_h = 0; % Quarter-chord sweep angle for horizontal tail in rad.
CebyCh = 0.4; % Elevator to Horizontal Tail Chord Ratio (Table 12.18 Sadraey)
W_h=S_h*MAC_h*tbyc_max_h*rho_mat*K_rho_h*((AR_h/(cos(sweep_qc_h)))^0.6)*(Lambda_h^0.04)*(V_h^0.3)*(CebyCh^0.4)
```

Vertical Tail Weight:

```
K_rho_v  = 0.052; % Vertical Tail Density factor for RC taken from 10.10 Sadraey
sweep_qc_v = 0; % Quarter chord sweep angle for vertical tail in rad.
CrbyCv = 0.3;% Rudder to Tail Chord Ratio (Table 12.18 Sadraey)
W_v=S_v*MAC_v*tbyc_max_v*rho_mat*K_rho_v*((AR_v/(cos(sweep_qc_v)))^0.6)*(Lambd
a_v^0.04)*(V_v^0.2)*(CrbyCv^0.4)
```

Fuselage weight:

```
L_f = 0.65; %Fuselage length.
Fuselage_Diameter = 0.323; %Max fuselage dia (assumed).
K_inlet = 1; % It is 1 only for inlets not on fuselage.
K_rho_f = 0.003; %Fuselage Density factor for RC & UAV taken from 10.11.
rho_mat_f = 1800;
W_f = L_f*(Fuselage_Diameter^2)*rho_mat_f*K_rho_f*(n_ult^0.25)*K_inlet
```

Landing Gear weight:

```
W_lg = 0.1; %Assumption
```

Installed Engine weight:

```
W_m_1+W_m_2; Total Motor Weight Taken from Matching Plot
W_airframe= W_lg + W_w + W_h + W_v + W_f + W_m_1+W_m_2 %Total Weight of the
Airframe
```

Notes:

Most values taken from tables of Chapter 10 of Sadraey book and the approximate midpoints of the ranges specified for those parameters in those tables. For the **fuselage density factor K_rho_f**, the book had 0.0021-0.0026 for UAVs and then 0.0015-0.0025. So, for this parameter, a value of 0.023 was assumed because it is approximately the midpoint for the UAV range but also lies within the range for RC vehicle, since our vehicle fits the description of both these classes.

12.8 Aileron Design

Step 1: Design Requirements

Low Cost

Manufacturability

Step 2+3: Roll Surface Configuration

Aileron only

Step 4: Aircraft Class and Critical Flight phase

Class: I

Flight Phase: B

Level of acceptability: 1

Step 5: Handling Quality Design Requirements

From Table 12.12 of Sadraey,

```
t_req = 2.5;
phi_des = 45;
I_xx = 0.71551;
```

Step 6: Aileron Position

```
bai_by_b = 0.7;
ba_by_b = 0.2;
bao_by_b = 0.9;
```

Step 7: Aileron Chord to Wing Chord Ratio

```
Ca_by_C = 0.2;
```

Step 8: Aileron Effectiveness Parameter

```
%Aileron-to-wing-chord ratio: 0.2

tau_a = 0.41
```

Step 9: Rolling Moment Coefficient Derivative

```
%15-20 percent of wing
yi = bai_by_b*b_w/2
yo = bao_by_b*b_w/2
C_r = 1.5*MAC_w*((1+lambda_w)/(1+lambda_w+lambda_w^2));
Cl_delta_A = ((2*CL_w_3d*tau_a*C_r)/(S_w*b_w))*((yo^2/2+(2/3*((lambda_w-
1)/b_w)*yo^3))-(yi^2/2+(2/3*((lambda_w-1)/b_w)*yi^3)))
```

Step 10: Maximum Aileron Deflection

```
delta_Amax = 20 %typical value in degree
```

Step 11: Aircraft rolling moment coefficient (Cl)

```
Cl = Cl_delta_A*delta_Amax*pi/180
```

Step 12: Aircraft rolling moment (LA)

```
V_app = 1.3*Vs
L_A = 0.5*rho_sea*(V_app^2)*S_w*Cl*b_w
```

Step 13: Steady-State Roll Rate

```
% Drag moment arm
y_D = 0.4*b_w/2 % assumption of 40 percent
% Wing horizontal/tail vertical tail rolling
% drag coefficient
C_D_R = 0.9
P_ss = ((2*L_A)/(rho_sea*(S_w + S_h + S_v)*C_D_R*(y_D^3)))^0.5
```

Step 14: Bank angle

```
%I_xx = 0.1129 kg-m^2;
phi_l = (I_xx*log(P_ss^2))/(rho_sea*(S_w + S_h + S_v)*C_D_R*(y_D^3))
```

Step 15: Aircraft rate of roll rate (P_dot)

```
P_dot = (P_ss^2)/(2*phi_l)
```

Step 16 & 17:

```
% Bank angle calculated in step 14 is compared with the bank angle of step 5. Since the bank angle calculated in step 14 is greater than the bank angle the time it takes the aircraft to achieve the bank angle of 30 deg is determined.
t_2 = ((2*phi_des*(pi/180)/P_dot)^1/2)
```

Step 18:

```
% If roll time obtained in step 16 or 17 is smaller than required roll time (treq) expressed in step 5 then continue else redesign.
```

Steps 19 and 20:

```
b_a = yo-yi
MAC_a = 0.2*MAC_w
S_a = 2*b_a*MAC_a
```

The solution is either to increase the aileron size (aileron span or chord) or to increase the aileron maximum deflection. Due to aileron stall concerns, and the location of the rear spar, the maximum aileron deflection and the aileron chord-to-wing chord ratio are not altered.

12.9 Elevator Design

Step 1: Low Cost & Manufacturability

Step 2: Find Take-off rotation acceleration (Skipped)

Step 3: Selection the Elevator Span

```
b_E = 0.8*b_h  % Elevator Span ( from table 12.3 Sadraey)
```

Step 4: Select max elevator deflection from table 12.3 of Sadraey

```
maxdefl_E = 15;    % Max Deflection of Elevator
```

Step 5-8: Skipped because related to Take-off Rotation

Step 9: Choose desired Tail lift coefficient

Step 10: Calculate angle of attack effectiveness of elevator using eq 12.75 (Sadraey)

```
effectiveness_E = ((Cl_h_req/CL_alpha_h_3d)-(i_h))/maxdefl_E % Attack
Effectiveness of Elevator
```

Step 11: Calculate Chord ratio of Elevator from Figure 12.12 of Sadraey

```
Chord_ratio_E = 0.05; % Use effectivenes_E in Figure 12.12

C_E = Chord_ratio_E*C_tip_h    % Elevator Chord
```

Step 12-15: Find Tail lift coefficient using CFD techniques at max negative elevator deflection and compare. If equal, you're good to go

Step 16: Calculate the Elevator Effectiveness Derivatives using eqs 12.51-53 of Sadraey

```
Cm_changedefl_E = (-CL_alpha_h_3d*eta_h*V_h*(b_E/b_h)*effectiveness_E);    %
Longitudinal Control Power Derivative

CL_changedefl_E = (CL_alpha_h_3d*eta_h*(S_h/S_w)*(b_E/b_h)*(effectiveness_E));
% Contribution of Elevator to Aircraft Lift

Cl_h_changedefl_E = (CL_alpha_h_3d*effectiveness_E);  % Contribution of the
Elevator to Tail Lift
```

Step 17: Calculate Elevator Deflection required for Longitudinal Trim

```
Cmo=-0.00848; % Aircraft cruise pitching moment

CL_slope=0.07626521; % Aircraft cruise lift curve slope

Cm_slope=0.00539271; % Aircraft cruise pitching moment curve slope

alpha_nose_calc = (Cmo*CL_changedefl_E)/((CL_slope*Cm_changedefl_E)-
(Cm_slope*CL_changedefl_E)) % Angle of Attack at which max deflection of
elevator required for longitudinal trim

def_E_calc = (Cmo*CL_slope)/((CL_slope*Cm_changedefl_E)-
(Cm_slope*CL_changedefl_E)) % required Deflection of Elevator for Longitudinal
trim
```

Step 18-22: Check if within the maximum permissible Elevator Deflection & check for horizontal tail stall

Step 23: Optimize Elevator

Step 24: Find Planform area of elevator and draw top view

```
S_E=b_E*C_E % Elevator Planform Area
```

12.10 Rudder Design

Steps 1+2: List data and identify cg locations, weight combination and altitude for spin recovery.

```
%Location of cg does not change.
```

Step 3: Determine the Aircraft AOA during Spin Maneuver.

```
alpha_spin = 40; %in degrees.
%This value is approximated as being close to (and beyond) the
%angle of attack of stall, and from Internet.
```

Step 4: Aircraft Mass Moments of Inertia in the body axis Coordinate System.

```
I_xx_B = 0.71551 %rolling inertia
I_zz_B = 2.23658 %yawing inertia
I_xz_B = 0.06072 %product of inertia
%Calculated via FEA of the model.
```

Step 5: Mass Moments of Inertia in the wind axis Coordinate System.

```
%Transformation Matrix
[I] = [(cosd(alpha_spin))^2 (sind(alpha_spin))^2 -(sind(2*alpha_spin));
(sind(alpha_spin))^2 (cosd(alpha_spin))^2 sind(2*alpha_spin);
0.5*sind(2*alpha_spin) -0.5*sind(2*alpha_spin) cosd(2*alpha_spin)]*[I_xx_B;
I_zz_B; I_xz_B]


I_xx_W = I(1,1) %rolling inertia
I_zz_W = I(2,1) %yawing inertia
I_xz_W = I(3,1) %product of inertia
```

Step 6: Desirable Rate of Spin Recovery

```
R_dot_SR = 1.4; %desired rate of yaw, taken from 12.122. of Sadraey. It is 80
in deg/s^2. This is the typical value used in aircraft design.
```

Step 7: Required Counteracting Yawing Moment.

```
N_SR = R_dot_SR*(((I_xx_W*I_zz_W)-(I_xz_W^2))/I_xx_W) %Eq. 12.120 of Sadraey
```

Step 8: Effective Vertical Tail Area

```
%It is the same as actual tail area because there are 2 vertical tails on
```

```
%top of which, the horizontal tail is sitting.
```

Step 9: Effective Vertical Tail Volume Ratio

```
V_v_e = V_v %Same as actual ratio.
```

Step 10: Rudder Span-to-Vertical Tail Ratio

```
span_ratio_R = 0.8; %Assumption from Table 12.3 (Sadraey) bR/bV
```

Step 11: Effective Rudder Span

```
%Same as actual.
```

Step 12: Max Rudder Deflection

```
delta_R = 30; %This is in +- degrees. Assumed from Table 12.3 of Sadraey
```

Step 13-15: Rudder AOA Effectiveness, Chord Ratio & Control Derivative

```
chord_ratio_R = 0.3; %Assumption from Table 12.3 CR/CV
tau_R = 0.525; %effectiveness approx from Figure 12.12 using chord_ratio_R
eta_v = 1;
C_n_delta_R = -CL_alpha_v_3d*V_v_e*eta_v*tau_R*span_ratio_R
```

Step 16: Rudder Span, Chord & Planform Area

```
b_R = 0.8*b_Vtail
C_R = 0.3*C_v_tip
S_R = b_R*C_R
```

Step 17: Rudder Design Validation

```
chord_ratio_R = 0.3; %Assumption from Table 12.3 CR/CV
delta_R_1 = (2*N_SR*57.298)/(rho_ceiling*(Vs^2)*S_w*b_w*C_n_delta_R)
if abs(delta_R_1) < delta_R && C_n_delta_R<0
    disp("Rudder geometry is acceptable.")
else
    disp("Rudder geometry is unacceptable.")
end
```

APPENDIX II: AUTOPILOT TUNING PARAMETERS

Q_A_ACCEL_P_MAX	110000
Q_A_ACCEL_R_MAX	110000
Q_A_ACCEL_Y_MAX	27000
Q_A_ANG_LIM_TC	1
Q_A_ANG_PIT_P	4.5
Q_A_ANG_RLL_P	4.5
Q_A_ANG_YAW_P	4.5
Q_A_ANGLE_BOOST	1
Q_A_INPUT_TC	0.2
Q_A_RAT_PIT_D	0.0036
Q_A_RAT_PIT_FF	0
Q_A_RAT_PIT_FLTD	10
Q_A_RAT_PIT_FLTE	0
Q_A_RAT_PIT_FLTT	20
Q_A_RAT_PIT_I	0.25
Q_A_RAT_PIT_IMAX	0.5
Q_A_RAT_PIT_P	0.25
Q_A_RAT_PIT_SMAX	50
Q_A_RAT_RLL_D	0.0036
Q_A_RAT_RLL_FF	0
Q_A_RAT_RLL_FLTD	10
Q_A_RAT_RLL_FLTE	0
Q_A_RAT_RLL_FLTT	20
Q_A_RAT_RLL_I	0.25
Q_A_RAT_RLL_IMAX	0.5
Q_A_RAT_RLL_P	0.25
Q_A_RAT_RLL_SMAX	50
Q_A_RAT_YAW_D	0
Q_A_RAT_YAW_FF	0
Q_A_RAT_YAW_FLTD	0
Q_A_RAT_YAW_FLTE	2.5
Q_A_RAT_YAW_FLTT	20
Q_A_RAT_YAW_I	0.018
Q_A_RAT_YAW_IMAX	0.5
Q_A_RAT_YAW_P	0.18
Q_A_RAT_YAW_SMAX	50

Q_A_RATE_FF_ENAB	1
Q_A_RATE_P_MAX	75
Q_A_RATE_R_MAX	75
Q_A_RATE_Y_MAX	75
Q_A_SLEW_YAW	6000
Q_A_THR_MIX_MAN	0.1
Q_A_THR_MIX_MAX	0.5
Q_A_THR_MIX_MIN	0.1
Q_ACCEL_Z	250
Q_ACRO_PIT_RATE	180
Q_ACRO_RLL_RATE	360
Q_ACRO_YAW_RATE	90
Q_ANGLE_MAX	3000
Q_ASSIST_ALT	0
Q_ASSIST_ANGLE	30
Q_ASSIST_DELAY	0.5
Q_ASSIST_SPEED	0
Q_AUTOTUNE_AGGR	0.1
Q_AUTOTUNE_AXES	7
Q_AUTOTUNE_MIN_D	0.001
Q_BACKTRANS_MS	3000
Q_ENABLE	1
Q_ESC_CAL	0
Q_FRAME_CLASS	1
Q_FRAME_TYPE	3
Q_FW_LND_APR_RAD	0
Q_FWD_MANTHR_MAX	0
Q_GUIDED_MODE	0
Q_LAND_ALTCHG	0.2
Q_LAND_FINAL_ALT	6
Q_LAND_ICE_CUT	1
Q_LAND_SPEED	50
Q_LOIT_ACC_MAX	250
Q_LOIT_ANG_MAX	15
Q_LOIT_BRK_ACCEL	50
Q_LOIT_BRK_DELAY	1

Q_LOIT_BRK_JERK	250
Q_LOIT_SPEED	500
Q_M_BAT_CURR_MAX	0
Q_M_BAT_CURR_TC	5
Q_M_BAT_IDX	0
Q_M_BAT_VOLT_MAX	0
Q_M_BAT_VOLT_MIN	0
Q_M_BOOST_SCALE	0
Q_M_HOVER_LEARN	2
Q_M_PWM_MAX	2000
Q_M_PWM_MIN	1000
Q_M_PWM_TYPE	0
Q_M_SAFE_DISARM	0
Q_M_SAFE_TIME	1
Q_M_SLEW_DN_TIME	0
Q_M_SLEW_UP_TIME	0
Q_M_SPIN_ARM	0.1
Q_M_SPIN_MAX	0.95
Q_M_SPIN_MIN	0.15
Q_M_SPOOL_TIME	0.25
Q_M_THST_EXPO	0.65
Q_M_THST_HOVER	0.35
Q_M_YAW_HEADROOM	200
Q_MAV_TYPE	0
Q_OPTIONS	0
Q_P_ACCZ_D	0
Q_P_ACCZ_FF	0
Q_P_ACCZ_FLTD	0
Q_P_ACCZ_FLTE	10
Q_P_ACCZ_FLTT	0
Q_P_ACCZ_I	1
Q_P_ACCZ_IMAX	800
Q_P_ACCZ_P	0.3
Q_P_ACCZ_SMAX	0
Q_P_ANGLE_MAX	0
Q_P_JERK_XY	2
Q_P_JERK_Z	5
Q_P_POSXY_P	1

Q_P_POSZ_P	1
Q_P_VELXY_D	0.35
Q_P_VELXY_FF	0
Q_P_VELXY_FLTD	5
Q_P_VELXY_FLTE	5
Q_P_VELXY_I	0.7
Q_P_VELXY_IMAX	1000
Q_P_VELXY_P	1.4
Q_P_VELZ_D	0
Q_P_VELZ_FF	0
Q_P_VELZ_FLTD	5
Q_P_VELZ_FLTE	5
Q_P_VELZ_I	0
Q_P_VELZ_IMAX	1000
Q_P_VELZ_P	5
Q_RC_SPEED	490
Q_RTL_ALT	15
Q_RTL_MODE	1
Q_TAILSIT_ENABLE	0
Q_THROTTLE_EXPO	0.2
Q_TILT_ENABLE	0
Q_TKOFF_ARSP_LIM	0
Q_TKOFF_FAIL_SCL	0
Q_TRAN_PIT_MAX	3
Q_TRANS_DECEL	2
Q_TRANS_FAIL	0
Q_TRANS_FAIL_ACT	0
Q_TRANSITION_MS	5000
Q_TRIM_PITCH	0
Q_VELZ_MAX	250
Q_VELZ_MAX_DN	0
Q_VFWD_ALT	0
Q_VFWD_GAIN	0
Q_WP_ACCEL	100
Q_WP_ACCEL_Z	100
Q_WP_JERK	1
Q_WP_RADIUS	200
Q_WP_RFND_USE	1

Q_WP_SPEED	500
Q_WP_SPEED_DN	150
Q_WP_SPEED_UP	250
Q_WP_TER_MARGIN	10
Q_WVANE_ANG_MIN	1
Q_WVANE_ENABLE	1
Q_WVANE_GAIN	1

Q_WVANE_HGT_MIN	0
Q_WVANE_LAND	-1
Q_WVANE_OPTIONS	0
Q_WVANE_SPD_MAX	0
Q_WVANE_TAKEOFF	-1
Q_WVANE_VELZ_MAX	0
Q_YAW_RATE_MAX	100

APPENDIX III: SPECIFICATIONS OF ELECTRONICS

13.1 T-Motor AT4125 (540 KV) Specifications

Figure 140. T-Motor AT4125 540 KV Long-Shaft BLDC [52]

Specifications			
Test Item	Long Shaft KV250	Weight (Incl. Cable)	350g
Motor Dimensions	Φ50*74mm	Internal Resistance	68mΩ
Lead	Enameled Wire 100mm	Configuration	12N14P
Shaft Diameter	IN：6mm OUT：6mm	Rated Voltage(Lipo)	12S
Idle Current(10V)	1.0A	Peak Current(180s)	50A
Max. Power(180s)	2200W	Recommendation	/
Test Item	Long Shaft KV540	Weight (Incl. Cable)	355g
Motor Dimensions	Φ50*74mm	Internal Resistance	14mΩ
Lead	Enameled Wire 100mm	Configuration	12N14P
Shaft Diameter	IN：6mm OUT：6mm	Rated Voltage(Lipo)	6S
Idle Current(10V)	2.6A	Peak Current(180s)	85A
Max. Power(180s)	2000W	Recommendation	/

Figure 141. Specifications of T-Motor AT4125 [72]

Type	Propeller	Throttle	Voltage (V)	Current (A)	Power (W)	RPM	Torque (N*m)	Thrust (g)	Efficiency (g/W)	Operating Temperature (℃)
AT4125 Long Shaft KV540	APC 15*8	40%	22.38	11.21	250.81	4943	0.341	1674	6.68	84 (Ambient Temperature:/)
		45%	22.34	13.58	303.32	5313	0.395	1929	6.36	
		50%	22.29	16.21	361.27	5650	0.452	2205	6.10	
		55%	22.24	19.14	425.84	5978	0.513	2492	5.85	
		60%	22.18	23.20	514.39	6382	0.595	2864	5.57	
		65%	22.10	27.69	611.87	6806	0.676	3233	5.28	
		70%	22.02	32.79	722.03	7193	0.766	3655	5.06	
		75%	21.93	38.58	845.87	7571	0.863	4081	4.82	
		80%	21.80	45.80	998.46	7963	0.970	4541	4.55	
		85%	21.68	52.89	1146.84	8301	1.072	4951	4.32	
		90%	21.52	62.57	1346.88	8577	1.213	5163	3.83	
		100%	21.36	72.77	1554.08	8879	1.344	5537	3.56	
	APC 16*8	40%	22.20	11.43	253.85	4637	0.378	1798	7.08	97 (Ambient Temperature:/)
		45%	22.16	13.89	307.76	4970	0.437	2069	6.72	
		50%	22.11	16.79	371.33	5309	0.502	2380	6.41	
		55%	22.05	20.26	446.90	5686	0.585	2771	6.20	
		60%	21.96	25.87	568.11	6118	0.694	3241	5.70	
		65%	21.86	31.71	693.11	6522	0.804	3738	5.39	
		70%	21.77	37.21	810.01	6873	0.896	4145	5.12	
		75%	21.66	44.10	955.01	7239	1.011	4635	4.85	
		80%	21.51	52.74	1134.53	7597	1.149	5207	4.59	
		90%	21.23	69.58	1477.35	8206	1.370	6054	4.10	
		100%	21.03	81.72	1718.70	8492	1.528	6618	3.85	

Note: Motor temperature is motor surface temperature @100% throttle running 10mins.
(Date above based on benchtest are for reference only, comparion with that of other motor types is not recommended.)

Figure 142. T-Motor AT4125 Test Data [72]

13.2 Gartt ML5210 (340 KV) Specifications

Figure 143. Gartt ML5210 (340 KV) Motor [55]

ML5210 MOTOR/340KV

Motor KV---------------------------------340KV RPM/V
Motor Resistance (RM)-----------------------0.0622 Ω
Idle Current (Io/10V)-------------------------0.7A/10V
Max Continuous Current --------------------------40A
Max Continuous Power--------------------------960W
Weight----------------------------------≈230g/8.11oz
Lipo Cell--6S-8S
Motor Diameter--------------------------60mm/2.36in
Motor Body Length----------------------30mm/1.18in
Configu-ration---------------------------------24N22P
Overall Shaft Length-------------------36.7mm/1.44in
Shaft Diameter-------------------------4.0mm/0.157in
Bolt holes spacing-----------------------25mm/0.98in
Bolt thread---------------------------------------M3×8

Figure 144. Specifications of VTOL Motor [55]

ML5210								
Item NO.	Volts (V)	Prop	Throttle	Amps (A)	Watts (W)	Thrust (g)	Efficiency (g/W)	Operating temperature(℃)
ML5210 340KV	24V	1555	50%	3.6	86.4	870	10.07	40℃
			54%	5	120.0	1100	9.17	
			57%	6	144.0	1260	8.75	
			62%	8	192.0	1530	7.97	
			66%	10	240.0	1800	7.50	
			70%	12	288.0	2050	7.12	
			74%	14	336.0	2280	6.79	
			78%	16	384.0	2510	6.54	
			81%	18	432.0	2740	6.34	
			100%	20	480.0	2920	6.08	
ML5210 340KV	24V	1755	50%	5.3	127.2	1230	9.67	61℃
			55%	8	192.0	1640	8.54	
			59%	10	240.0	1910	7.96	
			62%	12	288.0	2150	7.47	
			65%	14	336.0	2410	7.17	
			68%	16	384.0	2620	6.82	
			71%	18	432.0	2830	6.55	
			74%	20	480.0	3030	6.31	
			77%	22	528.0	3260	6.17	
			79%	24	576.0	3420	5.94	
			82%	26	624.0	3610	5.79	
			100%	28.3	679.2	3830	5.64	
ML5210 340KV	24V	1855	50%	6.8	163.2	1510	9.25	73℃
			52%	8	192.0	1720	8.96	
			55%	10	240.0	2040	8.50	
			58%	12	288.0	2210	7.67	
			61%	14	336.0	2480	7.38	
			63%	16	384.0	2670	6.95	
			65%	18	432.0	2910	6.74	
			68%	20	480.0	3120	6.50	
			70%	22	528.0	3330	6.31	
			73%	24	576.0	3510	6.09	
			75%	26	624.0	3660	5.87	
			78%	28	672.0	3840	5.71	
			80%	30	720.0	3950	5.49	
			82%	32	768.0	4070	5.30	
			100%	34.2	820.8	4180	5.09	
ML5210 340KV	24V	2055	50%	7.1	170.4	1600	9.39	78℃
			52%	8	192.0	1750	9.11	
			55%	10	240.0	2070	8.63	
			57%	12	288.0	2250	7.81	
			60%	14	336.0	2530	7.53	
			62%	16	384.0	2730	7.11	
			64%	18	432.0	2980	6.90	
			66%	20	480.0	3200	6.67	
			69%	22	528.0	3410	6.46	
			71%	24	576.0	3590	6.23	
			73%	26	624.0	3710	5.95	
			76%	28	672.0	3900	5.80	
			78%	30	720.0	4090	5.68	
			80%	32	768.0	4210	5.48	
			100%	36.8	883.2	4620	5.23	
Notes: The test condition oftemperature is motor surface temperature in 100% throttle while the motor run 10 min. environment temperature 26℃								

Figure 145. Test Data of VTOL Motor [55]

APPENDIX IV: FINANCES

Table 37 Bill of Materials

Category	**Product/Service**	**Qty.**	**Total Cost (Rs.)**
Airframe	Manufacturing	--	175000
Battery	TATTU 6S 22.2V 10000 mAh 25C Li-Po	1	32000
Flight Controller Kit	Holybro Pixhawk 5X + Baseboard + Power Module + M8N GPS + Power Distribution Board (PDB) + Cables	1	68500
Radio	FlySky FS-i6X Transmitter + FS-iA10B Receiver	1	13400
Telemetry	Holybro SiK Telemetry Radio V3	1	15500
Motor (Cruise)	T-Motor AT4125 (540 KV) Long Shaft BLDC Motor	1	21500
ESC (Cruise)	Hobbywing Skywalker 80A ESC	1	5400
Propeller (Cruise)	Gemfan 15x8 Nylon Propeller	1	1200
Motor (VTOL)	Gartt ML5210 (340 KV) 4.6 kg Thrust BLDC Motor	4	35600
ESC (VTOL)	Hobbywing X-Rotor 2-6S Li-Po 40A ESC	4	11000
Propeller (VTOL)	18x5.5 Carbon Fiber Propeller Pair	3	13350

BEC	UBEC	1	1250
Servo	Tower Pro SG90 9-Gram Mini Servo	5	1750
Servo Connections	Pushrods	5	150
Servo Connections	Control Horns	2	320
Servo Connections	Clevis	2	320
Servo Connections	Single Core Jumper Wires	5	250
Motor Connections	4mm Bullets	4	1200
Motor Connections	3.5mm Bullets	12	480
Connector	XT90	1	430
Connector	XT60	1	100
Wires	12” AWG Silicone Wire	6”	60
Wires	12” AWG Silicone Wire	1m	175
Wires	14” AWG Silicone Wire	5m	655
Wires	16” AWG Silicone Wire	5m	600

Pixhawk PDB Connections	Soldering	--	160
Motor Mounts	3D Printing	4	850
Tee Joints	3D Printing	8	4000
Total			**405,200**

APPENDIX V: ENGINEERING DRAWINGS

13.3 Exploded View

1	Fuselage
2	Right Wing
3	Left Wing
4	Right Winglet
5	Left Winglet
6	Vertical Tail
7	Horizontal Tail
8	CF Boom
9	Landing Gear Right
10	Landing Gear Left
11	VTOL Motor
12	VTOL Propeller
13	VTOL Mount
14	Cruise Motor
15	Cruise Propeller
16	Front Cutout
17	Back Cutout

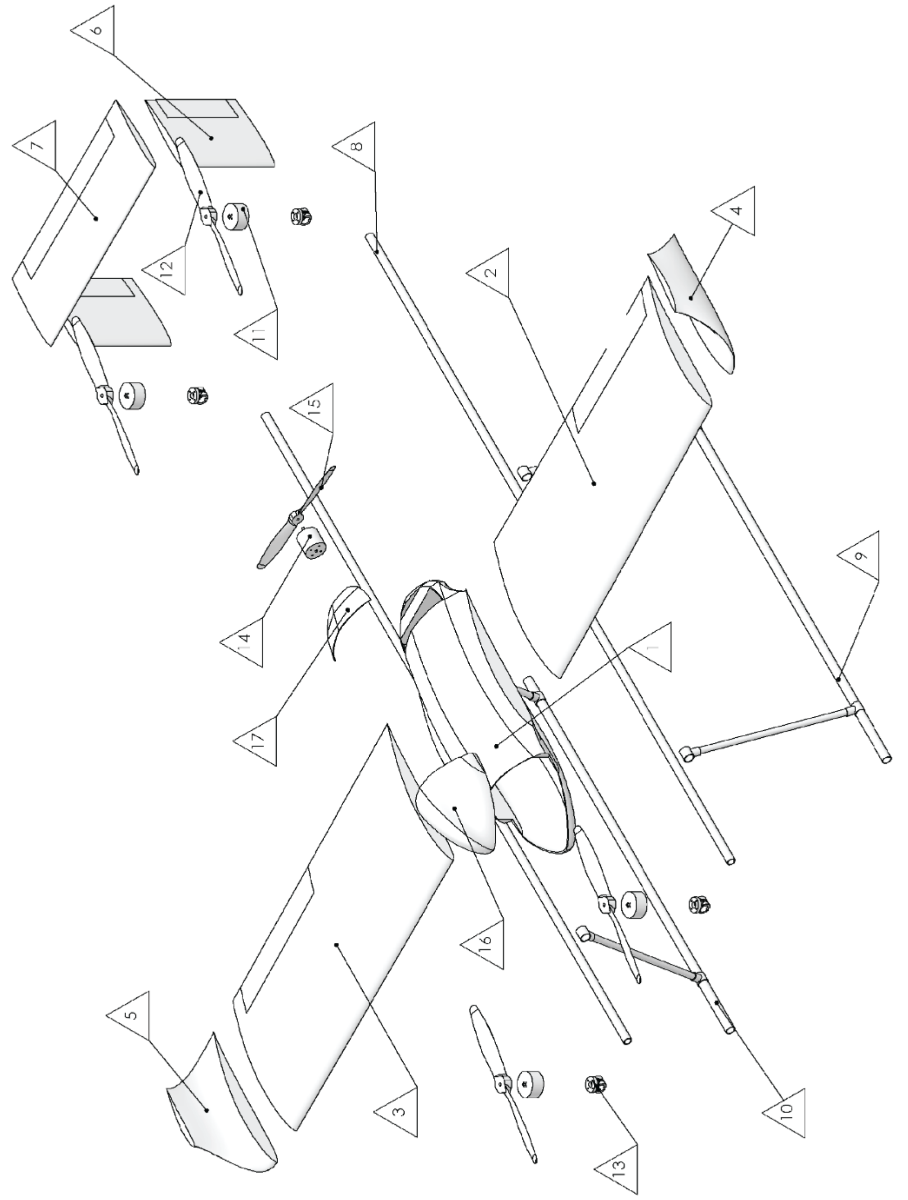

13.4 Assembly Drawing

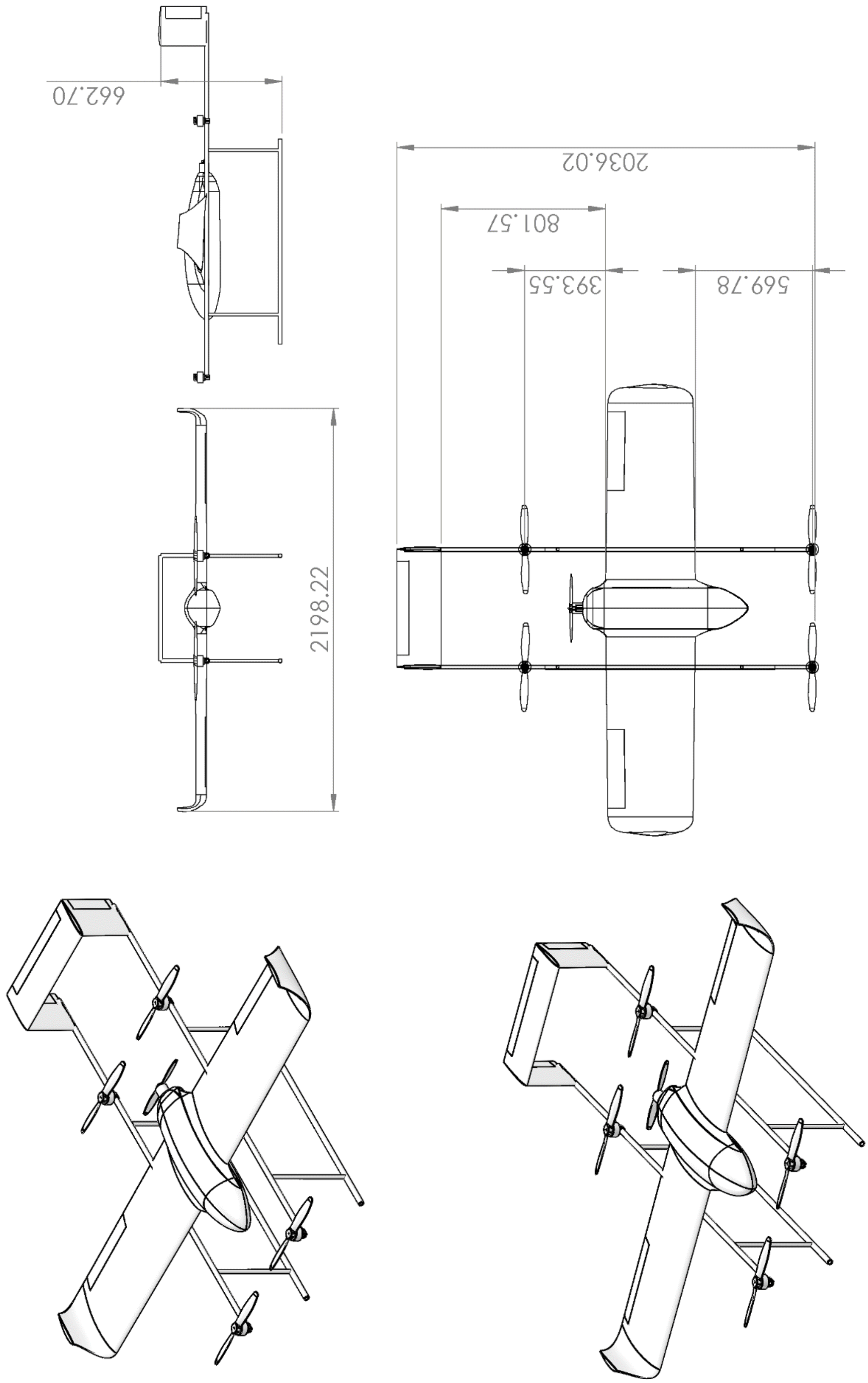

13.5 Wing

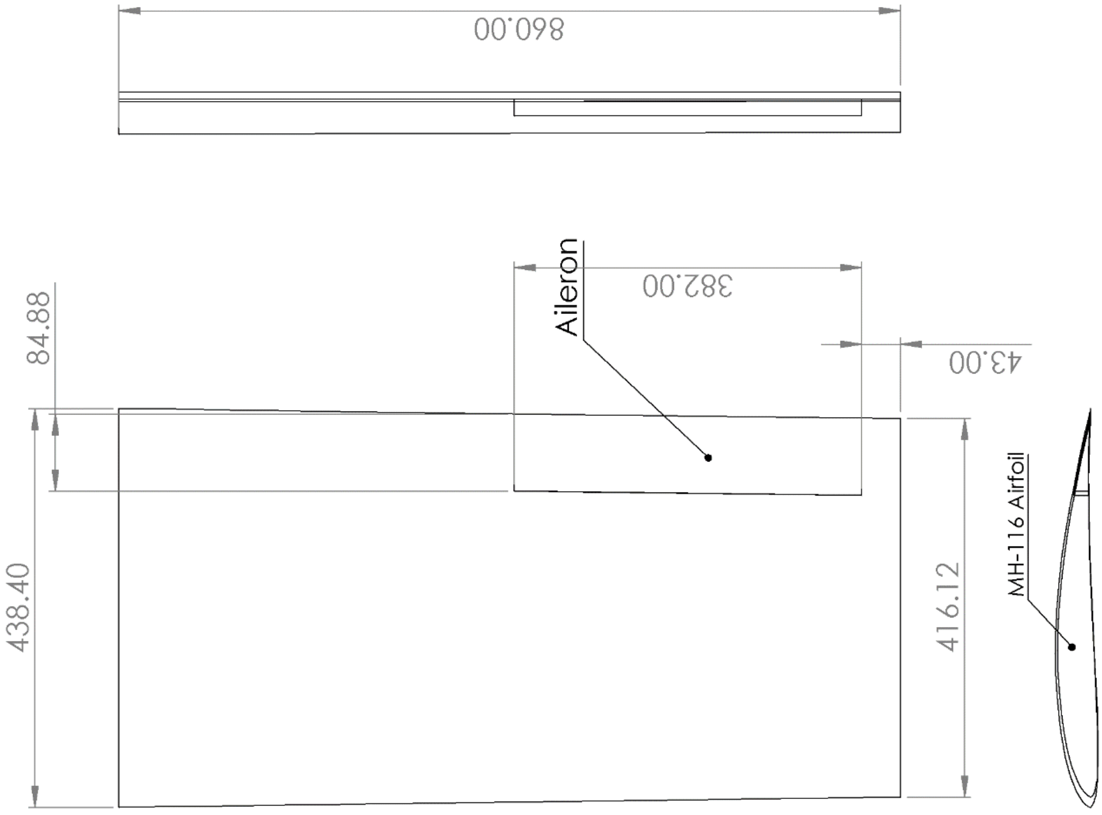

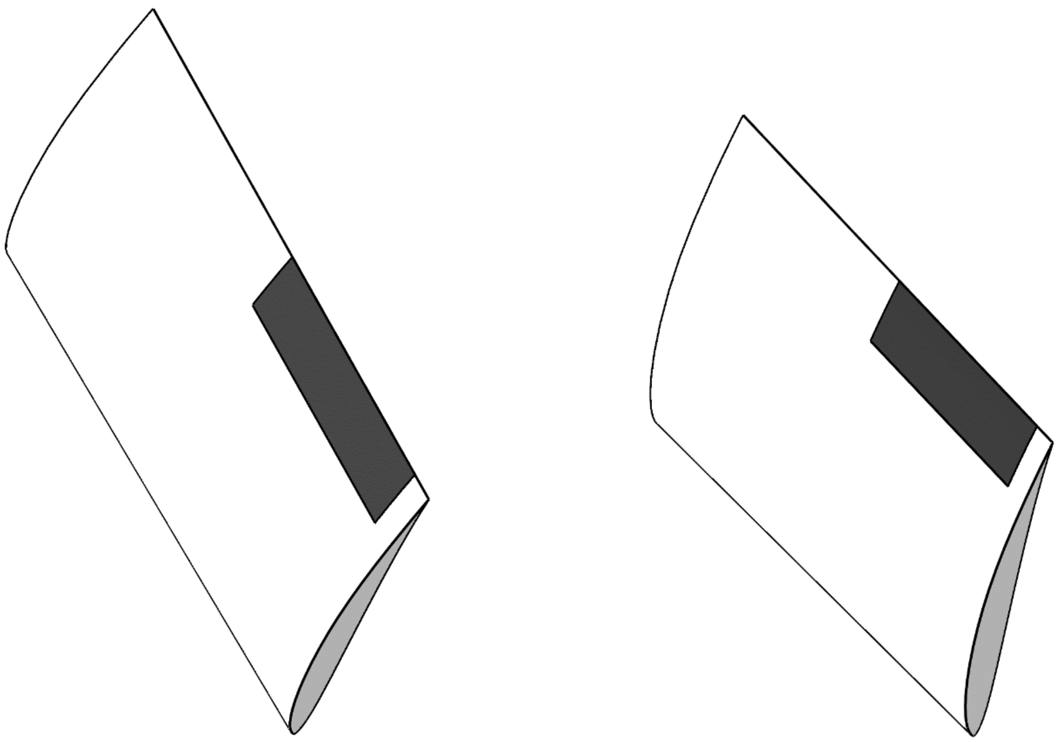

13.6 Winglet

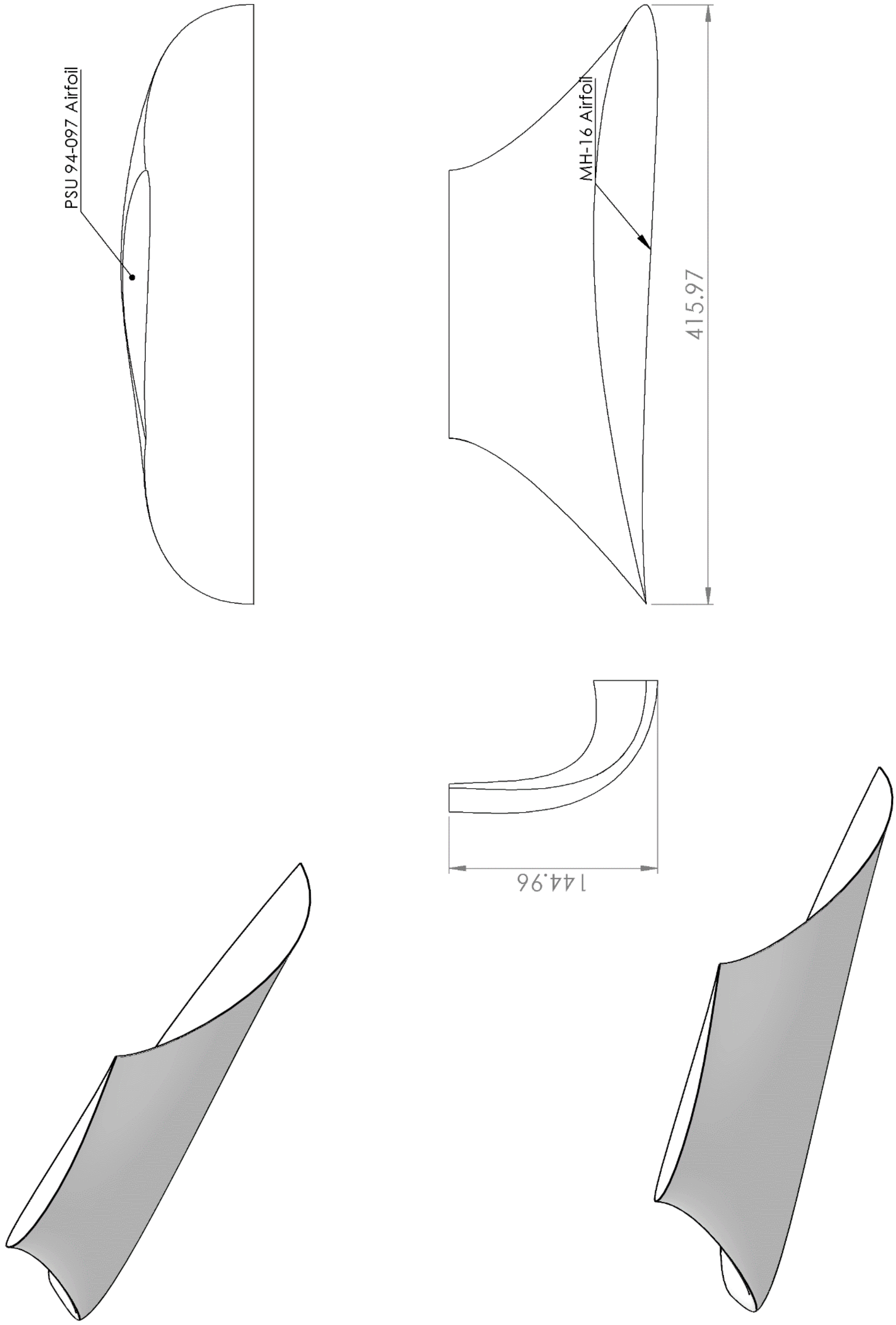

13.7 Horizontal Tail

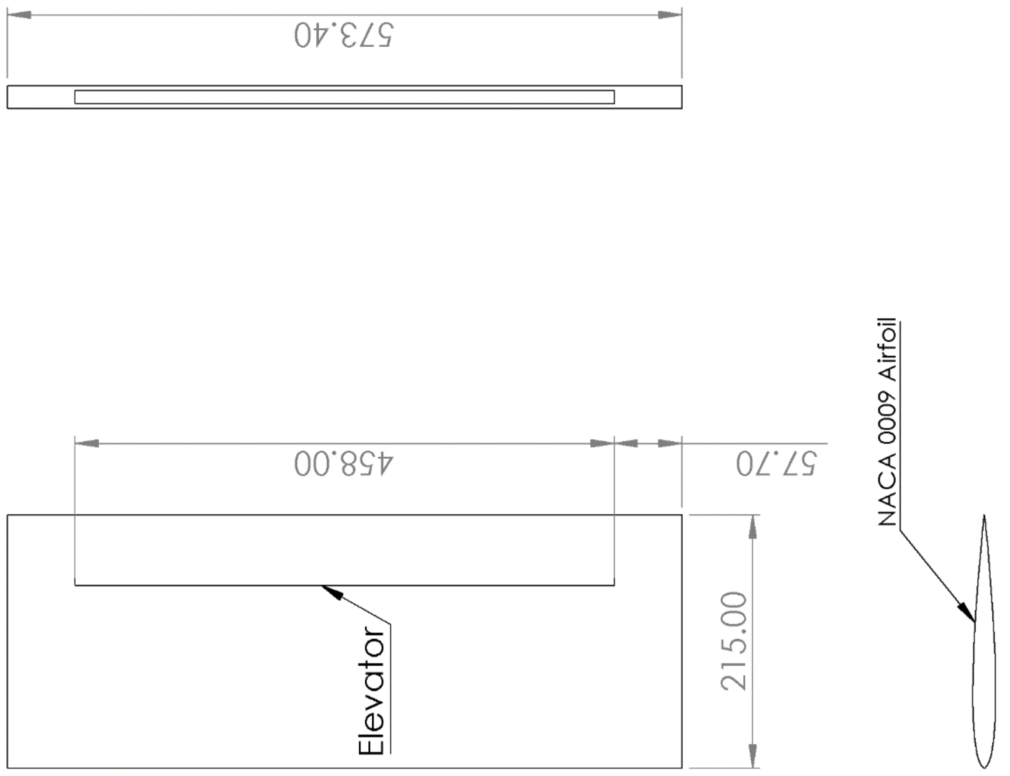

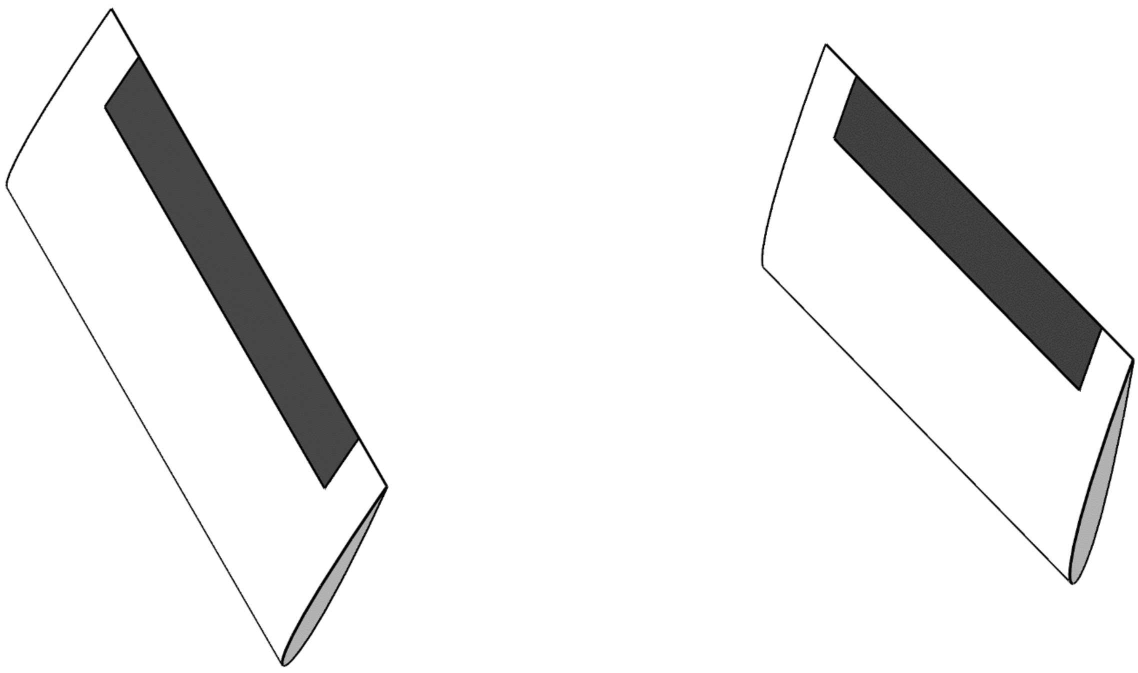

13.8 Vertical Tail

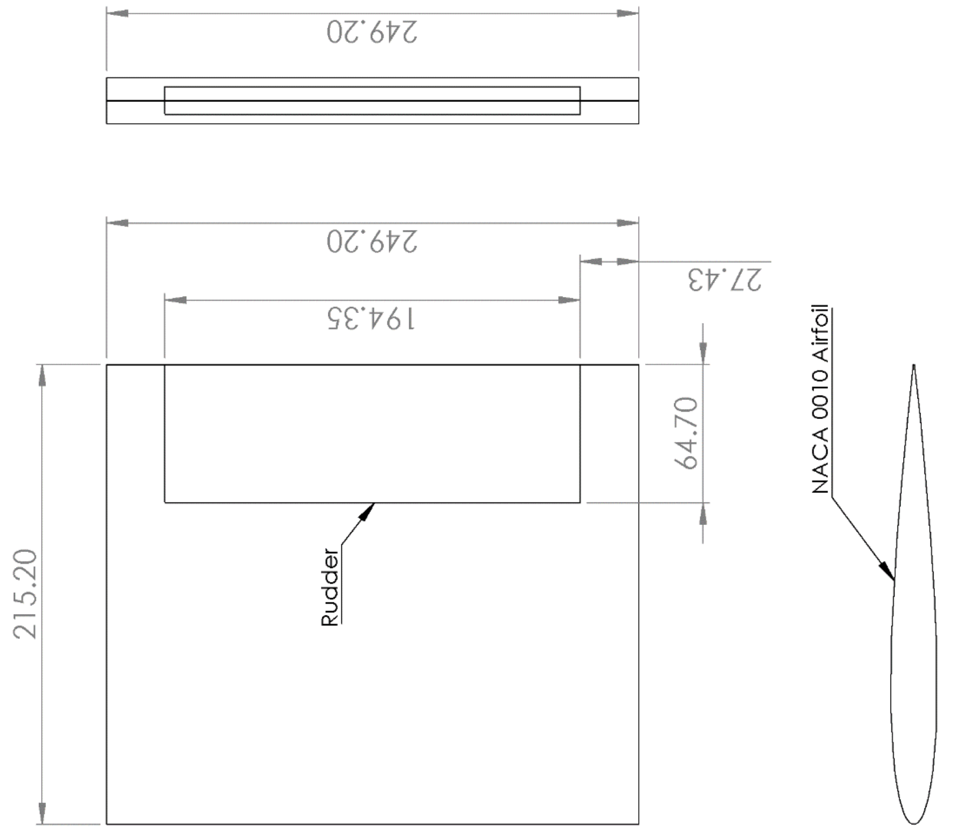

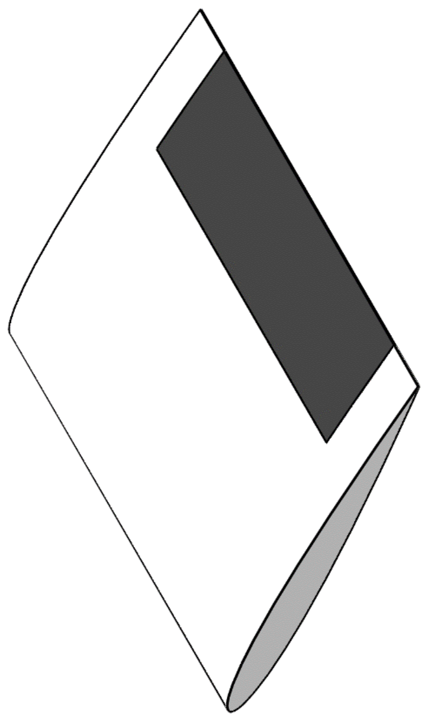

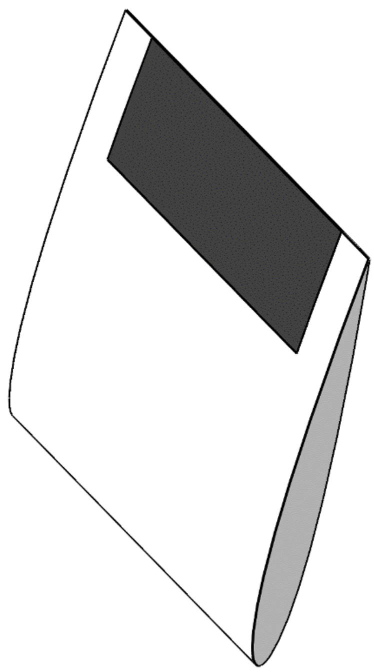

13.9 Fuselage

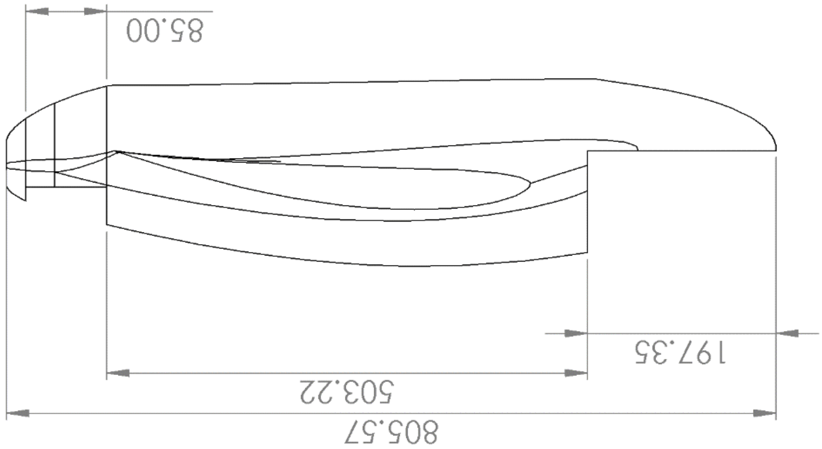

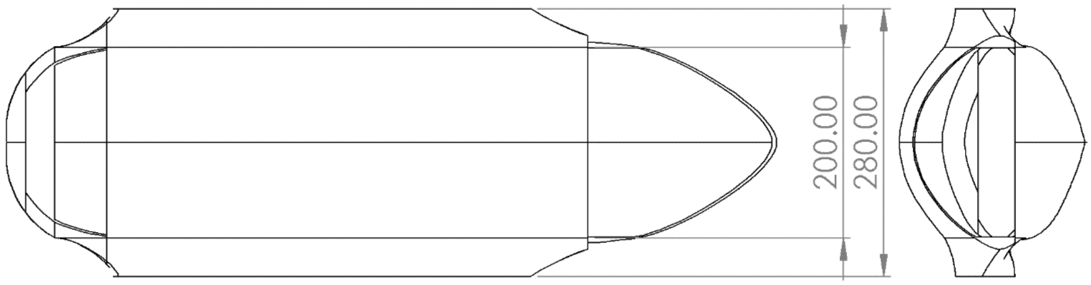

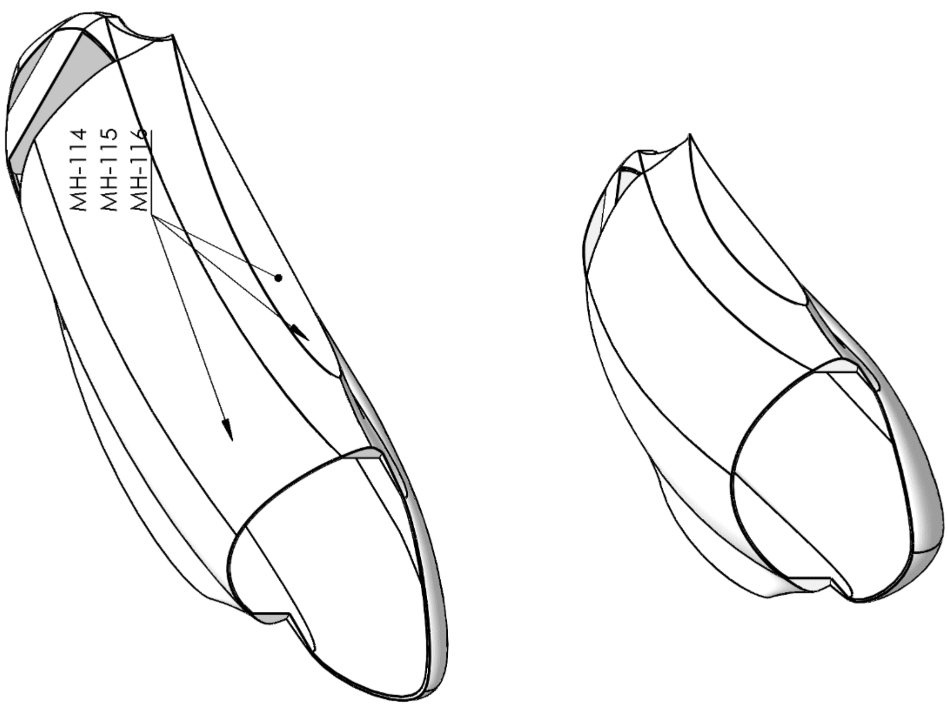

13.10 Landing Skid

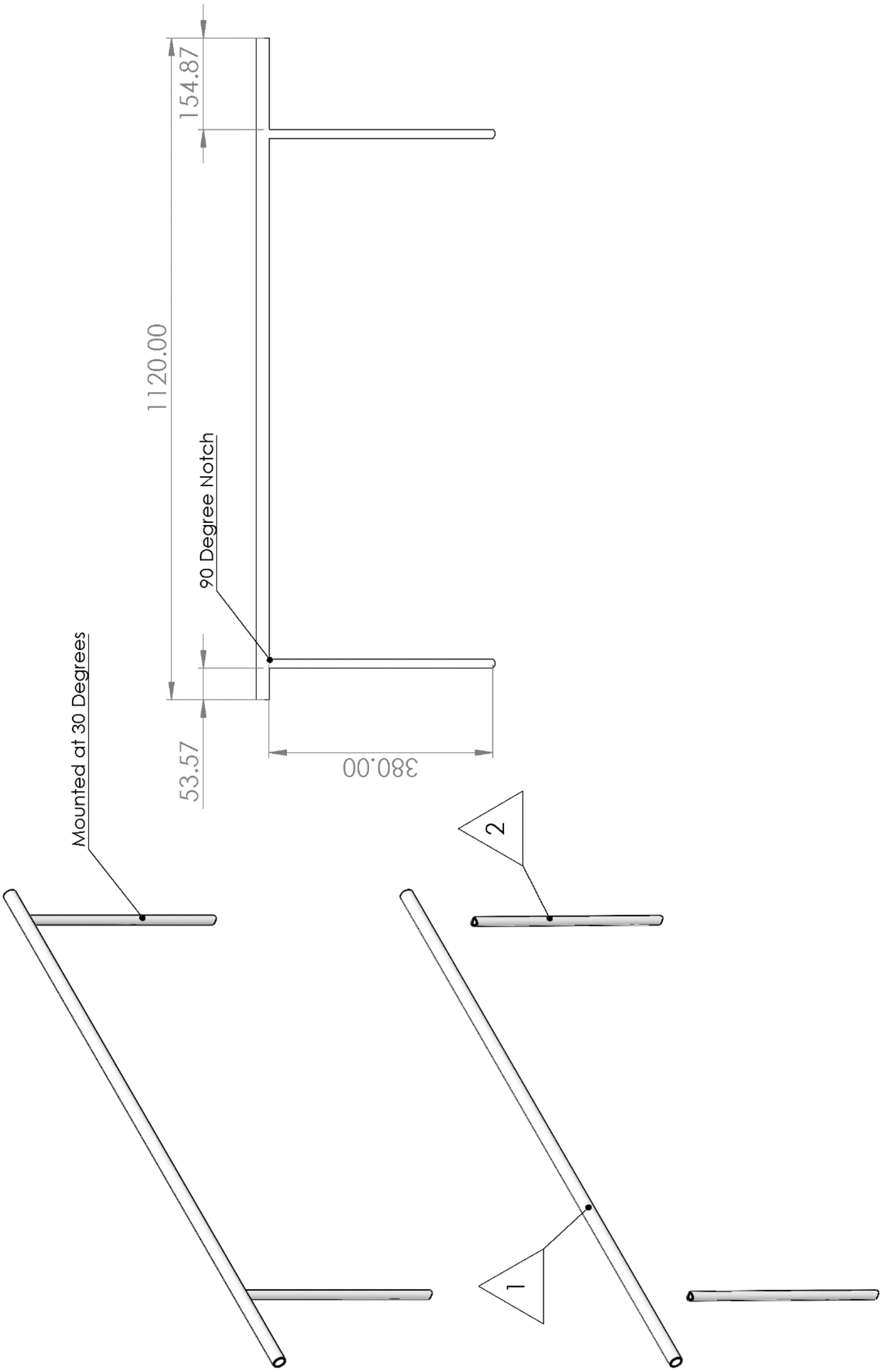

13.11 Boom

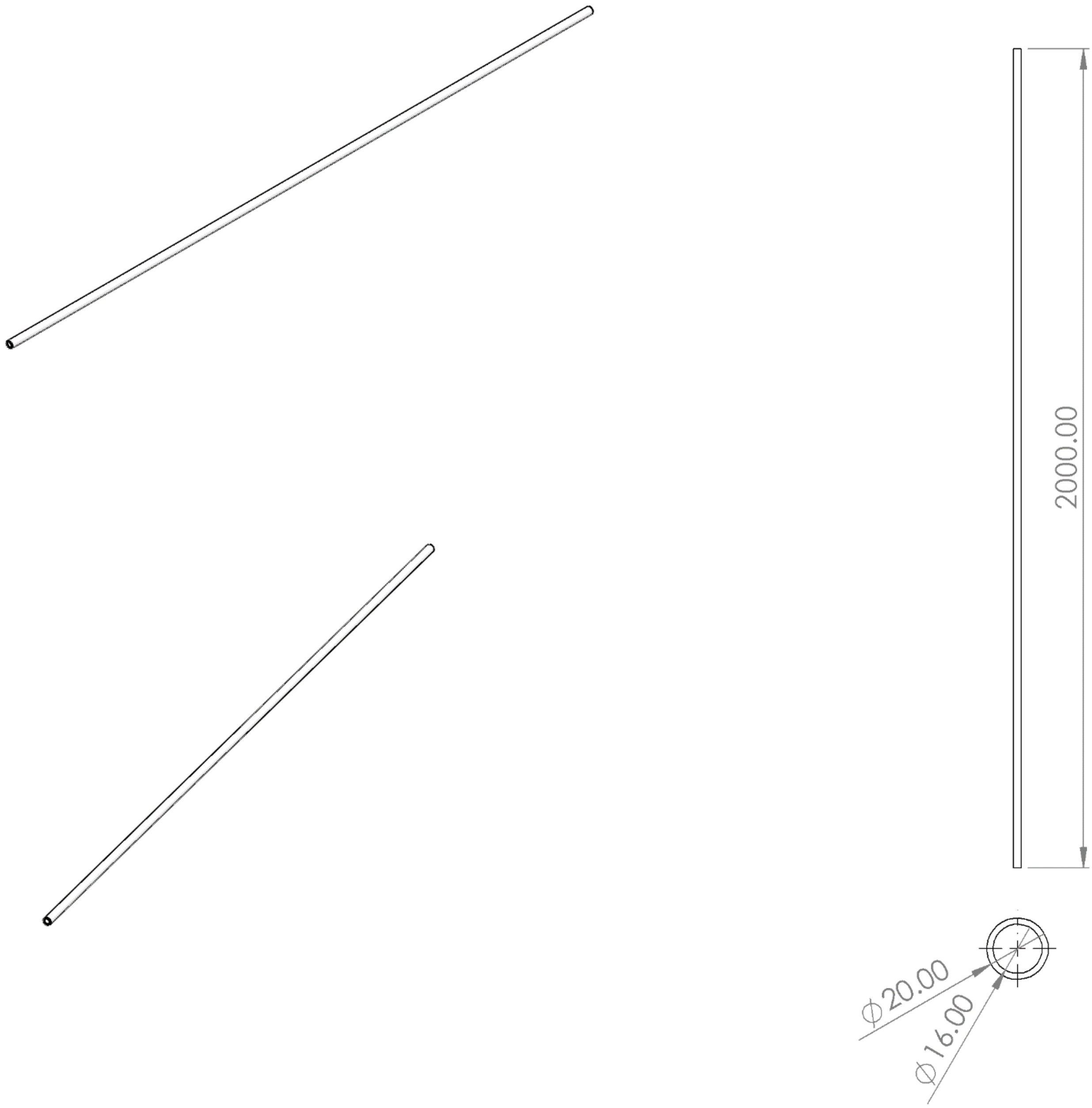

13.12 VTOL Motor Mount

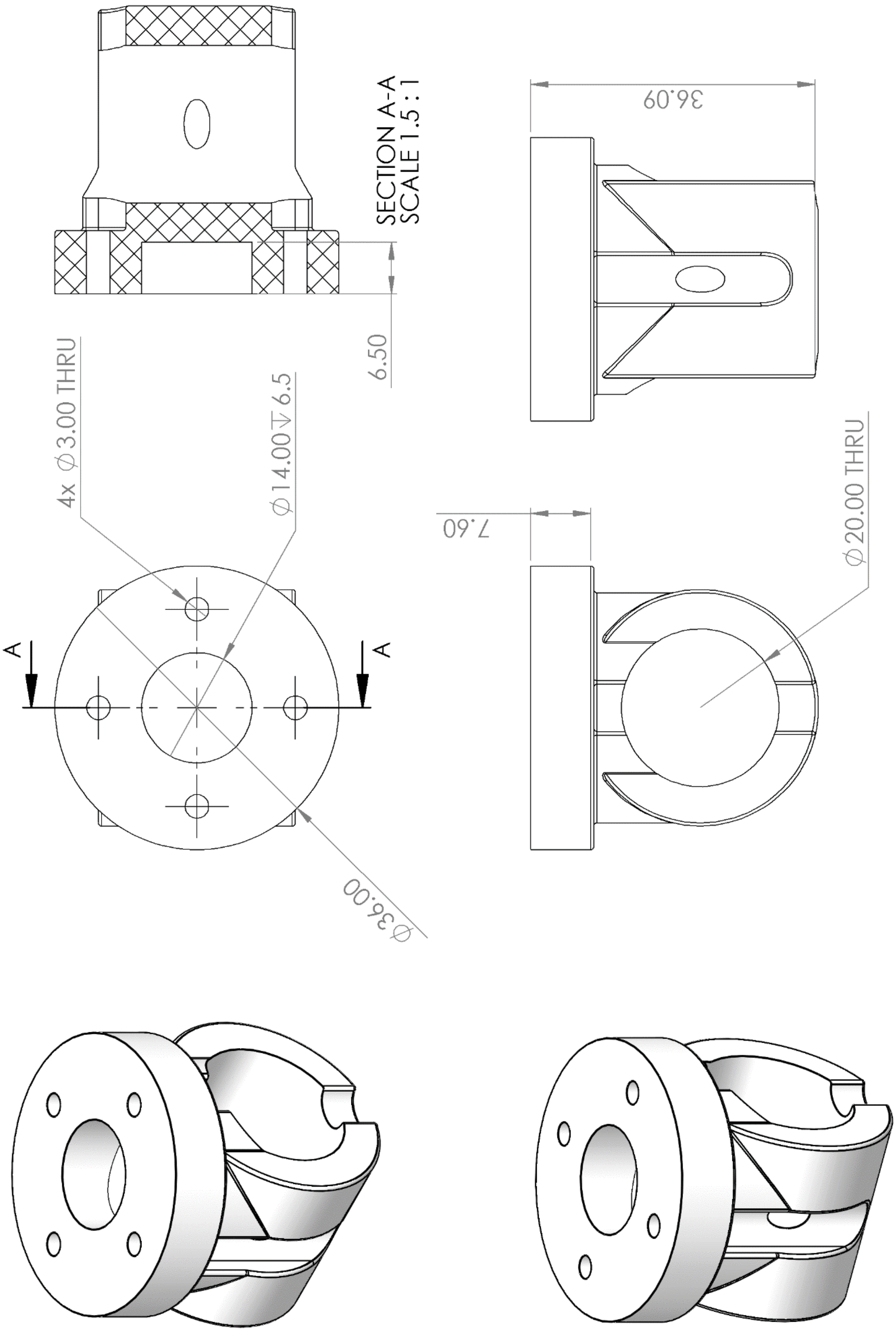

13.13 VTOL Motor (Gartt ML5210)

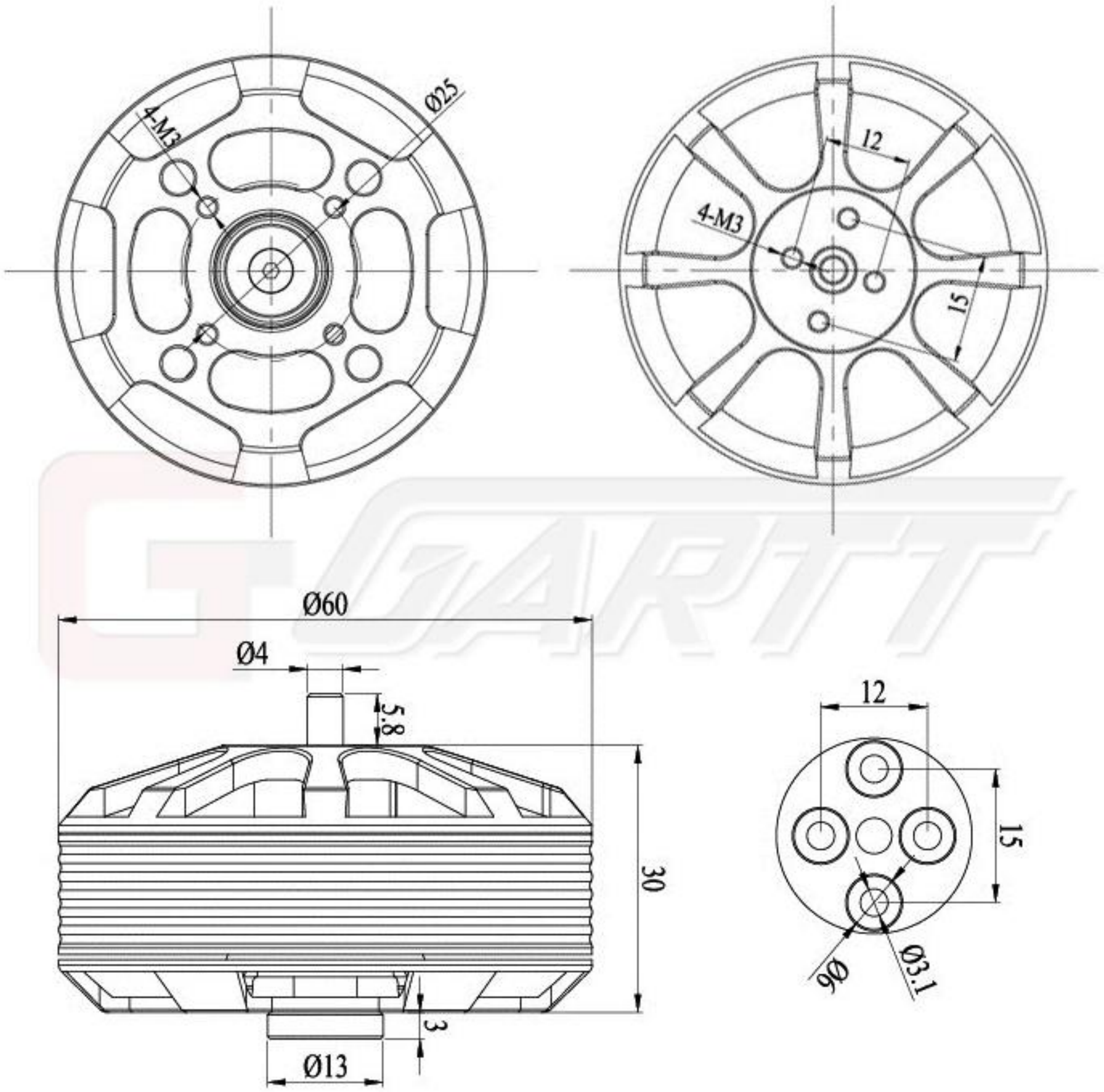

Figure 146. VTOL Motor Drawing [55]

13.14 Cruise Motor (T-Motor AT4125)

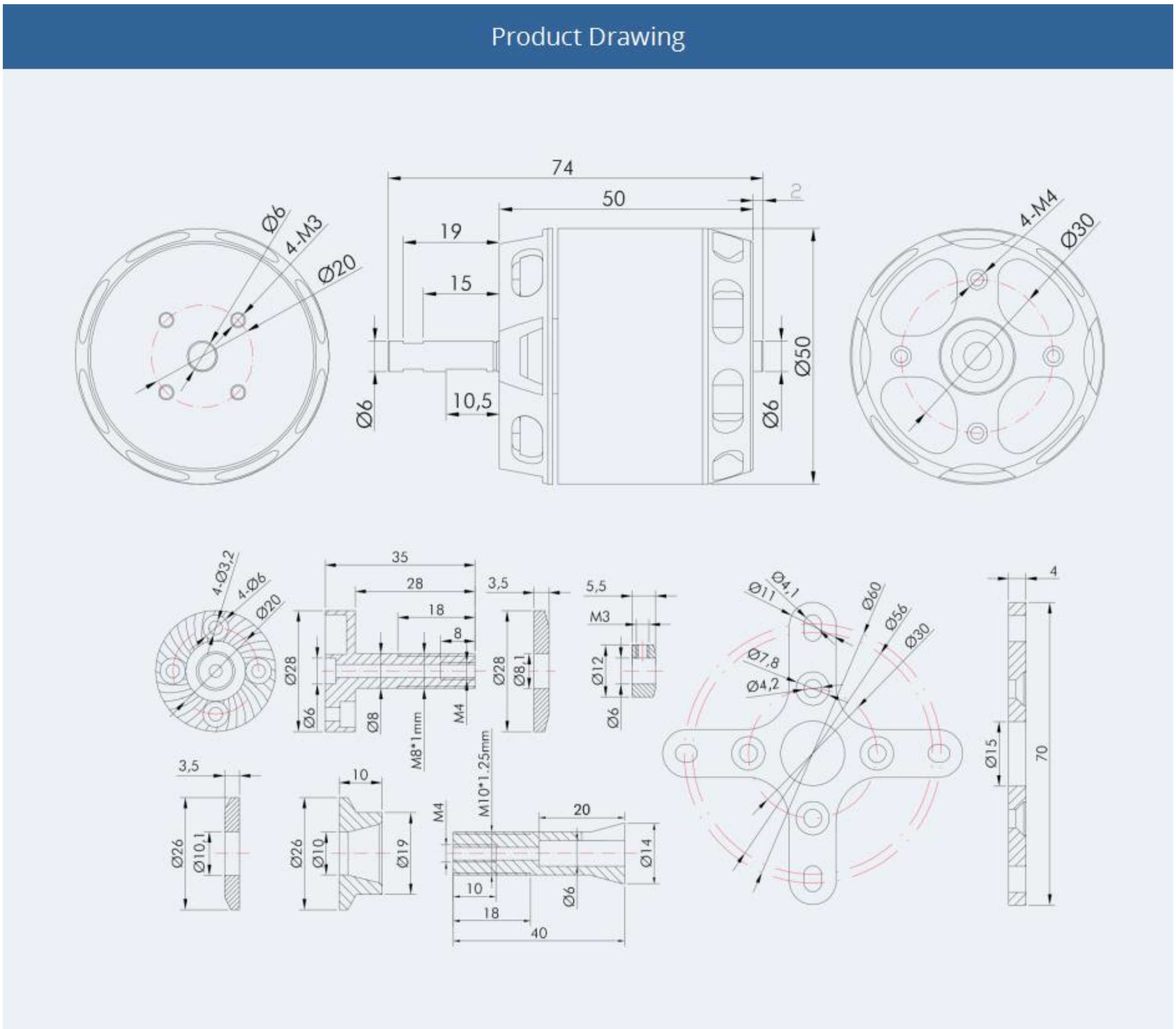

Figure 147. Cruise Motor Drawing [72]

BIBLIOGRAPHY

[1] "Quadcopter Pictures | Download Free Images on Unsplash," [Online]. Available: https://unsplash.com/s/photos/quadcopter. [Accessed January 2022].

[2] "Kettering Bug - Wikipedia," [Online]. Available: https://en.wikipedia.org/wiki/Kettering_Bug. [Accessed January 2022].

[3] "Hewitt-Sperry Automatic Airplane - Wikipedia," [Online]. Available: https://en.wikipedia.org/wiki/Hewitt-Sperry_Automatic_Airplane. [Accessed January 2022].

[4] "Lockheed D-21 - Wikipedia," [Online]. Available: https://en.wikipedia.org/wiki/Lockheed_D-21. [Accessed January 2022].

[5] "Tadiran Mastiff - Wikipedia," [Online]. Available: https://en.wikipedia.org/wiki/Tadiran_Mastiff.

[6] "IAI Scout - Wikipedia," [Online]. Available: https://en.wikipedia.org/wiki/IAI_Scout. [Accessed January 2022].

[7] "General Atomics MQ-1 Predator - Wikipedia," [Online]. Available: https://en.wikipedia.org/wiki/General_Atomics_MQ-1_Predator. [Accessed January 2022].

[8] "Mini Mugin 2600mm UAV T tail/V Tail Platform - Mugin UAV," [Online]. Available: https://www.muginuav.com/product/mini-mugin-2-6m-uav-t-tail-v-tail-platform/. [Accessed January 2022].

[9] "New Mugin 2930mm H Tail VTOL UAV Platform Frame Kit|uav," [Online]. Available: https://www.aliexpress.com/item/32858257526.html. [Accessed January 2022].

[10] M. Sadraey, Aircraft design a Systems Engineering Approach, Wiley.

[11] "Brushless DC electric motor," [Online]. Available: https://en.wikipedia.org/wiki/Brushless_DC_electric_motor.

[12] B. Zhang, Z. Song, F. Zhao and C. Liu, "Overview of Propulsion Systems for Unmanned Aerial Vehicles," 2021.

[13] "How do ESCs work," [Online]. Available: https://howtomechatronics.com/how-it-works/how-brushless-motor-and-esc-work/.

[14] "Propulsion Systems and their types for UAV," [Online]. Available: http://wiki.theuavguide.com/.

[15] "Dynamics of Flight," NASA, [Online]. Available: https://www.grc.nasa.gov/www/k-12/UEET/StudentSite/dynamicsofflight.html.

[16] "Modelling Aircraft Servos," [Online]. Available: http://deankmiller.com/model-aircraft-servos/.

[17] "Development of Unmanned Aerial Vehicle," SemanticScholar, [Online]. Available: https://www.semanticscholar.org/paper/Development-of-Unmanned-Aerial-Vehicle-Real-Time-Singh/6be0fbf2baf09c8bd761af3881bdd8edc4598866/figure/17.

[18] "Quadrotor in Y4 Configuration," [Online]. Available: https://www.semanticscholar.org/paper/Quadrotor-in-Y4-Configuration-Sagr%C3%A9n-Yun/db32fa6d90ee75977467ebbdd60226bc2cb4b1e3#references.

[19] B. Cuffari, "Using Sensors in Drones," AZOSensors, [Online]. Available: https://www.azosensors.com/article.aspx?ArticleID=1149.

[20] D. G. Hull, in *Fundamentals of Airplane Flight Mechanics*, 2007.

[21] J. D. A. Jr, Aircraft Performance and Design, McGraw-Hill, 1999.

[22] NASA, "Principle of Aerodynamics," [Online]. Available: https://slideplayer.com/slide/7471659/.

[23] "Wing Geometry Definitions," NASA, [Online]. Available: https://www.grc.nasa.gov/www/k-12/airplane/geom.html.

[24] Yankeemojo, "Flight Training Manual," [Online]. Available: http://yankeemojo.blogspot.com/2013/07/flight-training-manual.html.

[25] "1: General comparison between UAVs with VTOL and CTOL abilities....," [Online]. Available: https://www.researchgate.net/figure/1-General-comparison-between-UAVs-with-VTOL-and-CTOL-abilites_tbl1_267737119. [Accessed January 2022].

[26] "Advantages and disadvantages of multirotor, fixed-wing, and... | ...," [Online]. Available: https://www.researchgate.net/figure/Advantages-and-disadvantages-of-multirotor-fixed-wing-and-single-rotor-drones_tbl2_348954274. [Accessed January 2022].

[27] "Drone Types: Multi-Rotor Vs Fixed-Wing Vs Single-Rotor Vs Hybrid ...," [Online]. Available: https://www.auav.com.au/articles/drone-types/. [Accessed January 2022].

[28] A. S. Saeed, A. B. Younes, C. Cai and G. Cai, "A survey of hybrid Unmanned Aerial Vehicles," *Progress in Aerospace Sciences,* pp. 91-105, 2018.

[29] M. Sadraey, Design of Unmanned Aerial Systems, Wiley.

[30] Ngoc AnhVu, Duy KhangDang et al, Electric propulsion system sizing methodology for an agriculture multicopter.

[31] "Drone Laws in Pakistan," [Online]. Available: https://drone-laws.com/drone-laws-in-pakistan/.

[32] M. Hassanalian and A. Abdelkefi, "Classifications, applications, and design challenges of drones: A review," *Progress in Aerospace Sciences,* pp. 99-131, 2017.

[33] "de Havilland Sea Vixen - Wikipedia," [Online]. Available: https://en.wikipedia.org/wiki/De_Havilland_Sea_Vixen. [Accessed January 2022].

[34] "NACA 0009 9.0% smoothed (n0009sm-il)," [Online]. Available: http://airfoiltools.com/airfoil/details?airfoil=n0009sm-il. [Accessed January 2022].

[35] "AM480 3D_AM Series_Motors_Fixed_Wing_T-MOTOR Store-Official ...," [Online]. Available: https://store.tmotor.com/goods.php?id=1167. [Accessed May 2022].

[36] "Drone Motor Calculator," [Online]. Available: https://www.omnicalculator.com/other/drone-motor. [Accessed Jan 2022].

[37] "Smart Hobby - Gratt ML 5210," [Online]. Available: https://www.smarthobby.pk/product-page/gartt-ml-5210-340kv-4600gram-4-6kg-thrust-brushless-motor. [Accessed Jan 2022].

[38] D. P. Raymer, Aircraft Design. A Conceptual Approach, American Institute of Aeronautics and Astronautics Inc., 2018.

[39] "Products | TAIRYFIL Carbon FIber," [Online]. Available: http://www.fpc.com.tw/fpcwuploads/pdocument/pdocument_210916155019.pdf. [Accessed May 2022].

[40] "The Differences Between a CNC Router and a CNC Mill | ShopSabre ...," [Online]. Available: https://www.shopsabre.com/the-differences-between-a-cnc-router-and-a-cnc-mill/. [Accessed May 2022].

[41] "Good Price 1325 Cnc Router Wood Furniture Design Machine In India Pakistan," [Online]. Available: https://www.alibaba.com/product-detail/good-price-1325-cnc-router-wood_60727812393.html. [Accessed May 2022].

[42] "What Is Laser Cutting? - A Definitive Guide To The Process - TWI," [Online]. Available: https://www.twi-global.com/technical-knowledge/faqs/what-is-laser-cutting. [Accessed May 2022].

[43] "Training Guide: Hot Wire Foam Cutter," [Online]. Available: http://k12maker.mit.edu/uploads/9/7/5/8/97583140/hot_wire_guide.pdf. [Accessed May 2022].

[44] "B08G5CPXZX Hot Wire Foam Cutter Cutting Machine Fireproof Density," [Online]. Available: https://01sale.net/product/b08g5cpxzx-hot-wire-foam-cutter-cutting-machine-fireproof-density-board-styrofoam-sponge-cutter-working-stand-table-diy-tool-31-x-15/. [Accessed May 2022].

[45] "How to Hand Laminate & Vacuum Bag a Simple Carbon Fibre Part - ...," [Online]. Available: https://www.easycomposites.co.uk/learning/hand-laminate-vacuum-bag-simple-part. [Accessed May 2022].

[46] "Wet Layup - TotalBoat," [Online]. Available: https://www.totalboat.com/wet-layup-2/. [Accessed May 2022].

[47] "Amazon.com: Holybro Pixhawk - Juego estándar 5X + GPS M8N : ...," [Online]. Available: https://www.amazon.com/-/es/HolyBro-Pixhawk-Juego-est%C3%A1ndar-GPS/dp/B09N9R7G2R. [Accessed May 2022].

[48] "FlySky FS-I6X 10Ch 2.4 GHz Radio Remote Control in Pakistan," [Online]. Available: https://electrobes.com/product/flysky-fs-i6x-10ch-transmitter-2-4ghz-afhds-2a-rc-transmitter-with-fs-x6b-i-bus-receiver/. [Accessed May 2022].

[49] "IA10B-SPECIFICATIONS --- FlySkyRC," [Online]. Available: https://www.flysky-cn.com/ia10b-canshu. [Accessed May 2022].

[50] "SiK Telemetry Radio V3 - Holybro," [Online]. Available: http://www.holybro.com/product/transceiver-telemetry-radio-v3/. [Accessed May 2022].

[51] "Tattu 6s 22.2V 10000 mAh 25C LiPo Battery with xt90 Plug - Allrc," [Online]. Available: https://allrc.pk/product/tattu-6s-22-2v-10000mah-25c-lipo-battery-with-xt90-plug/. [Accessed May 2022].

[52] "T-Motor AT4125 540KV --- RC Diesel," [Online]. Available: https://rcdiesel.eu/products/t-motor-at4125-540kv. [Accessed May 2022].

[53] "Hobbywing Skywalker 80A Model aircraft brushless motor controller ...," [Online]. Available: https://www.conrad.com/p/hobbywing-skywalker-80a-model-aircraft-brushless-motor-controller-load-max-100-a-2108341. [Accessed May 2022].

[54] "Gemfan Composite Propeller 15x8 Grey | HobbyKing," [Online]. Available: https://hobbyking.com/en_us/gemfan-composite-propeller-15x8-grey.html?___store=en_us. [Accessed May 2022].

[55] "Gartt Ml 5210 340 kv Brushless Motor For Multicopter Quadcopter...," [Online]. Available: https://www.aliexpress.com/item/32809063233.html. [Accessed May 2022].

[56] "Hobbywing X-Rotor 2-6S Lipo 40A orignal | smarthobby," [Online]. Available: https://www.smarthobby.pk/product-page/hobbywing-x-rotor-2-6s-lipo-40a-orignal. [Accessed May 2022].

[57] "18x5.5 3K Carbon Fiber Propellers 18inch CW CCW 1855 Props for ...," [Online]. Available: https://www.aliexpress.com/item/32869573358.html. [Accessed May 2022].

[58] "Xt 90 Battery Connector Xt90 Plug Xt90 Socket For Rc Battery 1pair - ...," [Online]. Available: https://www.aliexpress.com/item/32656489753.html. [Accessed May 2022].

[59] "XT60 Connectors - Male Female Pair in Pakistan - Electronics Pro," [Online]. Available: https://epro.pk/product/xt60connectorsmalefemalepairinpakistan/. [Accessed May 2022].

[60] "Technical Hut JST XH 2.54 Male Female 3-Pin Connector Set 1 Pair, ...," [Online]. Available: https://www.indiamart.com/proddetail/jst-xh-2-54-male-female-3-pin-connector-set-1-pair-22986264555.html. [Accessed May 2022].

[61] "Servo Motors: Servo Mini Tower Pro 9g SG-90 Philippines ...," [Online]. Available: https://circuit.rocks/tower-pro-9g-sg-90-mini-servo. [Accessed May 2022].

[62] "Take Flight With H4WK - DIYODE Magazine," [Online]. Available: https://diyodemag.com/projects/part_three_take_flight_with_h4wk. [Accessed May 2022].

[63] "QSTABILIZE Mode - Plane documentation," [Online]. Available: https://ardupilot.org/plane/docs/qstabilize-mode.html. [Accessed May 2022].

[64] "QLOITER Mode - Plane documentation," [Online]. Available: https://ardupilot.org/plane/docs/qloiter-mode.html. [Accessed May 2022].

[65] "QHOVER Mode - Plane documentation," [Online]. Available: https://ardupilot.org/plane/docs/qhover-mode.html. [Accessed May 2022].

[66] "QRTL Mode - Plane Documentation," [Online]. Available: https://ardupilot.org/plane/docs/qrtl-mode.html. [Accessed May 2022].

[67] "QLAND Mode - Plane Documentation," [Online]. Available: https://ardupilot.org/plane/docs/qland-mode.html. [Accessed May 2022].

[68] "Tuning Process Instructions - Plane documentation," [Online]. Available: https://ardupilot.org/plane/docs/quadplane-vtol-tuning-process.html. [Accessed May 2022].

[69] "Mugin-2 2930mm H-Tail Fiberglass & Carbon Fiber VTOL UAV Platform...," [Online]. Available: https://www.muginuav.com/product/mugin-2-2930mm-h-tail-fiberglass-carbon-fiber-vtol-uav-platform/. [Accessed May 2022].

[70] "Foxtech Baby Shark VTOL 260 Drone | The Australian Drone Specialists," [Online]. Available: https://www.integraldrones.com.au/product/foxtech-baby-shark-drone/. [Accessed May 2022].

[71] "Foxtech BABY SHARK VTOL 260 for Inspection Mapping and Survey," [Online]. Available: https://www.foxtechfpv.com/foxtech-baby-shark-vtol.html. [Accessed May 2022].

[72] "AT4125 Long Shaft_AT_Series_Motors_Fixed_Wing_T-...," [Online]. Available: https://store.tmotor.com/goods.php?id=827. [Accessed May 2022].

[73] W. F. Phillips, "Lifting-Line Analysis for Twisted Wings and Washout," 2012.

[74] P. J. Swatton, Principles of Flight for Pilots, 2010.

[75] NASA, "Aircraft Control," [Online]. Available: https://slideplayer.com/slide/7471659/.

[76] "NACA 0010 (naca0010-il) Xfoil prediction polar at RE = 500,000," [Online]. Available: http://airfoiltools.com/polar/details?polar=xf-naca0010-il-500000. [Accessed January 2022].

[77] "Inclination Effects on Lift," NASA, [Online]. Available: https://www.grc.nasa.gov/www/k-12/airplane/incline.html.

[78] A. S. Saeed, A. B. Younes, S. Islam, J. Dias, L. Seneviratne and G. Cai, "A Review on the Platform Design, Dynamic Modeling and Control of Hybrid UAVs," pp. 1-10, 2015.

[79] "Drone Motor Calculator," [Online]. Available: https://www.halfchrome.com/drone-thrust-testing/. [Accessed Jan 2022].